

HYPERELECTRONIC POLARIZATION AND
RELATED ELECTRONIC PROPERTIES
OF MACROMOLECULAR SOLIDS:
ORGANIC SEMICONDUCTORS

By

ROGER D. HARTMAN

Bachelor of Arts
William Jewell College
Liberty, Missouri
1958

Master of Science
University of Arkansas
Fayetteville, Arkansas
1960

Submitted to the faculty of the Graduate College
of the Oklahoma State University
in partial fulfillment of the requirements
for the degree of
DOCTOR OF PHILOSOPHY
May, 1968

OCT 25 1968

HYPERELECTRONIC POLARIZATION AND
RELATED ELECTRONIC PROPERTIES
OF MACROMOLECULAR SOLIDS:
ORGANIC SEMICONDUCTORS

Thesis Approved:

Herbert A. Pohl

Thesis Adviser

W. J. Lewis

J. Paul DeWitt

K. D. Berlin

Betty D. Pollak

N. Durham

Dean of the Graduate College

688378

ACKNOWLEDGMENTS

The author wishes to express his sincere gratitude to his many friends and associates for their assistance and encouragement during the tenure of this study. To Professor H. A. Pohl, Thesis Chairman, go special thanks for his patience and guidance throughout this investigation. The author also wishes to express his appreciation to Professor J. Yahia and Professor M. Pollak for many valuable suggestions and stimulating discussions.

He is further indebted to: Mr. H. Hall and associates, and Mr. W. Adkins and associates for their assistance in design and construction of apparatus; Mr. D. Pohl, Mr. E. Engelhardt, Dr. S. Kanda, and Dr. J. Mason for their assistance in preparing materials studied; Professor E. E. Kohnke, Professor W. J. Leivo, and Professor T. G. Winter, and their respective groups for loan of equipment and apparatus; Mr. W. Hedgpeth and Mr. J. Wyhof for their assistance in taking and analyzing data; Mr. R. A. Van Nordstrand for assistance in X-ray diffraction studies; and Mrs. Paula Baum for the drawings in this manuscript.

He graciously acknowledges financial support of: The National Science Foundation in the form of a NSF Science Faculty Fellowship; The National Aeronautics and Space Administration in the form of a

Research Assistantship; and The University of Tulsa in the form of a Faculty grant. Further, he acknowledges support from Dr. H. E. Harrington and the Physics Department at Oklahoma State University.

Finally, to his wife, Dr. Wanda (who preempted him by some 4 months) for her patience, understanding, encouragement, and for her typing the manuscript, goes his sincere appreciation.

TABLE OF CONTENTS

Chapter	Page
I. THE PROBLEM.	1
Introduction	1
Historical Background	2
Statement of the Problem.	6
Characterization of Polymers.	7
Hyperelectronic Polarization	9
Superconducting Organic Polymers	12
II. PREPARATION OF MATERIALS	14
Experimental Synthesis and Purification	14
Elemental Analysis	20
Physical and Chemical Properties.	22
Color and Solubility	22
Density	23
Structure and Molecular Weight.	23
Electronic Characteristics	28
III. ORGANIC SEMICONDUCTORS	29
Conductivity	29
Insulators, Semiconductors, and Metals	30
Organic Crystals and Polymers	34
High Pressure Technique.	35
Hopping Model	37
Carrier Sources	40
Statement of the Problem	41
Experimental Apparatus and Procedure	41
Results and Discussion.	49
PAQR'S	49
Cu-Coordination Polymers	57
Electric Field - Molecular Lengths	73
Summary	74
Suggestions for Future Studies	76

IV. ELECTRON SPIN RESONANCE.	78
Detection of ESR	78
Determination of Spin Densities	82
Gaussian Curve	83
Lorentzian Curve	84
Power Determination	85
First Moments	86
Direct Conversion of ESR Signal	87
Literature Review	87
Statement of the Problem	91
Experimental Apparatus and Procedure	92
Results and Discussion	95
ESR Pressure and O ₂ Effects	97
ESR Temperature Effects	110
Summary	121
Suggestions for Further Studies	124
V. HYPERELECTRONIC POLARIZATION	125
Polarization	125
Polarization Mechanisms	128
Electronic Polarization	130
Atomic Polarization	130
Dipolar Polarization	131
Interfacial Polarization	131
Hyperelectronic Polarization	131
Literature Review	134
Ferroelectrics	135
Multiphase Materials	136
Organic Materials	142
Statement of the Problem	143
Experimental Apparatus and Procedure	144
Results and Discussion	152
$\sigma(P, \omega)$ and $\epsilon(P, \omega)$	155
$\sigma(T, \omega)$ and $\epsilon(T, \omega)$	173
$\sigma(\vec{E}, \omega)$ and $\epsilon(\vec{E}, \omega)$	188
Relaxation Times and Dispersion	196
Electrode Studies and Sample Morphology	202
Unpaired Spins and O ₂ Effects	211
Summary	213
Suggestions for Future Studies	217

VI. A SEARCH FOR ORGANIC SUPERCONDUCTORS. . . .	220
Introduction	220
Experimental Background	222
Theoretical Background	232
BCS Theory	233
Little's Organic Superconductor	239
Statement of the Problem	243
Experimental Apparatus and Procedure	244
Results and Discussion	252
Multilevel Semiconductors	269
Filamentary Superconduction	272
Summary	279
Suggestions for Future Studies	280
VII. SUMMARY AND CONCLUSIONS	282
BIBLIOGRAPHY	284

LIST OF TABLES

Table	Page
I. Semiconducting Polymer Compositions.	15
II. Elemental Analysis of Polymers	21
III. Resistivity and Activation Energy for 10 PAQR Polymers (After Being Subjected to 12 Kbar and 400°K) at 1.820 Kbar and 300°K	50
IV. Resistivity and Activation Energy for 10 PAQR Polymers (After Being Subjected to 32 Kbar and 450°K) at 1.820 Kbar and 300°K	52
V. Activation Energies for Several Polymers at Various Pressures as Measured from 300°K to 450°K	53
VI. Spin Concentration of Seven DPPH ESR Standards.	95
VII. Pressure Effects on ESR Signal.	105
VIII. ESR Data and Resistivities for Several Polymers at 300°K and 77°K After Extensive Outgassing	112
IX. Average Molecular Length of Several Polymers	122
X. Comparison of Activation Energies for Polymer JM85B	186
XI. Dependence of ϵ_r (1 KHz) upon A. C. \vec{E} -Field Strength	189
XII. Dependence of ϵ_r (1 KHz) upon D. C. \vec{E} -Field Strength	190
XIII. Estimated Parameters for Polymers	201
XIV. Relaxation Times of Macromolecular Solids	203
XV. Electrode, Thickness, and Shear Effects of Dielectric Constant of Polymer DPIA.	207
XVI. Activation Energies for Several Polymers at 8 Kbar in Various Temperature Ranges.	267
XVII. D. C. Resistivities of 13 Polymers Measured at 8 Kbar at Low Temperatures in a Chester-Jones Clamp	273

LIST OF FIGURES

Figure	Page
1. High Pressure Resistivity Cell.	42
2. Calibration Curve for 50 Ton Press	44
3. Calibration Curve for 12-1/2 Ton Press	45
4. Resistivity-Pressure Curves for Polymer DP1A at Various Temperatures	47
5. Resistivity-Temperature Curves for Polymer DP1A at Various Pressures	48
6. Resistivity-Pressure Curves for Several PAQR Poly- mers (Experiments I and III)	55
7. Resistivity-Pressure Curves for Several PAQR Poly- mers (Experiment II)	56
8. Resistivity-Temperature Curves for Polymer SK3A: (a) $T_{\max} = 75^{\circ}\text{C}$; and (b) $T_{\max} = 100^{\circ}\text{C}$	59
9. Resistivity-Pressure Curve for Polymer SK3A ($T_{\max} = 75^{\circ}\text{C}$)	60
10. Resistivity-Pressure Curve for Polymer SK3A ($T_{\max} = 100^{\circ}\text{C}$)	61
11. Resistivity-Pressure Curve for Polymer SK1A	62
12. Hysteresis of Piezoresistivity for Polymer SK3A	64
13. Effect of Shearing Stress on Resistivity of Polymer SK3A	70
14. Effect of Shearing Stress on Resistivity of Polymer SK1A	71
15. Effect of Shearing Stress on Resistivity of Polymer DP1A	72

16.	Variation of the Normalized Conductivity vs. \vec{E} -Field Strength for Various Average Molecular Lengths L.	75
17.	Block Diagram of ESR Spectrometer	93
18.	Calibration Curve for ESR Spectrometer	94
19.	Typical Resonance Line for DPPH Standard	96
20.	Ensuing Decay of ESR Signal of Polymer DP1A Following Pressure Treatments	98
21.	Strip Chart Recordings of ESR Signal of Sample DP1A After Pressure Treatment	100
22.	Effect of O ₂ Adsorption on the ESR Signal of Polymer DP1A	102
23.	Strip Chart Recordings of ESR Signal of Highly Out-gassed Polymer DP1A as a Function of O ₂ Pressure Induced on the Sample	103
24.	Strip Chart Recordings of ESR Signal of Polymer DP1A with H ₂ O Vapor Adsorbed as a Function of O ₂ Pressure	104
25.	Correlation of Unpaired Spin Concentration with Peak to Peak Signal Half Width	114
26.	Correlation Between Spin Concentration and Charge Carrier Concentration	115
27.	Schematic Diagram of Electrical Polarization Mechanisms: (A) Maxwell-Wagner; (B) Dipolar; (C) Atomic; (D) Electronic; and (E) Hyperelectronic	129
28.	Schematic Diagram of Exciton and Ion Monopole Formation in Long Ekaconjugated Polymers: (a) in the Absence; and (b) in the Presence of an External \vec{E} -Field.	132
29.	Equivalent Lumped Parameter Representations of a Multiphase Dielectric.	138
30.	Theoretical Dispersion of R _p and C _p for a Multiphase Dielectric.	140

31.	Bridge Circuit for the Determination of the AC Resistivity and Dielectric Constant of Polymeric Semiconductors.	147
32.	High Pressure Dielectric Cell	149
33.	Pressure and Frequency Dependence of the Dielectric Constant and Resistivity for Polymer JM96A (No Premold Pressure Treatment)	156
34.	Pressure and Frequency Dependence of the Dielectric Constant and Resistivity for Polymer JM96A (Premolded at 10.4 Kbar)	157
35.	Premolding Pressure and Frequency Dependence of the Dielectric Constant and Resistivity for Polymer JM77B	159
36.	Pressure and Frequency Dependence of the Dielectric Constant and Resistivity for Polymer JM97A (Premolded at 9.6 Kbar)	160
37.	Pressure and Frequency Dependence of the Dielectric Constant and Resistivity for Polymer JM89B (Premolded at 8.3 Kbar)	161
38.	Pressure and Frequency Dependence of the Dielectric Constant and Resistivity for Polymer DP1A (Premolded at 3.4 Kbar)	162
39.	Pressure and Frequency Dependence of the Dielectric Constant and Resistivity for Polymer SK3A (Premolded at 10.6 Kbar)	163
40.	Pressure and Frequency Dependence of the Dielectric Constant and Resistivity for Polymer JM85B (Premolded at 10.9 Kbar)	164
41.	Pressure Dependence of the Dielectric Constant and A.C. Conductivity Measured at 1 KHz for Several Polymers	167
42.	Pressure Dependence of the Resistivity for Polymer JM96A at Various Frequencies.	172
43.	Temperature and Frequency Dependence of the Dielectric Constant and Resistivity for Polymer DP1A	174

44.	Temperature and Frequency Dependence of the Dielectric Constant and Resistivity for Polymer JM82. . .	176
45.	Temperature and Frequency Dependence of the Dielectric Constant and Resistivity for Polymer JM77B. . .	177
46.	Temperature and Frequency Dependence of the Dielectric Constant and Resistivity for Polymer JM50. . .	178
47.	Temperature and Frequency Dependence of the Dielectric Constant and Resistivity for Polymer DP1A. . .	179
48.	Temperature and Frequency Dependence of the Dielectric Constant and Resistivity for Polymer JM85B. . .	180
49.	Temperature Dependence of the Dielectric Constant for Polymer DP1A at Various Frequencies.	182
50.	Temperature Dependence of the Dielectric Constant for Polymer JM85B at Various Frequencies.	183
51.	Temperature Dependence of the Dielectric Constant for Polymer JM77B at Various Frequencies.	184
52.	Temperature Dependence of the Dielectric Constant for Polymers JM85B and JM77B at 1 KHz (Possible Ferroelectric Effect).	187
53.	Frequency Dependence of the Dielectric Constant for using Various Electrodes and Mechanical Shearing Stress.	210
54.	Cross Sectional View of the Chester-Jones High Pressure Clamp.	245
55.	View of the Liquid Helium Cryostat.	247
56.	Schematic of the Complete Vacuum System and Exchange Gas System for the Liquid Helium Cryostat.	249
57.	Temperature Dependence of the D.C. Resistivity for Polymer JM85A.	253
58.	Temperature Dependence of the D.C. Resistivity for Polymer JM85B.	254

59.	Temperature Dependence of the D.C. Resistivity for Polymer JM82.	255
60.	Temperature Dependence of the D.C. Resistivity for Polymer DP1A	256
61.	Temperature Dependence of the D.C. Resistivity for Polymer HAP1	257
62.	Temperature Dependence of the D.C. Resistivity for Polymer JM50.	258
63.	Temperature Dependence of the D.C. Resistivity for* Polymer JM42.	259
64.	Temperature Dependence of the D.C. Resistivity for Polymer SK3A.	260
65.	Temperature Dependence of the D.C. Resistivity for Polymer JM84A	261
66.	Temperature Dependence of the D.C. Resistivity for Polymer JM84B	262
67.	Temperature Dependence of the D.C. Resistivity for Polymer JM83A	263
68.	Temperature Dependence of the D.C. Resistivity for Polymer JM83B	264
69.	Temperature Dependence of the D.C. Resistivity for Polymer JM77B	265
70.	Resistivity-Temperature Curve (Pumped Liquid N ₂ Temperature) for Polymer DP1A	268
71.	Anomalous Behavior of the Resistivity of Several Poly- mers at Low Temperatures	274

CHAPTER I

THE PROBLEM

Introduction

Macromolecular solids, particularly organic compounds, have deeply interested and fascinated scientists and engineers from a wide variety of disciplines in the past two decades. This is largely due to the fact that many of these solids, usually considered as high quality electrical insulators, have been made to conduct electronically, and to conduct quite well (up to 10^4 mho/cm). In addition, many of these solids tend to exhibit a variety of other interesting properties such as: photoconduction, semiconduction, and thermoelectric effects. Certain types of them possess unusually large dielectric constants (up to 50,000); and it has even been suggested that organic macromolecules with particular structures may be superconducting at room temperature.

In view of these many fascinating properties, this study was undertaken to: (1) classify a group of newly synthesized polymers as electronic semiconductors, and to study the effect on electronic conductivity brought about by the systematic change of the monomeric acene and anhydrides from which the polymers are formed; (2)

investigate the nature of the unusually high dielectric constant (hyper-electronic polarization) exhibited by many of these macromolecular solids; and (3) examine a number of these solids at low temperatures in an effort to find a superconductor. The problems at hand will be discussed in more detail in what follows.

Historical Background

Investigations into the electronic behavior of organic compounds date back to the turn of the century when in 1906, Pochettino (1) observed photoconduction in anthracene. The subject essentially lay dormant until 1941, when Szent-Györgi (2) suggested that our understanding of certain biological processes could be enhanced by considering such structures as having properties akin to semiconductors. In the late forties and early fifties, work was carried out by Eley and coworkers (3) and by Vartanyan (4) on phthalocyanines.

Although there have been scattered studies of the electronic properties of organic compounds for some sixty years, it was not until the late fifties that a serious effort to understand and develop organic semiconductors was underway. This sharp increase in research efforts in the area of organic materials was brought about largely by an erroneous report from the Soviet Union in 1959, which indicated they had successfully developed a plastic transistor (5). Although this report actually discussed a new organic semiconductor material, rather than a plastic transistor, the incorrect translation had a very

positive effect on the search for organic semiconductor materials.

During the late fifties and early sixties, a group of researchers at the Princeton University Plastics Laboratory, headed by H. A. Pohl, succeeded in synthesizing and characterizing over one hundred polymeric semiconductors. The types of polymers studied by Pohl and coworkers (6-22) included: polyacene quinone radical (PAQR) polymers, polyacetylenes, polybenzimidazoles, pyropolymers, and Schiff's base polymers. The range of conductivities of these polymers varied from 10^4 to 10^{-12} mho/cm. In brief, it was found that most of these organic macromolecular solids exhibited a number of striking features which included: (1) photoconductivity; (2) extreme dependence of conductivity on applied pressure; (3) high thermoelectric powers (Seebeck coefficients); and (4) rectification properties.

A study of the correlation between electronic conductivity and unpaired spin concentration was made by Pohl and Chartoff (21) and Pohl and Opp (17). Effects of pressure and temperature on conductivity have been investigated (6-22), and a quantitative theory, relating conductivity to pressure and temperature was developed and reported by Pohl, Rembaum, and Henry (16) based on absolute reaction rate theory. This model is applicable to the solids reported in this study.

Concurrent with this work by the Princeton group, was a study of the electronic properties of charge exchange complexes, in particular tetracyanoquinodimethane (TCNQ) complexes. These polymers

also exhibit very high conductivities. Particularly significant have been the contributions made by Kepler and coworkers (23-25), Inokuchi, et. al. (26-28), Labes and coworkers (29, 30), and Kommandeur and others (31-33). Most of these measurements were performed with very little or no pressure on the sample. Drickamer and his group at Illinois (34, 35) studied TCNQ polymers at extreme pressures (up to 500 kbar) and found that the resistivity decreases with pressure (corresponding to earlier reports by Pohl for PAQR's) quite rapidly, then minimizes, and starts to increase as the pressure is increased further. This was attributed to an irreversible chemical change which had been induced in the sample. Eyring and coworkers (36, 37) have recently investigated the pressure behavior of several charge exchange complexes as well.

Further investigation by Pohl and coworkers on the PAQR's has led to a very interesting result, in that these polymers tend to exhibit unusually large dielectric constants. Pohl and Rosen (38, 39) first reported dielectric constants of up to 800 at room temperature, and a frequency of 1 KHz for a PAQR composed of anthraquinone and pyromellitic dianhydride. Since that time, the author of this paper has reported even higher dielectric constants for similar polymers (40-43). Rosen and Pohl termed this high polarization effect "hyperelectronic."

In 1964, a rather striking prediction was made by W. A. Little (44). He suggested the possibility of synthesizing an organic superconductor, which would be capable of exhibiting superconducting

properties at room temperatures.

That the above findings and predictions are surprising should be evident from the fact that these macromolecular solids are, by and large, highly purified hydrocarbon derivatives, i. e., organic polymeric solids. One would certainly not expect most organic polymers to exhibit exalted electronic behavior such as semiconduction, superconduction, and hyperelectronic polarization. On the contrary, organic polymers tend to be thought of as very high quality electrical insulators.

Consider a variety of organic compounds such as: rubbers, plastics, textiles, leathers, papers, and woods. There is not a good electrical conductor in the lot. Yet, when one synthesizes a particular type of organic polymer, one finds many of these exalted electronic properties present. The possibility of achieving such properties is attributed to the enhanced π -electron transfer from molecule to molecule as suggested earlier by Szent-Györgi (2).

The purpose of this study is to investigate the origin of the unusually high dielectric polarization as exhibited by certain macromolecular solids; and to perform a search for the existence of superconductivity in organic macromolecular solids. This brief historical background is not meant to be an extensive literature survey on organic semiconductors, since there are a number of adequate review articles in print [e. g. Pohl (20,45), Rembaum, Moacanin, and Pohl (46), Airapetyants and Davydov (47), Becher and Mark (48), Hatano (49) and

Rozenšhtein (50, 51)], In addition, a relatively new reference book by Gutmann and Lyons (52) capably and adequately discusses all related phenomena associated with organic semiconductors and the macromolecular solid state. The reader is referred to the reference works as listed above for further studies.

Statement of the Problem

The problem, as investigated in this study, is divided into three parts. It consists of:

- I. Experimentally studying the electronic properties of a group of newly synthesized organic polymers in an effort to characterize them as electronic polymeric semiconductors, and to investigate the effects on electronic conductivity induced by a systematic change in the monomeric acene and anhydride system;
- II. Investigating both theoretically and experimentally the effect of unusually high polarization exhibited by many of the macromolecular solids; and
- III. Performing a search for an organic superconductor from the likely candidates characterized in part (I).

Broadly speaking, the three phases of the investigation are concerned with the energetics of carrier formation, the mobilities of carriers, and the effects on these parameters of morphology and impurity. These effects may be enhanced by applying externally produced

pressure and electric (\vec{E}) fields to the specimen and studying their effects on the conductivity.

This study is also concerned with the relative roles in the electrical polarization mechanism of the variously excited electronic states such as (1) uncoupled spin states, (2) Frönkel excitons, (3) von Hippel polarons, and (4) free carrier electrons [cf. Pohl (45)]. By studying the effect of temperature and pressure variation on the electron spin resonance signal (ESR) and conductivity, one determines the activation energy for production of unpaired spins and for production of free charge carriers, respectively. This provides a means of establishing the energetics of carrier formation and transport, and of spin related processes. A.C. measurements provide further insight into the polarization mechanisms; and by examining the effect of temperature and pressure on the dielectric constant, one can obtain more information regarding the source of the hyperelectronic polarization.

Characterization of Polymers

For the purpose of this study, a semiconductor shall be defined as any material which conducts electronically as opposed to ionically, with the conduction σ exhibiting a positive temperature dependence given by:

$$\sigma = \sigma_0 \exp(-E_g/2kT), \quad (1)$$

where E_g is the energy interval, measured in eV; k is the Boltzmann constant, in eV/°K; T is the absolute temperature (°K); and σ_0 is

the reference conductivity at $T = 0^\circ\text{K}$. For an "intrinsic" semiconductor, the activation energy, $E_a = E_g/2$. Further, we shall limit our definition of semiconductors to those materials possessing a conductivity within the following range: $10^{-12} \leq \sigma \leq 10^4$ mho/cm.

In order to characterize the sample as an electronic semiconductor, one is required to establish the conductivity as being truly electronic in nature along with the validity of Eq (1). To do this involves the measurement of D.C. resistance of the material at various temperatures, while showing that there is no degradation in resistance as a function of time if the system is in thermodynamic equilibrium. Further, one must check for D.C. polarization. If the sample is truly an electronic semiconductor, there should be no change in resistance when the electrodes to the sample are interchanged.

Generally speaking, the specimens are examined for the dependence of σ on variations in externally produced pressure, temperature, and electric (\vec{E}) field. Where applicable, the theoretical model proposed by Pohl, et.al. (15, 39, 45) is applied to calculate the molecular lengths from \vec{E} -field dependency of σ . Electron spin resonance (ESR) measurements are made, and the number of unpaired spins per gram are correlated with the conductivity. In this manner, one can study the effect on conductivity of changing the acene monomer and/or the anhydride. Where applicable, ESR temperature dependence is examined, and molecular lengths are calculated for the respective samples, after a model developed by Pohl, et.al. (21, 45). A comparison

of these two methods for determining molecular lengths is made. This work is reported in Chapters III and IV.

Hyperelectronic Polarization

Several polymers, characterized as electronic semiconductors in Part I, are investigated for the dependence of A.C. polarization and A.C. conductivity on variations in externally applied pressure, temperature, frequency, and \vec{E} -field. Characteristics of the electrical properties of high dielectric constant polymeric semiconductors which have been observed include: the resistivity $\rho (= 1/\sigma)$ is strongly pressure and temperature dependent, and moderately sensitive to the magnitude of the applied \vec{E} -field; the dielectric constant, ϵ_r , is observed to be strongly pressure and temperature dependent, increasing with either or both parameters, but is inversely dependent upon the magnitude and frequency of the applied \vec{E} -field (38-43). Regarding the large polarization effects, Rosen and Pohl (38, 39) first suggested a new type of polarization mechanism, namely, that of hyperelectronic polarization. Hyperelectronic polarization differs from ordinary polarization in the following ways.

1. Normal electronic polarization is considered to be due to a slight shift of the centers of positive and negative charge in atoms when an external electric field is applied. This type of polarization usually results in a bulk polarizability which is linearly proportional to the applied electric field for a wide range of field strengths. With

respect to dispersion, this polarization mechanism exhibits relaxation at a frequency, $\nu_e \approx 10^{15}/\text{sec}$; or a relaxation time, $\tau_e \approx 10^{-15}$ sec.

2. Hyperelectronic polarization may be considered as due to the pliant interaction of charge pairs of excitons, localized temporarily on long highly polarizable molecules, with an external electric field. These carriers, which are thermally produced by exciting intermolecular ionization levels of long conjugated molecules ($L \approx 1000-4000\text{\AA}$), are molecularly separated, and range over molecularly limited domains. When an external electric field is applied, these highly mobile carriers, spending most of their time in extraordinarily long regions of near-zero resistance, form a collection of highly polarizable monopoles, and therefore, exhibit a very high bulk polarizability. Hyperelectronic polarization is observed to be nonlinearly dependent upon the applied electric field, and exhibits dispersive relaxation at a frequency, $\nu_h \approx 10^3/\text{sec}$; or a relaxation time, $\tau_h \approx 10^{-3}$ sec.

Since polarization effects in this frequency region are generally attributed to Maxwell-Wagner surface polarization (53); and since, in fact, the polymers studied are not single crystalline, but are rather polycrystalline in nature; one must establish that, indeed, hyper-electronic polarization, rather than surface polarization is what has been observed in these investigations.

Many investigators (53-60) have reported high dielectric constants in oxide semiconductors. Normally they contribute this effect to the existence of a two-phase material, that is, a bulk property, and

an oxide property due to the layer of oxide over the grains of the sample. In particular, Verwey (54), Volger (55), Koops (56), Hilborn (57), Huggins and Sharbaugh (58), Sillars (59), and Van Uiter (60) have observed such effects. They treated the sample as above, and were able to describe the observed dispersion in resistivity and dielectric constant by assuming multi-phase properties, and discussed the dispersion in terms of lumped parameters. In all cases, the relaxation time of the dispersion was in the region of $\tau = 10^{-3}$ sec.

It is the purpose of this portion of the study to establish the mechanism of hyperelectronic polarization as being the principal contributor to the high polarizabilities as observed in a number of macromolecular solids. This is accomplished by showing that ϵ_r and σ : (1) are independent of the electrode used (WC, Pt, Au); (2) are not effected significantly after subjecting the sample to extreme shearing stresses (which would tend to rupture the oxide or other insulating layer around the grains); (3) are directly related to the number of spins and carriers in the sample; (4) are both activated parameters; and (5) exhibit a relaxation time ($\tau \sim 10^{-3}$ to 10^{-4} sec) which can only be resolved with theoretical values by employing a model suggested by Pollak (61, 62).

Pollak's model assumes that for long needle like molecules, the normally expected relaxation time of dispersion must be modified by the square of the ratio of the molecular length to the molecular diameter. From high frequency measurements, the bulk properties are inferred.

Using these values, one finds for the Maxwell-Wagner relaxation time for ordinary surface polarization, $\tau_{\text{MW}} \sim 10^{-10}$ to 10^{-11} sec, while the observed time, $\tau_{\text{obs}} \sim 10^{-3}$ to 10^{-4} sec. Using Pollak's model, and the molecular lengths determined in Part I, one finds, then, $\tau'_{\text{MW}} \sim (10^{-10}) \times (L/d)^2 \sim 10^{-3}$ to 10^{-4} sec, which agrees with the observed value. These findings are discussed in Chapter V.

Superconducting Organic Polymers

It has been suggested by Little (44, 63, 64) that certain types of organic macromolecular solids might be expected to be superconductors if one applies the present theoretical model of the superconducting state to them. He also points out that if such a polymer were isolated, it should exhibit superconduction properties at temperatures as high as 2000°K . The limit of presently known transition temperatures, T_c , is about 18°K . If such a polymer could be found, it would certainly have a revolutionary effect on the world.

This portion of the study is involved with performing a search for superconductivity in the most likely candidates of organic semiconductors which were available. A suitable criterion for the observation of superconductivity in semiconductors (as opposed to metallic systems) has been given by Cohen and others (65, 66). It had been predicted that if a semiconductor were to undergo a superconduction transition, it would be necessary that the semiconductor satisfy the following criteria: (1) Must possess a high carrier concentration;

(2) Must have a large effective mass; (3) Must possess many valleys in the energy bands; and (4) Must exhibit a very large dielectric constant. Indeed, when superconduction was observed in the oxide semiconductor, SrTiO_3 (67), it was found that the above criteria were sufficient.

In order to increase the number of carriers for the organic materials under study above what one would normally expect, a high pressure technique was employed. A Chester-Jones Clamp (68) was constructed, and the samples were studied at liquid He temperatures under pressures of ≈ 8 kbar. The results of this investigation are discussed in Chapter VI. It is suggested that filamentary superconduction has been observed in several of the organic macromolecules herein under study.

CHAPTER II

PREPARATION OF MATERIALS

The materials reported in this study were for the most part synthesized and purified in a manner similar to that described by Pohl and Engelhardt, and Pohl and other coworkers (12-15, 20, 69). The composition of each of the 31 polymers studied is contained in Table I. Those polymers listed with JM, DP, EHE, SK, and HAP preceding the sample numbers were prepared by J. W. Mason, D. G. Pohl, E. H. Engelhardt, S. Kanda, and H. A. Pohl, respectively. Only five of the polymers listed (DP1A, SK1A, SK2A, SK3A, and HAP1) were prepared in our laboratory at Oklahoma State University.

Experimental Synthesis and Purification

Each of the JM polymers are polyacene quinone radical types (PAQR). The monomeric starting materials were repeatedly recrystallized until each had a melting range of 2°C or less. An intimate mixture of the desired reactants was prepared by grinding them together in a mortar and pestle. This mixture was then heated at $295 \pm 2^{\circ}\text{C}$ for a period of 24 hours under a nitrogen atmosphere. The hard, black polymeric products were ground to fine powder and triturated exhaustively with 1% hydrochloric acid and water in order

TABLE I. SEMICONDUCTING POLYMER COMPOSITIONS

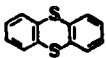
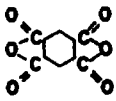
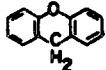
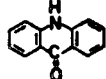
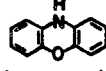
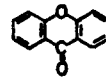
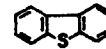
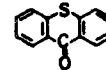
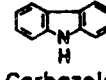
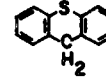
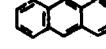
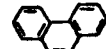
Sample No.	Acene	Anhydride ^(a)	Catalyst	Reaction Temp (°C)	Ratio (moles) ^(b)	Type ^(c)
JM39	 Thianthrene	 PMA	ZnCl ₂	295	1:1:2	PAQR
JM40	 Xanthene	PMA	ZnCl ₂	295	1:1:2	PAQR
JM41	 Acridone	PMA	ZnCl ₂	295	1:1:2	PAQR
JM42	 Phenoxazine	PMA	ZnCl ₂	295	1:1:2	PAQR
JM43	 Xanthone	PMA	ZnCl ₂	295	1:1:2	PAQR
JM46	 dibenzothiophene	PMA	ZnCl ₂	295	1:1:2	PAQR
JM48	 9-Thioxanthene	PMA	ZnCl ₂	295	1:1:2	PAQR
JM49	 Carbazole	PMA	ZnCl ₂	295	1:1:2	PAQR
JM50	 9-Thioxanthene	PMA	ZnCl ₂	295	1:1:2	PAQR
JM77B	 Anthracene	PMA	ZnCl ₂	295	1:1:2	PAQR
JM78B	 Phenanthrene	PMA	ZnCl ₂	295	1:1:2	PAQR

TABLE I. (Continued)

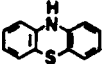
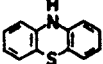
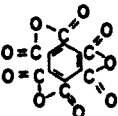
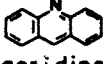
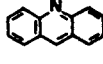
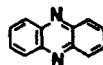
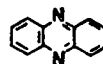
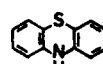
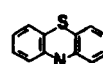
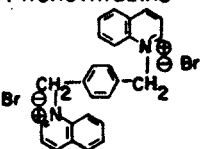
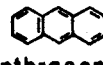
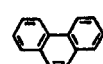
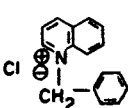
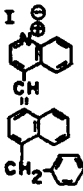
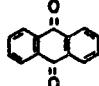

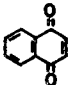
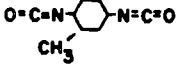
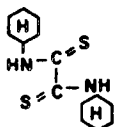
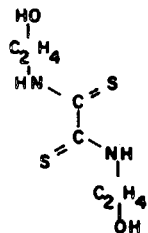
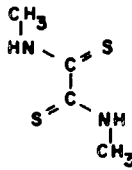
Sample No.	Acene	Anhydride ^(a)	Catalyst	Reaction Temp (°C)	Ratio (moles) ^(b)	Type ^(c)
JM80	 Phenothiazene	PMA	ZnCl ₂	295	1:1:2	PAQR
JM82	 Phenothiazene	 MTA	ZnCl ₂	295	1:1:2	PAQR
JM83A	 acridine	PMA	ZnCl ₂	295	1:1:2	PAQR
JM83B	 Acridine	MTA	ZnCl ₂	295	1:1:2	PAQR
JM84A	 Phenazine	PMA	ZnCl ₂	295	1:1:2	PAQR
JM84B	 Phenazine	MTA	ZnCl ₂	295	1:1:2	PAQR
JM85A	 Phenothiazene	PMA	ZnCl ₂	295	1:1:2	PAQR
JM85B	 Phenothiazine	MTA	ZnCl ₂	295	1:1:2	PAQR
JM89B		MTA	ZnCl ₂	295	1:1:2	PAQR
JM92B	 anthracene	MTA	ZnCl ₂	295	1:1:2	PAQR
JM93B	 Phenanthrene	MTA	ZnCl ₂	295	1:1:2	PAQR
JM96A		PMA	ZnCl ₂	295	1:1:2	PAQR

TABLE I. (Continued)

Sample No.	Acene	Anhydride (a)	Catalyst	Reaction Temp (°C)	Ratio (moles) (b)	Type (c)
JM97A		PMA	ZnCl ₂	295	1:1:2	PAQR
DP1A	 Anthraquinone	PMA	ZnCl ₂	306	1:1:2	PAQR
EHE59	 Fluoranthene	PMA	ZnCl ₂	306	1:1:2	PAQR
EHE102	 1,4-Naphthoquinone	 P-TODI		100	1:1	Schiff's Base
SK1A		Cu(OCOCH ₃) ₂ Cupricacetate		100	1:1	Cu Coordination Polymer
	NN-dicyclohexyl-dithiooxamide - Cu(II)					
SK2A		Cupricacetate		100	2:1	Cu Coordination Polymer
	NN'-di(βhydroxyethyl)-dithiooxamide-Cu(II)					
SK3A		CuSO ₄ CupricSulfate		100	1:1	Cu Coordination Polymer
	NN-dimethyl-dithiooxamide - Cu(II)					
HAP1	Cellulose char			1000		Pyropolymer

- (a) PMA = pyromellitic dianhydride; MTA = mellitic trianhydride; P-TODI = p-toluene diisocyanate. (b) acene:anhydride:catalyst. (c) PAQR = polyacene quinone radical.

to remove the ZnCl_2 catalyst. They were then extracted first with boiling ethyl alcohol followed by boiling benzene for periods of 24 hours each in a Soxhlet extraction apparatus to remove all traces of soluble material. Finally, the insoluble products were ground to a fine powder once more and dried in a high vacuum over phosphorous pentoxide. The dry samples were kept in a desiccator until ready for use (70).

Polymer DP1A, also a PAQR polymer, was prepared by mixing a one to one mole ratio of anthraquinone with PMA, using zinc chloride as a catalyst. The actual weights of the reactants were as follows: 210.22 g anthraquinone; 118.02 g pyromellitic dianhydride; and 136.29 g zinc chloride. The mixture was heated 24 hours at 300°C in a nitrogen atmosphere, after which the product was finely ground, leached with dilute HCl , and then extracted in a Soxhlet apparatus with boiling H_2O for 12 hours. Subsequent to this treatment, the sample was then extracted with hot toluene, ethanol, and benzene, in that order, each for 24 hours. The insoluble residue was finely ground once again and the sample was dried 36 hours at 50°C . After drying, it was stored in a desiccator until it was to be examined. DP1A is a resynthesis of polymer IS1 reported by Pohl and Rosen (38, 39) in 1965 and 1966. The newly synthesized polymer was in a more purified state than the original IS1. Investigations of the new polymer, DP1A, have been reported by Hartman and Pohl (40-43).

The last PAQR polymer reported in the study is polymer EHE59. It was synthesized by mixing 1 to 1 to 2 mole ratios of fluoranthene,

to PMA to $ZnCl_2$, and heating at $306^\circ C$ for 24 hours in air. At the completion of polymerization, it was ground to a fine powder, leached for 12 hours with dilute HCl, and then extracted in a Soxhlet apparatus with water (12 hours), ethanol (24 hours), and benzene (12 hours) in that order. It was then dried for 12 hours at $50^\circ C$, was again finely ground, and was then stored in a desiccator (15, 69).

Sample EHE102, was formed by reacting 1-4 naphthaquinone with p-toluene diisocyanate in the absence of air, at $100^\circ C$. It was ground and purified in a manner described in the above paragraph (15, 69).

Attempts by Kanda and others (71-75) have been successful in synthesizing polymers through coordination with metallic ions. When bi-functional coordinating units enter into chemical combination with a metallic ion, it is possible to form linear polymers of the type ...A-M-A-M-A.... This system may be effected by arraying the metallic ion (M) and the chelating agent (A) in an alternate fashion as indicated. Polymers SK1A, SK2A, and SK3A are such types and were formed by mixing aqueous cupric salt solution with an alcoholic solution of rubeanic acid. They were prepared in our laboratory under a slightly different procedure from the original materials reported by Kanda (72, 74), in that the organic ligands were recrystallized from ethanol.

Polymers SK1A and SK2A were prepared by mixing NN'-dicyclohexyl-dithiooxamide in warm benzene solution and NN'-di-(β -hydroxyethyl)-dithiooxamide in warm ethanol-water solution,

respectively, with equi-molar copper acetate ethanol solution. A black precipitate was formed almost immediately upon mixing the two. The precipitate was so fine that it was necessary to centrifuge the mixture to separate the polymer from the liquid. The gelatinious precipitate was then extracted in a Soxhlet apparatus for 72 hours with hot benzene followed by 24 hours with hot water. It was then dried at 50°C for 24 hours and stored in a desiccator until needed (76, 77).

The preparation of polymer SK3A was accomplished by mixing one equivalent mole of the purified NN'-dimethyl-dithioamide in hot 50% ethanol-water mixed solvent and one equivalent mole of copper sulphate in hot water. After centrifugal separation, the precipitate was extracted in a Soxhlet apparatus for 120 hours with ethanol and for 36 hours with water to remove the non-ionic and ionic impurities (42, 43, 76, 77).

Elemental Analysis

Carbon, hydrogen, oxygen, nitrogen, and sulphur analyses have been made for several PAQR polymers prepared from equi-molar quantities of acene and PMA or MTA. Also, carbon, hydrogen, nitrogen, sulphur, and copper analyses have been obtained on the three Cu(II) coordination polymers. Experimentally observed atomic percents are compared with the calculated values in Table II. Calculated values are based on one to one mole ratios in all cases. Where data has been reported for similarly prepared polymers, the previous results are

TABLE II
ELEMENTAL ANALYSIS OF POLYMERS

Sample No.	Percent by Weight					
	C	H	O	N	S	Cu
DP1A	(a) Calc.	73.80	1.54	24.60		
	Obs.	86.57	3.80	9.63		
JM77B	Calc.	80.00	2.00	18.00		
	Obs.	80.92	3.74	15.44		
JM83A	Calc.	76.40	1.90	17.80	3.90	
	Obs.	68.34	3.33	25.55	2.78	
JM83B	Calc.	72.30	1.21	23.10	3.40	
	Obs.	69.97	3.42	23.56	3.05	
JM85A	Calc.	69.30	1.84	16.80	3.70	8.40
	Obs.	66.18	3.36	21.55	3.90	6.01
SK1A	Calc.	48.50	6.40	18.60	8.10	18.40
	(b) Obs.	48.70	6.74	18.29	7.67	18.60
	Obs.	48.30	6.29	18.41	8.30	18.70
SK2A	Calc.	26.70	3.71	23.60	10.37	35.62
	Obs.	26.10	4.40	22.50	9.31	37.89
SK3A	Calc.	22.90	2.89	30.20	13.40	32.67
	(b) Obs.	22.80	3.35	28.60	12.20	33.05
	Obs.	21.20	2.96	31.30	12.20	32.34

(a) Calculated for 1:1 molar ratios. Activation analysis indicated less than 5 ppm $ZnCl_2$ in the polymers catalyzed by zinc chloride.

(b) Elemental analyses were performed on two separate syntheses of SK1A and SK3A.

compared with the current analysis. It can be seen that the agreement is quite satisfactory.

Physical and Chemical Properties

Color and Solubility

The ZnCl_2 - catalyzed PAQR polymers, were in all cases, black, insoluble, infusible materials, with melting points well in excess of 600°C . Several of the polymers were heated to 600° to 800°C with the indication that considerable pyrolysis had occurred.

It was possible to form a small pellet of most of the materials, by applying high pressure (up to 10 kbar) and slight heat (50° - 100°C). Occasionally, a material was found which would not fuse together. Polymer EHE102, which was a Schiff's base polymer, deep brown in color, was one such polymer, along with JM84A. However, after several hours under extreme pressure, a pellet resulted in all cases. As a whole, the degree of incompressibility, insolubility, and infusibility exhibited by these polymers indicates the occurrence of a high degree of cross linking in these polymers.

Colors of the Cu-coordination polymers ranged from deep brown to black. In general, they appeared to be more fusible and compressible than the PAQR's, indicating a much smaller degree of cross-linking, if any. Polymer SK1A dissolves to some extent in CHCl_2 , CCl_4 , and dioxane, at room temperature; however, the other coordination complexes are all quite insoluble in water and common organic

solvents (74). Evidence of decomposition above 90°C and hysteresis, due to long periods of application of high pressure to the specimen, have also been reported for these polymers (72, 76, 77).

Density

Densities of the materials studied varied at most by a factor of two; no direct density measurements were made, but from the physical dimensions and weights, densities were calculated to range from ~ 1.1 g/cc to ~ 1.9 g/cc. The density was found to be somewhat dependent on the premolding pressure, probably due to inaccurate thickness measurements of the sample.

Structure and Molecular Weight

Since the polymers tend to be insoluble, not much can be said about their structure nor molecular dimensions except by inference. In earlier work on Cu-coordination polymers, Kanda (71) succeeded in forming a colloidal suspension of $\text{CuC}_6\text{H}_2\text{O}_4$ (formed from reacting 2-5 dihydroxy-benzoquinone with Cu(II) salt) which exhibited streaming birefringence. This work, together with electron micrographs, indicated the molecules to be rod-like, approximately $1000 - 5000 \text{ \AA}$ in length, and 500 \AA in diameter. Work on similar coordination compounds exhibited similar results, with the molecular length calculated as $1000 - 2000 \text{ \AA}$ (75). X-ray and electron micrographic measurements indicated crystalline structure which was indicative of a linear one-dimensional solid in the earlier work. In fact, Kanda reports

some single crystals were grown approximately 1 mm in length.

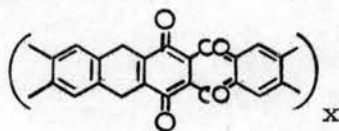
X-ray diffraction measurements on the currently studied Cu-coordination polymers SK1A, SK2A, and SK3A indicate some degree of crystallinity in that rotation camera pictures show two diffuse haloes corresponding to short range ordering (diameter of pattern $\sim 1 \text{ \AA}$ and 10 \AA). X-ray data on polymer DP1A, taken on a diffraction monochromator, indicated a very strong reflection at 7.63 \AA , two rather strong reflections at 6.11 \AA and 3.83 \AA , and several weaker but detectable reflections at 3.77 \AA , 3.51 \AA , 3.35 \AA , 2.64 \AA , 2.60 \AA , 2.42 \AA , 2.28 \AA , 2.06 \AA , and 2.04 \AA . The background diffraction pattern indicated amorphous material was also present to some degree (78).

Pohl and coworkers (39,21) have suggested two alternate ways in which one may obtain information regarding the molecular size and weights of these insoluble polymers. The first method makes use of the effective change of electrical conductivity with externally applied electrical field variations. Rosen and Pohl (39) have developed a model which assumes contribution to charge carrier formation from the applied electric field. Relating the average electric field appearing internally across an average molecular length to the conduction, a formal expression is obtained from which one can infer the "average molecular length." Making use of this model (which will be discussed in more detail in Chapters III and V), the molecular lengths are estimated to be from 1200 \AA to 5500 \AA .

An alternate method involves the measurement of the electron spin resonance (ESR) signal, as a function of temperature. Pohl and Chartoff (21) have suggested that the activation energy for creating free radicals can be related to the energy of an electron, treated quantum mechanically as a particle in a box of length equal to the average molecular dimension. From this treatment (to be elaborated on in Chapter IV), one arrives at molecular lengths from $\sim 800 \text{ \AA}$ to 4400 \AA .

That these molecular lengths as calculated by the two methods are reasonable, is substantiated by observing the relaxation of "hyper-electronic" polarization. This observed relaxation time can best be related to the theoretically expected relaxation time by applying the Pollak model (61, 62) which assumes the observed relaxation time must be modified by the square of the ratio of the molecular length to the molecular width. Using molecular lengths of $1000 - 4000 \text{ \AA}$, and average chain diameters of $\approx 4 \text{ \AA}$, one finds the anomaly between the observed and expected relaxation times is resolved.

The degree of polymerization of the polymers studied can be estimated by using the aforementioned molecular lengths to determine an average polymerization number. For Sample DP1A, from Table I, one may write the possible monomer unit as:

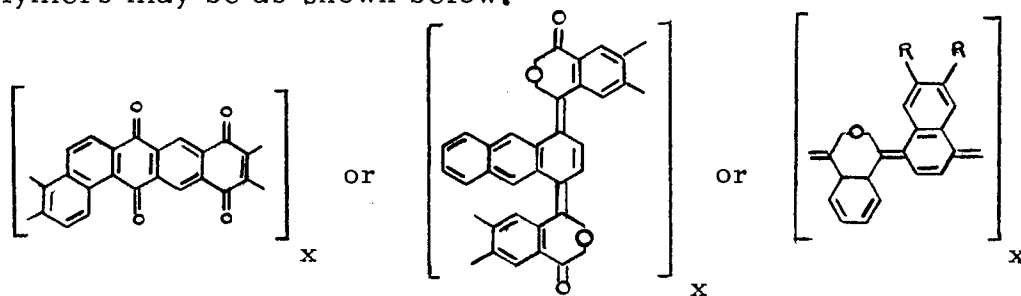


The monomer unit length is then $12 \times L$, where L is the projected C-C bond length. Using simple trigonometry, one finds $L = \sqrt{3}/2 L_0$, where

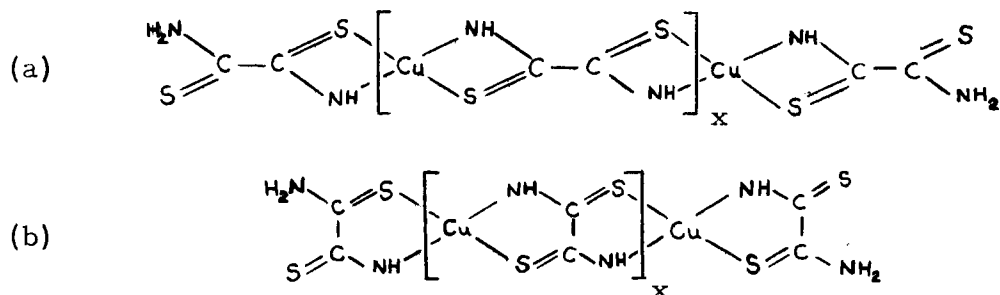
$L_0 = \text{C-C bond length } (1.4 \text{ \AA})$. One then finds $L \approx 0.8(1.4 \text{ \AA}) \approx 12 \text{ \AA}$.

Since the estimated molecular length for DP1A is $\approx 1500 \text{ \AA}$, one then obtains the polymerization number, $x \approx 125$. By similar computations it may be shown that x varies from ~ 100 to ~ 300 for the polymers studied.

Rosen and Pohl (39) have suggested the structure of typical PAQR polymers may be as shown below.

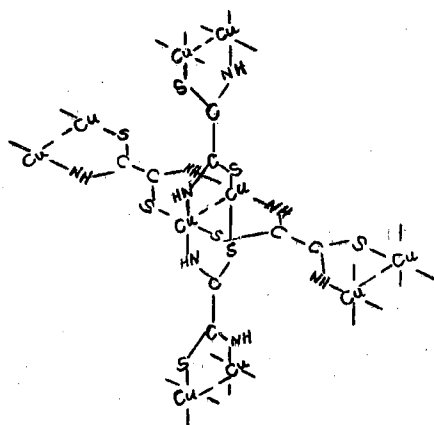


Three possible molecular structures for the Cu-complexed polymers, two one-dimensional chain structures, and a two-dimensional structure, have been proposed. Jensen (79), and Evans and Gibson (80) proposed the one-dimensional chain structures shown below as (a) and (b), respectively. From elemental analysis of a precipitated sample

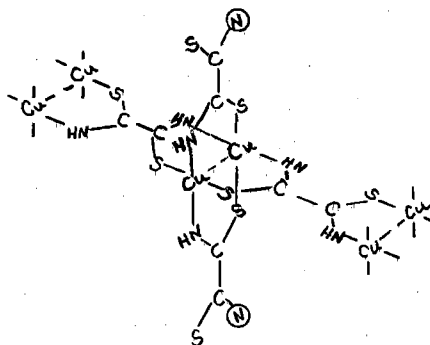


of the Cu-polymer, a 1:1 molar ratio of Cu:rubeanic radical is indicated. Thus, either of the proposed one-dimensional structures could be possible. Kanda, et.al. (81) state the five membered ring is more probable.

A two-dimensional model, of the copper acetate-type, was proposed by Kishita and Kubo (82) in order to account for the anomalously small magnetic susceptibility at room temperatures. This structure, as shown, meets the analytical requirements for a crystalline form of the polymer. Kanda, et.al. (81) have suggested from X-ray data, and magnetic susceptibility measurements that the crystalline structure and the precipitate structure may be recognized as one and the same if one terminates the two-dimensional chain after one C-C bond length has been established above and below the main one-dimensional chain.



Kanda's proposed model is shown below. This model limits the cross-linking, and tends to support earlier mentioned results regarding the fusibility and solubility of these materials.



Electronic Characteristics

All of the materials examined in this study, were found to be electronic type semiconductors with specific resistivities at 1.8 kbar and room temperatures ranging from 300 ohm-cm for polymer JM85B to $> 10^{10}$ ohm-cm for polymer SK2A. For those polymers examined, it was found that they exhibit: (1) electrical field dependency on the conductivity; (2) strong pressure dependency on the conductivity; (3) frequency dependency on the polarization and conductivity with a characteristic relaxation time of $\tau_h \simeq 10^{-3}$ to 10^{-4} sec; (4) strong negative temperature dependency on the resistivity; (5) strong ESR signals at $g \cong 2.0$, with the number of spins/g $\simeq 10^{19}$ to 10^{20} ; (6) strong pressure dependency on the ESR signal; (7) strong affinity for O_2 as indicated by ESR signal; (8) correlation from polymer to polymer between conductivity and the number of spins per gram; (9) unusually high dielectric constants (hyper-electronic polarization); (10) evidence that the dielectric constant is a function of free carriers, bound electrons, permanent dipoles, and unpaired spins in the specimen; and (11) evidence of filamentary superconduction near 77°K .

These interesting and unusual properties will be discussed in the following chapters.

CHAPTER III

ORGANIC SEMICONDUCTORS

Conductivity

The amount of electrical current passed through a given material for a given \vec{E} -field is found to depend upon: (1) the number of available charge carriers, (2) the net charge of each carrier, and (3) the rate at which they are transported through the material bulk. The conductivity, σ , is defined as the amount of charge transported across a unit cross-sectional area per second per unit applied \vec{E} -field. For a material which has n carriers per unit volume with each carrier having a charge q , we may write from Ohm's law:

$$\vec{J} = \sigma \vec{E} = nq\vec{v}; \quad (1)$$

or:
$$\sigma = nq\bar{v}/|\vec{E}| = nq\mu \quad (2)$$

where \vec{v} is the drift velocity of the carriers, and $\mu = \bar{v}/|\vec{E}|$ is the mobility of the carrier.

If there are several different types of charge carriers available, then

$$\sigma = \sum_i n_i q_i \mu_i = \sum_i z_i |e| n_i \mu_i, \quad (3)$$

where $q_i = z_i |e|$, $|e|$ being the absolute electronic charge; and z_i is an integer representing varying degrees of ionic charge carriers.

For the present, the discussion is limited to electronic type semiconductors only ($z_1 = 1$). Further, it will be assumed that impurities are not dominant. In such case, the conductivity becomes:

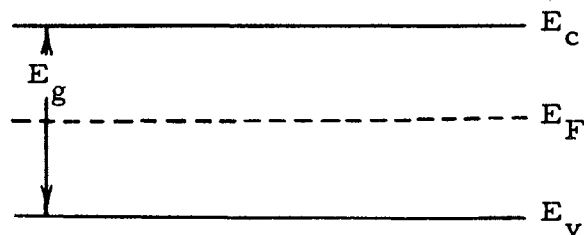
$$\sigma = n |e| \mu. \quad (4)$$

Insulators, Semiconductors, and Metals

The phenomenon of semiconduction was observed some 130 years ago by Michael Faraday (11) when he noted that under a given electric field, silver sulfide does not conduct as well as metals, but certainly more than insulators. It was some one hundred years later before a practical application of this effect was made. Prior to Faraday's observation, materials were, by and large, thought of as insulators, or conductors. Since most metals are good electrical conductors, the words "metal" and "conductor" came to be synonymous.

When a normal conductor (metal) is heated, it is observed that its resistance increases; while for a semiconductor and insulator, an inverse effect is found, i. e., the resistance drops. These effects can best be understood in terms of the band model. Using this model (cf. diagram below), one considers electrons in the conduction band,

or else the holes in the valence band as charge carriers. The gap between the bands is conveniently known



as the forbidden gap. Most solids may be characterized by their

Fermi level (E_F).

A simple example of this band gap model is seen by considering covalent bonding. When two "covalent" atoms (e.g., hydrogen) are brought close together, their electronic wave functions overlap, producing a new wave function given by:

$$\psi = \psi_A^1 \psi_B^2 \pm \psi_A^2 \psi_B^1 = \psi_A \pm \psi_B \quad (5)$$

where the symmetrical function $\psi_A + \psi_B$ and the antisymmetric function $\psi_A - \psi_B$ correspond to the ground state and excited state of the molecule formed by the two atoms respectively. The separation in the ground state and the excited state is inversely dependent on the distance between the two atomic centers, A and B. The two atoms are thus joined together through their valence electrons which are shared mutually by each atom in molecular orbitals.

As one allows more and more atoms to interact, such as is the case for a large number of atoms which are held in close proximity by the crystalline lattice of a solid, then more and more of the covalent bondings occur, and many such energy levels are formed. Thus, conduction bands and valence bands may result due to the many levels in the excited and ground states respectively, and are separated by a forbidden energy gap, E_g .

The population of the excited levels, or the conduction band, for an insulator or semiconductor is usually small at, and below, normal room temperature. The Fermi energy, E_F , a measure of the thermodynamic potential per unit charge carrier, is the energy at which the

probability of a given energy level being occupied is exactly 1/2. Population of the conduction levels is normally achieved via thermal excitations. Quantum mechanically, Fermi-Dirac statistics must be used to discuss the occupation density of energy states, since the electron is subject to the Pauli exclusion principle; however, for temperatures such that $T \gg E_F/k$ (where k is the Boltzmann constant), the Fermi-Dirac distribution goes over to its classical limit, the Maxwell-Boltzmann distribution function (84, 52).

If the semiconductor is intrinsic (i. e., the conductivity is due to inherent properties of the material rather than to impurities) as the temperature is increased above absolute zero, electrons thermally excited from the valence band to the conduction band leave behind vacancies, or holes in the valence band. Both the electrons and holes may act as carriers. The number density of electrons and holes acting as carriers is given by:

$$n = 2(2\pi m_e kT/h^2)^{3/2} \exp \left[(E_F - E_g)/kT \right] \quad (6)$$

$$p = 2(2\pi m_h kT/h^2)^{3/2} \exp (-E_F/kT) \quad (7)$$

where m_e and m_h are the electron and hole mass respectively, and h is the Planck constant. (Cf., for example, Kittel (84) for a derivation of the above.)

On multiplying Eqs (6) and (7), one obtains:

$$np = 4(2\pi kT/h^2)^3 (m_e m_h)^{3/2} \exp (-E_g/kT). \quad (8)$$

For the intrinsic semiconductor, $n = p$, and:

$$n^2 = A^2 \exp (-E_g/kT), \quad (9)$$

$$\text{or} \quad n = A \exp(-E_g/2kT) \quad (10)$$

where A^2 is the factor preceding the exponential in Eq (8). Hence, the excitation of carriers depends on the exponential factor, $\exp(-E_g/2kT)$. The activation energy E_a is defined as: $E_a = E_g/2$. If the masses are equal (i.e., $m_e = m_h$), then $E_F = E_g/2 = E_a$, i.e., the Fermi level lies in the center of the forbidden gap.

Over the intrinsic temperature range, the population of carriers may be approximated by the Boltzmann distribution function as:

$$n = n_0 \exp(-E_a/kT). \quad (11)$$

Substitution of Eq (11) into Eq (4) yields:

$$\sigma = n_0 |e| \mu \exp(-E_a/kT). \quad (12)$$

But, $n_0 |e| \mu$ is, by definition, σ_0 . Hence,

$$\sigma = \sigma_0 \exp(-E_a/kT). \quad (13)$$

In terms of the resistivity of a material ($\rho = 1/\sigma$), then

$$\rho = \rho_0 \exp(E_a/kT). \quad (14)$$

Metals, insulators, and semiconductors may be characterized in terms of the band model as follows. Metallic behavior is exhibited if the bands are partially filled, or if overlapping of a filled and empty band occurs. In an intrinsic semiconductor, a filled valence band lies closely below an empty conduction band, such that thermal excitations may populate the empty band to some degree, leaving partially filled and partially empty bands as in the case of a metal. Insulators are characterized by completely filled bands.

Materials may be characterized by their conductivities, which in

turn are dependent on the number of charge carriers and the mobility of the material. They may be somewhat arbitrarily classified according to their conductivities as follows: metals for $10^4 \leq \sigma \leq 10^8$ mho/cm; semiconductors for $10^{-12} \leq \sigma \leq 10^4$ mho/cm; and insulators for $10^{-22} \leq \sigma \leq 10^{-12}$ mho/cm. In addition, metals usually possess $\sim 10^{22}$ to 10^{23} carriers/cc, and exhibit mobilities from 10 to 10^6 cm²/volt-sec; while for semiconductors, $n \sim 10^{11}$ to 10^{20} /cc, and $\mu \sim 10^{-4}$ to 10^5 cm²/volt-sec (10, 52). For a more thorough discussion of solids and semiconductors, the reader is referred to standard references and texts (83-87).

Organic Crystals and Polymers

That semiconduction would be exhibited by organic substances was, until quite recently, completely overlooked. It is now known, however, that many such materials do exhibit semiconduction. That they are semiconductors is often due to the π -orbital overlap and to an extended degree of conjugation (45).

One of the main difficulties in treating organic solids (molecular and macromolecular) both experimentally and theoretically is their lack of order. In some instances, it has been possible to grow single crystals of organic monomers large enough to experimentally examine their electrical properties. Examples of such are naphthalene, anthracene, tetracene, pentacene, quaterrylene, perylene, and others. Even in the case of these single crystals, the symmetry of

the organic crystal is much lower than that of inorganic crystals.

On the other hand, large single crystals of polymeric solids are not commercially available. Efforts to grow them have not as yet succeeded. Pohl (45) in a recent review discusses the handicaps associated with the molecular (both monomeric and polymeric) solids. It appears very unlikely that polymeric single crystals will ever be achieved to any degree of size due to the fact that the net free energy of crystallization per orderable unit is much smaller for a polymer than for most crystalline inorganic solids.

Hence, polymers at best are available as polycrystalline, aperiodic solids with low short-range order. Since the theoretical model of conduction assumes single crystalline material, it is seen that polymers must either be treated in an approximate, or at best semiempirical fashion. If one is to experimentally study polymeric solids, it appears that it will be necessary to increase the long range order in the polycrystalline solid.

High Pressure Technique

One way to increase the degree of order in a polycrystalline material is by the application of extreme pressure to the sample. Molecules or complexes which have a tendency to crystallize in a layered structure either in a series of planes or in a herringbone structure, may be greatly influenced through pressure application. In each case, the π -orbital overlap increases rapidly with pressure. Hence, by

applying high pressure technique, a very dense highly compacted and sintered pellet, a "pseudo single crystal," with longer range ordering present is achieved.

High pressure techniques were pioneered by P. W. Bridgman. (A collection of Bridgman's published works may be found in reference 88.) Drickamer and the Illinois Group (34, 35, 89-93), using Bridgman's technique have advanced pressure studies on materials up to ~ 600 kbar. In general, they find the resistivity of organic materials to decrease rapidly with pressure up to ~ 150 kbar, where the tendency reverses. As the pressure is released, the resistivity curve does not exhibit the initial behavior. They attribute this phenomena to the occurrence of irreversible chemical changes at the higher pressure. Recently, they found (93) these irreversible changes could be overcome if the sample were kept at liquid N_2 temperatures.

Akamatsu and Inokuchi (94), Eley and coworkers (95, 96), and Pohl and the Princeton group (10-22) were the first to examine organic semiconductors at high pressures. Prior to the Princeton group's efforts, it had been thought that pressure application to a polycrystalline organic solid would, at best, reduce the number of voids via compaction. However, Pohl and coworkers found the conductivity of polymeric semiconductors to be highly dependent in a reversible manner upon the pressure applied. In fact, certain polymers (PAQR's) exhibited an increase of more than 100 fold in conductivity in a pressure range where metals exhibit only a two fold change. Pohl,

Rembaum, and Henry (16) developed a semiempirical model to explain the pressure effect, based on absolute rate reaction theory. It will be discussed shortly.

Other investigators who are studying high pressure effects on organic solids include Eyring and coworkers (36, 37), Labes and coworkers (29, 30), and Bradley, et.al. (97). In all cases, the conductivity of organic solids is reported to radically change with the application of high pressure. Gutmann and Lyons adequately review these effects (52).

Hopping Model

Since we have seen that polymeric solids are polycrystalline, and as such must be treated in an approximate method as far as the theory is concerned, the question arises as to how carriers are transported intermolecularly.

As a rule, the band theory of solids is not applicable, since the potential is non periodic. If the solid were periodic throughout the bulk of the material, the band theory could be applied. In some cases however, polymeric semiconductors are treated as band type solids (98), and often the band theory is applied to molecular crystals to make order-of-magnitude calculations and predictions of the mobility of charge carriers in such crystals.

Ordinarily, the charge carriers in organic solids must overcome a very high energy barrier between the molecule to molecule gap.

Hence, the carrier is normally assumed to quantum mechanically "tunnel" or "hop" the barrier. Tunneling has been invoked by several investigators to explain how carriers are transported in a typical molecular crystal (96, 99, 100). To apply the tunneling model, one usually requires at least a high degree of local order, such that a region of periodicity in the potential may be achieved. As such, several molecules interacting split the energy level of the associated π -orbital into bands rather than definite energy levels. This can result in a lowering of the expected quantum mechanical barrier and increase the probability of transition of the carrier.

When one treats the interaction between adjacent molecules only, such that the interaction is essentially a 2 body type, the transfer of carriers is usually called hopping. However, quite frequently, hopping and tunneling are equated.

Pohl, Rembaum, and Henry (16) and Pohl and Opp (17), in a study of pressure effects on the conductivity and mobility of PAQR polymers developed a hopping model, to account for the observations, which is based on the transition rate theory. They postulated that hopping or tunneling depends upon the π -orbital overlap as seen in terms of an effective "area of contact" for the activated state. The pressure increment required to produce a given increment in effective area of contact was assumed proportional to the effective area of contact, i. e., $dP/dA \propto A$. This led to the development of a semiempirical relation for the dependency of the conductivity upon pressure and temperature:

$$\sigma(P, T) = \sigma_0 \exp(-E_a'/kT) \exp(b''P^{1/2}/k) \quad (15)$$

$$\text{where: } E_a' = E_a - b_0 P^{1/2} \quad (16)$$

with b_0 and b'' being appropriate constants. For zero pressure,

Eq (15) becomes:

$$\sigma(O, T) = \sigma_0 \exp(-E_a/kT)$$

as expected [cf. Eq (13), this chapter]. Hence:

$$\sigma(P, T) = \sigma(O, T) \exp \left[\frac{P^{1/2}}{k} (b'' + b_0/T) \right]. \quad (17)$$

Taking the log of Eq (17) results in:

$$\ln \left[\frac{\sigma(P, T)}{\sigma(O, T)} \right] = \frac{P^{1/2}}{k} (b'' + b_0/T). \quad (18)$$

At constant temperature, a log plot of σ versus $P^{1/2}$ then yields a straight line. As T is varied, a family of straight lines results.

Rosen and Pohl (39) further related the dependency of conductivity to variations in applied electrical fields. Assuming a random distribution of highly conjugated segments of polymers in a macromolecular solid, they obtained a relation for the carrier density which was dependent upon the "molecular length" and the applied \vec{E} -field. By comparing the carrier density n , at a given \vec{E} -field with the density at \approx zero field, they obtained:

$$\frac{n(\vec{E}, T)}{n(O, T)} = \frac{2kT}{|e| \mathcal{E} L} \left[\exp (|e| \mathcal{E} L/2kT) - 1 \right], \quad (19)$$

where L is the average molecular length, and \mathcal{E} is the average \vec{E} -field across the molecule.

Now Eq (19) may be introduced into Eq (15) to give:

$$\sigma(E, P, T) = \sigma_0 \exp \left[-E_a / kT \right] \exp \left[\frac{P^{1/2}}{kT} (b''_T + b_0) \right] \times \left[\frac{2kT}{|e| L \mathcal{E}} \left(\exp \left[\frac{e \mathcal{E} L}{2kT} \right] - 1 \right) \right]. \quad (20)$$

If one holds pressure and temperature constant, then

$$\sigma(E) = C \frac{V}{a} \left(\exp \left[\frac{V}{a} \right] - 1 \right), \quad (21)$$

where C is a constant, V is the potential applied across a sample of thickness x , and $a (= 2kTx / |e| L)$ is a constant for a given sample.

Thus by comparing the conductivity at different fields to the conductivity at \approx zero field, one obtains:

$$\frac{\sigma(\vec{E})}{\sigma(\vec{E} \approx 0)} = \frac{a}{V} \left(\exp \left[\frac{V}{a} \right] - 1 \right). \quad (22)$$

Hence, by examining the \vec{E} -field dependence of the conductivity, then, one may obtain an idea of the average molecular length of the polymer.

Carrier Sources

Pohl (45) has recently reviewed the energetics associated with the production of carriers, as to their origin, mobility, the effects of impurity and morphology upon the conductivity, and the interactions of the various electronic ground and excited states with electric fields. (This was briefly discussed in Chapter I.) He also discusses the effect of conjugation on the electrical properties. The reader is referred to this review and to Gutmann and Lyons (52), Chapter 6 for further discussion of the electronic behavior of macromolecular solids.

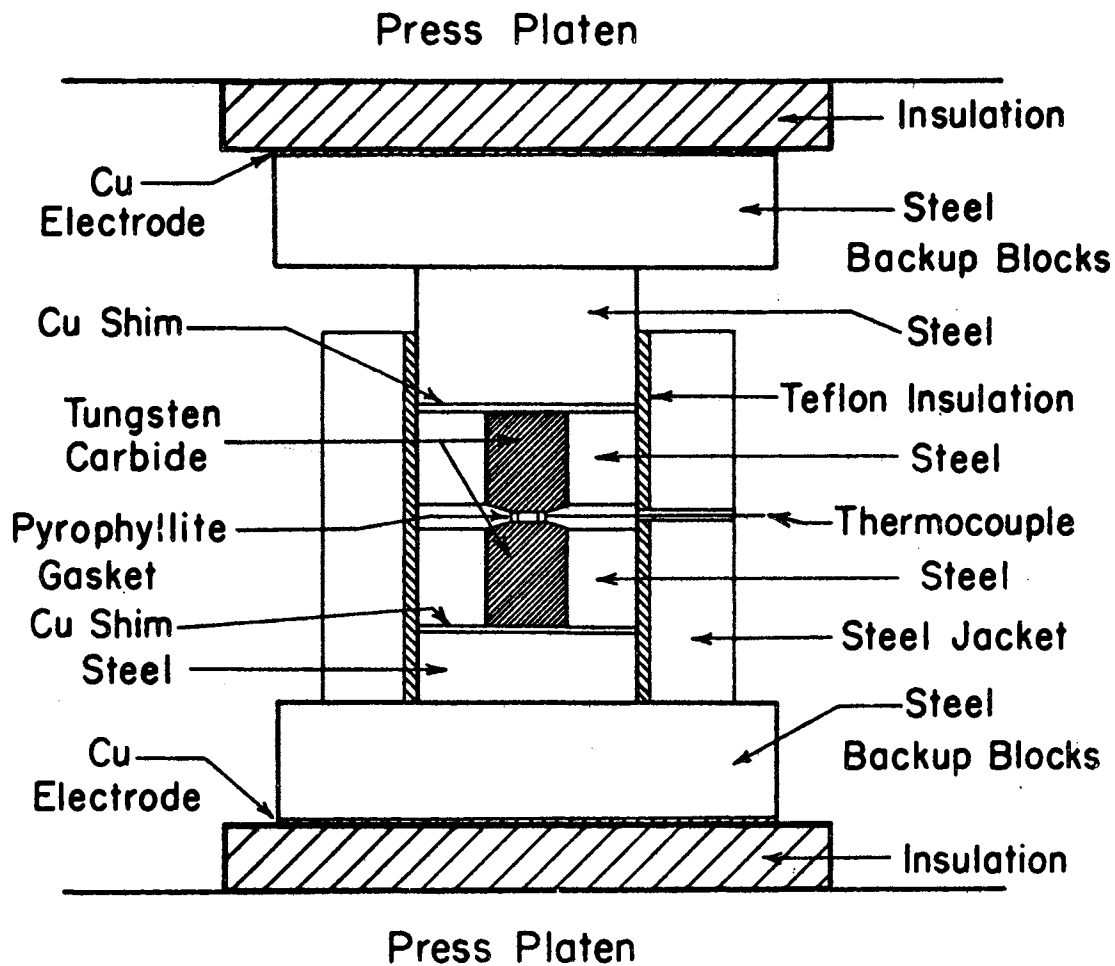
Statement of the Problem

The first phase of this investigation deals with a study of newly synthesized organic polymers. The polymers are examined for electronic semiconducting behavior, and the effects of pressure and electric fields on the conductivity as well as the effect of varying the acene and anhydride system is studied. The polymers are classified as organic semiconductors if they satisfy the criterion listed in Chapter I.

Experimental Apparatus and Procedure

In order to study the electrical properties of polycrystalline samples, it is necessary to either resort to high pressure techniques, and thus, eliminate voids in the sample, or to high frequency A.C. measurements. This section discusses D.C. measurements under high pressures, while A.C. measurements are discussed in Chapter V.

Piezoresistance measurements were made on 25 samples in a Bridgman opposed-anvil high pressure cell. The specific cell resistance was on the order of 10^{14} ohm. It is shown in cross section in Figure 1. Pressures up to 32 kbar were employed with this system with the aid of a 50 ton Model SB230 C and a 12-1/2 ton Model SB 240 Pasadena Hydraulic Inc. press. The presses were calibrated with the aid of a Wheatstone bridge composed of 4 strain gages mounted on a



Sample Retaining Ring (Pyrophyllite)

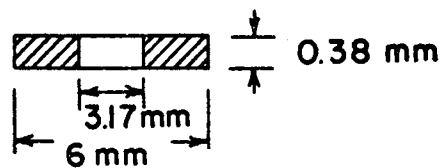


Figure 1. High Pressure Resistivity Cell

steel bar, such that two of the gages were under compression and two under tension. The calibration curves for the presses (calibrated to the highest pressure in each case) are shown in Figures 2 and 3.

Before starting a high pressure high temperature study, the sample is premolded in a one-eighth inch or a one-fourth inch diameter die under a pressure of up to 8 kbar. The resulting compacted pellet (whose thickness should be ~ 0.010 inch to 0.015 inch) is first weighed, is inserted into the pyrophyllite retaining ring (0.015 inch thick), and is then placed in the high pressure cell as shown in Figure 1.

The samples are first subjected to the highest pressure and temperature of each experiment. The pressure is then released and measurements are made as the pressure is increasing. Then the procedure is repeated at the next lower temperature. The sample temperature is determined by a copper-constantan thermocouple in close proximity to the sample.

Since organic solids exhibit electric field dependence [Eq (15); also cf. reference (39)] it is necessary that the field be held constant during the experimentation. To achieve this, a Heathkit 1 P-32 D.C. power supply is used as a constant voltage source of 5 volts together with a Keithley 610 B electrometer as an ammeter and a Simpson 260 meter as a voltmeter. Knowing the voltage drop across the Keithley and the sample, as well as the current through the sample, the resistance is determined. Sample area and thickness are determined at the

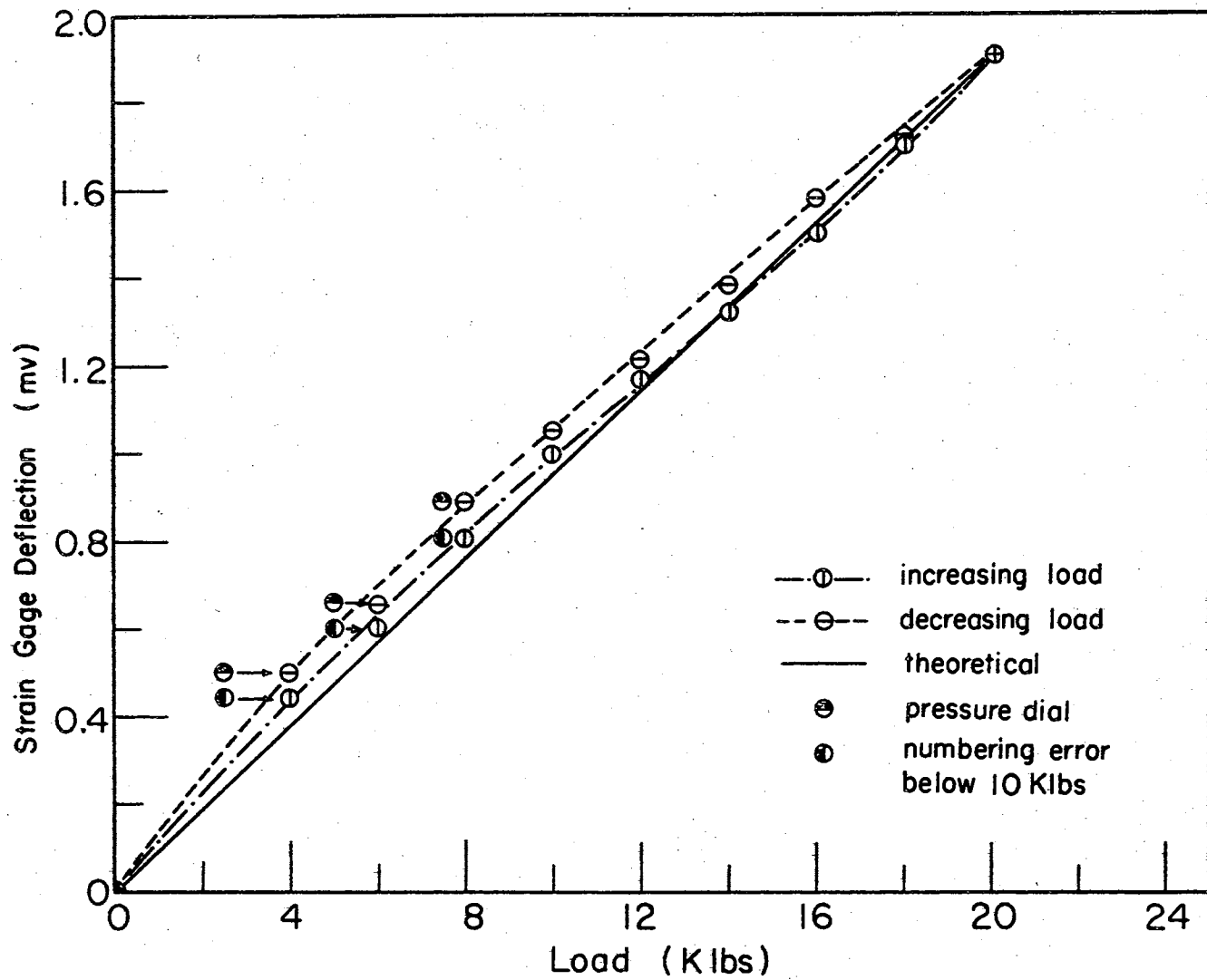


Figure 2. Calibration Curve for 50 Ton Press

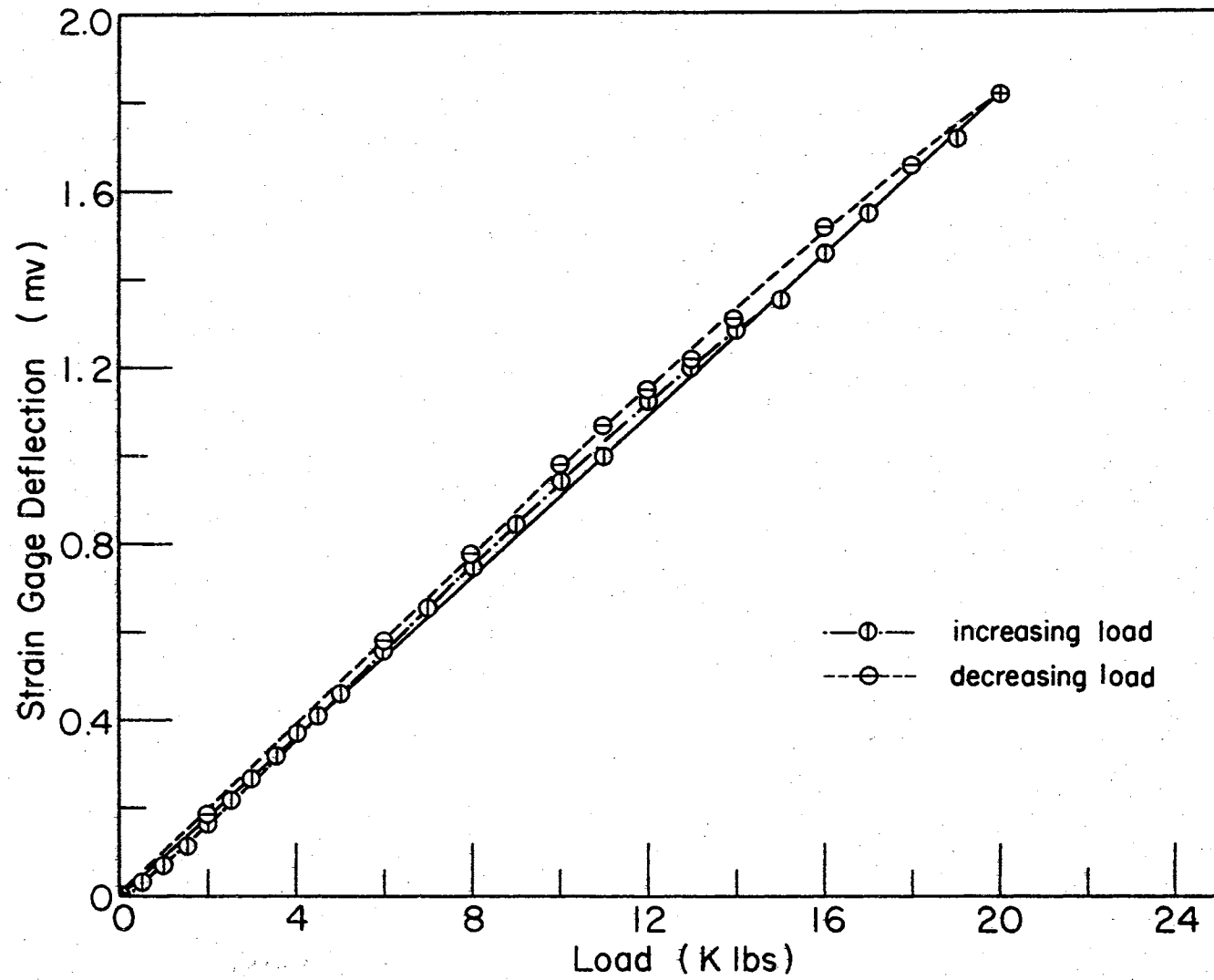


Figure 3. Calibration Curve for 12-1/2 Ton Press

conclusion of each experiment, from which the resistivity can then be determined, according to the relation:

$$\rho = \frac{RA}{x} , \quad (23)$$

where R is the resistance in ohms, A is the sample cross section in cm^2 , and x is the thickness in cm. A and x are measured directly on the sample after compression.

Polymer DP1A, a highly purified resynthesis of an earlier polymer studied by Pohl and coworkers (39) is used as a reference material since it has been extensively studied in our laboratory.

Plots of the resistivity versus the square root of pressure at fixed temperatures are then made [after Pohl (16)] according to Eq (18). A typical result for Polymer DP1A is shown in Figure 4.

By plotting the resistivity obtained against reciprocal temperature at various fixed pressures, a second family of curves result. Again, a typical result for polymer DP1A is given in Figure 5. These lines are plots of the equation given earlier in this chapter,

$$\rho = \rho_0 \exp (E_a/kT).$$

The slope of these lines is thus a measure of the activation energy. It is seen in Figure 5 that the activation energy is pressure dependent as expected (21).

Although the actual energy dependence on pressure for Sample DP1A is not plotted, it will be seen in Table V that it exhibits the expected dependence throughout the range in which it was examined.

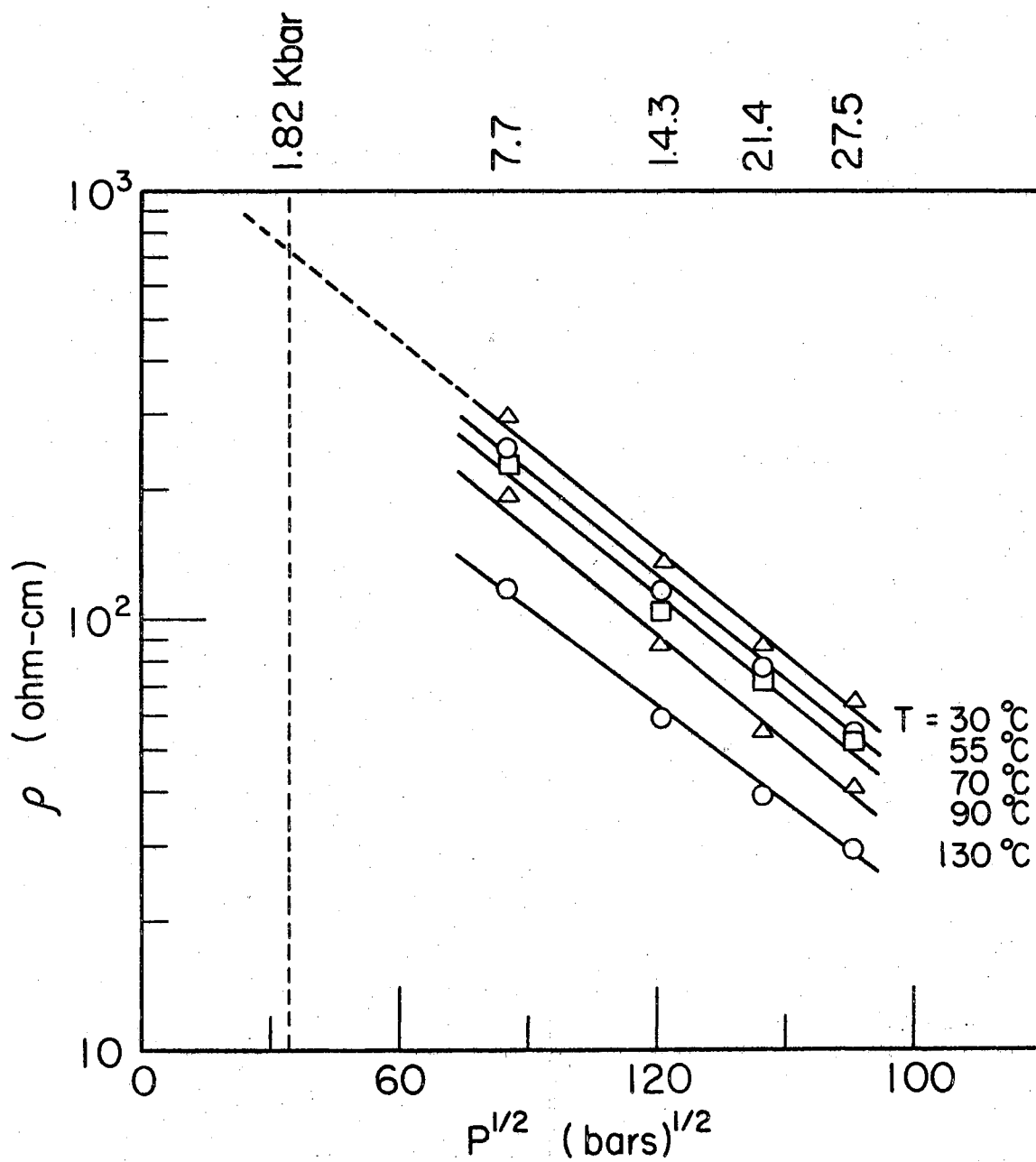


Figure 4. Resistivity-Pressure Curves for Polymer DPIA at Various Temperatures

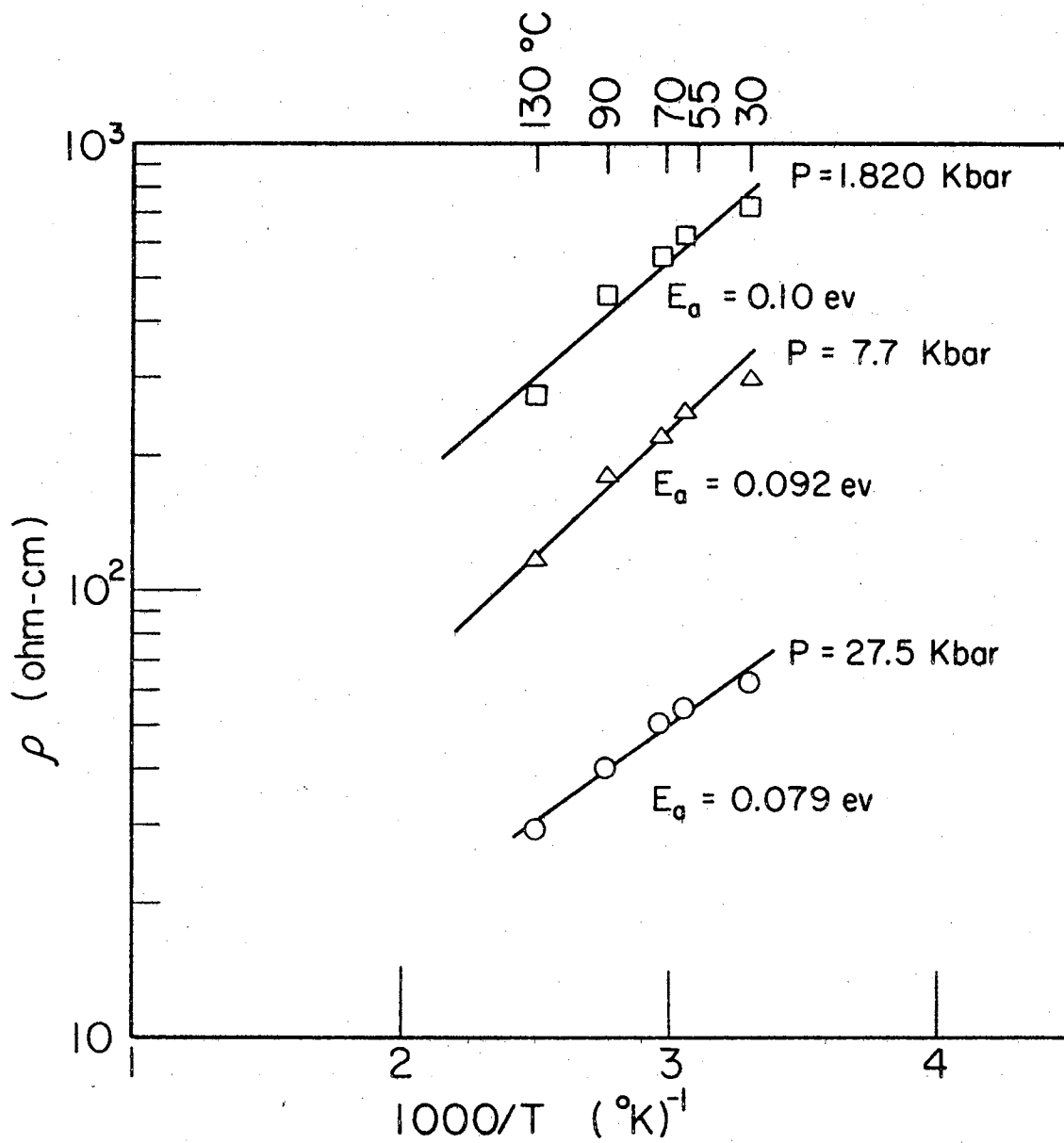


Figure 5. Resistivity-Temperature Curves for Polymer DPIA at Various Pressures

Results and Discussion

PAQR'S

Experiment I. The initial study was performed on 10 PAQR polymers (JM78B, 93B, 77B, 92B, 83A, 83B, 84A, 84B, 85A, and 85B) formed from heterocyclic aromatic acenes (phenanthrene, anthracene, acridene, phenazine, and phenothiazene) and anhydrides (PMA and MTA) to examine the effect on conductivity of the addition of groups which stabilize radical electrons. It has previously been reported by Pohl and coworkers (15-19) that a correlation between conductivity and such factors as unpaired spin concentration and structure of the monomeric acenes and anhydrides exists. This investigation was directed toward the development of materials with as high a conductivity as possible, by (1) adding groups which stabilize radical electrons, and by (2) studying the effect of MTA as opposed to PMA. MTA derivatives of PAQR polymers have not been reported previously.

These polymers, prepared as discussed in Chapter II, were subjected to pressures up to 12 kbar as was outlined in the previous section. The results of the study are summarized in Table III. The value of resistivity at 1.820 kbar (ρ_0) has previously been taken as a standard; thus, for comparison purposes, it is used here.

It is evident from Table III that this approach to increased conductivity in the PAQR's has been successful. The addition to the polymer structure of heterocyclic atoms which can stabilize unpaired

TABLE III

RESISTIVITY AND ACTIVATION ENERGY FOR 10 PAQR POLYMERS (AFTER BEING
SUBJECTED TO 12 KBAR AND 400°K) AT 1.820 KBAR AND 300°K

Acene	MTA			PMA		
	Sample No.	ρ_0 (Ohm-cm)	E_a (eV)	Sample No.	ρ_0 (Ohm-cm)	E_a (eV)
Phenanthrene	JM93B	8.65×10^7	0.337	JM78B	1.72×10^6	0.214
Anthracene	JM92B	1.6×10^6	0.242	JM77B	5.78×10^5	0.246
Acridine	JM83B	4.20×10^4	0.196	JM83A	4.25×10^5	0.253
Phenazine	JM84B	6.65×10^4	0.312	JM84A	2.20×10^5	0.303
Phenothiazine	JM85B	1.0×10^3	0.197	JM85A	1.08×10^4	0.259

electrons leads to enhanced conductivity; and the use of comonomers with multiple anhydride groupings (MTA as opposed to PMA) appears to enhance conductivity still further. This work has been reported by Mason, Pohl, and the author (70).

Experiment II. The same 10 PAQR polymers were re-examined in the same fashion as before, over an extended pressure (to 32 kbar) and temperature (to 450°K) range. Again, the activation energies and resistivities were determined. Standard values of E_a and ρ_0 (taken at 1.820 kbar) are shown in Table IV. By comparing Table IV and Table III, it can be seen that the PMA polymers behave as expected; but the MTA polymers tend to exhibit anomalous behavior. It still is evident that addition of heterocyclic atoms which can stabilize the unpaired spins leads to enhanced conductivity. Also, it is evident that the activation energy has been effected by the extreme pressure. In general, it has been lowered according to Pohl, et. al. (16). [Cf. Eq (16) this chapter.] The activation energy for these polymers at various pressures is shown in Table V.

Experiment III. Due to the anomalous behavior of the MTA polymers, additional work was limited to the PMA series. Nine new PAQR polymers (JM39, 40, 41, 42, 43, 46, 48, 49, and 50) formed from heterocyclic aromatic acenes (thianthrene, xanthene, acridone, phenoxazine, xanthone, dibenzothiophene, 9-thioxanthone, carbazole, and 9-thioxanthene) and PMA were recently synthesized as new members in the series reported in Experiments I and II. In addition,

TABLE IV

RESISTIVITY AND ACTIVATION ENERGY FOR 10 PAQR POLYMERS (AFTER BEING
SUBJECTED TO 32 KBAR AND 450°K) AT 1.820 KBAR AND 300°K

Acene	MTA			PMA		
	Sample No.	ρ_o (Ohm-cm)	E_a (eV)	Sample No.	ρ_o (Ohm-cm)	E_a (eV)
Phenanthrene	JM93B	1.7×10^6	0.211	JM78B	1.1×10^5	0.225
Anthracene	JM92B	2.2×10^7	0.215	JM77B	6.9×10^4	0.263
Acridine	JM83B	3.4×10^4	0.269	JM83A	4.2×10^4	0.235
Phenazine	JM84B	1.1×10^5	0.145	JM84A	3.2×10^4	0.245
Phenothiazine	JM85B	3×10^2	0.15	JM85A	8.4×10^2	0.130

TABLE V

ACTIVATION ENERGIES FOR SEVERAL POLYMERS AT VARIOUS
PRESSURES AS MEASURED FROM 300°K TO 450°K

Sample No.	E_a (eV)				
	P(kbar) 1.82	P(kbar) 7.85	P(kbar) 15.7	P(kbar) 23.5	P(kbar) 31.4
DP1A	0.105	0.092	0.085	0.079	0.060
JM85B	0.155		0.142		0.122
JM85A	0.150		0.115		0.125
JM84B	0.145	0.137	0.167	0.158	0.170
JM77B	0.263	0.252	0.252	0.241	0.267
JM83B	0.269	0.130	0.143	0.120	0.101
JM84A	0.245	0.229			0.258
JM83A	0.235	0.227			0.187
JM93B	0.211	0.177	0.185	0.190	0.189
JM78B	0.225	0.314	0.285		0.265

polymers JM80 and JM82, resyntheses of polymers JM85A and JM85B respectively have been made. They have all been examined at room temperature only, up to 12 kbar. The respective ρ_0 's have been determined, but no activation energies have been obtained.

The resistivity dependency on pressure is shown in Figure 6 for the above eleven polymers together with the data from Experiment I (each polymer being subjected to a maximum of 12 kbar pressure). Data from Experiment II is shown in Figure 7 (each polymer being subjected to a maximum of 32 kbar).

From Figure 6, it appears that the new syntheses of polymers JM85B (now JM82) and JM85A (now JM80) have produced materials with somewhat different resistivities.

It is apparent by now that the conductivity of polymers may be affected by either adding heterocyclic atoms or groups which stabilize the unpaired spins, or by varying the multiple anhydride groupings of the comonomers. Figure 6 shows evidence of some six orders of magnitude change in resistivity by such variations.

There has been speculation that polymers such as the polyacene-quinones are, in fact, good conductors within the individual molecules, and that the resistance observed on the macroscopic scale is the result of the many barriers to conductivity between the molecular chains. If this is the case, improvements in macroscopic conductivity must be the result of improvements in intermolecular interactions which lower the conduction barriers, rather than improvements in the

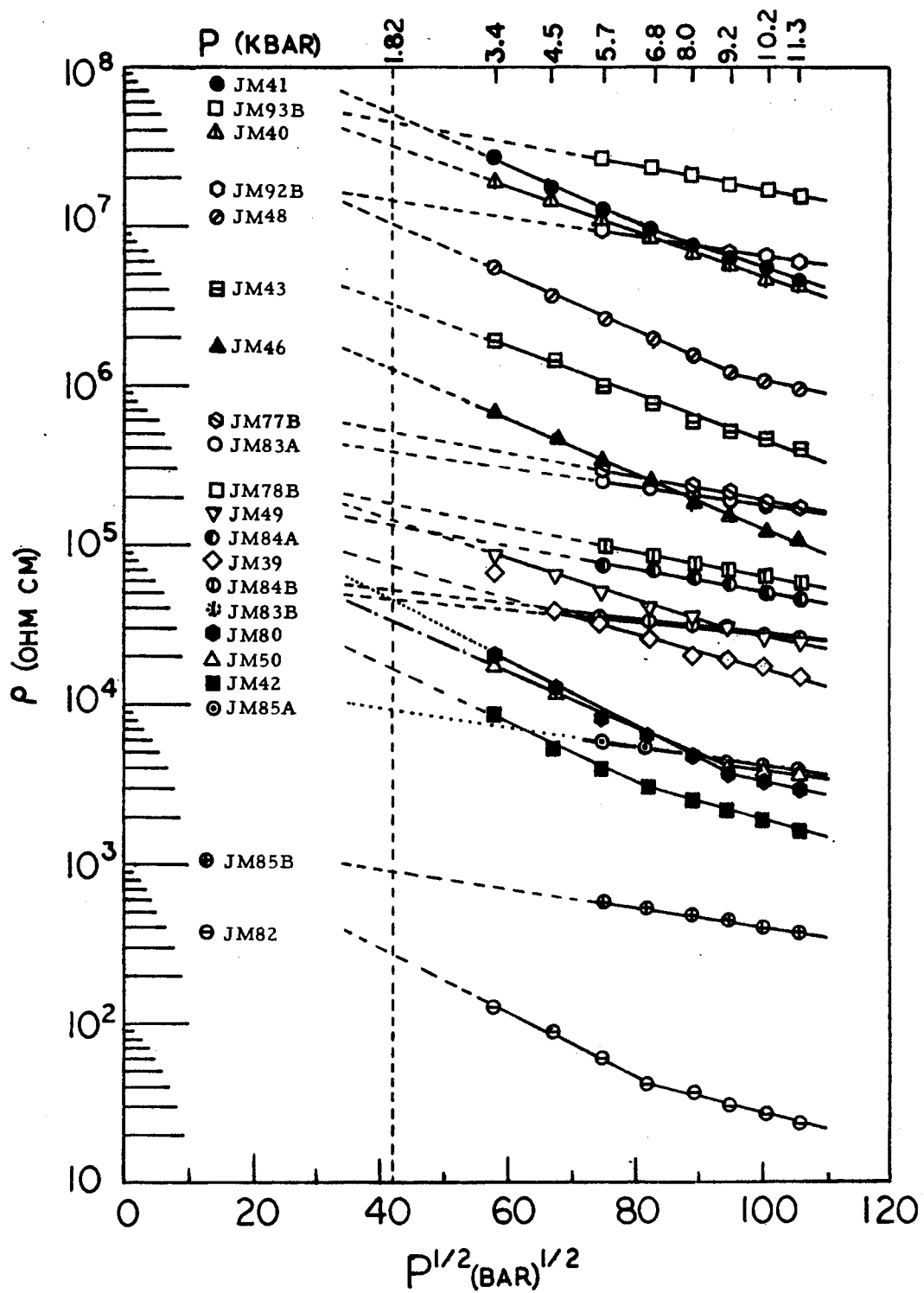


Figure 6. Resistivity-Pressure Curves for Several PAQR Polymers (Experiments I and III)

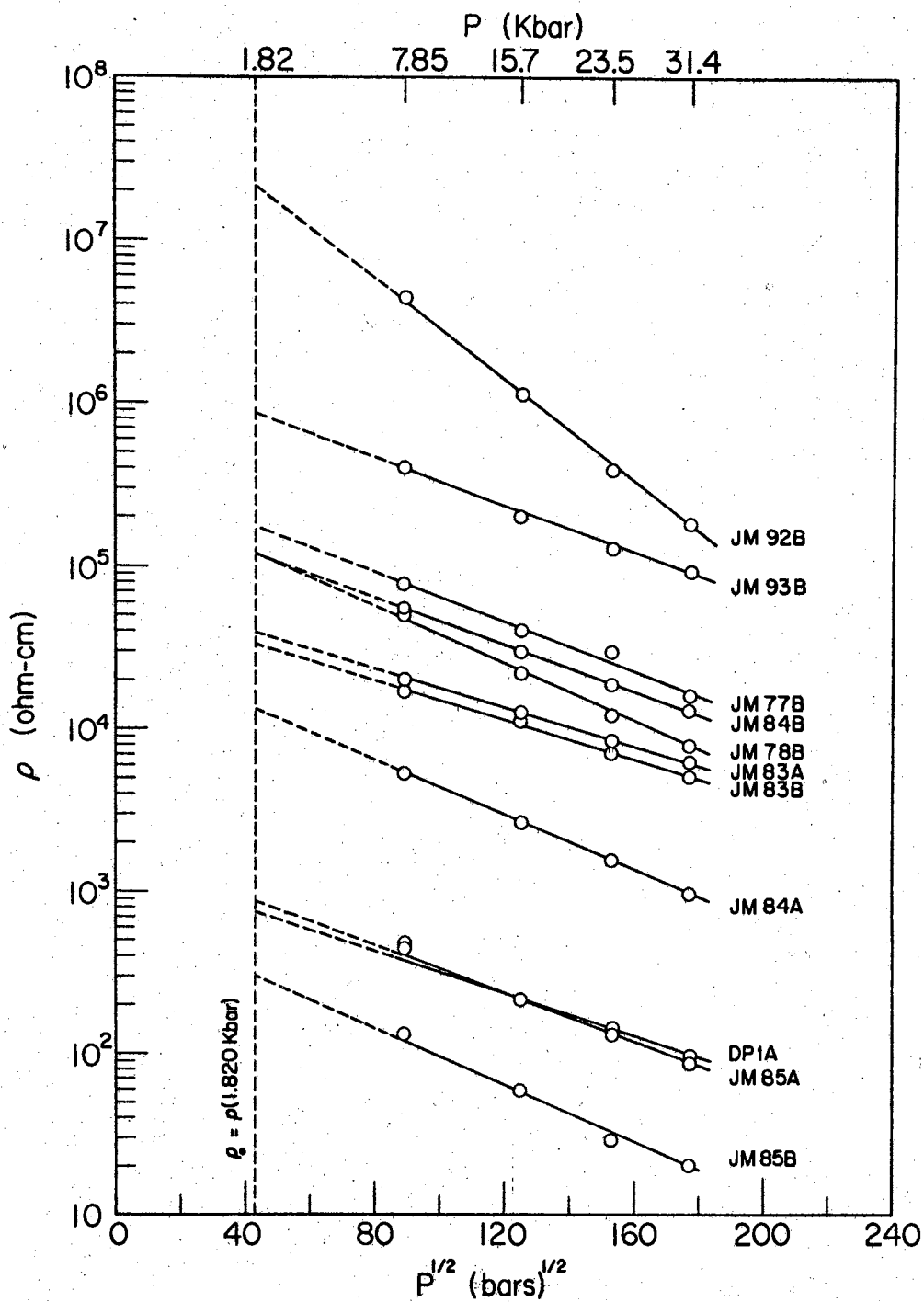


Figure 7. Resistivity-Pressure Curves for Several PAQR Polymers (Experiment II)

conductivity of the molecular structure itself. The results with the heterocyclic polymers tend to support this hypothesis. The polymers appear to have high concentrations of unpaired spins, as discussed in the next chapter, and the spin concentrations correlate well with conductivity. A high number of unpaired electrons, which reside mainly on specific centers in the polymer structure--exactly the situation which seems to pertain in the heterocyclic polymers--would be expected to enhance the interactions between molecules, and lead to reduction of the intermolecular conduction barriers.

Before definite conclusions can be put forth as to the mechanism responsible for the increased macroscopic conductivity in the series studied, it will be necessary to investigate the last 9 polymers at elevated temperature and pressure; and to relate the change in conductivity to the microscopic molecular system in some way (such as to an increase in π -orbital overlap).

Cu-Coordination Polymers

Piezoresistance measurements of three Cu-coordination polymers (SK1A, SK2A, and SK3A) were made according to the method discussed earlier, at pressures up to 14 kbar. The resistivity was observed to increase upon either recycling the pressure, or allowing the sample to remain at a fixed temperature and pressure for extended time.

Hysteresis Effects. Initial evidence of this hysteresis effect

in the Cu-coordination polymers was reported by Hartman and Kanda in 1965 (122). Further investigations have been reported by Hartman, Kanda, and Pohl (76). Figure 8 shows a typical resistivity versus temperature curve for SK3A; curve (a) corresponding to the initial set of data with maximum temperature 75°C . The pressure was maintained constant at 14 kbar. From curve (a), the activation energy is found to be 0.35 eV.

After cooling back to room temperature, the specimen was heated to 100°C with curve (b) resulting. Since curves (a) and (b) differ only slightly in slope, the activation energies appear to be nearly the same. However, the absolute values of resistivity has approximately doubled. Typical resistivity-pressure curves for SK3A are shown in Figures 9 and 10. It can be seen that the pressure dependence is quite different for the 75°C maximum temperature sample and the 100°C one.

Data on SK1A is shown in Figure 11. The sample is kept under a constant pressure of 14 kbar. At about 80°C , the resistivity begins to increase (as indicated by arrows \uparrow in Figure 11), and as the sample is left at 100°C for one week, the resistivity increases by about a factor of 7. As the sample is allowed to cool, a considerable difference in slope is noted. This would be measured as a change in activation energy. It is significant, however, that as the sample approaches room temperature again, the slope begins to match the initial slope.

Sample SK2A exhibited similar behavior, but in general its

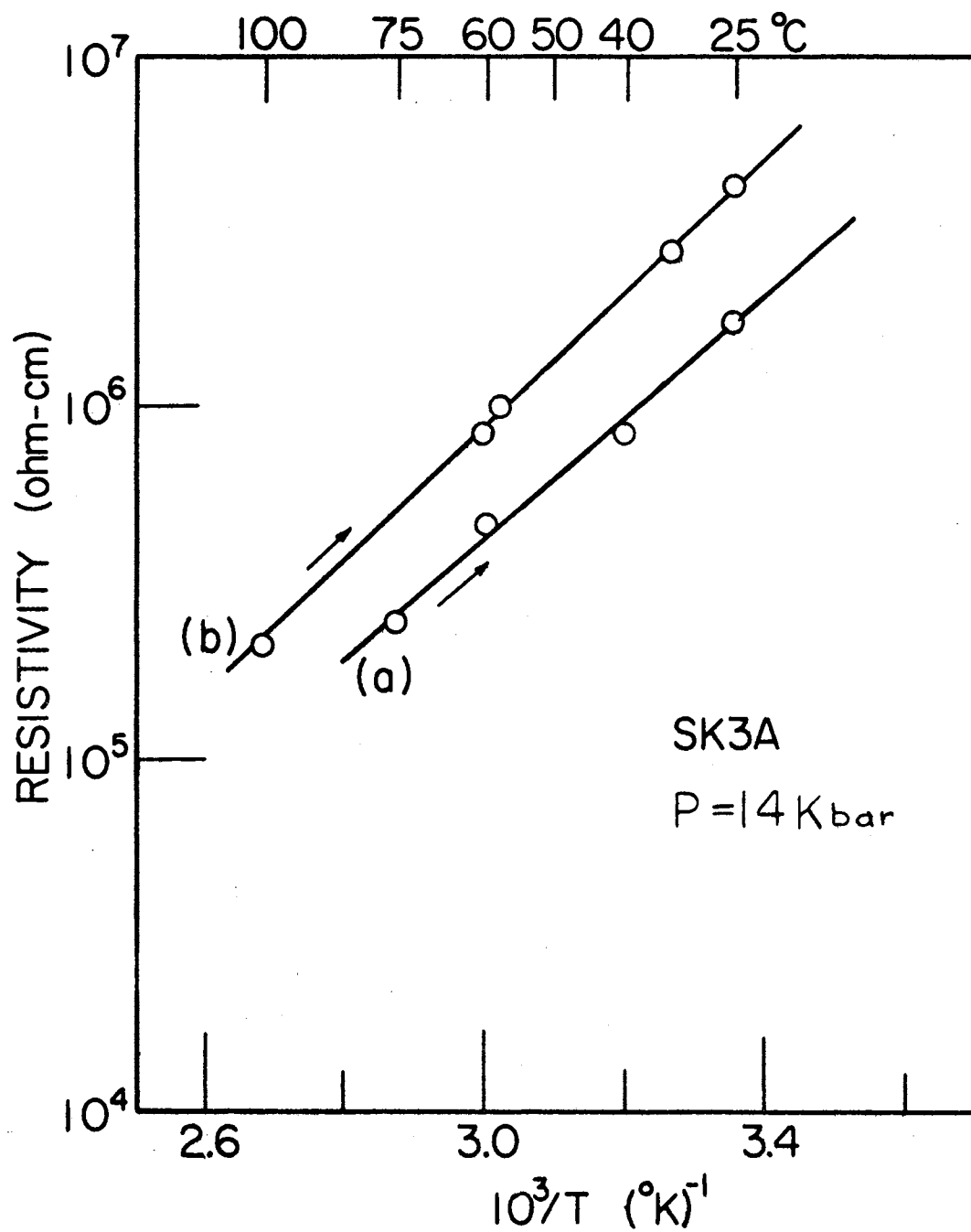


Figure 8. Resistivity-Temperature Curves for Polymer SK3A:
(a) $T_{\max} = 75^{\circ}\text{C}$; and (b) $T_{\max} = 100^{\circ}\text{C}$

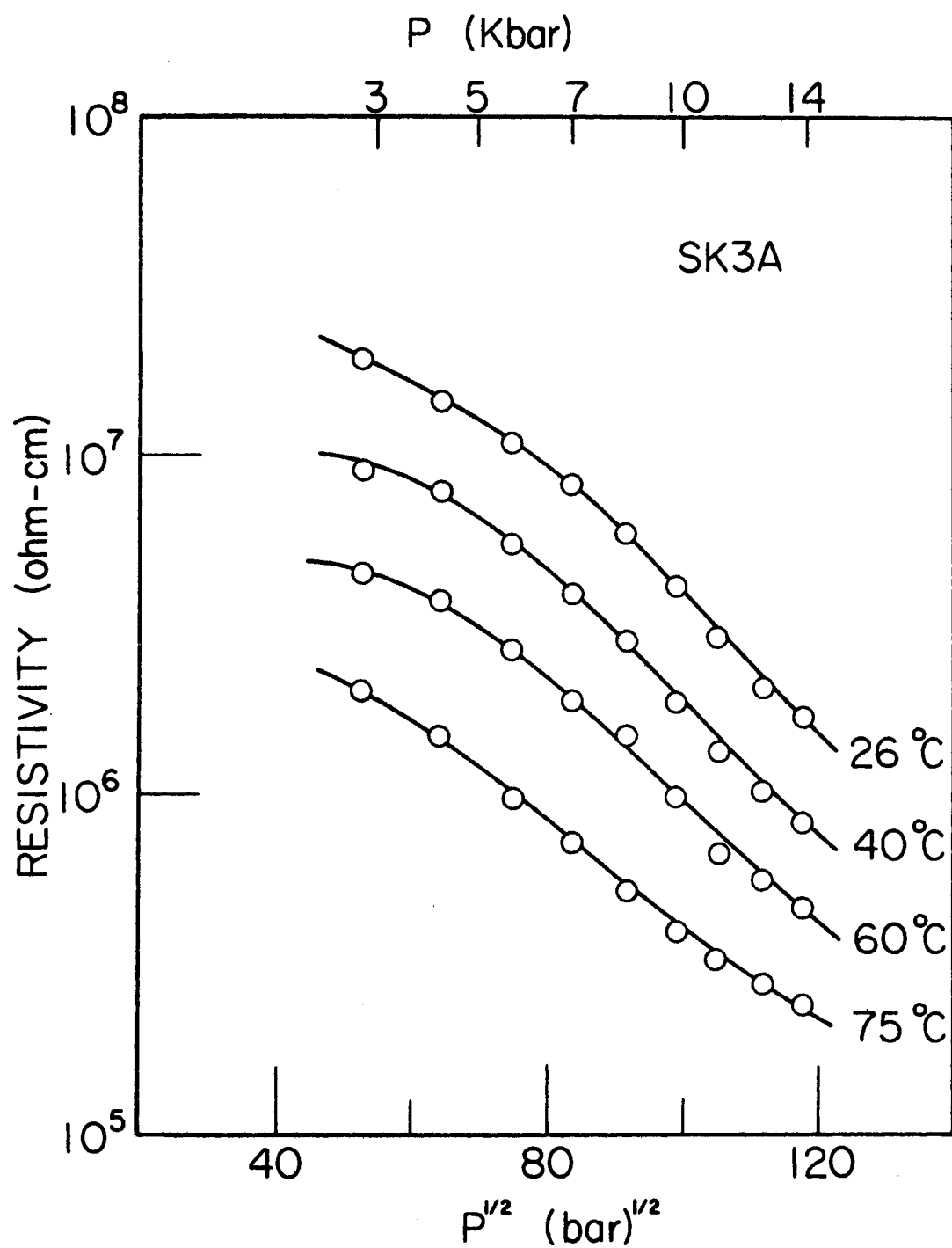


Figure 9. Resistivity-Pressure Curve for Polymer SK3A
($T_{\text{max}} = 75^\circ\text{C}$)

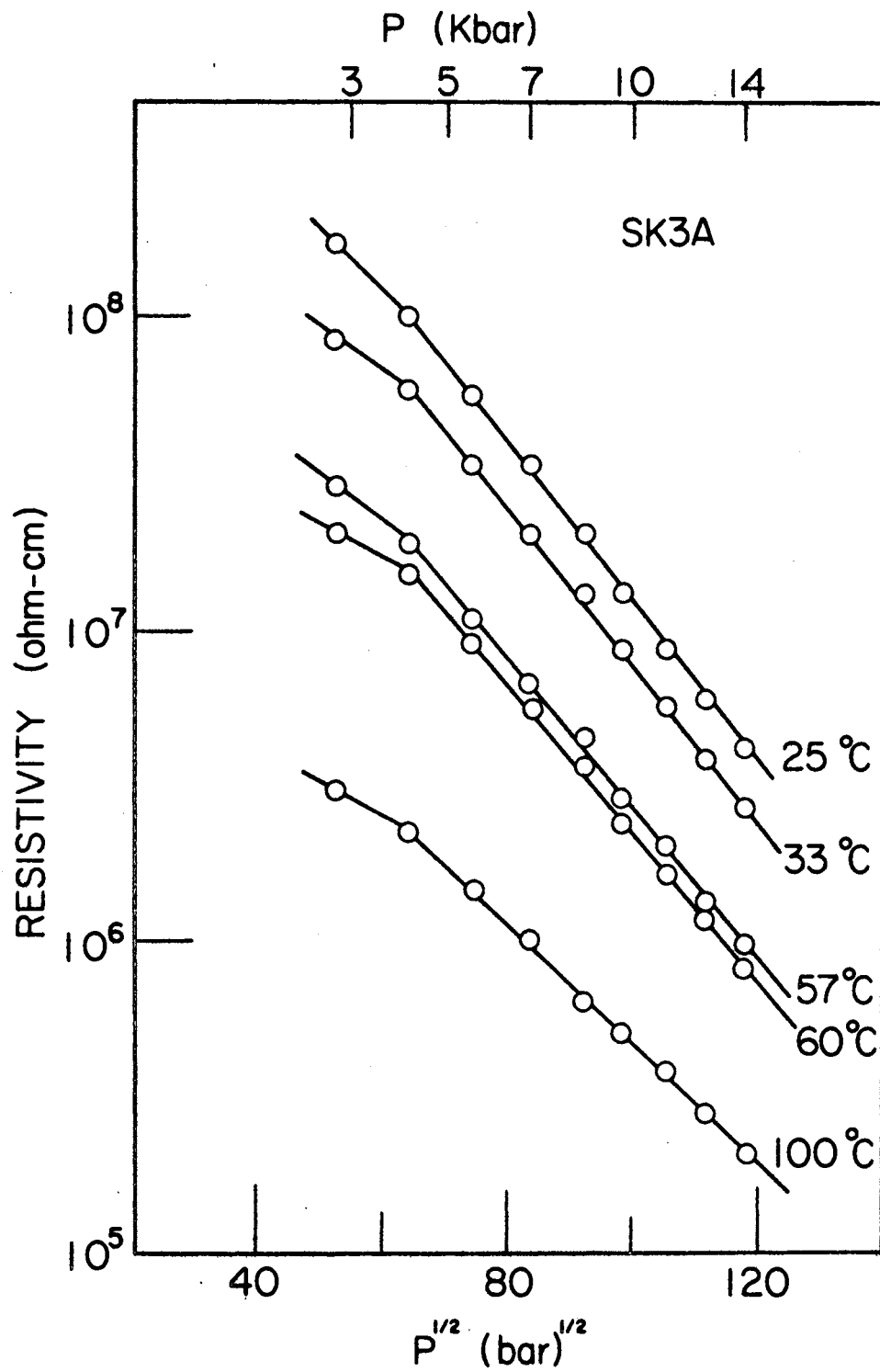


Figure 10. Resistivity-Pressure Curve for Polymer SK3A
($T_{\max} = 100^{\circ}\text{C}$)

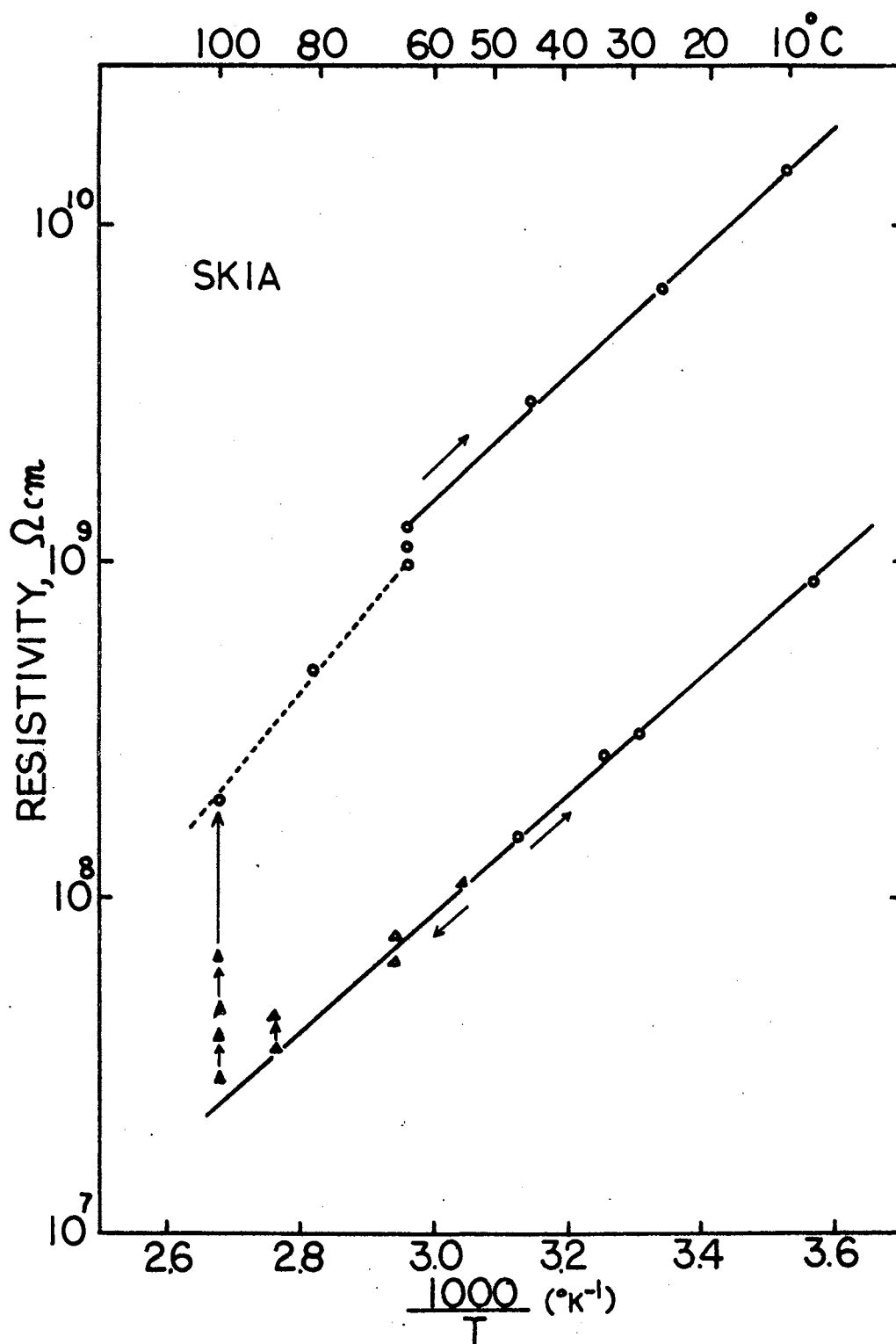


Figure 11. Resistivity-Pressure Curve for Polymer SK1A

resistance was too high to obtain conclusive results. It exhibited resistance values in excess of 10^{11} ohms.

In view of the change in resistivity exhibited by Figures 8 through 11, it was decided to look at the behavior of the polymers over an extended period of time. This resulted in a "quasi-closed" hysteresis loop being obtained.

A typical hysteresis curve for polymer SK3A is shown in Figure 12. This curve is an idealization of the actual data taken, but no loss of generality has been introduced since the actual data portrayed the same type of behavior.

In obtaining a curve such as that shown in Figure 12, the resistance of the sample was first measured at room temperature (T_1) and a pressure of 14 kbar. This value of resistivity is represented by ρ_1 . The pressure was then released and the sample was heated to higher temperature (T_2). Again the sample pressure was increased to 14 kbar, and the resistance was measured (ρ_2). Two different procedures were then followed.

First, the pressure was held at 14 kbar and the sample was quickly cooled back to room temperature, where the resistance was again measured (ρ_2'). The pressure was then released and the sample was allowed to relax. The resistance which was periodically measured (always at 14 kbar while the temperature was held constant) slowly increased back to its original value (ρ_1).

After returning to point (1), the sample was again heated to T_2 ,

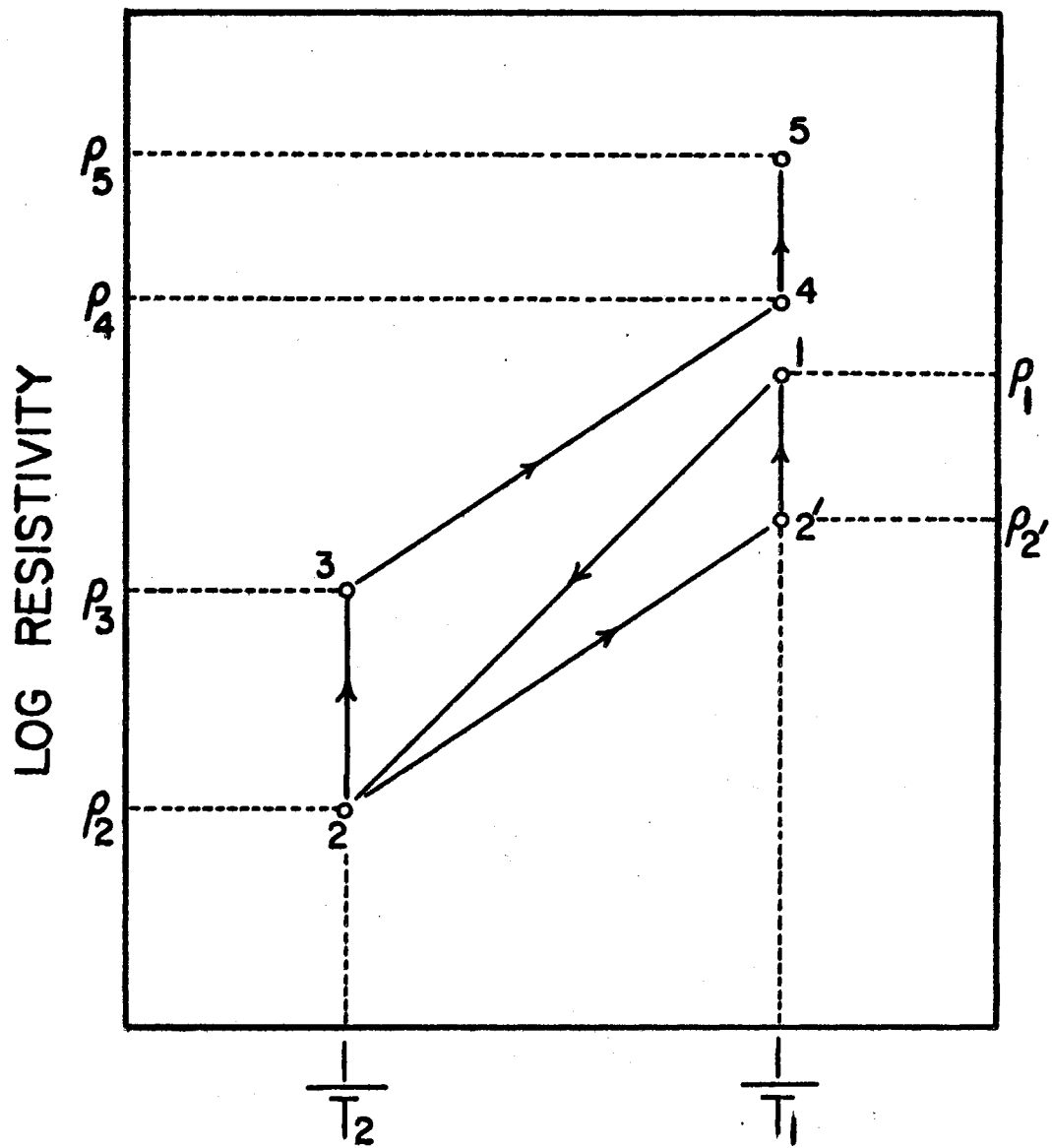


Figure 12. Hysteresis of Piezoresistivity for Polymer SK3A

and point (2) was reproduced. This time, however, the sample was held at 14 kbar and the resistance was periodically measured over a period of several hours. In this manner, point (3) was obtained. Upon cooling to room temperature, the resistivity was measured at 14 kbar as ρ_4 .

In order to convert ρ_4 back to ρ_1 , it was necessary to anneal the sample under zero pressure for several hours. Otherwise, the resistivity tended to creep upward to a value ρ_5 , quite similar to the transition from ρ_2 to ρ_1 .

In this manner, a "quasi-closed" hysteresis loop resulted for the resistivities of the Cu-coordination polymers.

In view of the complex behavior of these polymers, it appears that the conductivity, as measured, is some complicated function of pressure, temperature, and time. Investigations of macromolecular solids frequently yield anomalous results, such as a functional dependence of resistance on pressure recycling (36, 37, 76, 122, 123) and functional dependence of resistance on time as pressure and temperature are held constant (34-37, 72, 76, 77, 124, 125).

There are many processes which may account for such behavior of resistivity. Among them are electrolytic, thermal, and chemical decomposition; phase change; and molecular orientation. Electrolytic decomposition was ruled out as the sample resistance remained constant upon the passing of large amounts of current through the sample for long periods of time. Thermal and chemical decomposition were

also ruled out as it was possible to return the sample to its original resistivity by heating at atmospheric pressure. This then leaves molecular orientation and phase change as prime suspects.

A semiempirical model, such as a coexistence of two phases, with the two phases being reversibly changed back and forth may be invoked to qualitatively explain hysteresis. Since these "phases" may be "true" phases, or "pseudo" phases (i. e., orientation could be considered as a "pseudo" phase), the model may account for either molecular orientation or phase changes.

Consider the solid to be composed of two coexisting forms, these forms may represent different phases or different bonding of the copper ions with the complexes. On the basis of this "two form" solid, the net conductivity will also be dependent upon the concentration of each, since each form may have different conductivities. Functionally writing this dependence of conductivity upon the parameters, one obtains:

$$\sigma = \sigma(T, P, t, f), \quad (24)$$

where T is temperature; P is pressure; t is time; and f represents the relative concentration of the form of the material present.

For a well behaved intrinsic semiconductor, the conductivity was given in Eq (4) as:

$$\sigma = |e| n \mu.$$

With reference to the proposed "two-form" solid, we must choose one of several available empirical forms for the conductivity. The

simplest one is perhaps that of direct additivity, i. e.,

$$\sigma \approx \sigma_1 f_1 + \sigma_2 f_2 \quad (25)$$

where: $\sigma_1 = |e| n_1 \mu_1 ; \quad (26)$

and $\sigma_2 = |e| n_2 \mu_2 . \quad (27)$

Hence, σ may be written as:

$$\sigma \approx |e| [n_1 \mu_1 f_1 + n_2 \mu_2 f_2] . \quad (28)$$

Now according to Eq (24), Eq (28) must show the proper dependence upon the variables P, T, and t.

The normal temperature dependence is due to the carrier concentration dependence which was given in Eq (11) as:

$$n = n_0 \exp (-E_a / kT).$$

This dependence is of course observed; however, there may be another type of T dependence, perhaps through the specific rates of formation of the two forms, f_1 and f_2 , i. e., $f_1 = f_1(T, t)$ and $f_2 = f_2(T, t)$.

The time dependence may be introduced through the rates of formation of f_1 and f_2 . At any instant of time, we assume the rate of formation is given by:

$$\left. \frac{\partial f_1}{\partial t} \right)_{T, P} = k_f f_2 - k_b f_1 , \quad (29)$$

where k_f and k_b represent the forward and backward rate constants. The subscripts, T and P, indicate that temperature and pressure are being held constant, since the rate of formation is more than likely temperature and pressure dependent. Eq (29) may be integrated to

obtain a time dependence by recalling that the fractional amount of concentration must sum to 1, i. e.,

$$f_1 + f_2 = 1. \quad (30)$$

It should be noted however, that Eq (29) is not rigorously true if the two forms of the solid are represented by different bondings. In that case, the linear dependence upon f_1 and f_2 must be replaced by a higher order dependence.

The inclusion of the pressure dependence may be realized from a thermodynamic consideration of the activity coefficients of the two forms of the solid. This dependence appears to indicate an exponential pressure dependence upon the rate constants in Eq (29).

In addition to the above mentioned pressure dependence, it is possible that the mobilities, μ , are also pressure dependent. Pohl, et.al. (16) have seen such a dependence in several polyacene quinone radical polymers.

It can be seen, at least qualitatively, that the semiempirical formulation of the conductivity given by Eq (25) will have the necessary dependence upon the variables involved.

Shearing Effects. To further study the anomalous piezoresistivity of the Cu-coordination polymers, the effect of shearing stress on the conductivity was investigated. It was compared to the behavior of PAQR polymer DPLA, which normally exhibits negligible hysteresis.

Effects of shear on the sample's resistivity were determined as follows. The premolded sample pellet was inserted in a pyrophyllite

retaining ring as previously described. The specimen was placed on a 10 mm diameter Bridgman steel anvil, and a 40 cm long rectangular bar was inserted between the sample and the upper anvil. Lubrication was used between the shearing bar and the upper anvil (126, 127).

Each polymer was sheared through several cycles, each cycle corresponding to 7° of arc, with samples DP1A and SK3A being under 14 kbar uniaxial pressure, and polymer SK1A under 11 kbar uniaxial pressure. The results of shearing stress on the resistivity of each is shown in Figures 13 through 15.

X-ray data on the sheared specimen DP1A (which in the polycrystalline form indicated a high degree of structure as mentioned in Chapter II) indicated no detectable reflections when examined with an X-ray monochromator. The sheared sample was also examined in a rotation camera. There tended to be a diffuse innermost halo indicating some long-range ordering had occurred.

Monochromator data was not obtained on the Cu-coordination polymers; however, rotational camera pictures indicated a slight broadening of the innermost halo upon shearing, as was observed for DP1A.

Thus, X-ray data tends to suggest that after shearing, polymer DP1A is amorphous, with long short-range ordering, and likewise for polymers SK1A and SK3A. However, the shearing effect on resistivity indicates a decrease in ρ for DP1A, while it tends to increase ρ

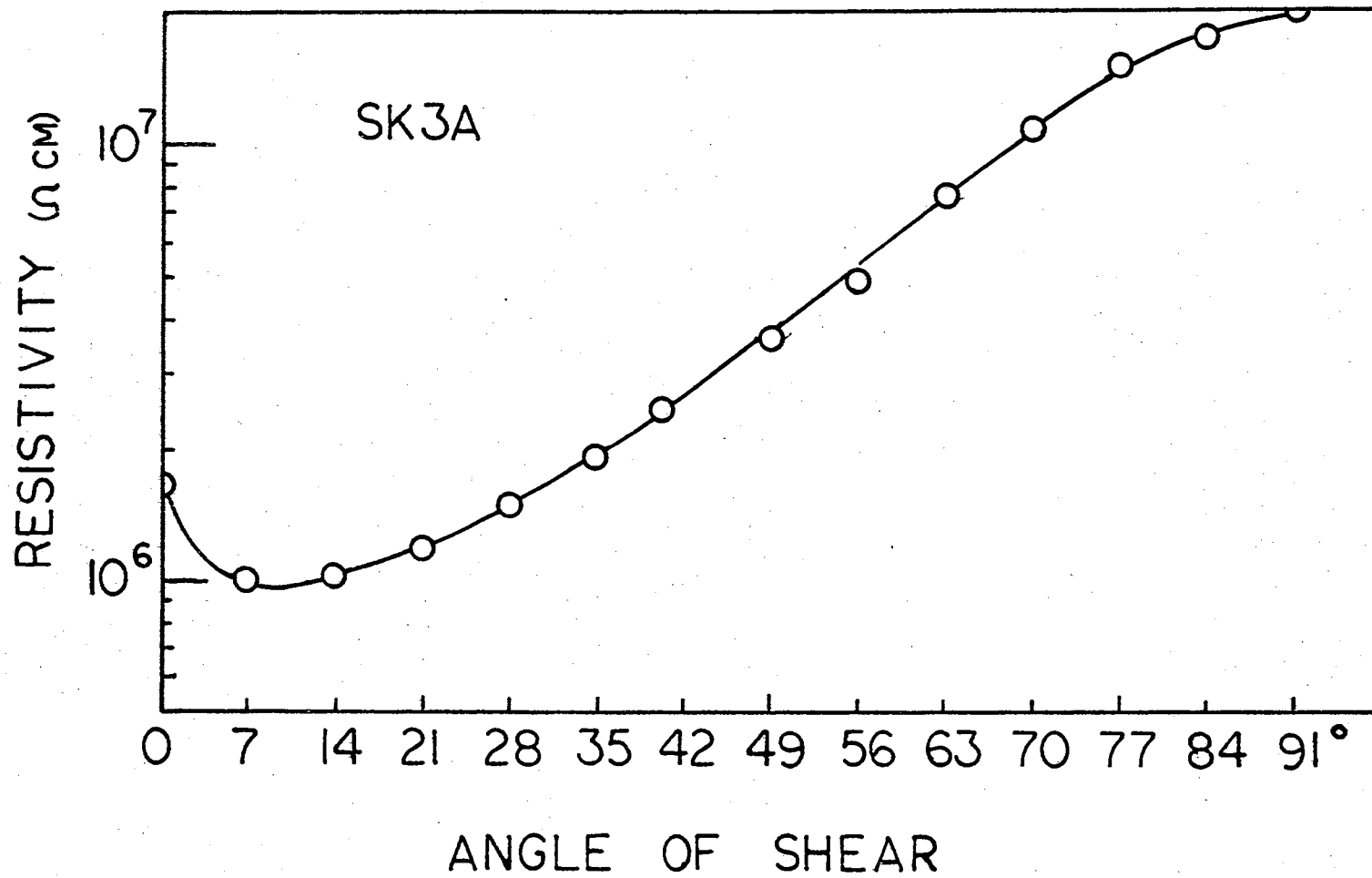


Figure 13. Effect of Shearing Stress on Resistivity of Polymer SK3A

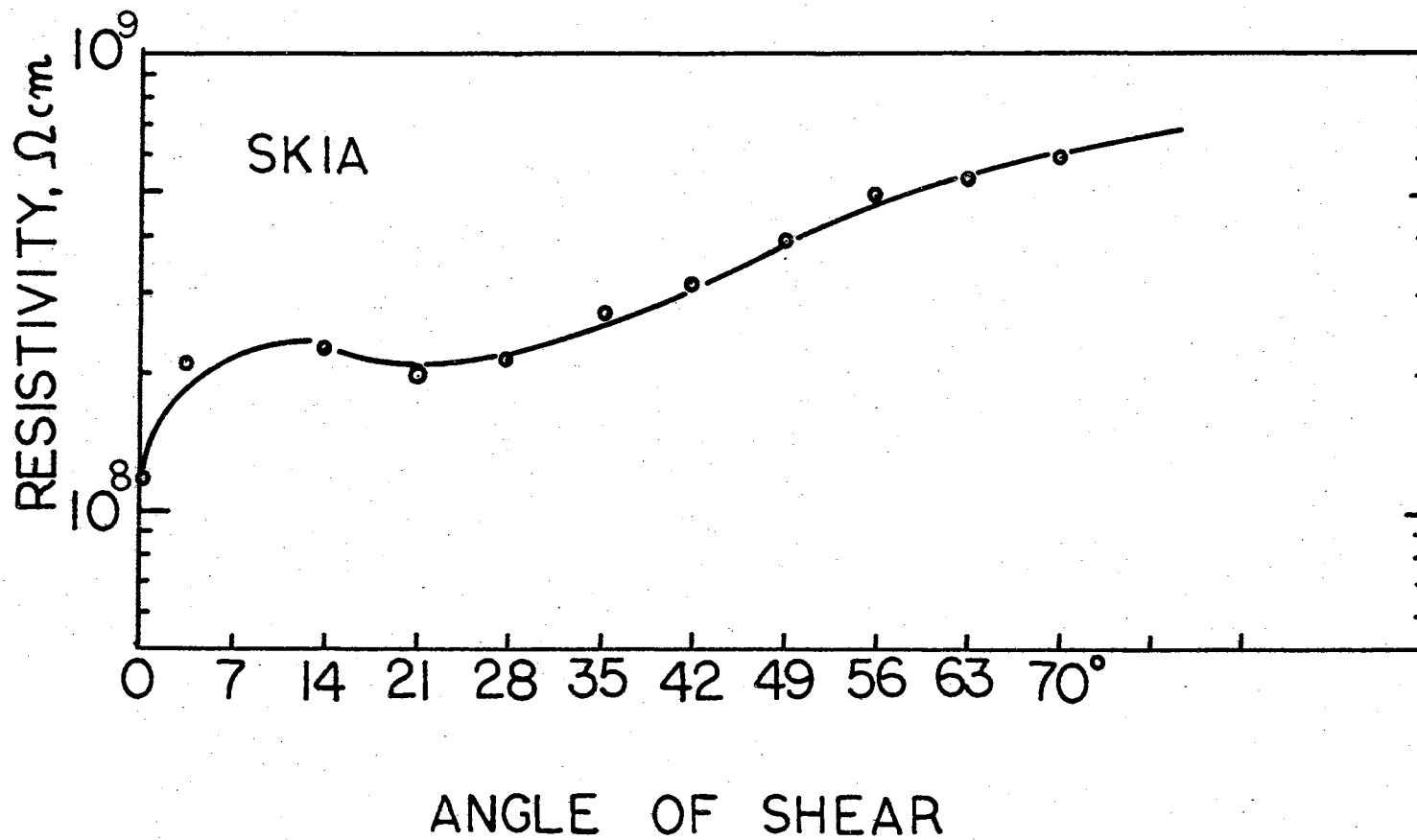


Figure 14. Effect of Shearing Stress on Resistivity of Polymer SK1A

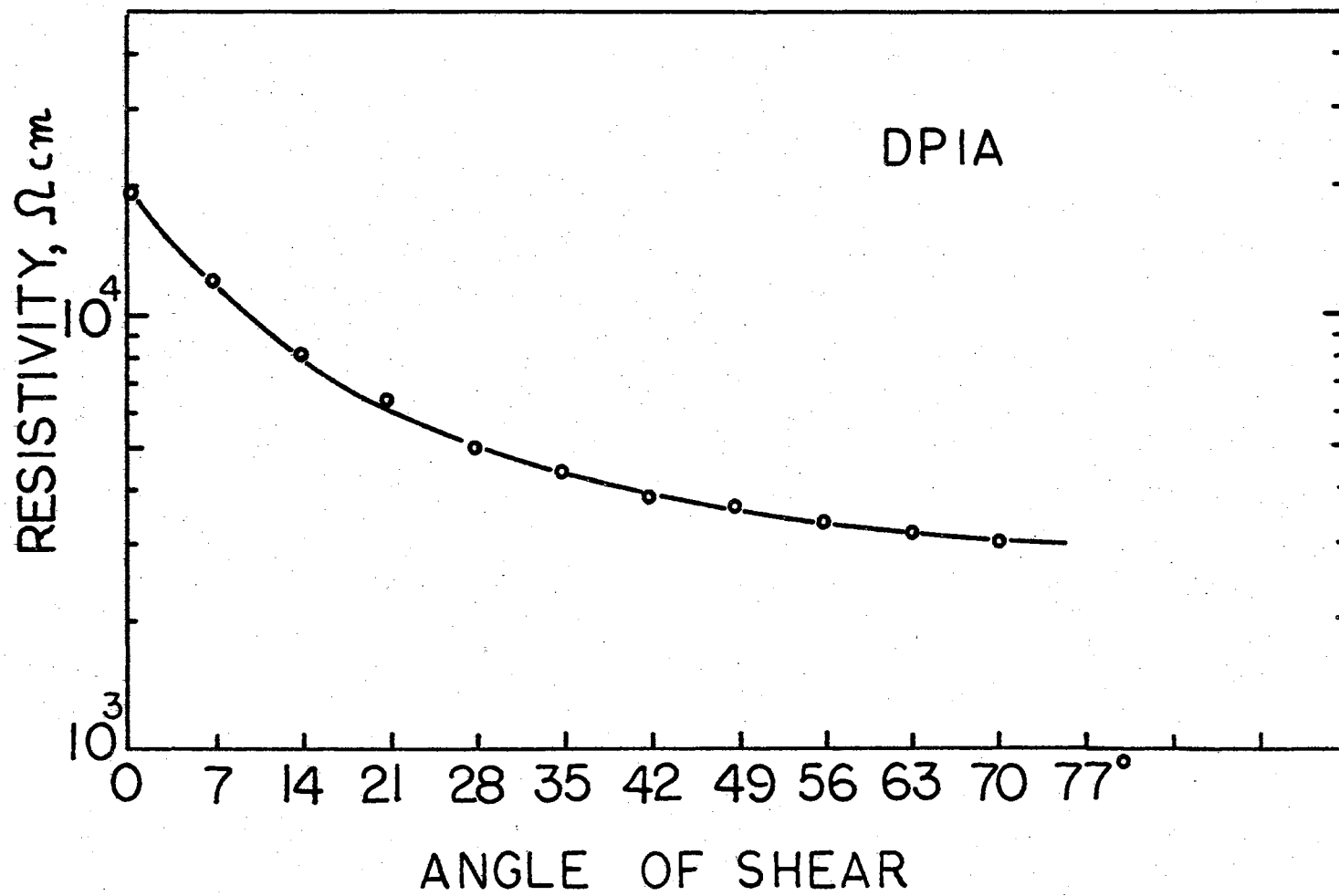


Figure 15. Effect of Shearing Stress on Resistivity of Polymer DPIA

in the two Cu-coordination polymers.

The behavior of the Cu-coordination polymers is not at all clear. If shearing were primarily causing molecular orientation, one would normally expect the resistivity to increase with shearing, due to the reasoning that shearing would tend to align the molecules in a plane perpendicular to the anvil axis. This corresponds to producing an anisotropic specimen which should have lower resistance along the molecular length and high resistance across the molecular layers. Longitudinal and transverse resistivities which were measured agreed with this viewpoint. On the other hand, if shearing primarily causes compaction of the sample, the resistance would probably continue to decrease with shearing.

This would at first, tend to suggest that polymers SK1A and SK3A are being oriented, while sample DP1A is being compacted. The Cu-coordination polymers are quite soft, and it would probably be easy to either orient the molecules or change the bonding with pressure. At this point, it does not appear conclusive that either a change of phase or orientation of the molecules occur when pressure is applied. Additional data on the ESR signal of polymer SK3A (as mentioned in the following chapter) when exposed to pressure, tends to support the "two phase" or change in bonding, however.

Electric Field - Molecular Lengths

As was discussed earlier, a measure of the effective chain length or average molecular length in a macromolecular solid may be

obtained by examining the dependence of conductivity upon the applied \vec{E} -field. [Cf. Eq (22) and reference (39)].

The D. C. conductivity \vec{E} -field dependence was measured on several polymers. The normalized plot of σ / σ_0 for these polymers is shown in Figure 16. The theoretical curves are plots of Eq (22) as calculated with the various molecular lengths as indicated. From Figure 16, it is seen that the average molecular length for the polymers examined varies from 1000 Å to 4000 Å. These values will be seen to compare with the molecular lengths as obtained from temperature ESR data to be discussed in Chapter IV.

In measuring the \vec{E} -field dependence on conductivity, extreme care should be taken to have the anvils flat, and the sample should not be exposed to very high pressure at long time intervals during field measurements. This will tend to cause cupping of the anvils, and the sample thickness, x , then is no longer uniform. This results in anomalous behavior for σ versus \vec{E} -field studies, since there is a mixing of several sample thicknesses, which in turn will cause a distribution of potentials to appear across the molecules. One then has, in effect, a weighted distribution of several equivalent molecular lengths, which gives an invalid result.

Summary

Twenty two newly synthesized organic polymers have been examined and classified as electronic semiconductors. A study of the

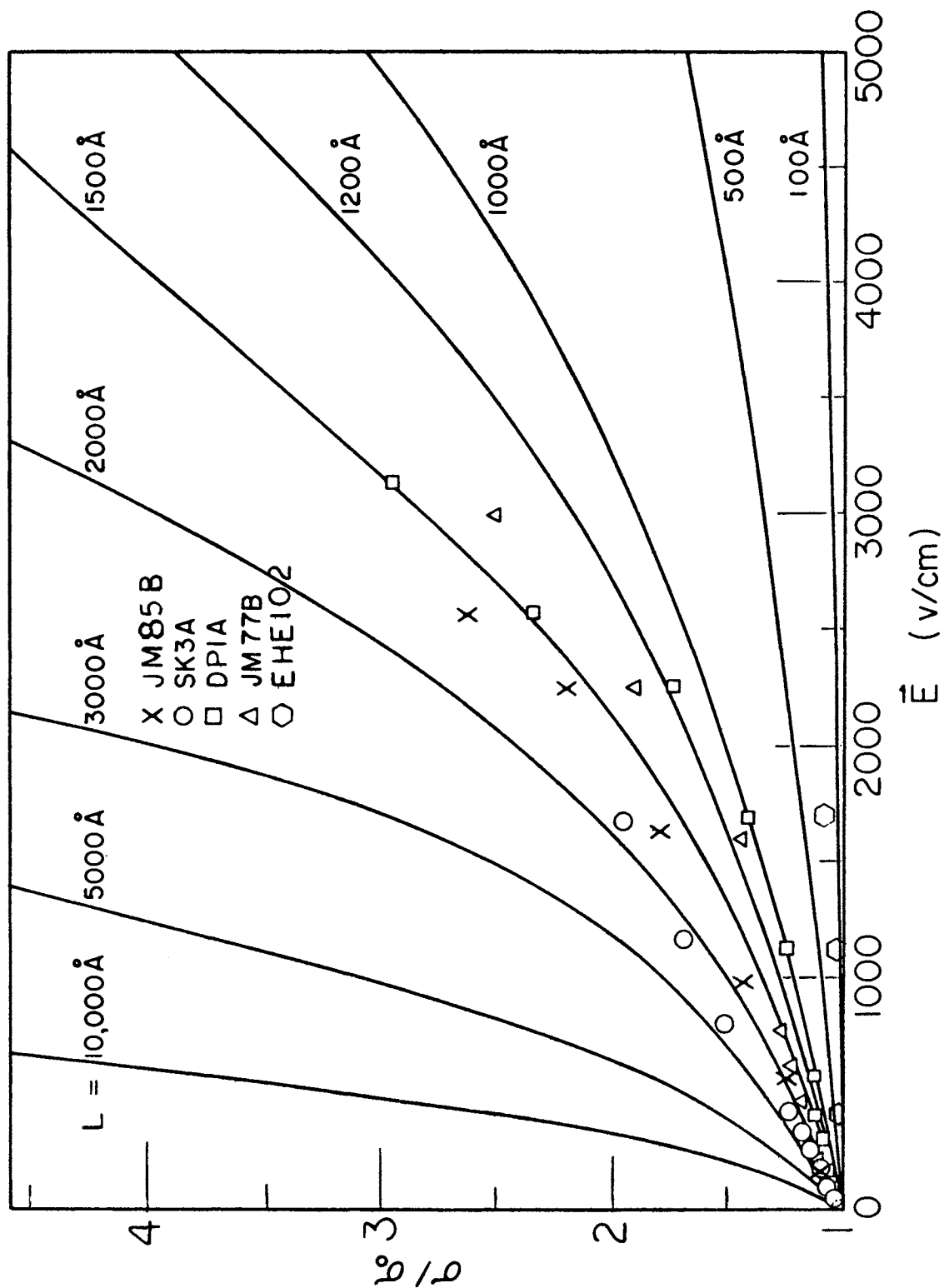


Figure 16. Variation of the Normalized Conductivity vs. \vec{E} -Field Strength for Various Average Molecular Lengths L

effect on conductivity of systematically changing the acene by the addition of heterocyclic atoms which stabilize unpaired electrons, resulted in producing a change of six orders of magnitude in σ . The activation energies were found to be pressure dependent, and the conductivities were found to be pressure and \vec{E} -field dependent as expected [Pohl, et. al. (16)] .

Three Cu-coordination semiconductors, which were studied, exhibited an anomalous dependence of conductivity upon pressure, temperature, and time of compression. Shearing stress effects on their conductivities were made, and X-ray data was also obtained. It is suggested that these polymers are capable of coexisting in two separate phases or forms, the two being mixed and reversibly transforming from one form into the other. This effect could quite possibly be due to a change in bonding or molecular orientation. It is suggested that a change in bonding occurs; therefore, semi-permanently effecting the structure. By annealing the sample at low pressures, the initial structure is obtained.

Suggestions for Future Studies

With regard to the decrease in conductivity of a given polymeric series by the addition of heterocyclic atoms or groups, it would be well to relate this effect to the speculated lowering of intermolecular conduction barriers by a theoretical molecular orbital approach.

As to the hysteresis effect observed in the Cu-coordination

polymers, it will be very difficult to assign the proper mechanism to this complex behavior. Perhaps by examining optical, X-ray, and ESR spectra, as well as electrical conductivity while the sample is actually exposed to high pressure, one could unscramble the anomalous behavior.

CHAPTER IV

ELECTRON SPIN RESONANCE

The existence of electron spin resonance (ESR) depends upon the fact that electrons possess charge, mass, angular momentum, magnetic moments; and hence, mutually interact with their surroundings. When a sample containing unpaired electrons, exhibiting gyromagnetism, is placed in an appropriate D.C. magnetic field, and is simultaneously irradiated by a proper, much weaker, rotating R.F. magnetic field, the sample responds transmitting vital information as to its constituency such as: impurities, electrons in unfilled conduction bands, odd molecules and free radicals, triplet electronic states, and so on. If one is to observe such effects, it is necessary only that the sample have a resultant electronic magnetic moment such that the material is paramagnetic (101-103).

Detection of ESR

One may conveniently describe a spinning charge in terms of a current loop, which may be represented by an equivalent magnetic moment. Thus, a spinning electron may be described as a tiny gyroscope having a magnetic moment along the axis of angular momentum.

Sands (103) has used the gyroscopic analog of the electron to discuss ESR. For the simple gyroscope, if one applies a force normal to the axis of rotation, a torque results which causes the gyroscope to precess. Likewise, if one could exert a torque on the spin axis of the electron, precession should result. One may effect this situation via a strong external magnetic field \vec{H}_0 interacting with the magnetic moment of the electron. A torque results, which causes precession of the spin axis of the electron about the magnetic field \vec{H}_0 . The frequency of precession, known as the Larmor precession, is proportional to the electronic magnetic moment and to the magnitude of the applied \vec{H}_0 -field. It is given by

$$\omega = \gamma |\vec{H}_0| \quad (1)$$

where γ is the gyromagnetic ratio, i.e., the ratio of the electronic magnetic moment to angular momentum, and ω is the angular frequency of precession. Eq (1) may be seen from considering the energy necessary to reorient the magnetic moment. Since electrons are subject to the rules of quantum mechanics, we may equate the work done by the external magnetic field to the Planck energy, i.e.,

$$\hbar \omega = 2 \vec{\mu} \cdot \vec{H}_0 \quad (2)$$

where $\vec{\mu}$ is the magnetic moment of the electron. Then

$$\omega = \mu H_0 / (1/2 \hbar) \quad (3)$$

but electronic angular momentum is $1/2 \hbar$. Thus, from the definition of γ , we have the Larmor equation:

$$\omega = \gamma |\vec{H}_0|$$

For a free electron ω is given by:

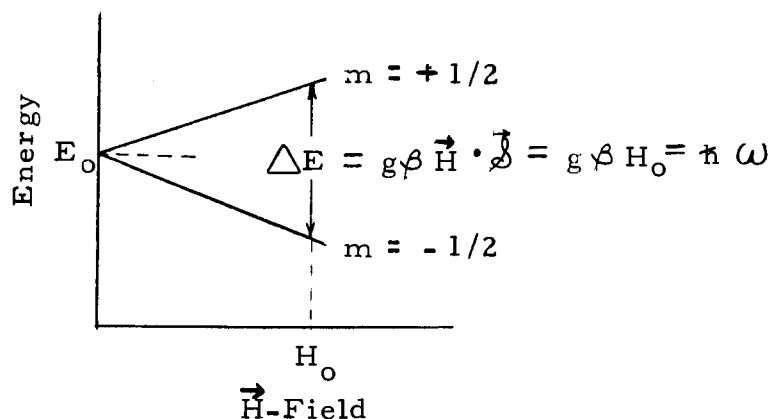
$$\omega = 2\pi \cdot 2.8026 H_0 \text{ MHz/gauss.} \quad (4)$$

In order to obtain resonance, one must correlate the unpaired electrons. If a sample containing many such electrons were placed in a strong D.C. magnetic field, \vec{H}_0 , one would not observe resonance, since each electron would be precessing at a random phase with respect to its neighbors. Hence, no bulk precessing magnetic moment would result. One must then correlate the precessions such that they are in phase. This is accomplished by applying a rotating magnetic field \vec{H}_1 perpendicular to \vec{H}_0 , having a rotational frequency equal to the Larmor frequency. The precessions are thus made coherent, and a torque is exerted on each of the electrons tending to tip its magnetic moment relative to the strong D.C. field, \vec{H}_0 . This small torque perturbs the electron, thus altering its energy. This excess energy, which is absorbed by the electron, is furnished from that stored in the rotating field \vec{H}_1 . Hence, a multitude of electrons absorbing energy in phase constitutes a strong resonance.

When a strong magnetic field \vec{H} is applied to a paramagnetic material having S total unpaired spins, which have been correlated by an additional field, \vec{H}_1 , the degenerate spin states will be split such that s_1 of the spins are aligned parallel, and s_2 are aligned antiparallel to the direction of the field. This first order interaction is known as the Zeeman interaction and is given by:

$$\mathcal{H} = g\beta \vec{H}_0 \cdot \vec{S} = g\beta H_0 S \quad , \quad (5)$$

where \mathcal{H} is the Hamiltonian; g is the Lande factor as observed in normal Zeeman effects; β is the Bohr magneton; and \mathcal{J} is the intrinsic electronic spin. This effect is pictorially indicated below. [For free electrons, $g = 2.0023$. In most free radicals g lies very close to this value, i.e., $2.002 \leq g \leq 2.004$ (104)].



On examining Eqs (1) and (5), and the figure above, it is seen that one may choose any frequency for the rotating field \vec{H}_1 , as long as the magnitude of the strong field \vec{H}_0 is correspondingly changed.

From a phenomenological approach, the resultant microscopic electronic magnetic moments in the sample tend to produce an overall observable bulk magnet moment per unit volume proportional to the applied field, \vec{H}_0 , i.e.,

$$\vec{M}_0 = \chi_0 \vec{H}_0, \quad (6)$$

where χ_0 is the static paramagnetic susceptibility of the sample given by:

$$\chi_0 = S\mu^2 \mathcal{J} (\mathcal{J} + 1) / 3kT; \quad (7)$$

where S represents the total number of unpaired electron spins in the sample, \mathcal{J} is the intrinsic spin, μ is the magnetic moment of an

individual electron, k is the Boltzmann constant, and T is the absolute temperature. Equation (7) may be rewritten as:

$$\chi_o = Sg^2 \beta^2 / 4kT = C/T ; \quad (8)$$

where β is the Bohr magneton ($\beta = \mu / \sqrt{3}$) and C is the Curie constant. Equation (8) is known as the Curie law, due to the $1/T$ dependence of the magnetic susceptibility. See for example, Sands (103) or Kittel (84) for a more thorough treatment of the phenomenological approach. In the event one is dealing with a ferromagnetic or ferroelectric material, Eq (8) is replaced by the Curie-Weiss form, i.e.,

$$\chi_o = \frac{C}{T - \Theta} , \quad (9)$$

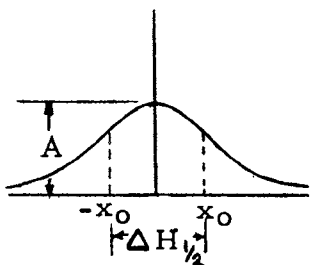
where Θ is the paramagnetic Curie point.

Determination of Spin Densities

With modern technology, the present limit of detecting free radicals or triplet states has been extended to $\approx 10^{10}$ total spins (105). Since the sensitivity of detection depends upon the width of the resonance line (the wider the line, the poorer the sensitivity) it is necessary to see how line shapes effect the computed spin densities. It will be assumed that a standard free radical sample (such as DPPH) whose spin density is known can be obtained for comparison with the unknown density signal. Since most detecting systems actually measure a difference in energy absorbed per unit change in frequency, the standard ESR output signal is a differential plot of the resonance absorption line.

Hence, it will be necessary to consider the differential of the assumed line shape, and relate the area under the curve of the "absorption line" to the peak half width ($\Delta H_{1/2} = 2x_0$) and the amplitude (h_0) of the differential signal.

Gaussian Curve



Gaussian Curve

Consider an absorption line as represented by a Gaussian curve as shown, and given by:

$$f(x) = A \exp(-a^2 x^2 / 2). \quad (10)$$

Taking the derivative results in:

$$f'(x) = -a^2 x f(x), \quad (11)$$

When $x = -x_0$, $f'(x) = h_0$, and is a maximum. Hence, equating the second derivative to zero gives:

$$x_0^2 = \frac{1}{a^2}. \quad (12)$$

Substitution of Eq (12) into Eq (11) yields:

$$f'(-x_0) = h_0 = \frac{1}{x_0} A \exp(-1/2) \quad (13)$$

or

$$A = h_0 x_0 \exp(1/2). \quad (14)$$

Now, substitution of Eq (12) and (14) into Eq (10) gives:

$$f(x) = h_0 x_0 \exp(1/2) \exp\left(-\frac{1}{2x_0^2} x^2\right). \quad (15)$$

Since the area under the curve represents the total energy absorbed

during resonance, which is in turn a measure of the total number of unpaired spins in the sample, we have:

$$S \propto \text{Area}$$

or

$$S = BA = B2 \int_0^{\infty} f(x) dx \quad (16)$$

where B is a proportionality constant. Integration of Eq(16) yields:

$$S = 2 \sqrt{2\pi} B \exp(1/2) h_0 x_0^2, \quad (17)$$

or

$$S = 8.28 B h_0 x_0^2. \quad (18)$$

Lorentzian Curve

Next, we shall consider the absorption line to have a Lorentzian shape given by:

$$f(x) = \frac{A}{x^2 + a^2} \quad (19)$$

Differentiating Eq (19), one obtains:

$$f'(x) = \frac{2Ax}{(x^2 + a^2)^2} \quad (20)$$

Using the same notation as before, and maximizing Eq (20) gives:

$$x_0^2 = a^2/3. \quad (21)$$

Since $f'(x)$ is maximum at $x_0^2 = a^2/3$, then

$$f'(x_0) = h_0 = \frac{9}{8} \frac{A}{x_0^3}, \quad (22)$$

or

$$A = \frac{8}{9} h_0 x_0^3. \quad (23)$$

Substituting this value for A into Eq (19) and integrating gives:

$$S = G2 \int_0^{\infty} \frac{8}{9} h_0 x_0^3 \frac{dx}{(x^2 + 3x_0^2)}, \quad (24)$$

or
$$S = \frac{8}{9} \frac{\pi}{\sqrt{3}} G h_o x_o^2, \quad (25)$$

where G is the proportionality constant between the number of spins and the integrated area under the resonance curve. Evaluating S , one obtains:

$$S = 1.63 G h_o x_o^2. \quad (26)$$

Upon comparing Eq (26) and Eq (18), one sees that if the proportionality constants, B for the Gaussian curve, and G for the Lorentzian curve, are not significantly different, then there is a factor of 5 difference in the results. Since it is not known how B and G agree, it is best to compare the product of the height with the square of the peak half width $\Delta H_{1/2} (= 2x_o)$ of the unknown sample to the same quantity for a known sample whose spin concentration has been previously determined, assuming the Lorentzian shape for both samples. The proportionality of spins per unit weight, or per unit volume of the unknown sample is determined from:

$$S_{\text{unk}} (\text{spin/gm}) = \frac{[h_o (\Delta H_{1/2})^2]_{\text{unk}}}{[h_o (\Delta H_{1/2})^2]_{\text{std}}} \times \frac{S_{\text{std}}}{W_{\text{unk}}}, \quad (27)$$

where unk and std represent the unknown sample and the known standard respectively, and W_{unk} is the weight of the specimen whose spin concentration is desired.

Power Determination

The number of spins per gram may be determined more precisely by measuring the power absorbed. Ingram(105) derives it as:

$$S(\text{spins/g}) = \frac{6 k T P}{H^2 \omega_0^2 \beta^2 g (\Delta + 1) \pi \omega_0 g(\omega - \omega_0)}, \quad (28)$$

where P is the power absorbed, ω_0 is the frequency at which resonance occurs, and $g(\omega - \omega_0)$ is the line shape function. (The rest of the factors appearing in Eq (28) have previously been defined. In practice, one normally measures the integrated intensity, I , under the line traced on the recorder chart and calculates the spin concentration from: (Cf. reference 52.)

$$S(\text{spins/g}) = \frac{b I T}{H^2 \omega_0^2}, \quad (29)$$

where b is evaluated by comparison with the curve obtained from a reference source (e. g., DPPH).

First Moments

Estimation of free-radical concentrations are often based on first moment calculations (involving second integrals) from the differential ESR signal versus magnetic field. This may be accomplished either by performing a numerical integration of the differential curve (i. e., a reconstruction of the resonance absorption line from the differential curve by applying Simpson's rule of calculus); or by experimental means. Experimentally, one can, for example, carefully cut the ESR signal out of the strip chart paper, and place it in a "moment balance," a very sensitive balance, which is calibrated in terms of a reference source.

Direct Conversion of ESR Signal

Recently, a method for determining spin concentrations was presented which was based on a direct conversion of the differential ESR signal to the area under the absorption curve. Randolph (106) performed error calculations for both Lorentzian and Gaussian line shapes as dependent upon the finite scan width of the experimental apparatus, miscentering of the scan with respect to the absorption spectrum, linear drift of the base line, and the bias in estimating the base line. Errors were determined for both second integral and first moment calculations. A simple analytical method was suggested which tends to minimize errors associated with spin concentration determinations. He described a simple feedback circuit which reduces the dependence of the second integral method on baseline bias and drift, and allows one to double integrate the signal electronically, and thus obtain the area with a minimum or error.

Literature Review

This portion of the investigation deals primarily with spin concentration determination of the polymers characterized in Chapter III, and with the temperature, pressure, and ambient dependence of the ESR signal, along with the correlation of spin densities with conductivities. As such, this literature review is not meant to be complete, but will rather be limited to those specific topics as relate to this study. Norberg (111), in a recent literature review, points out that

more than 500 papers on magnetic resonance were published in 1962, alone. With regard to ESR studies on organic solids, Gutmann and Lyons (52) should be consulted. They review the literature quite well in Chapter 2, and list some 60 recent references. For a general overall understanding of magnetic resonance, the reader is referred to the works listed in the bibliography (52, 105, 101, 111-116).

As was mentioned in Chapter I, the overall concern of this study is related to the energetics of carrier and unpaired spin formations, and how they are interrelated. A knowledge of the spin population in a sample is most important for the understanding of the electrical properties, but it is quite often difficult to correlate with the charge carrier population. Quite often, the number of spins in a molecular crystal does not equal the number of carriers.

Pohl and Opp (17) reported for a group of PAQR polymers a spin concentration of $\sim 10^{19}/\text{cc}$, while the charge carrier density was $\sim 10^{17}/\text{cc}$. It was also found that $\Delta H_{1/2} \sim 6$ to 7.5 gauss. Pohl and Engelhardt (15) found the spin densities to vary from $5 \times 10^{16}/\text{g}$ to $2 \times 10^{20}/\text{g}$ while the charge carrier densities, as deduced from Hall measurements were on the order of $10^{16}/\text{cc}$ to $10^{18}/\text{cc}$. They also observed that the higher the resistivity, the smaller the spin density. In a study of polybenzimidazoles, polyacetylenes, and PAQR's, Pohl and Chartoff (21) found the respective spin densities to be less than $10^{17}/\text{g}$ for the polybenzimidazoles; $10^{17}/\text{g}$ to $10^{18}/\text{g}$ for the polyacetylenes; and $\sim 10^{18}/\text{g}$ to $10^{20}/\text{g}$ for the PAQR's. Again, a positive correlation

between conductivity and spin density was observed.

In such cases where the carrier density is different from the spin density, a study of each with the variation of temperature may provide significant information. One may not, in general, expect a simple temperature dependence of the spin population, however. For example, amine-quinone complexes show a temperature dependence which follows the Curie law, Eq (8), that is, the spin density is found to be proportional to $1/T$. (Cf. reference 52.) On the other hand, aromatic hydrocarbon-halogen complexes tend to show an exponential temperature dependence, indicating an activation process. The spin activation energy is found to agree with the carrier activation energy (52, 30). Pohl and Chartoff (21) found exponential temperature dependence of spins for several PAQR polymers, and computed the activation energies as ~ 0.01 to 0.025 eV. Besides considering the normal $1/T$ Curie dependence, and the activated dependence on carriers and spins, one must also consider temperature effects on the mobility. In the work reported in the previous paragraph, the temperature dependence on the mobility is negligible; however, in other materials, if a change in mobility with temperature occurs it will greatly complicate matters.

Other types of temperature dependence of the spin density has also been observed. Chestnut and Phillips (117) observed anomalous temperature effects of ESR signals in ion radical salts. In such cases, an increase in temperature tended to increase the spin density. This was attributed to a transition from a singlet spin state to a triplet

spin state. Coupling between pairs of unpaired spins situated on different molecules was forming both singlet and triplet states, with the triplet lying at higher energies (118, 119). Recent work by Rembaum and Hermann (120, 121) on the temperature dependence of the spin density of poly (N-vinyl carbazole) iodine complex also indicates a similar transition is occurring in this polymer, since the spin concentration tends to increase with temperature.

In some cases, there is a very close correlation between carrier density and spin density as a function of temperature. This led Singer and Kommandeur (33) to deduce that the observed radicals are charged (e.g. perylene-iodine). In other cases, one finds the spin density to be completely temperature independent. In general, one expects the correlation to be greater when the spins are associated with ionic radicals than when they are associated with uncharged radicals.

Gutmann and Lyons (52) point out the lack of correlation between the spin density with such properties as activation energy and thermopower in a comparison of 3,10-diaminopyrene-chloranil (3:1) and 3,8-diaminopyrene-iodanil (1:1). These two charge transfer complexes have identical conductivity ($\sigma = 10^{-6}$ mho/cm at room temperature), a similar temperature dependence of conductivity ($E_a = 0.82$ eV and 0.80 eV, respectively) and similar Seebeck coefficients ($Q = 4 \times 10^{-4}$ volt/degree and 7×10^{-4} volt/degree). Yet the former has a spin density of 1.1×10^{23} /mole, while the latter had no detectable spin signal.

In order to resolve the various anomalies in the temperature

dependence of the spin concentration for organic materials in general, it is necessary that one be able to assign the proper mechanism to the population of the various spin states. The nature of paramagnetic centers which gives rise to an ESR signal in conjugated polymers is not completely understood. In some cases, the source of spins may be the conduction electrons transferred into the conduction band by thermal excitation; in other cases, perhaps it is a transition from the singlet to the triplet spin state, or the production of new radicals, either charged or uncharged. Until the various mechanisms are completely understood, the anomalous results will be observed.

A review of the literature reveals only a few scattered references to pressure effects on ESR. In general, the investigations are being carried out on crystals, and the effect on spin signal is of interest rather than the correlation between spins and carriers. Here, one can observe effects on the line shape due to the change in the symmetry of the crystalline lattice, and hence, the crystal field.

Statement of the Problem

The purpose of this phase of the study is to investigate the energetics of unpaired spin production, and to seek to correlate it with the conductivity measurements reported in Chapter III. ESR measurements on samples were made at room temperature and at liquid N_2 temperature, from which spin activation energies were estimated. The ESR signal for several samples is examined as a function of

pressure, and is further investigated as a function of various ambient gases.

Experimental Apparatus and Procedure

The principal piece of apparatus used in this part of the investigation was an Alpha Scientific Laboratory Model AL 340 SY Electron Spin Resonance Spectrometer. It consists of the following: electromagnet with 6 in. diameter x 1.875 in. gap pole faces and magnetic power supply; 60 cycle sweep unit, for use with visual display; master oscillator power supply; phase detector; 100 KHz modulator unit, including a regulated power supply for the modulator and the phase detector; master oscillator detector amplifier (MODA) with integral probe assembly; and strip chart recorder with a full scale sensitivity of 100 mV. The sensitivity of the spectrometer is $\sim 10^{15}$ spins/gauss linewidth (i. e., it can detect as little as 1 μ g of DPPH). A block diagram of the spectrometer is shown in Figure 17.

The spectrometer was calibrated against seven DPPH standards of spin concentration varying from 5.842×10^{18} spins to 1.528×10^{15} spins. The standards were prepared by S. Kanda from purified DPPH crystals in solution using micro-chemistry techniques. Table VI gives the spin concentration of each of the standards. A log-log plot of "spins" as given in Table VI versus weight of the sample should yield a straight line for proper calibration, after normalizing the readings at some one concentration. Such a graph is shown in Figure 18.

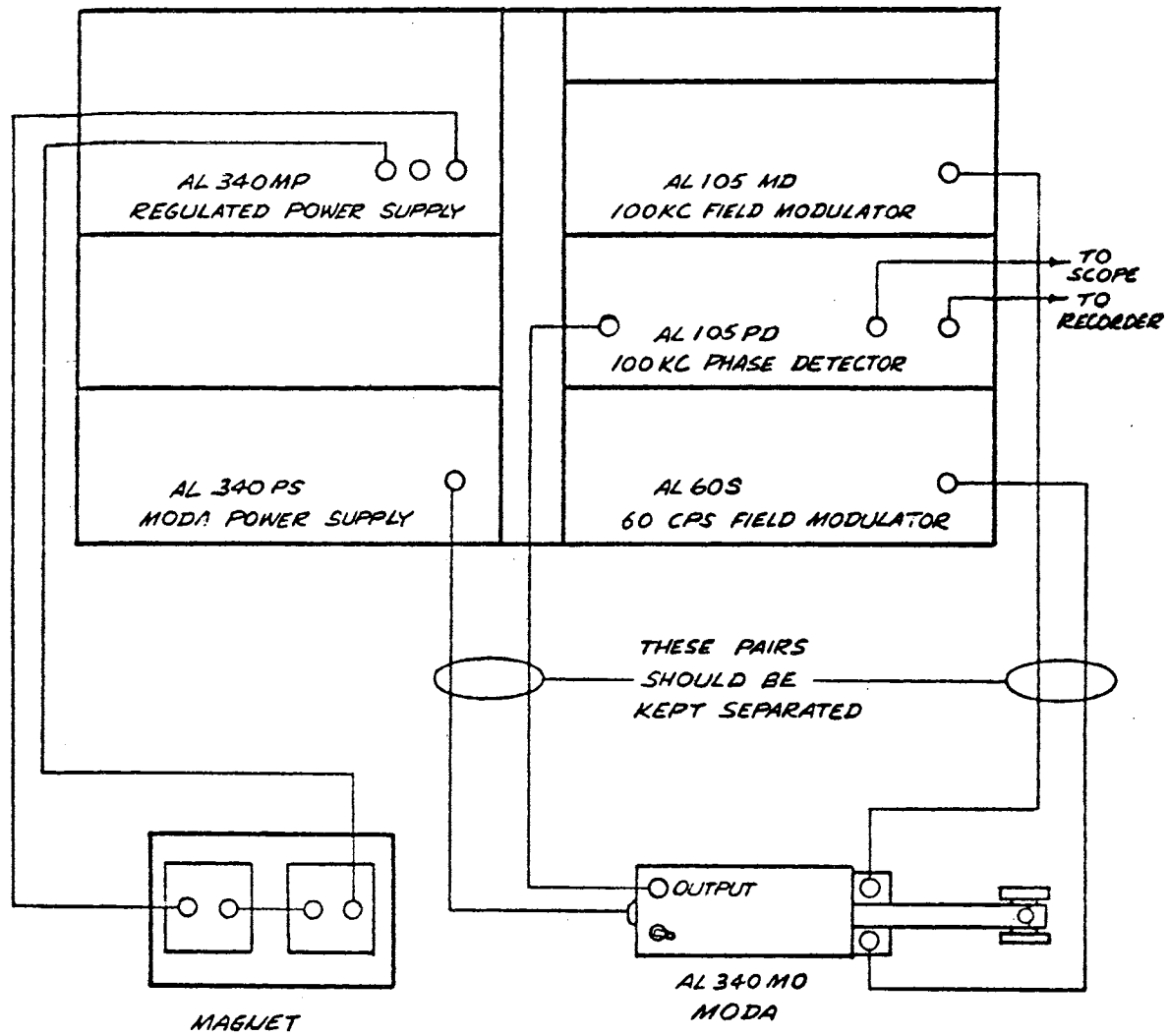


Figure 17. Block Diagram of ESR Spectrometer

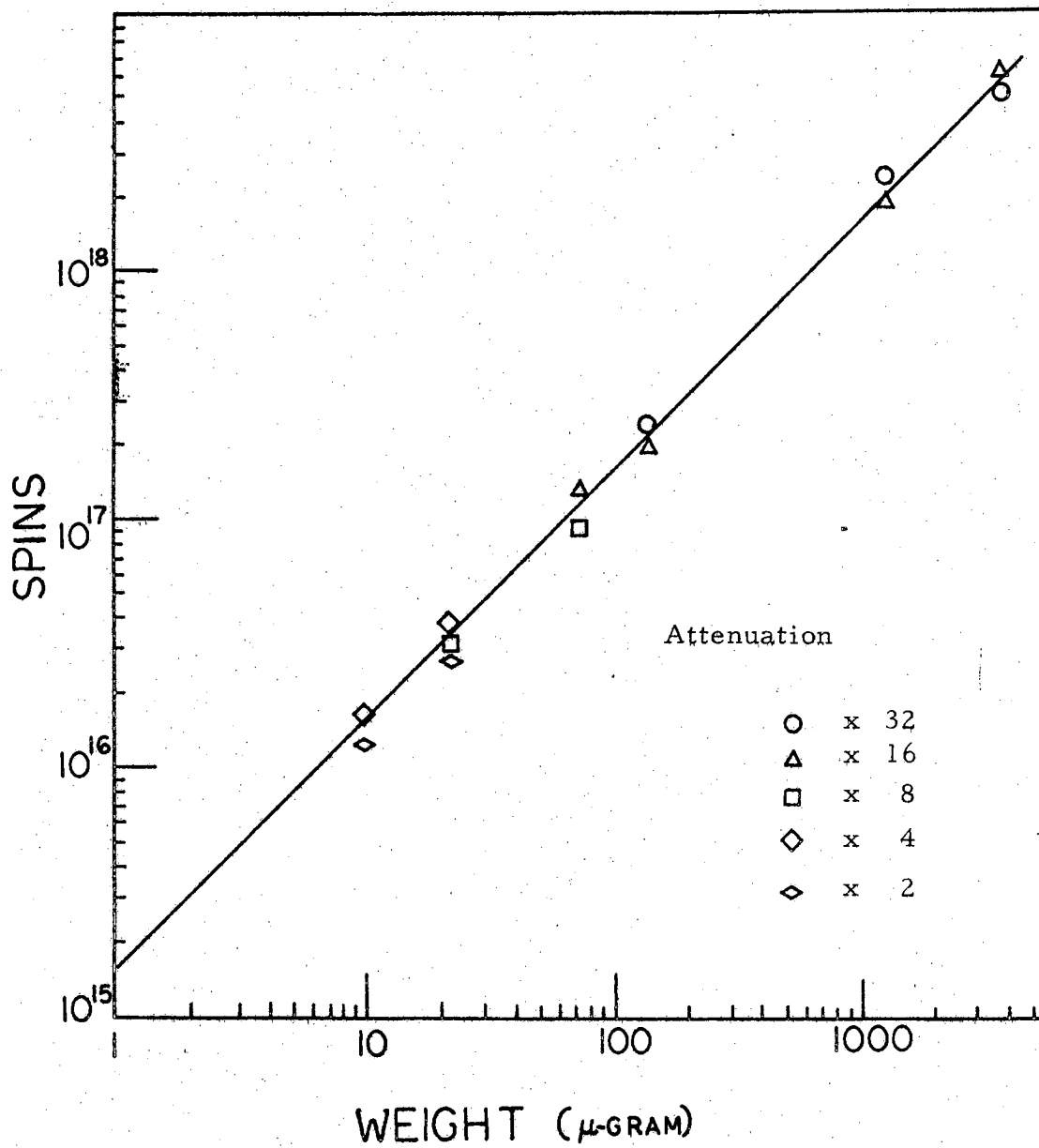


Figure 18. Calibration Curve for ESR Spectrometer

TABLE VI

SPIN CONCENTRATION OF SEVEN DPPH ESR STANDARDS

Sample No.	Weight (μg)	S (spins) (Calculated)
DPPH 1	3820	5.842×10^{18}
DPPH 2	1270	1.941×10^{18}
DPPH 3	140	2.138×10^{17}
DPPH 4	74	1.132×10^{17}
DPPH 5	24	3.762×10^{16}
DPPH 6	10	1.528×10^{16}
DPPH 7	1	1.528×10^{15}

A typical resonance line for DPPH-1 (with 0.025 gauss, 100 KHz modulation field, gain = 3, phase balance = 1, normal phase reversal, attenuation x 16, fast magnetic sweep, time constant = 1 sec, and slow writing speed) is shown in Figure 19. The width $\Delta H_{1/2}$ is determined to be 2.5 gauss from knowing the rate of sweep of the H-field. Since DPPH has a $\Delta H_{1/2} \approx 2.7$ gauss, the speed was compensated so the measured $\Delta H_{1/2} = 2.7$ gauss, in agreement with the theoretical value.

Results and Discussion

Initially ESR data was taken on specimen which had been exposed to high pressures and temperatures in the Bridgman high pressure cell, while conductivity measurements were being taken (as were

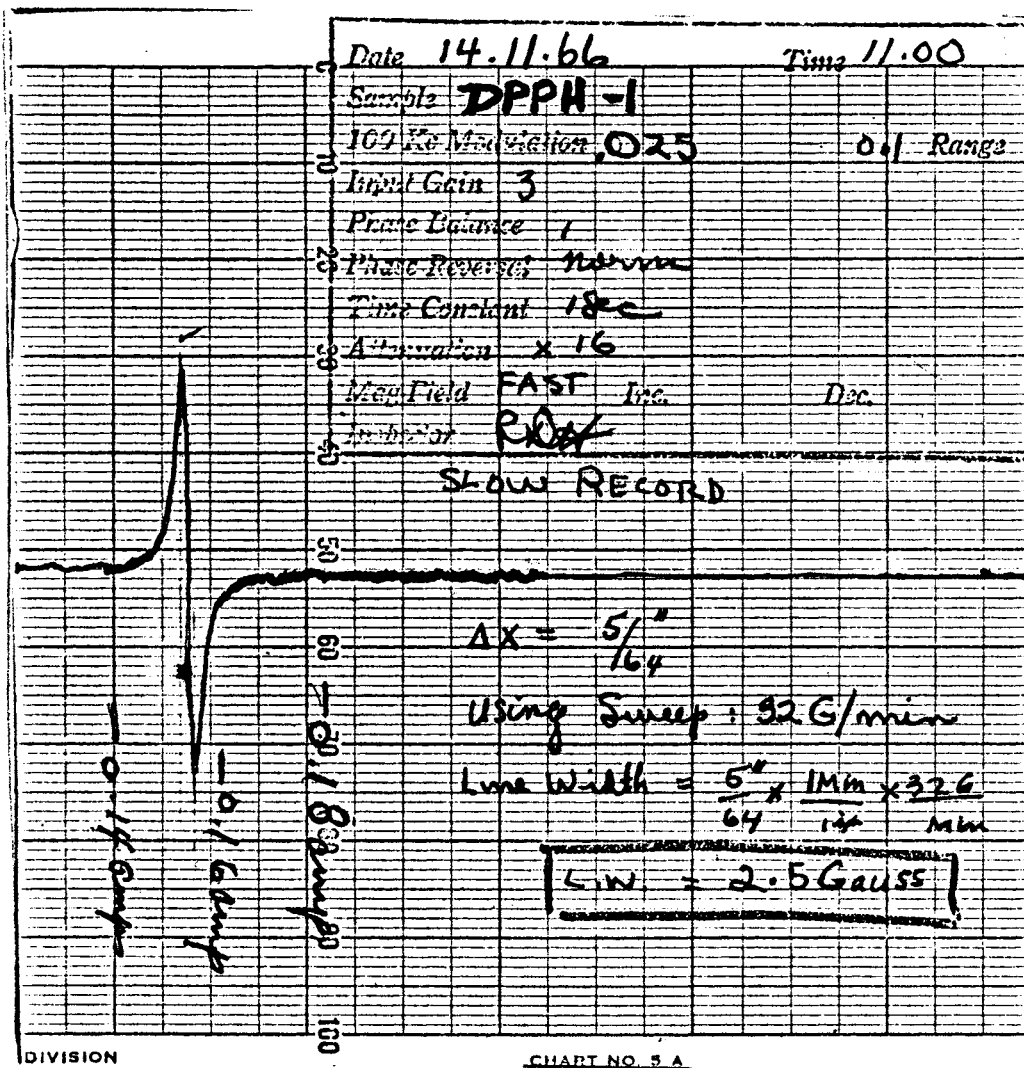


Figure 19. Typical Resonance Line for DPPH Standard

discussed in Chapter III). It was noted, when the spin density of a given sample was rechecked a few days later, the intensity of the differential signal was much smaller and wider. That the effect was real was indicated by the ability of the spectrometer to reproduce the DPPH standard resonance line. Hence, the spectrometer calibration had not changed, but rather the spin signal of the polymeric semiconductor under study had changed drastically.

A systematic study of this effect followed. After considerable examination, it was attributed to a pressure induced O_2 effect.

ESR Pressure and O_2 Effects

Briefly, it was found that a narrowing of the resonance absorption line together with an increase in amplitude of the line resulted after pressing the samples at about 30 kilobar when this line is compared to that observed in the unpressed sample. The ESR signal from the pressed sample was observed to return to its former width and amplitude after some time. It was further determined that pressure cycling from 7 to 30 kilobar of the sample enhances the ESR signal to a greater extent than does the application of steady high pressure, while shearing it while under pressure reduces its signal to a value similar to that of the unstressed powder sample.

The pressure and time effects on the amplitude and line width are shown in Figure 20. (a) The sample is first weighed and ESR data is taken on the polycrystalline powder. The amplitude and width are

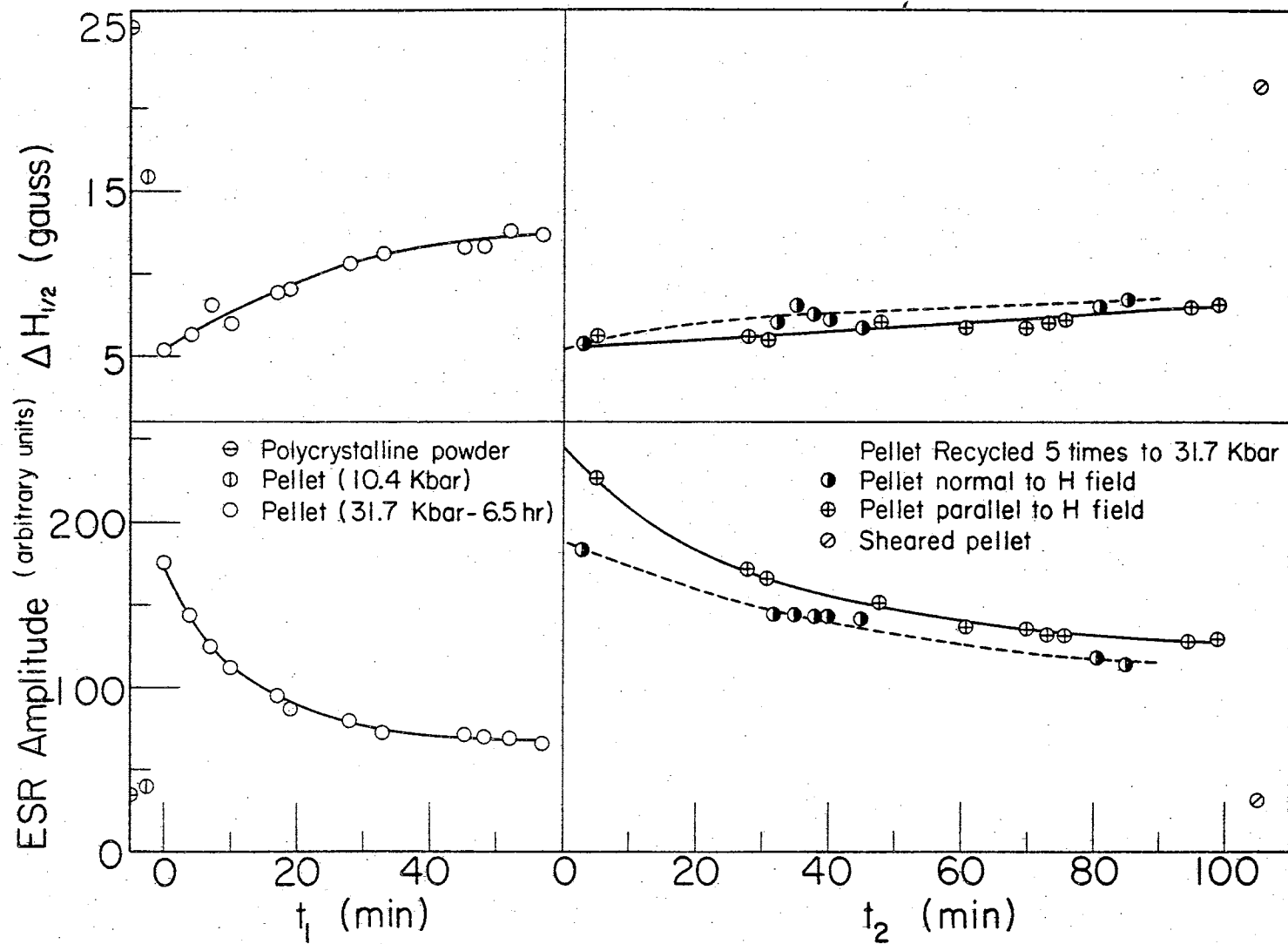


Figure 20. Ensuing Decay of ESR Signal of Polymer DP1A Following Pressure Treatments

shown at the extreme left of the graph as (\ominus). (b) Next, this specimen was premolded into a pellet at 10.7 kbar and at 300°K. The pellet signal exhibited a slight increase in amplitude over the powder signal, and a considerable degree of sharpness. Data on the pellet is shown as (\oplus) slightly displaced to the right of the powder data. (c) Following this, the pellet was returned to the press and was left under 31.7 kbar overnight (6 1/2 hrs at 300°K). The signal was increased considerably in amplitude and sharpness, but tended to decay in time (t_1) as shown. (d) After 1 hr., the sample was again returned to the press and was quickly recycled 5 times from 7 to 31.4 kbar. The resulting change in the signal is plotted against time (t_2). (e) After considerable time, the specimen was put in a shearing apparatus and was sheared through 6° of arc, while a uniaxial pressure of 2 kbar was maintained on the sample. The results of the shearing effect on the sample are shown at the extreme right side of the graph (\oslash). After shearing, the amplitude and width of the line are quite similar to the initial powder values.

Actual strip chart recordings of the signal for cases (a), (b), (c), and (d) above, together with the time change of the signal in case (d), are shown in Figure 21.

The narrowing of the width and increase in amplitude of the resonance line after pressing the sample was considered to be due to either:

- (1) molecular orientation and thus spin alignment;
- (2) breaking of bonds, which creates free radicals, thus

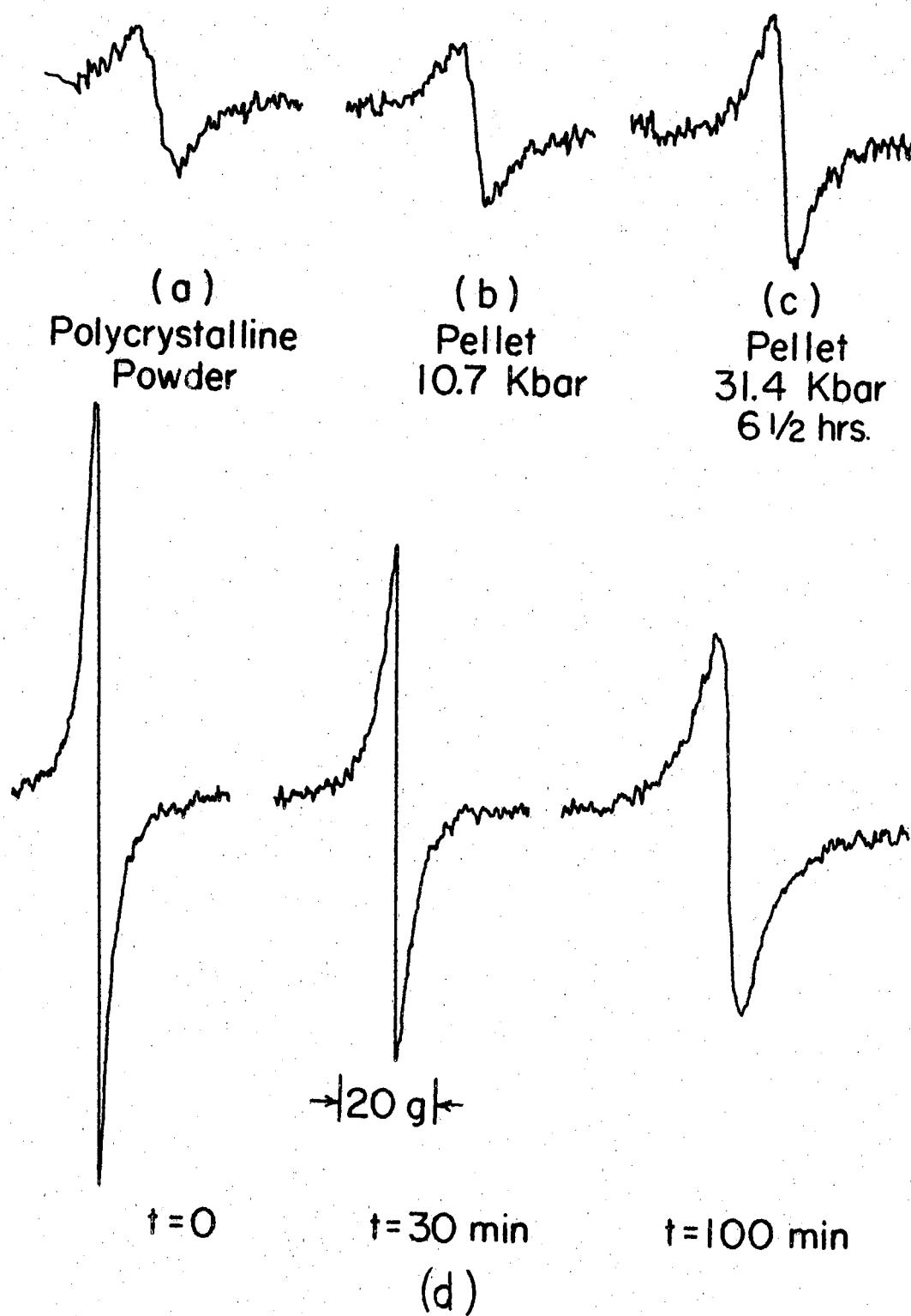


Figure 21. Strip Chart Recordings of ESR Signal of Sample DP1A after Pressure Treatment

providing more spins, which are slowly removed by O_2 adsorption from the atmosphere; or

- (3) the removal of O_2 which was initially adsorbed on the sample, either by chemically combining it with molecules of the sample, or by forcing it out of the bulk of the sample by the application of high pressure.

In cases (2) and (3), the time decay of the signal would be due to the adsorption of O_2 from the atmosphere, while in case (1), it would be due to the relaxation of the orientation. It will now be discussed how this was resolved.

The spin signal of a typical polymer (DP1A) has been examined under various ambients. For a powdered specimen, after it has been outgassed sufficiently, the following results were observed:

- (1) O_2 will completely remove the signal of a dry outgassed sample at partial pressure of O_2 greater than about 300 mm. (Cf. Figure 22.)
- (2) H_2O vapor does not effect the signal, except that its presence on the sample partially excludes the O_2 effect. When the sample possesses H_2O vapor, and is then exposed to O_2 , the O_2 is not adsorbed in the same extent that it is on a clean sample. (Cf. Figure 22.)
- (3) N_2 does not effect the sample. Actual strip chart recordings of the above effects are shown in Figures 23 and 24.

Furthermore, it was found that sufficient outgassing of the

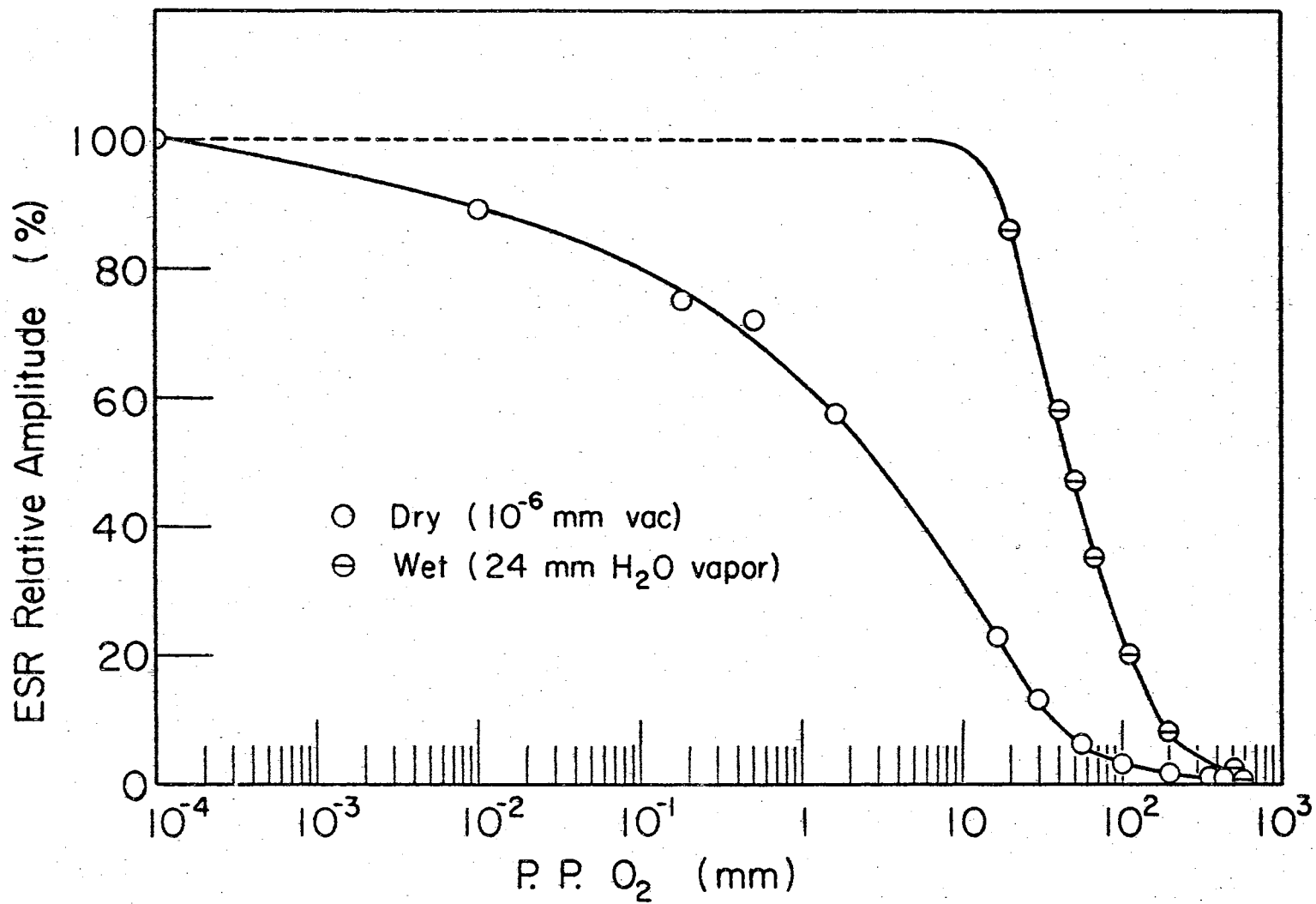


Figure 22. Effect of O_2 Adsorption on the ESR Signal of Polymer DPIA

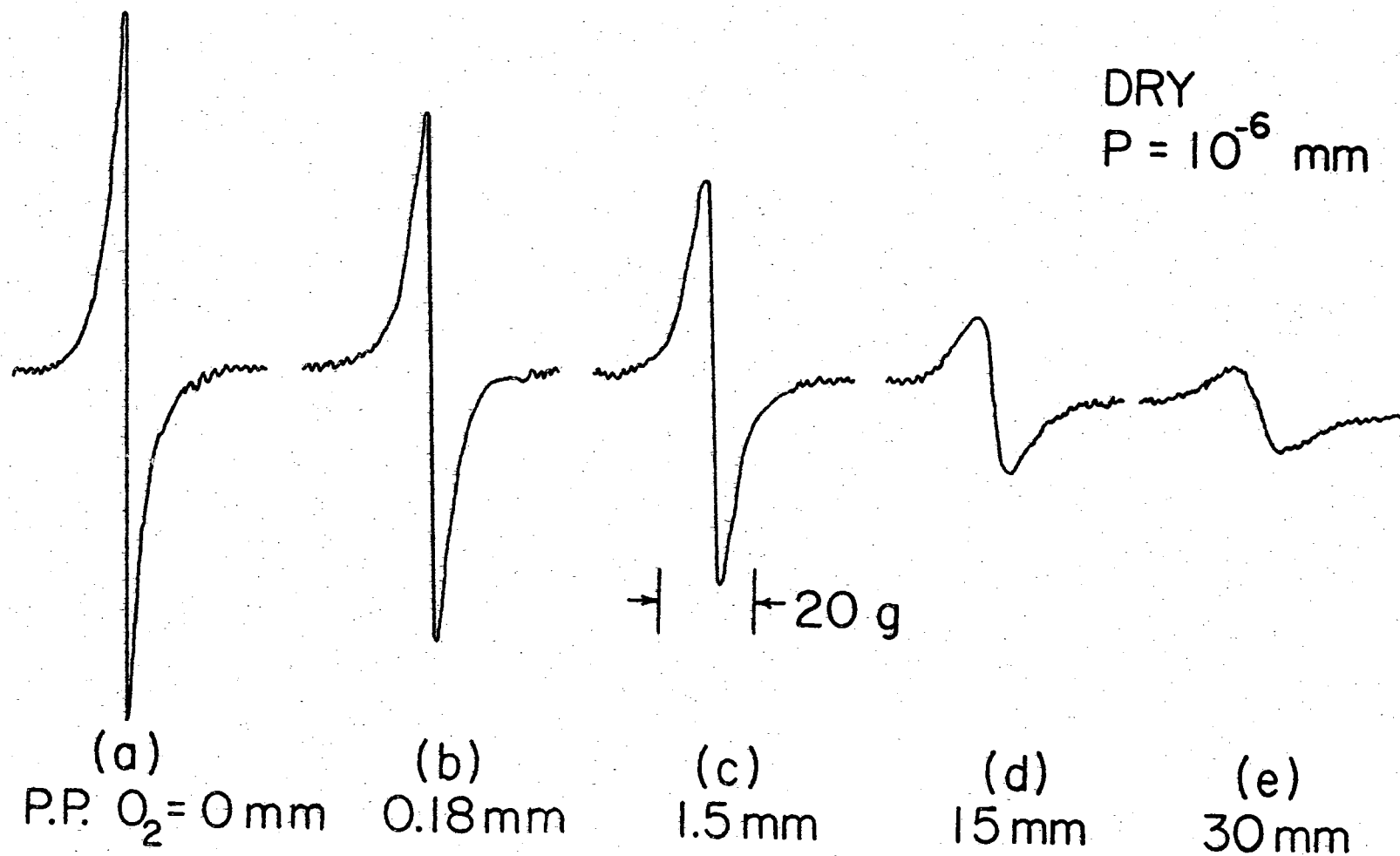


Figure 23. Strip Chart Recordings of ESR Signal of Highly Outgassed Polymer DPIA as a Function of O_2 Pressure Induced on the Sample

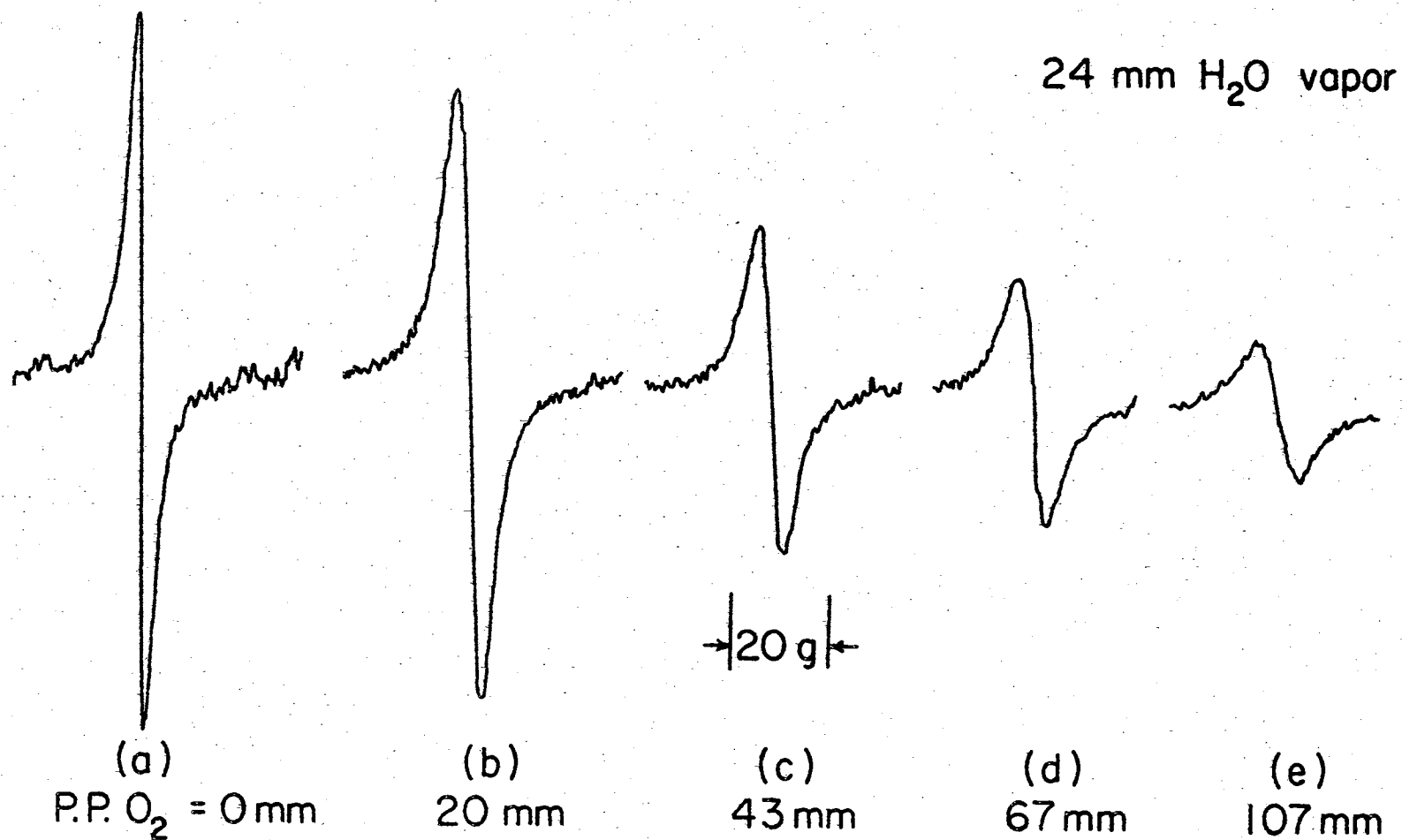


Figure 24. Strip Chart Recordings of ESR Signal of Polymer DP1A with H₂O Vapor Adsorbed as a Function of O₂ Pressure

powdered specimen sharpens the signal much the same as does the high pressure effect. Table VII displays data supporting this.

TABLE VII
PRESSURE EFFECTS ON ESR SIGNAL

Sample No.	Powder		Outgassed		High Pressure	
	$\Delta H_{1/2}$ (gauss)	$S(10^{20})$ sp/gm	$\Delta H_{1/2}$ (gauss)	$S(10^{20})$ sp/gm	$\Delta H_{1/2}$ (gauss)	$S(10^{20})$ sp/gm
DP1A	8.1-10.9	1.8-2.6	2.7	1.3-2.0	2.7	1-2.5
JM77B	8.8- 9.5	0.8-1.2	5	0.9-1.8	4.0	
JM85B	10.5	1.23	5	1.6	3.9	~ 2
SK3A	∞		∞		9	0.44
EHE102	∞		∞		∞	

Case 1. In order to see if the O_2 were effecting the D.C. resistance measurements, a specimen was premolded at 10.7 kbar pressure, and was then outgassed at $120^\circ C$ in a vacuum of 10^{-6} torr for 20 hours. It was then enclosed in a N_2 ambient, and resistance measurements were taken at 31.4 kbar. The D.C. resistivity and the ESR signal were not appreciably changed from that obtained under normal atmosphere ambient, except that the ESR signal did not exhibit a time dependence as long as it was kept under N_2 atmosphere. When air atmosphere was introduced, the signal was quickly reduced in amplitude and broadened in width, exhibiting the same sort of time behavior as shown in Figures 20 and 21. Since no appreciable time dependence was exhibited

as long as the sample was under N_2 ambient, molecular orientation (case 1) was not thought to have been observed. However, the ESR signal amplitude and width did exhibit \vec{H} -field orientation effects, as shown in Figure 20. This amplitude orientation effect is probably due to the field inhomogeneity in the cavity. (Also, on a couple of occasions after several hours with the sample in N_2 , the ESR signal had dropped $\sim 10\%$. However, this was attributed to fluctuations in the spectrometer.)

Case 2. To within limitations of experimental measurement, it presently appears that the number of spins is not increased with pressure, although it is difficult to be definite about this. This would exclude case (2) mentioned above. However, in the case of SK3A, a definite effect was produced by the high pressure treatment (cf. Table VII), while the outgassing did not produce a detectable signal.

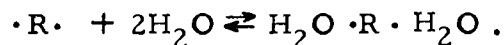
An extremely broad signal was observed for SK3A powder, if enough of the material were used (~ 50 mg, as opposed to ~ 2 mg normally needed for most of the samples studied). However, no spin density calculation was possible, since the width was several hundred gauss wide, and the amplitude was extremely small. Kanda, et.al. (81) have reported ESR measurements on a similar Cu-coordination complex. They found a symmetrical broad ESR line at $g = 2.075$; the half width of the signal being 292 gauss ($T = 300^\circ K$), 228 gauss ($T = 213^\circ K$), and 268 gauss ($T = 138^\circ K$), and calculated the spin concentration to be 9.6×10^{22} /mole at $300^\circ K$. This spin concentration

was used to calculate the magnetic susceptibility, which agreed quite well with the susceptibility as measured directly.

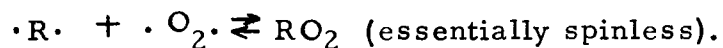
Kanda, et.al. further state that the ESR absorption did not appear to be dependent upon the degree of crystallinity of the sample. For instance, they measured essentially the same absorption intensity for a crystal, polycrystalline powder, and a colloid. Since the current study of the ESR signal of SK3A indicates a line width of 9 gauss after premolding while it was several hundred prior to stressing the sample, it would appear that either orientation or a phase change has occurred. Other effects observed on SK3A (e.g. hysteresis) lead us to conclude a phase change has occurred.

Case 3. In chemical terms, one may describe the events for case (3) as follows:

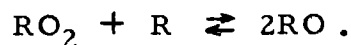
1. There is a normal, reversible uncoupling of electron pairs of the host polymer molecules at room temperature as indicated by the equilibrium, $R \rightleftharpoons \cdot R \cdot$.
2. Water can be reversibly bound at the spin sites with little effect on the total ESR signal,



3. Molecular oxygen can be reversibly sorbed at the spin sites, in this case masking the ESR signal. (Oxygen is itself a diradical.)



4. High pressure (or high temperature) can bring about an irreversible oxidation of the host polymer,



Thus, following a high temperature or high pressure experiment, the apparent ESR signal is increased because the spinless polymer-oxygen complex is destroyed leaving normal dissociation of the polymer to spin active entities to be displayed as if oxygen were absent. When this polymer is exposed to atmosphere, after high pressure treatment, the O_2 gradually makes its way back onto the spin sites, and the signal broadens correspondingly in time. If sufficient H_2O has been adsorbed on the sample before its being exposed to air, the O_2 will not be adsorbed to equilibrium, i. e., H_2O on the sites partially interferes with O_2 adsorption and interaction.

It now appears that case (3) is the cause of the signal changing with pressure and time. However, if orientation is occurring, it is not possible to detect it under the present arrangement. Hence, if one is to completely resolve the problem of pressure effects, it will be necessary to develop a new method of examining ESR signals while the sample is actually under stress, rather than exposing it to atmosphere to make measurements. The latter way of performing the measurements allows O_2 from the air to be adsorbed, which tends to effect the signal in the same way that orientation relaxation would.

It is interesting to note that Piette (128), in discussing the application of ESR to the study of surface chemistry, mentions an effect

very similar to the one which has been discussed in the previous paragraphs. Normal carbon black, when measured in air, has a rather broad ESR line, with $\Delta H_{1/2} \sim 15$ gauss. When the sample is outgassed sufficiently, it displays a very sharp ESR signal, with $\Delta H_{1/2} \sim 7$ gauss. Following the evacuation process, if oxygen is introduced onto the sample, the line immediately broadens to \sim twice the half-width initially observed ($\Delta H_{1/2} \sim 30$ gauss). In each of these cases, the line intensity (and hence the number of spins) does not change. The shape of the line changes, but it does so in such a manner as to keep the product, $h_o(\Delta H_{1/2})^2$, constant.

If the carbon is again evacuated and nitrogen is admitted on the sample, followed by pure oxygen exposure, the line shape remains the same as it did under vacuum conditions; i. e., N_2 adsorption on the surface excludes the O_2 effect.

Piette suggests that initially in air, the partial pressure of O_2 on the surface traps unpaired electrons. Evacuating the sample frees these trapped electrons and allows them to resonate in phase with their neighbors. When an atmosphere of pure O_2 is put onto the freshly evacuated sample, it can adsorb to completion, as indicated by a severe broadening of the line. The subsequent outgassing and exposure to N_2 results in the trapped spins being covered with N_2 , which is inert to the trapping of the spins.

Up to this point, the observations on the polymeric semiconductor and on the carbon black are in correspondence. However, the

next step does not agree, i.e., when O_2 is introduced onto the carbon covered with N_2 , the signal is unchanged; while for the polymeric semiconductor, the O_2 quickly replaces the N_2 on the sample and the line is broadened. Hence, water vapor on the polymer plays the role that N_2 plays on carbon black.

ESR Temperature Effects

ESR temperature measurements can indicate the concentration and type of unpaired electron spins in a material. This can give useful insight into the nature and source of the carriers in organic semiconductors. The polymers examined here are of highly extended conjugation type, (as opposed to those using donor-acceptor charge transfer structures).

The samples were carefully weighed and outgassed extensively to $150^{\circ}C$, after which they were sealed in a tiny quartz finger, approximately 1 mm in diameter by 20 mm in length. They were then placed in a larger quartz container (~ 6 mm diameter by 75 mm length), which sat in the spectrometer cavity between the magnet pole faces and served as a dewar. After taking room temperature spectrum, the samples were individually cooled to $77^{\circ}K$ by slowly pouring liquid N_2 over the sample into the quartz dewar, and another spectrum was taken. Likewise, spectra for the DPPH standard was obtained at the two reference temperatures in the same manner.

Following the discussion in the last section, if one is to obtain

reasonable ESR data, the measurements must be done in vacuum. Hence, all of the data reported in this section was obtained on highly outgassed powdered specimen, having been heated to $\sim 150^{\circ}\text{C}$ for 20 hours or more.

The spin concentrations as calculated from Eq (27), were determined at room temperature (300°K) and at liquid N_2 temperature (77°K). This data is shown in Table VIII.

Spin Lifetimes. The data obtained, as tabulated in Table VIII, shows the ESR peak width to be greater for those semiconducting polymers with lower spin concentrations. Assuming, for example, a Lorentzian distribution in the response signal, the mean relaxation time, $\bar{\tau}$, obtained from ESR measurements of the peak width at half peak power, ΔW , is a measure of the mean lifetime during which a particular molecular electronic configuration exists. Writing the thermal relaxation time T_2 for a Lorentzian distribution (21, 104, 105), one has:

$$T_2 = 0.577 / \Delta W \approx \bar{\tau}$$

$$\Delta W = 1.8 \times 10^{-7} (\Delta H_{1/2}) \text{ sec}^{-1}; \text{ (if } \Delta H_{1/2} \text{ is in gauss)}$$

$$\bar{\tau} \approx 3.1 \times 10^{-8} / (\Delta H_{1/2}).$$

For example, for the range of $\Delta H_{1/2}$ values observed here of 3 to 11 gauss,

$$\bar{\tau} = 0.3 \text{ to } 1.0 \times 10^{-8} \text{ sec.}$$

In terms of this mean spin lifetime then, it is seen that the spin life -

TABLE VIII

ESR DATA AND RESISTIVITIES FOR SEVERAL POLYMERS
AT 300°K AND 77°K AFTER EXTENSIVE OUTGASSING

Sample No.	Resis- tivity (a) (ohm-cm)	T = 300°K ^(b)		T = 77°K ^(b)		E _s (eV)
		$\Delta H_{1/2}$ (gauss)	S (Spins/gm)	$\Delta H_{1/2}$ (gauss)	S (Spins/gm)	
JM85B	3.0×10^2	6.5	1.9×10^{20}	5.1	1.8×10^{18}	0.021
JM82	3.8×10^2	4.4	5.4×10^{19}	6.4	1.9×10^{19}	0.009
DP1A	7.2×10^2	3.4	1.5×10^{20}	2.7	3.9×10^{18}	0.033
JM85A	8.4×10^2	4.5	4.5×10^{19}			
JM42	2.2×10^4	8.1	1.2×10^{20}	7.9	1.4×10^{20}	~0
JM84A	3.2×10^4	5.4	1.4×10^{20}			
JM83B	3.4×10^4	8.4	6.8×10^{19}			
JM83A	4.2×10^4	5.1	3.4×10^{19}			
JM50	4.6×10^4	3.6	3.6×10^{20}	3.7	2.6×10^{20}	0.003
JM80	5.7×10^4	9.2	2.3×10^{19}	10.7	2.4×10^{19}	~0
JM77B	6.9×10^4	6.6	6.0×10^{19}	6.9	4.0×10^{18}	0.024
JM39	8.9×10^4	10.0	3.4×10^{19}	9.3	8.8×10^{18}	0.012
JM84B	1.1×10^5	6.6	6.8×10^{19}			
JM78B	1.1×10^5	10.7	4.7×10^{19}			
JM49 (c)	1.6×10^5	broad		5.3	1.5×10^{20}	
SK3A (c)	3.8×10^5	9.0	4.4×10^{19}			
JM46	1.6×10^6	7.0	8.7×10^{19}	5.6	3.9×10^{19}	0.007
JM93B	1.7×10^6	8.1	6.1×10^{19}			
JM43	4.1×10^6	4.4	1.1×10^{19}	9.3	3.2×10^{20}	0.01
JM48	1.3×10^7	6.8	4.5×10^{19}	6.4	2.8×10^{18}	0.003
JM92B	1.8×10^7	4.8	2.0×10^{19}			
JM40	4.0×10^7	8.0	7.1×10^{19}	8.8	4.2×10^{18}	0.005
JM41	6.8×10^7	6.0	7.7×10^{19}	5.6	6.8×10^{19}	0.001
EHE102(c)	10^{10}	broad	10^{15}	broad	10^{15}	

(a) Measured at 1.820 kbar and 300°K after high pressure compaction to 31.7 kbar at elevated temperatures (410-450°K).

(b) Measured on polycrystalline powdered specimen after outgassing at 10^{-6} torr and 450°K for 40 hours.

(c) JM49 exhibited broad signal, but no qualitative results could be obtained at room temperature. SK3A exhibited an extremely broad signal, while EHE102 did not appear to be detectable. The data for SK3A was obtained after high pressure treatment.

time is directly proportional to the spin concentrations as we proceed among the polymers. Since the more stable of the free radicals are expected to have a smaller specific rate of return to the ground state, the observed trend in Table VIII and shown in Figure 25 may be understood. A few of the samples (JM43, JM82, JM83A, JM85, and JM92B), do not follow this trend, however. It is probably due to inaccuracy in spin determination. There are two alternate, but closely analogous explanations as pointed out earlier by Pohl and Chartoff (21), i. e. involving nuclear spins via exchange narrowing or delocalization narrowing as well as the above mentioned radical lifetime mechanism.

Spins and Carriers. Since the polymer molecules are the source or precursors of both unpaired electrons observable in ESR measurements, and of the carriers as observable in conduction measurements, and both unpaired spins and carriers are expected to be produced by (separate) thermal activation processes (21, 30), we then expect to find some direct correlation between the observed spin concentration and the observed conduction on comparing these for conjugated polymers. Indeed, just such a correlation is seen among the polymers studied here, as is indicated by Table VIII and Figure 26. The empirical equation fitted to the graph agrees well with the one postulated by Pohl and Chartoff (21).

Energetics of Spin Formation. From the temperature dependence of the electron paramagnetic susceptibility, assuming Curie type of

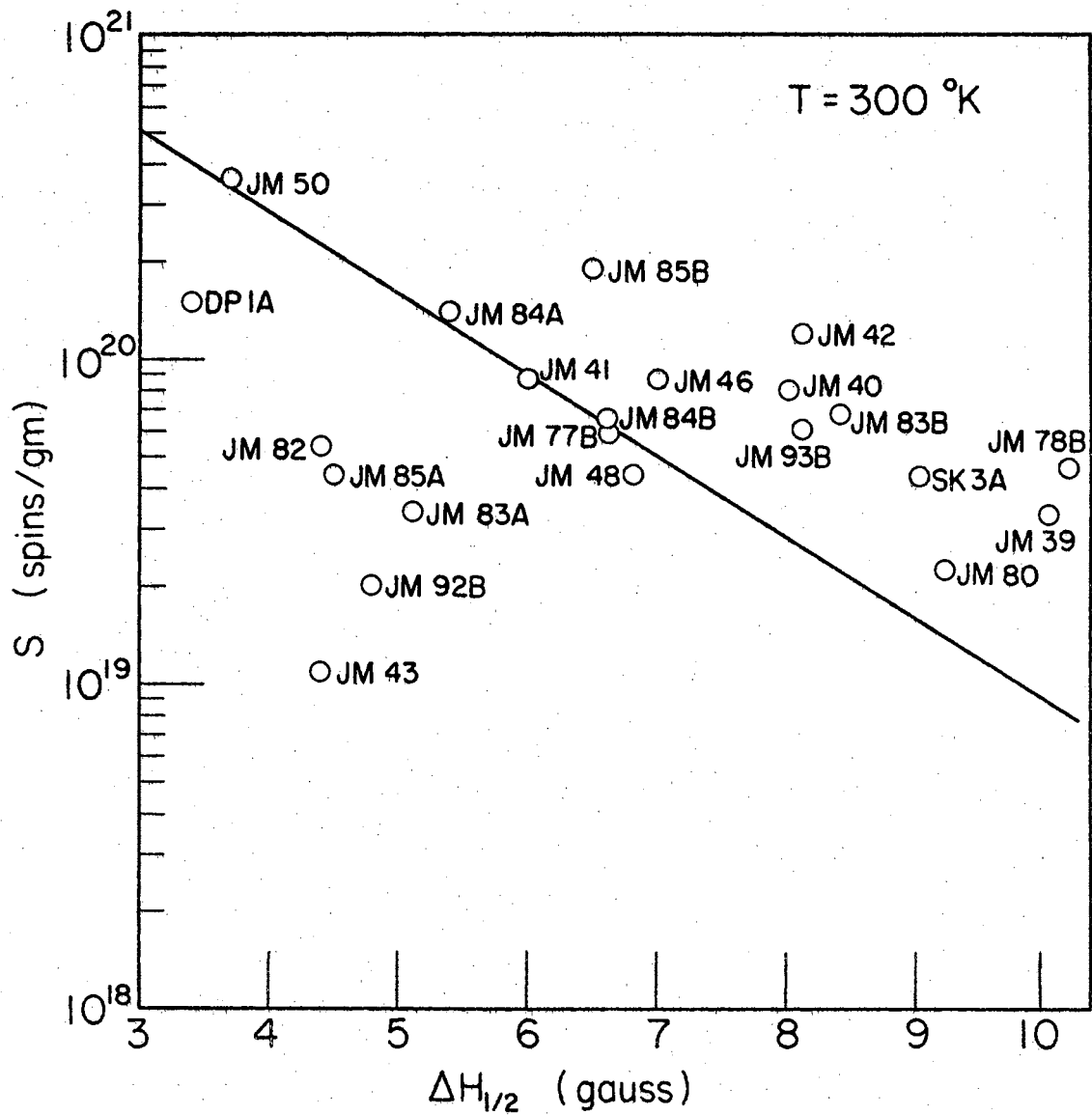


Figure 25. Correlation of Unpaired Spin Concentration with Peak to Peak Signal Half Width

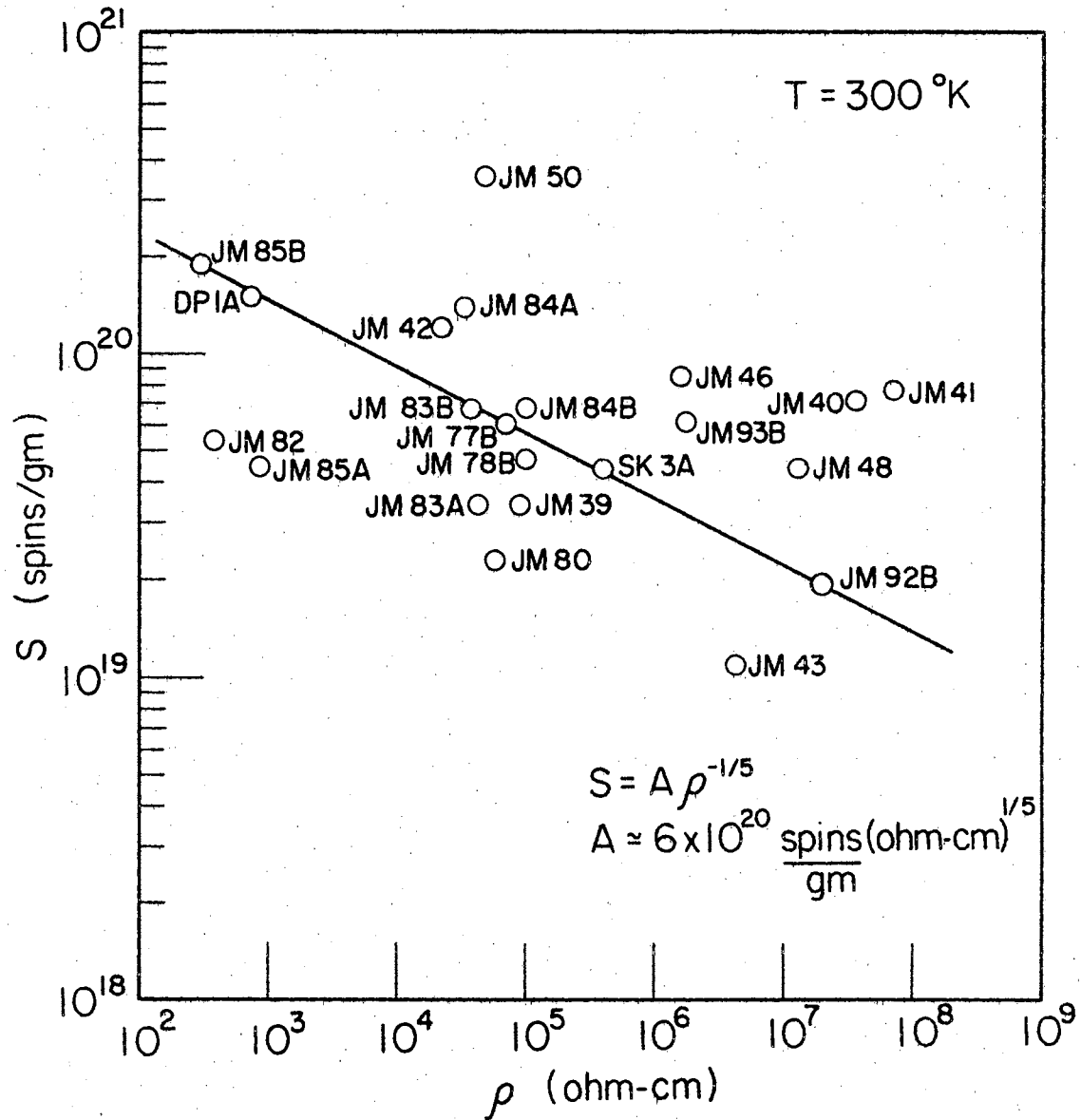


Figure 26. Correlation between Spin Concentration and Charge Carrier Concentration

behavior, one can obtain an activation energy for the formation of unpaired spins. The observed susceptibility of the present polyacene quinone radical polymers appears to vary with temperature in a manner interpretable for most polymers simply as that obeying a Boltzmann distribution (21, 22), both as to birth of unpaired spins and as to their alignment with the field, e. g.

$$S = S_0 \exp(-E_s/kT), \quad (30)$$

where S is the number of spins per gram and E_s is the spin activation energy.

We have seen earlier in this chapter that the number of spins detected is proportional to the area under the absorption curve. In particular, for a Lorentzian shape, we saw [Eq (26)] :

$$S = 1.63 G h_0 x_0^2 .$$

Now, it is actually the magnetic susceptibility which is being detected and plotted by the spectrometer. In reality, then, the above should be written as:

$$\chi = \text{Const } h_0 (\Delta H_{1/2})^2 ; \quad (31)$$

where $\Delta H_{1/2} = 2x_0$. Calling $(h_0 \Delta H_{1/2})^2$ an area, A , then:

$$\chi = \text{Const } A . \quad (32)$$

Since χ is assumed temperature dependent according to the Curie law [Eq (8)], we have, upon substitution of Eq (30) into Eq (8) and using Eq (32):

$$\chi(T) = \frac{S_0 g \beta}{4kT} \exp(-E_s/kT) = \text{Const } A(T) \quad (33)$$

Thus:

$$\chi_{2u}/\chi_{1u} = (T_1/T_2) \exp \left[-\frac{E_s}{k} \left(\frac{1}{T_2} - \frac{1}{T_1} \right) \right] = A_{2u}/A_{1u}; \quad (34)$$

where the subscript, u, designates the signal of the unknown. Later the subscript s will be used to refer to the standard sample.

For nonactivated spin processes, Eq (34) becomes

$$\chi_{2u}/\chi_{1u} = T_1/T_2. \quad (35)$$

Hence, Eq (35) gives the theoretical limit for the change in susceptibility with temperature. For the case at hand, $T_2 = 77^\circ\text{K}$, and $T_1 = 300^\circ\text{K}$. Thus, $\chi_{2u}/\chi_{1u} = 3.89$ is the Curie limit.

A DPPH standard was examined at 300°K and 77°K , with the calculated susceptibility ratio being found as:

$$\chi_{2s}/\chi_{1s} = (A_{2s}/A_{1s})_{\text{std}} = 4.1,$$

or about 5% greater than the theoretical value. This is well within the experimental expectations for this particular method of determining spin concentrations (i. e., by comparing areas).

Returning to the discussion of activated spin states, from Eq (34) one finds the activation energy to be:

$$E_s = 8.9 \times 10^{-3} \log_e \left[\frac{\chi_1 T_1}{\chi_2 T_2} \right]. \quad (36)$$

Since $\chi_1/\chi_2 = A_1/A_2$ and $T_1/T_2 = 300/77 = 3.89$, we then have:

$$E_s = 8.9 \times 10^{-3} \log_e \left[3.89 A_{1u}/A_{2u} \right] \text{ (eV)}, \quad (37)$$

where $A_{1u} \equiv A_u(T_1) = \left[\frac{\Delta H_{1/2}^2}{h \nu} \right]_{u, T_1}$. After obtaining E_s ,

the spin density at T_2 may be calculated with the aid of Eq (30), i. e.,

$$S_{2u}/S_{1u} = \exp \left[-\frac{E_s}{k} \left(\frac{1}{T_1} - \frac{1}{T_2} \right) \right], \quad (38)$$

or for the particular temperatures involved in this study:

$$S_{2u} = S_{1u} \exp \left[-1.123 \times 10^2 E_s \right] \quad (39)$$

where E_s is in eV.

An alternate method for obtaining spin activation energies is from a comparison of the unknown signal to the DPPH standard signal at each temperature. From Eq (27), using the same notation for area as above, we see:

$$S_{1u} = (A_{1u}/A_{1s}) S_s. \quad (40)$$

The spin signal of the standard source does not appear to be temperature dependent, so the temperature subscript is left off of S_s . Likewise for the second temperature,

$$S_{2u} = (A_{2u}/A_{2s}) S_s. \quad (41)$$

Now to obtain the activation energy, we again may employ Eq(30) at the two respective temperatures and take a ratio of the spins S_{1u} to S_{2u} . This results in:

$$E_s = 8.9 \times 10^{-3} \log (S_{1u}/S_{2u}) \quad (\text{eV}). \quad (42)$$

The spin concentrations and activation energies as calculated from both of the above methods, were found to agree to within experimental error.

Upon examining the data in Table VIII, it is apparent that a couple

of the samples (JM42 and JM80) are not properly described by a spin activation process, since the spin concentration is greater at 77°K than at 300°K. However, the actual susceptibility ratios for these samples were 4.62 and 4.36, respectively. This is not too far removed from the theoretical value predicted by the Curie law (3.89). Possibly the anomalous behavior of these two polymers is due to errors in determining the areas. (Recall that the ratio for DPPH was 4.1).

On the otherhand, it may be that the Curie law is inadequate, i. e., perhaps the Curie-Weiss law [Eq (9)] should be applied. For the case of the Curie-Weiss law, Eq (37) becomes:

$$E_s = 8.9 \times 10^{-3} \log_e \left[\frac{A_{1u}(300 - \Theta)}{A_{2u}(77 - \Theta)} \right] \text{ (eV)}. \quad (43)$$

It is seen that for $\Theta < 77^\circ\text{K}$, E_s remains defined, and positive, and as Θ increases from 0 to 77°K, E_s likewise increases. Hence, Eq(43) could also explain the anomalous behavior. Since values for Θ (assuming the existence of such for these materials) have not been determined, this discussion cannot be carried further.

It will be seen in Chapter V that examination of the dielectric constant at low temperatures indicates an anomalous behavior for several polymers in the temperature range of $\sim 150^\circ\text{K}$ to $\sim 200^\circ\text{K}$. Hence, it may be that a modified form of Eq (43), allowing Θ to be larger than 77°K could be used.

Although no mobility measurements were made in this study, previous measurements of mobility and ESR spectra on PAQR polymers

tend to indicate that the spin densities exceed the carrier density by some few hundred. This is also expected from a comparison of the activation energies for the two phenomena.

Molecular Length. Since macromolecules showing appreciable inherent conduction are generally insoluble, it is not easy to make determinations of the chain length by the various usual osmotic, viscosimetric, light-scattering, or related means in solution. Pohl, et.al. (21, 39, 45), have suggested one method, making use of the temperature variation of ESR response, which gives an approximate value for the effective molecular lengths of the conjugated regions giving birth to the unpaired spins. If one assumes that the activation energy of unpaired spins, E_s , is equal to the energy 1E to promote an electron from the highest occupied molecular orbital (HOMO) to the lowest empty molecular orbital (LEMO), and that in turn the unpairing energy is small so that ${}^1E \simeq {}^3E$, then one can use the free-electron model approximation (which should be a good approximation here) to estimate the orbital domain length, i.e., the effective linear segment length of ekaconjugation. Then:

$$E_s \simeq {}^1E = h^2 / 4mL_0z \simeq {}^3E, \quad (44)$$

where h is Planck's constant, m is the electron mass, L_0 is the C-C bond length, and z is the number of successively ekaconjugated C-C bonds in the linear segment. Putting the proper values into Eq(44) yields E_s in eV as:

$$E_s \simeq 38.4/z \text{ (eV)}. \quad (45)$$

Hence, after determining E_s , one calculates z from Eq (45) and the effective linear segment length L by:

$$L = 1.4 z (\text{\AA}), \quad (46)$$

where $L_0 = 1.4 \text{\AA}$ is the C-C bond length. Eq (46) assumes a linear chain.

If the molecule were a string of fused benzenoid rings, each carbon bond would have a linear projected length of $L_0 \cos 60^\circ = 1.21 \text{\AA}$, and thus:

$$L = 1.21 z (\text{\AA}). \quad (47)$$

Using the spin activation energies determined, the overall maximum chain lengths are calculated from Eq (47), since it is more appropriate for polymers than the linear form of Eq (46). The "molecular lengths" range from 1400\AA to $46,000 \text{\AA}$ for the polymers examined. This is in rather good agreement with the chain lengths calculated from the field-dependence of the conductivities in these polymers as discussed in Chapter III. The lengths, as determined by the two methods, are compared in Table IX.

Summary

ESR measurements as a function of temperature, pressure, pre-heating, and ambient gas have been made on several PAQR polymers, a Cu-coordination complex, and a Schiff's base polymer. Specifically, 24 polymers were examined in vacuo at room temperature after considerable outgassing, and 14 were examined at liquid N_2 temperature.

The observed spin concentrations correlate with the observed conductivity as reported in Chapter III, indicating the conjugated molecules are a common source for unpaired spins and carriers. Judging from the differing activation energies for the two phenomena, the unpaired spin den-

TABLE IX

AVERAGE MOLECULAR LENGTH OF SEVERAL POLYMERS

Sample No.	Spin Activation Measurements ^(a)			\vec{E} -field- σ Measurements ^(b)
	E_s (eV)	z (Å)	L_s (Å)	$L_{\vec{E}}$ (Å)
DP1A	3.3×10^{-2}	1165	1410	1200 - 1500
JM77B	2.4×10^{-2}	1600	1935	1300 - 1800
JM85B	2.1×10^{-2}	1826	2215	1600 - 2000
JM39	1.2×10^{-2}	3200	3840	
JM43	1.0×10^{-2}	3840	4640	
JM82	9.0×10^{-3}	4280	5190	
JM46	7.0×10^{-3}	5490	6630	
JM40	5.0×10^{-3}	7670	9250	
JM48	3.0×10^{-3}	12800	15480	
JM50	3.0×10^{-3}	12800	15480	
JM41	1.0×10^{-3}	38400	46100	
SK3A				2000 - 3000
EHE102				100 - 200

(a) z and L_s are determined from Eqs (45) and (47), Chapter IV, respectively.

(b) Interpolated values from Figure 16, Chapter III.

sity is several hundred times the carrier density. The ESR spectra half-widths, $\Delta H_{1/2}$, were correlated with the spin densities, indicating a mean lifetime, \bar{T} , for free radicals ~ 0.3 to 1×10^{-8} sec. The mean spin lifetime is seen to be directly proportional to spin concentration from polymer to polymer. To within experimental error, the magnetic behavior could be fitted to the Curie form.

From the spin activation energy, E_s , one can determine an average molecular length for the pi-conjugated chain. The range of molecular lengths determined were from 1400 \AA to $46,000 \text{ \AA}$, which is in agreement with independently determined molecular lengths from E-field effects, for the same samples reported in Chapter III.

Other investigations include the effects of various gasses sorbed onto the samples. It was found that: O_2 will completely quench the spectra of a dry outgassed sample at a partial pressure of O_2 in excess of 300 cm; H_2O vapor does not effect the signal, except that its presence on the sample partially excludes the O_2 effect, i. e., the O_2 is not absorbed to the same extent on a wet sample as it is on a dry sample; and N_2 does not effect the signal, either directly, or indirectly.

High pressure effects on the ESR signal were also examined. It was found that a narrowing of the resonance absorption line together with an increase in amplitude of the line resulted, upon pressing the specimen at ~ 30 kbar when this line is compared to that observed in the unstressed sample. The ESR signal from the pressed sample was observed to return to its former width and amplitude after some time. It was further determined that pressure cycling between two fixed points enhances this effect to a greater extent, while shearing it under a uniaxial pressure reduces

its signal to a value similar to that of the initially unstressed powder sample. This effect has been attributed to a slowly reversible, induced oxygen effect, although molecular orientation is a possibility.

Suggestions for Further Studies

In order to more closely correlate the spin density and carrier density of organic polymers, it would seem that an experimental investigation of spin population and shape of the ESR line under pressure would be in order. This particularly suggests itself after the present brief investigation of pressure effects. Since the conductivity is also a function of applied pressure, one could develop a cell which would allow both the ESR spectra and the conductivity to be measured simultaneously while varying the pressure on the sample. In this way, one could observe direct pressure effects on a clean specimen, free from O₂ effects as experienced in this study.

Also, since the conductivity has been shown to be related to the spin concentration, together with the polarization measurements (to be discussed in the next chapter), it would seem in order to carefully examine the spin signal as a function of temperature in some continuous or nearly continuous manner. At least, in view of the anomalous behavior of several samples reported in this chapter, it would be well to monitor the spins at as many fixed temperature points as possible. If one is to use the pressure cell mentioned in the first paragraph, then one could observe continuous pressure and temperature effects on the ESR signal and on the conductivity directly and simultaneously. These experiments should aid considerably in assigning proper mechanisms to conduction and polarization phenomena.

CHAPTER V

HYPERELECTRONIC POLARIZATION

Polarization

From a phenomenological approach, polarization is a macroscopic term generally associated with a dielectric material, i.e., a material which increases the charge storage capability of a capacitor when inserted between the metallic electrodes. This increase of storage capacity is accomplished by the neutralization of charges at the electrode surfaces which would normally contribute to the external field. The application of an external \vec{E} -field to a dielectric separates the positive and negative charge centers and results in electrical and mechanical distortion of the material. Under the influence of the \vec{E} -field, dipole chains are formed which tend to bind counter charges with their free ends at the metallic electrodes.

The electric polarization vector, \vec{P} , is defined in terms of the bound charge density of a material as (MKS units):

$$\vec{P} = \vec{D} - \epsilon_0 \vec{E}, \quad (1)$$

where \vec{D} is the dielectric displacement vector associated with the true, or total charge concentrated on the body (bound charge plus the free charge); \vec{E} is the electric field intensity vector associated with the

free charge; and ϵ_0 is the dielectric constant or permittivity of free space.

We define the electric susceptibility, χ_e , as the ratio of the bound charge density to the free charge density, i. e.,

$$\chi_e = \frac{1}{\epsilon_0} \frac{d\vec{P}}{d\vec{E}} \quad (2)$$

or:
$$\vec{P} = \chi_e \epsilon_0 \vec{E}. \quad (3)$$

Comparing Eq (3) with Eq (1), it is seen that:

$$\chi_e = \frac{|\vec{D}|}{\epsilon_0 |\vec{E}|} - 1. \quad (4)$$

Now, for isotropic bodies,

$$\vec{D} = \epsilon \vec{E}, \quad (5)$$

where ϵ is the permittivity of the dielectric. Hence,

$$\chi_e = \frac{\epsilon}{\epsilon_0} - 1 = \epsilon_r - 1, \quad (6)$$

where ϵ_r is the relative dielectric constant or relative permittivity of the dielectric media. In terms of ϵ_r , Eq (3) becomes:

$$\vec{P} = (\epsilon_r - 1) \epsilon_0 \vec{E}. \quad (7)$$

From a molecular approach, the polarization vector, \vec{P} , is defined as the dipole moment per unit volume by:

$$\vec{P} = N \vec{\mu}_a, \quad (8)$$

where N is the number of elementary particle dipoles interacting with the \vec{E} -field, and $\vec{\mu}_a$ is the average dipole moment. The dipole moment is proportional to the localized \vec{E} -field acting on the particle, i. e.,

$$\vec{\mu}_a = \alpha \vec{E}, \quad (9)$$

where α is the polarizability, and \vec{E} is the average local \vec{E} -field.

Thus, Eq (9) substituted into Eq (8) yields:

$$\vec{P} = N\alpha\vec{E}. \quad (10)$$

Comparing Eq (10) to the macroscopic form for \vec{P} , as given by Eq (3),

$$\vec{P} = \chi_e \epsilon_0 \vec{E},$$

it is seen that the two approaches are linked together, in terms of the macroscopic electric susceptibility and the externally applied \vec{E} -field, and the molecular quantities N , α , and \vec{E} . In general, $\vec{E} \neq \vec{E}$ due to polarization of the surrounding media.

In 1850, Mosotti (53) developed a relation between the molecular quantities and the macroscopic quantities by assuming the dielectric media to be continuous outside a spherical region of finite domain in the immediate proximity of a test molecule. He further assumed the system to be dilute, and as such, the contribution of other molecules within the domain of the test molecule could be neglected. The Mosotti equation relates the local average field, \vec{E} , to the macroscopic applied field, \vec{E} , as:

$$\vec{E} = \frac{\vec{E}}{3} (\epsilon_r + 2). \quad (11)$$

Substitution of Eq (11) into Eq (10) and equating to Eq (7) yields:

$$\frac{N\alpha}{3\epsilon_0} = \frac{\epsilon_r - 1}{\epsilon_r + 2}. \quad (12)$$

For very dilute systems, $\epsilon_r \approx 1$, and thus, $\epsilon_r + 2 \approx 3$. Hence,

Eq (12) becomes:

$$\frac{N\alpha}{\epsilon_0} \approx \epsilon_r - 1 = \chi_e. \quad (13)$$

The Mosotti equation was modified by Clausius in 1879 to account for the dependence of polarization on the density of the media. The number of molecules per mole is the Avogadro number,

$$N_o = NM/d, \quad (14)$$

where M is the molecular mass, and d is the density. Substituting Eq (14) into Eq (12) gives:

$$\frac{N_o \alpha}{3} = \left[\frac{\epsilon_r - 1}{\epsilon_r + 2} \right] \frac{M}{d} . \quad (15)$$

Eq (15), known as the Clausius-Mosotti equation, gives the polarizability per mole, rather than per unit volume.

Polarization Mechanisms

The previous discussion on polarization has been limited to D. C. \vec{E} -fields only. When A. C. \vec{E} -fields are applied to dielectric materials, it is found, in general, that the polarization, and hence, the dielectric constant, decreases with increasing frequency. Furthermore, the polarization does not decrease smoothly, but rather in a stepwise fashion as shown in Figure 27. There are, in general, four regions of polarization: interfacial polarization, dipolar or orientation polarization, atomic polarization, and electronic polarization (labeled in Figure 27 as A, B, C, and D, respectively). Each of these polarization mechanisms, dominant in a particular frequency region, are characterized by a relaxation time τ , as indicated.

In addition to the four polarization mechanisms mentioned above,

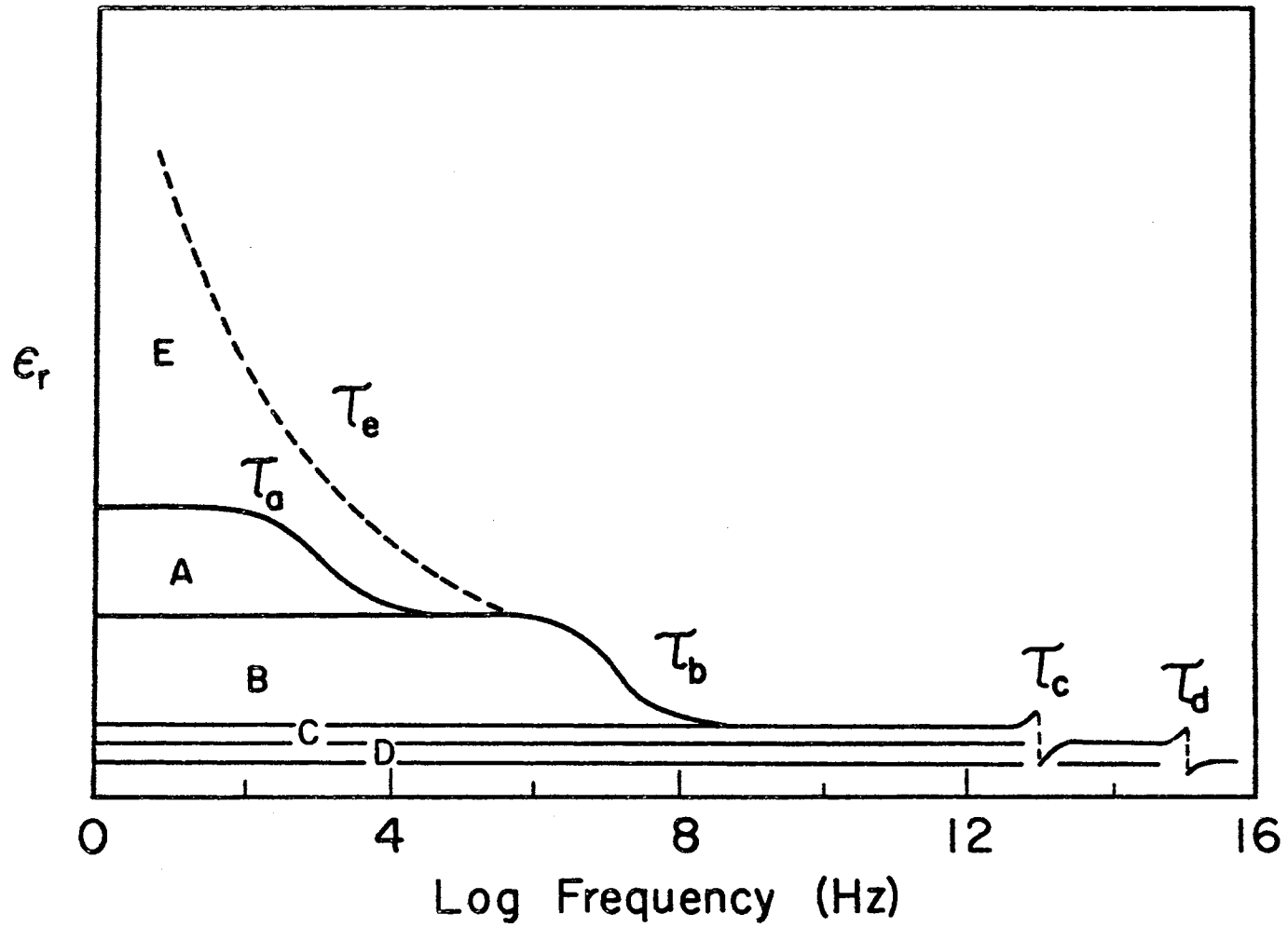


Figure 27. Schematic Diagram of Electrical Polarization Mechanisms: (A) Maxwell-Wagner; (B) Dipolar; (C) Atomic; (D) Electronic; and (E) Hyper-electronic

a new type has been suggested, that of "hyper-electronic" polarization (labeled in Figure 27 as E). As was mentioned in Chapter I, Rosen and Pohl (38, 39) first suggested this model to account for the unusually high dielectric constants observed in polymeric semiconductors. These polarization mechanisms will be briefly discussed in what follows (Cf. Figure 27).

Electronic Polarization

Electrically speaking, matter consists of positively charged nuclei surrounded by negatively charged electron clouds. When an \vec{E} -field is applied, the electronic cloud is shifted, resulting in an elongated electronic orbit. This type of polarization usually results in a bulk polarizability which is linearly proportional to the applied \vec{E} -field and exhibits dispersion at $\approx 10^{15}$ Hz (or a relaxation time $\tau \approx 10^{-15}$ sec).

Atomic Polarization

Atoms which form molecules or crystals normally do not share their electrons symmetrically if atoms of several different kinds are involved. This asymmetrical charge distribution causes some atoms to be positively charged, while others are left negatively charged. When an \vec{E} -field is applied, a displacement of these charged atoms within the molecule results, and is known as atomic polarization. It exhibits dispersion at $\approx 10^{13}$ Hz or $\tau \approx 10^{-13}$ sec.

Dipolar Polarization

In addition to the above effects of asymmetrical charge distribution, it also gives rise to the existence of permanent dipole moments, which are present in the absence of an \vec{E} -field. Hence, application of an \vec{E} -field results in the alignment of these dipoles, and is known as dipolar or orientation polarization. Dispersion occurs at $\approx 10^7$ Hz or $\tau \approx 10^{-7}$ sec.

Interfacial Polarization

Interfacial polarization (Maxwell-Wagner) involves the storage of ions at the interfaces between crystals or grain boundaries, or between substances of different compositions. It is a "long range" effect, where the other types mentioned above are microscopic effects. When such charge is stored at an interface, a macroscopic distortion in the local \vec{E} -field results, and to an outside observer, it appears as an increase in polarization. It relaxes at $\approx 10^3$ Hz or $\tau \approx 10^{-3}$ sec.

Hyperelectronic Polarization

Hyperelectronic polarization (38-43, 129), pictorially displayed in Figure 28, is considered as due to the interaction of charge pairs localized temporarily on long highly polarizable molecules ($\sim 4000 \text{ \AA}$) with an external \vec{E} -field. These highly mobile carriers, thermally produced (at points A and B in Figure 28 a) by exciting intermolecular ionization

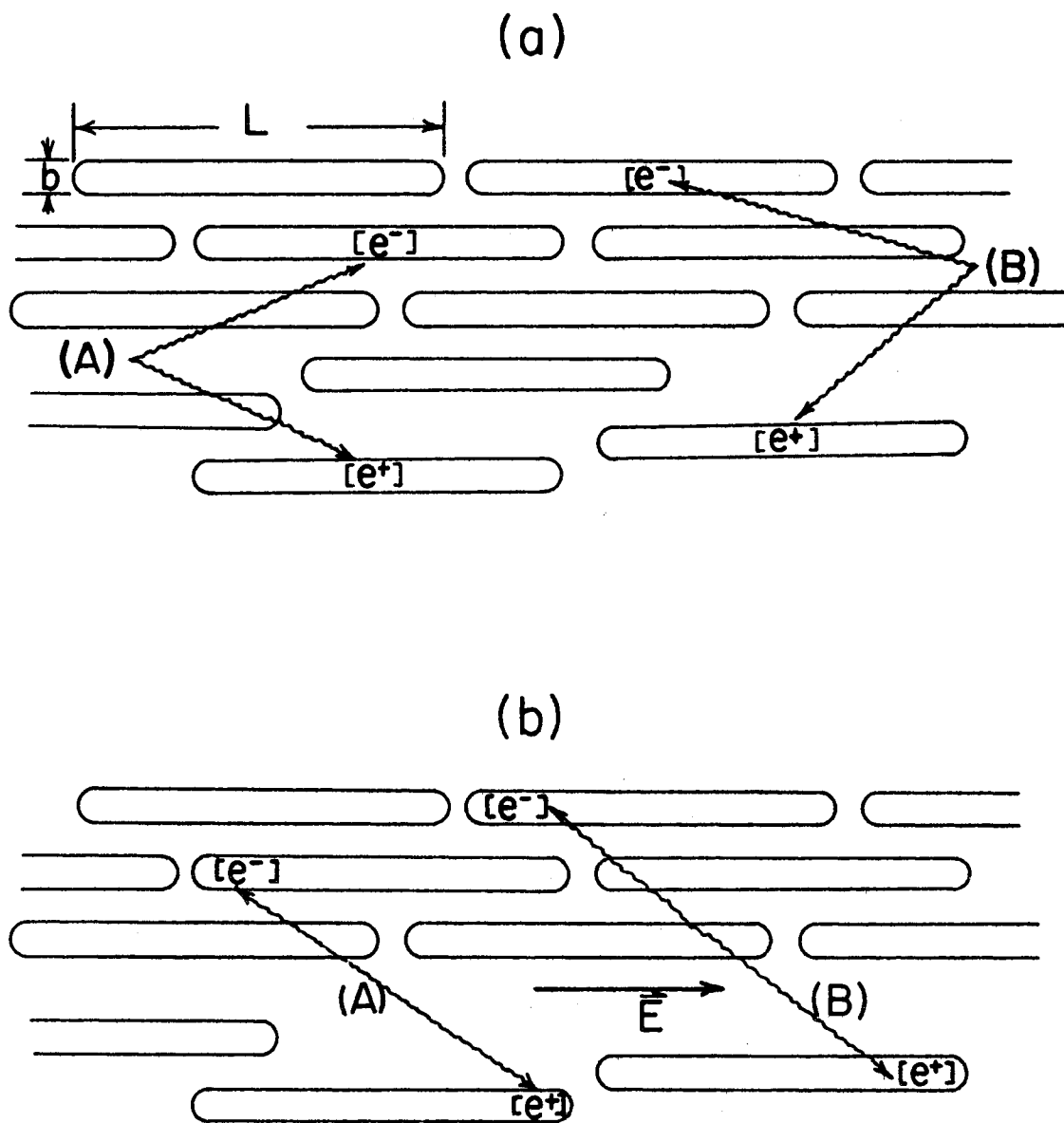


Figure 28. Schematic Diagram of Exciton and Ion Monopole Formation in Long Ekaconjugated Polymers: (a) in the Absence of; and (b) in the Presence of an External \vec{E} -field

levels of long highly conjugated molecules, lie individually in extended regions of near zero resistance (i. e., extraordinarily long sequences of associated π -orbitals), which limit the domain of the carrier to the molecular boundary.

In the absence of an external \vec{E} -field, these carriers will mutually interact to form domains of spiralled and cyclized links of polarization. There is, of course, a certain amount of delocalization of the carriers (indicated in Figure 28 a by brackets), but the overall collection exhibits a near-zero dipole moment. When an external \vec{E} -field is applied, these highly mobile carriers, spending most of their time in extraordinarily long regions of near-zero resistance, form a collection of highly polarizable monopoles, and therefore, exhibit a very high bulk polarizability. Hyperelectronic polarization is observed to be directly dependent upon temperature and pressure, and is inversely dependent upon the frequency and magnitude of the applied A.C. \vec{E} -field. Further, it exhibits dispersion near a frequency of 10^3 Hz, or $\tau \approx 10^{-3}$ sec (Cf. Figure 27). It is particularly pronounced in molecular solids composed of long polymeric molecules having extensive regions of electronic orbital delocalization. Hence, hyperelectronic polarization is a "long range" effect as is interfacial polarization.

Assuming each of the polarization mechanisms as discussed to act independently of the others, the total polarizability of a dielectric material may be written as the sum of each of the terms, i. e.,

$$\alpha = \alpha_e + \alpha_a + \alpha_d + \alpha_s + \alpha_h, \quad (16)$$

where the subscripts e, a, d, s, and h represent electronic, atomic, dipolar, surface, and hyperelectronic polarization, respectively.

Up to this time, it has been assumed that ϵ is a real quantity. This is true for D.C. measurements, but for A.C. studies, in a lossy dielectric, a phase shift results between the external driving \vec{E} -field and the resulting polarization. In order to account for such effects, one normally treats the dielectric constant, and hence α , as complex, i. e.,

$$\tilde{\epsilon}_r = \epsilon'_r - i \epsilon''_r; \quad (17)$$

and thus Eq (17) and (10) become:

$$\vec{P} = (\tilde{\epsilon}_r - 1) \epsilon_0 \vec{E} = N \tilde{\alpha} \vec{E}. \quad (18)$$

The imaginary part of Eq (17) is related to the loss current in the media as $\sigma = \omega \epsilon''_r$, while the real part (ϵ'_r) is related to the storage of charge (capacitance).

Literature Review

Concerning materials which exhibit unusually large polarizabilities, or dielectric constants, a search of pertinent literature reveals they may be generally classified into two groups. On the one hand are the ferroelectric materials which exhibit high bulk polarizability; while on the other hand are the artificial dielectrics, composed of two or more different "phases" of materials, which exhibit high polarizability due to grain boundaries (interfacial polarization). Exceptions to this rule are the organic macromolecular solids which have been reported to

possess large bulk dielectric constants, due to "hyper-electronic" polarization (38-43, 129).

Ferroelectrics

Ferroelectricity is the spontaneous electric polarization or alignment of electric dipoles within a material by mutual interaction. Characteristic ferroelectric materials which have been identified include Rochelle salt; potassium sodium tartrate, found to be ferroelectric by Valasek in 1921 (130); potassium dihydrogen phosphate and potassium dihydrogen arsenate, by Busch and Scherrer (131) in 1935; and barium titanate by Wainer and Salomon in 1942 (132) and by von Hippel and coworkers at M.I.T. in 1943 (133); additional titanates have been found by Matthias (134-138). There are now ca. 100 known ferroelectrics (52).

A ferroelectric material exhibits both spontaneous electric polarization and hysteresis effects of the polarization with respect to the applied \vec{E} -field, within specific temperature ranges. The upper temperature limit of these observations is called the Curie temperature, above which the ferroelectric obeys the Curie-Weiss law (discussed in Chapter IV), i. e.,

$$\epsilon = \epsilon_0 + \frac{C}{T - T_c} \quad (19)$$

In the vicinity of the Curie temperature, the dielectric constant becomes very large.

Since the dielectric constant exhibits an anomaly at the transition temperature and is \vec{E} -field dependent due to the observed hysteresis

effects, investigators normally study ϵ_r as a function of T or \vec{E} . However, recent investigations have been made as to the frequency dependence of ϵ_r for many ferroelectrics. In general, an anomalous dispersion is observed at the Curie temperature. In polycrystalline media, ϵ_r is observed to decrease with frequency systematically.

Multiphase Materials

For almost 100 years, it has been recognized that the anomalous dispersion in the conductivity and dielectric constant exhibited by certain polycrystalline or amorphous materials is due to the presence of impurities, grain boundaries, or voids which exhibit considerably different σ 's and ϵ_r 's than the bulk material.

Theoretical Models. Maxwell (139), employing a simple inhomogeneous two layered dielectric model consisting of plane sheets of materials possessing differing σ 's and ϵ_r 's, was able to qualitatively explain the anomalous behavior actually observed in real dielectrics. Of course, this is a purely phenomenological approach, and in many cases, Maxwell's simple model does not do much more than indicate a trend in the dispersion. One can, however, extend the two layered model to an n-layered model, and greatly improve the agreement of the theory with observed results.

Following Maxwell's two layered model, Wagner (140) assumed an inhomogeneous dielectric to be composed of an insulating matrix with spherical conducting particles dispersed throughout the matrix. In such

a manner, an improvement was made on the agreement between the theoretical model and the observed dispersion.

In 1937, Sillars (59), in an attempt to explain the lack of agreement of the "Maxwell-Wagner" model with observed results on a water-wax suspension, extended the model to include spheroidal particles (from flat dish types to elongated needle types) dispersed in an insulating matrix.

Equivalent Circuit Characterization. On the basis of the success of the Maxwell-Wagner, or the Maxwell-Wagner-Sillars phenomenological models, it has become quite customary for investigators to automatically treat the dispersion observed in multiphase systems in terms of such.

Consider, for example, a capacitor consisting of a set of parallel plate electrodes, filled with an inhomogeneous dielectric as shown in Figure 29 a. Here, the inhomogeneity could be due to either the grain boundaries, the voids or air gaps, or a thin insulating oxide layer surrounding the bulk particles. An enlarged view of a section of the dielectric is shown in Figure 29 b, where R_b , C_b and R_g , C_g represent the bulk and gap resistance and capacitance, respectively.

If one assumes an idealized case of cubic particles (Figure 29 c) and neglects sidewise admittance, the material may be characterized as a number of different electrical equivalent circuits as shown in Figure 29 d-f. These few cases are certainly not exhaustive. One may imagine any number of combinations of electrical parameters as long

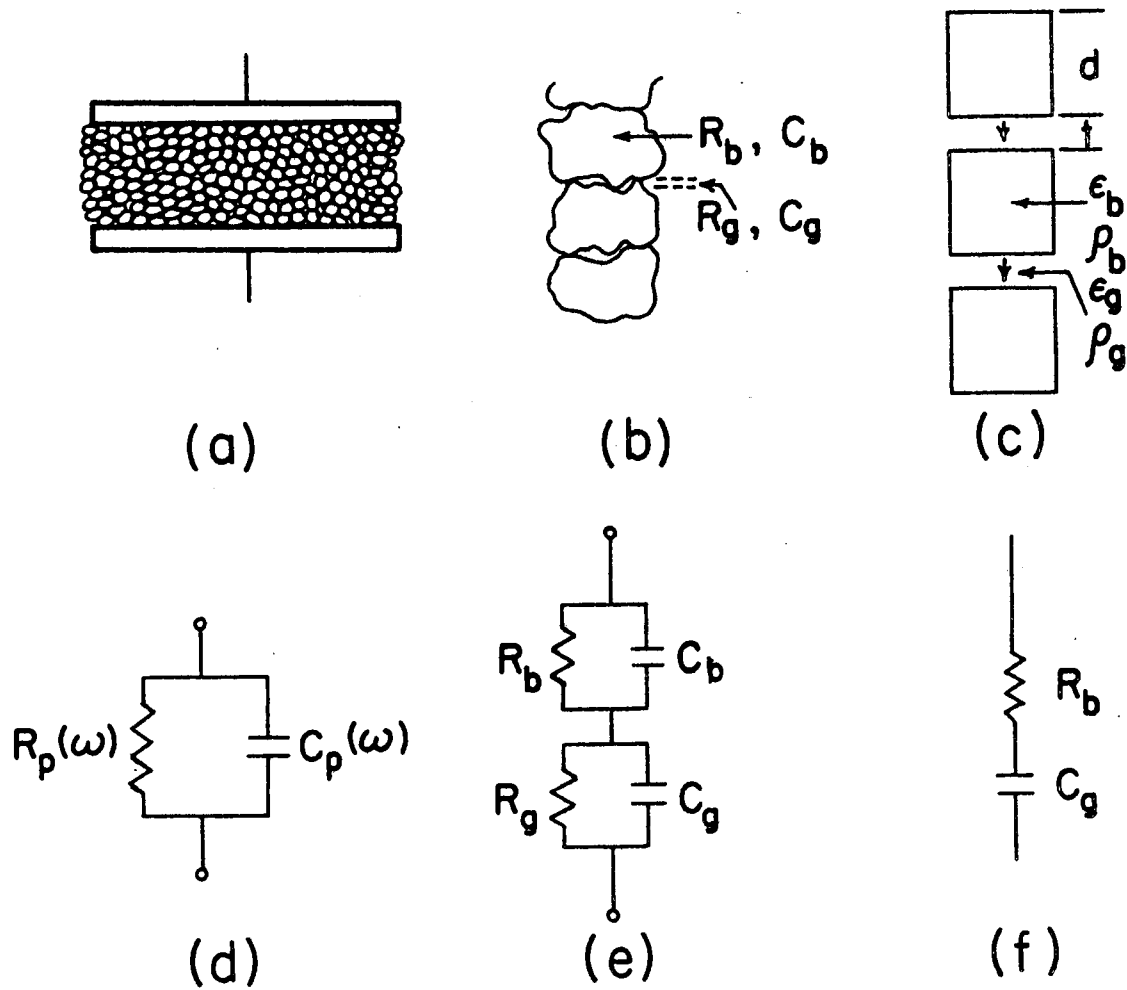


Figure 29. Equivalent Lumped Parameter Representations of a Multiphase Dielectric

as the circuits are "equivalent." Case (e) corresponds to the two layer model of Maxwell.

The equivalent circuit shown in Figure 29 d is the normal characterization of a material which exhibits dispersion, i. e., for lossy dielectrics, one normally measures the parallel resistance and capacitance. Since R_p and C_p are frequency dependent, a network transformation may be made on the circuit to relate it to the "bulk" and "surface" R and C , i. e., the surface or gap parameters may be lumped as one parallel network and the bulk parameters are similarly lumped as a second parallel network in series with the first (Figure 29 e). It can be shown that at high frequencies, for a material such that $C_g \gg C_b$ and $R_g > R_b$, $C_p(\omega) \rightarrow C_b$ and $R_p(\omega) \rightarrow R_b$ as $\omega \rightarrow 0$. [See, for example Gutmann and Lyons (52), p. 51.] A typical plot of the dispersive behavior of $R_p(\omega)$ and $C_p(\omega)$ is shown in Figure 30.

Ferrites and Oxides. A number of investigators at the N. V. Philips' Gloeilampenfabrieken in Eindhoven, Netherlands, have found unusually high dielectric constants in sintered metal oxides and ferrites. Verwey (54) found ϵ_r 's up to 2000 at room temperature and 100 Hz for a sintered disk of $\text{Ni}_{0.4}\text{Zr}_{0.6}\text{Fe}_2\text{O}_4 + 0.1\% \text{Fe}_3\text{O}_4$. Both ϵ_r and ρ indicated a dispersion similar to that shown in Figure 30. A two-phase oxide-bulk system (as in Figure 29 e) was employed to match the observed dispersion curves. The relaxation time for the dispersion was observed to be $\sim 10^{-3}$ sec. Verwey mentioned that for certain ceramic semiconductors with a rather low D.C. resistivity, the apparent di-

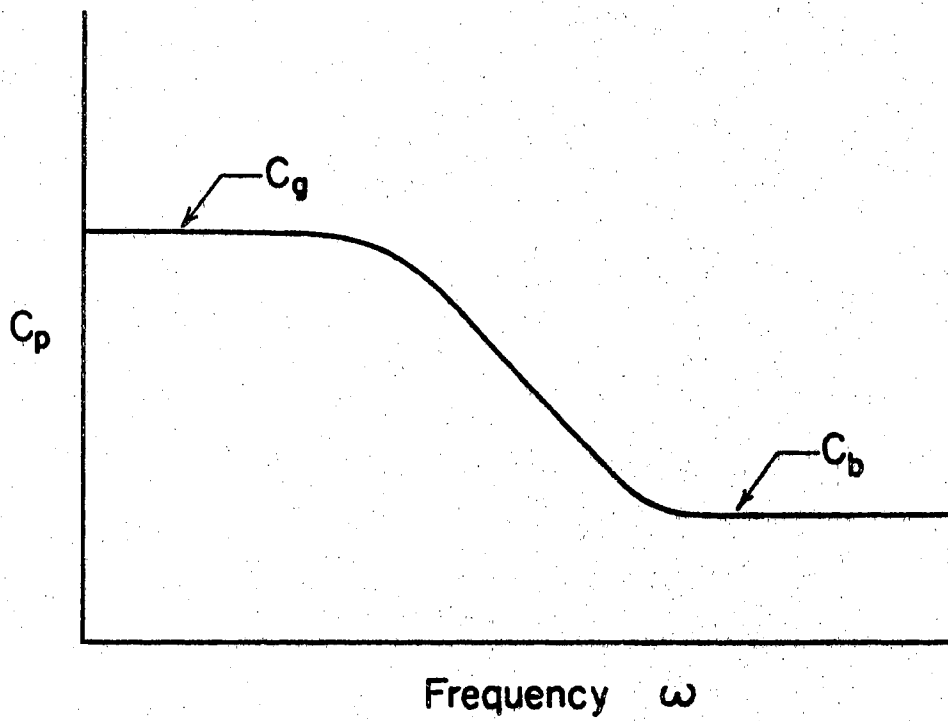
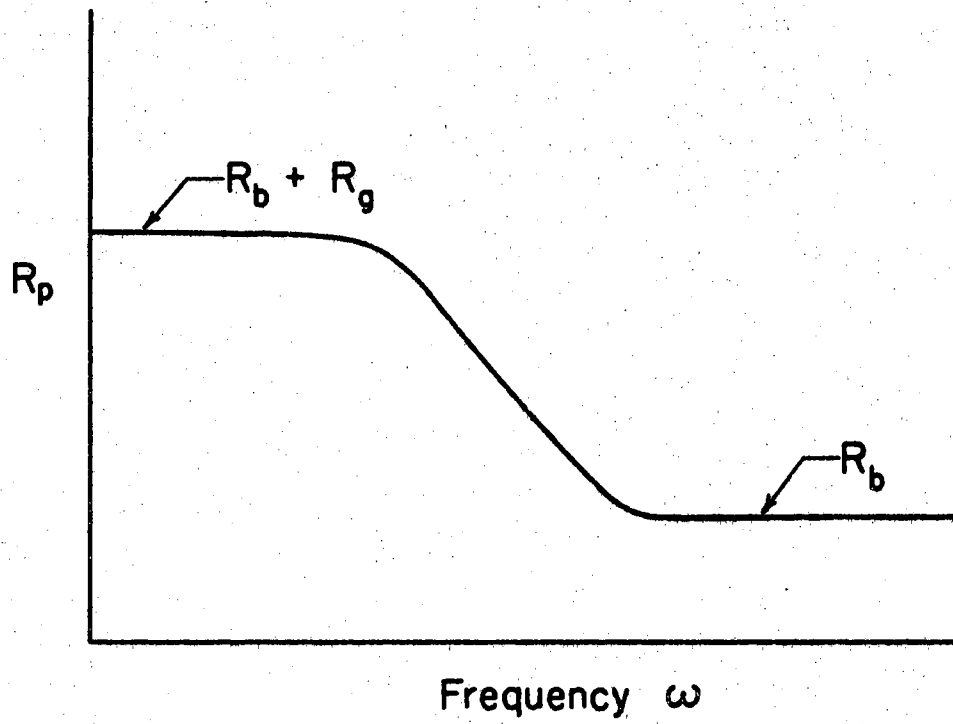


Figure 30. Theoretical Dispersion of R_p and C_p for a Multiphase Dielectric

electric constant was found to reach values as high as 10^6 .

Similar dispersive results on another ferrite, $\text{La}_{0.9}\text{Sr}_{0.1}\text{MnO}_3$ were observed by Volger (55). He reported dielectric constants as high as 3×10^5 at liquid air temperatures (91°K). A three component equivalent circuit was employed to fit the experimental dispersion curves (i. e., the capacitance of the barrier layer, C_g , was set equal to zero, leaving R_g in series with the parallel $R_b + C_b$). The oxide layer around the grains was estimated to be 20 to 30 \AA . Volger also found the conductivity was dependent on the \vec{E} -field strength applied.

Koops (56, 141) also reported high dielectric constants (up to 2000) and anomalous dispersion for a nickel zinc ferrite similar to the material studied by Verwey. He treated the dispersion in terms of the equivalent circuit of Figure 29 e, but further developed a qualitative model based on a linear inhomogeneous solid consisting of alternate layers of bulk material and insulating layers.

Other investigators which have observed similar effects in sintered ferrites and oxides include Van Uitert (60), Blechschmidt (142), Brockman, et. al. (143), Möltgen (144), and Hilborn (57). Van Uitert employed the model proposed by Koops to explain the dispersion in a number of ferrites (with ϵ_r up to 10^5), while Hilborn used a multilayer model (n-layered), and derived a relaxation distribution function for the "n" parallel combinations of R and C. Brockman, et. al., found $\epsilon_r \sim 10^5$ in a manganese zinc ferrite; and Möltgen found similar values for ϵ_r 's in copper zinc ferrites, and employed a model very similar to that of

Koop to fit the dispersion curves.

Further discussions of multiple-phase materials are given by von Hippel (53, 145). He discusses the effect of dispersing conducting particles in an insulating matrix and presents data on "thiokol," an organic polysulphide insulating matrix with zinc oxide and carbon black dispersed throughout. Dielectric constants up to 18,000 at room temperature and 1 KHz have been observed. The relaxation time for the dispersion was observed to be 10^{-6} to 10^{-7} sec.

Hence, in view of the above, it is seen that macroscopic scale Maxwell-Wagner (interfacial) polarization which depends sensitively upon the morphology of the materials present, can account for the anomalously high dielectric constants and for the unexpected dispersion as observed in multiphase materials. Furthermore, the materials can be simulated "theoretically" by curve fitting using lumped circuit equivalents with a complex of virtual resistors and capacitors in various series and parallel arrays.

Organic Materials

That organic materials, in particular highly purified polymeric semiconductors, should exhibit unusually high dielectric constants is quite surprising. Typical values for ϵ_r 's of most types of pure polymers lie in the range of 2 to 10 (53, 146).

A review of the literature fails to yield evidence of such, with the exception of that reported by Pohl and coworkers (38-43, 129). As was

mentioned in Chapter I, and earlier in this chapter, dielectric constants up to 50,000 have been observed on certain PAQR type polymers, with the polymers exhibiting anomalous dispersion, relaxing at $\sim 10^{-3}$ to 10^{-4} sec. This effect has been attributed to hyperelectronic polarization, i. e., a Maxwell-Wagner polarization on the molecular scale.

Statement of the Problem

In view of the foregoing discussion on multiphase materials, and the similarities between interfacial polarization and hyperelectronic polarization; and in view of the fact that the polymers to be studied are not single crystalline, but are rather polycrystalline in nature, one must establish in some way that hyperelectronic polarization indeed is the mechanism observed.

The purpose of this phase of the study, then, is to examine the polarizability of a number of highly purified organic polymeric semiconductors at extreme pressures and temperatures, in order to provide homogeneous, void free materials. In addition, the polarizability is examined after severe shearing of the sample under uniaxial pressure. If there is a thin oxide or other poorly conducting layer surrounding the conducting region, violent shearing of the sample should rupture this layer, and hence, change the dielectric constant and conductivity accordingly.

Also, polarization effects are observed as a function of various electrode materials, and as a function of various thicknesses and ge-

ometries for a given polymer. Dispersion of ϵ_r and ρ for the various polymers at frequencies up to 100 KHz are obtained. The effect of A.C. \vec{E} -field on ϵ_r and ρ are examined, as well as the dependency of ϵ_r upon the unpaired spin concentration.

With regard to the relaxation time of hyperelectronic polarization, the model proposed by M. Pollak (61, 62), as discussed in Chapter I, is applied to resolve the anomaly in the expected and observed relaxation times.

Experimental Apparatus and Procedure

An imperfect dielectric may be characterized in terms of a number of equivalent circuit configurations as was discussed in the last section (Cf. Figure 29). If one is to measure the A.C. conductivity and polarizability of such a material, it is necessary to assume either a parallel RC or a series RC equivalent circuit, i. e., one can measure either the equivalent series capacitance and resistance, C_s and R_s , or the equivalent parallel capacitance and resistance, C_p and R_p of the sample. The usual procedure is to measure C_s and R_s if the dielectric is of high quality (i. e., non-lossy) and to measure C_p and R_p if the material exhibits a significant degree of lossiness.

In making A.C. measurements on a dielectric, one must keep in mind that the impedance of the unknown is a complex quantity, and hence, the impressed voltage and current are out of phase. The impedance may be written as:

$$\tilde{Z}_u = Z \exp(i\Theta), \quad (20)$$

where $Z (= \sqrt{R^2 + C^2})$ is the magnitude of the complex impedance, and Θ is the phase angle. Eq (20) may also be written as:

$$\tilde{Z}_u = R_u - iX_u, \quad (21)$$

where R_u and $X_u (= 1/\omega C_u)$ represent the resistance and capacitive reactance of the unknown, respectively.

To determine R_u and C_u , the usual procedure is to employ an impedance bridge which compares the unknown impedance with a standard impedance. A simple A.C. impedance bridge is shown below. When proper balance is obtained (both the phase and amplitude of the unknown and standard impedances must be balanced), one has:

$$I_1 \tilde{Z}_A = I_2 \tilde{Z}_B \quad (22)$$

$$I_1 \tilde{Z}_s = I_2 \tilde{Z}_u. \quad (23)$$

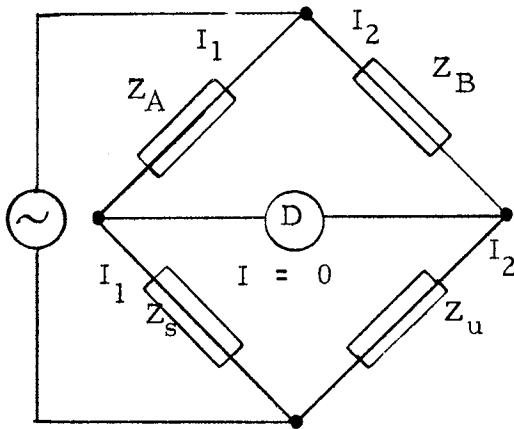
Division of Eq (22) by Eq (23)

gives:

$$\frac{\tilde{Z}_A}{\tilde{Z}_s} = \frac{\tilde{Z}_B}{\tilde{Z}_u}, \quad (24)$$

or:

$$\tilde{Z}_u = \tilde{Z}_s \frac{\tilde{Z}_B}{\tilde{Z}_A}. \quad (25)$$



Now, if \tilde{Z}_A and \tilde{Z}_B are purely resistive, i.e., $\tilde{Z}_A = R_A$ and $\tilde{Z}_B = R_B$; and furthermore, if the unknown is measured in the series mode (i.e., $\tilde{Z}_s = R_s - i/\omega C_s$), one has:

$$\tilde{Z}_u = R_B/R_A (R_s - i/\omega C_s) = R_u - i/\omega C_u. \quad (26)$$

Since the real and imaginary parts of the left and right hand side of Eq (26) must be separately equal, one has for the series mode:

$$R_u = \frac{R_B}{R_A} R_s \quad (27)$$

$$C_u = \frac{R_A}{R_B} C_s \quad (28)$$

Now for a lossy dielectric, which is to be characterized by the parallel mode, one may either employ the same bridge described for the series mode, or one may replace the standard series circuit by a standard parallel combination. In case the former is used, the unknown parallel components are found to be frequency dependent, and require several steps of calculation to yield C_u and R_u . However, the latter method would directly compare the unknown to a parallel mode standard circuit, and hence, Eqs (27) and (28) become

$$R_u = \frac{R_A}{R_B} R_p \quad (29)$$

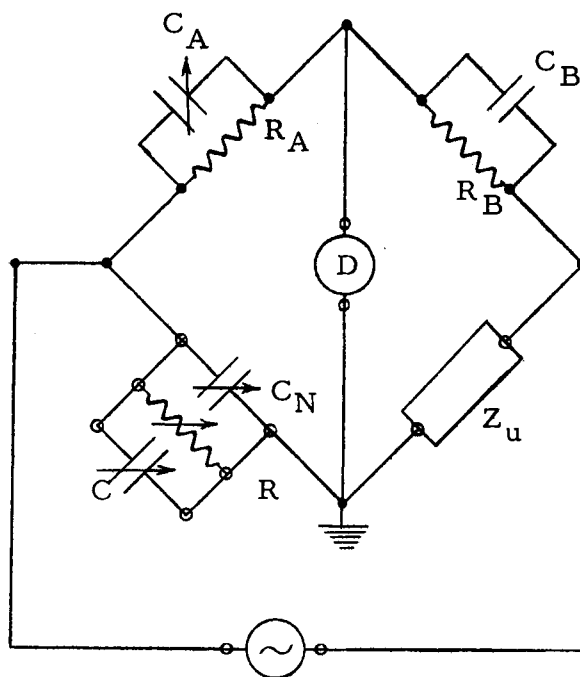
$$C_u = \frac{R_B}{R_A} C_p \quad (30)$$

The inversion in the ratio multiplier comes about from considering the admittances, \tilde{Y} , for parallel circuits rather than impedances, \tilde{Z} , as for series circuits ($\tilde{Y} = \tilde{Y}_1 + \tilde{Y}_2$, where $\tilde{Y}_1 = 1/\tilde{Z}_1$, and $\tilde{Y}_2 = 1/\tilde{Z}_2$).

The parallel mode bridge as described above is often called a comparison bridge, or a Koops (56, 141) bridge, since Koops developed and used it in his studies of ferrites as discussed earlier. For a detailed discussion of bridges, the reader is referred to Malmstadt,

Enke, and Toren (147).

The actual bridge employed in this study on A.C. electrical properties of organic semiconductors was a General Radio 716 C capacitance bridge, modified into a comparison bridge of the Koop's type. A schematic diagram of the bridge circuit is shown below. Other bridges used as auxiliary apparatus were a General Radio 1650 impedance bridge, and a General Radio 716 B capacitance bridge.




Key:

R_A, R_B, C_A, C_B, C_N = Internal (GR 716-C Bridge) components.

R_{std} = GR 1434-G precision decade (0.1Ω - $1.111110\text{ M}\Omega$).

C_{std} = GR 1434 precision decade ($50\mu\mu\text{f}$ - $1.111110\mu\text{f}$).

Z_u = Unknown impedance (parallel mode).

 = Hewlett-Packard Model 200 CD audio oscillator (0-22V RMS).


 = Hewlett-Packard Model 200 B oscilloscope.

Figure 31. Bridge Circuit for the Determination of the AC Resistivity and Dielectric Constant of Polymeric Semiconductors

To provide high pressure on the specimen while determining R_p and C_p , three different high pressure cells were employed. For low pressures (< 5 kbar), a mycalex cell similar to one employed by Rosen and Pohl (39) was used. It is shown in Figure 32. The inside bore of the mycalex container is 0.25 inch. Tungsten carbide pistons, ground flat on each end, are used to transmit the pressure onto the sample. The pressure was obtained by means of the Pasadena Hydraulic presses in our laboratory. They have been discussed in Chapter III.

The second high pressure cell used, which provides a much higher pressure on the sample has been described in Chapter III (Cf. Figure 1). Pressures of up to 20 kbar were applied to the sample while measuring the dielectric constant and the A.C. conductivity.

The third high pressure chamber used in this study was designed especially for low temperature measurements. It provides a means of locking the sample in place while maintaining a fixed pressure (up to ~ 10 kbar) on the specimen. It is then immersed in liquid N_2 or He to study the behavior of the dielectric constant at very low temperatures. Since the design and construction of this cell [Chester-Jones (68) clamp] is more pertinent to the low temperature studies reported in the next chapter (Chapter VI), it is discussed in detail there (Cf. Figure 54).

The background capacitances of the test cells employed were carefully checked by substituting blanks of mica, teflon, polyethylene, and polystyrene for the sample. During actual measurements of the

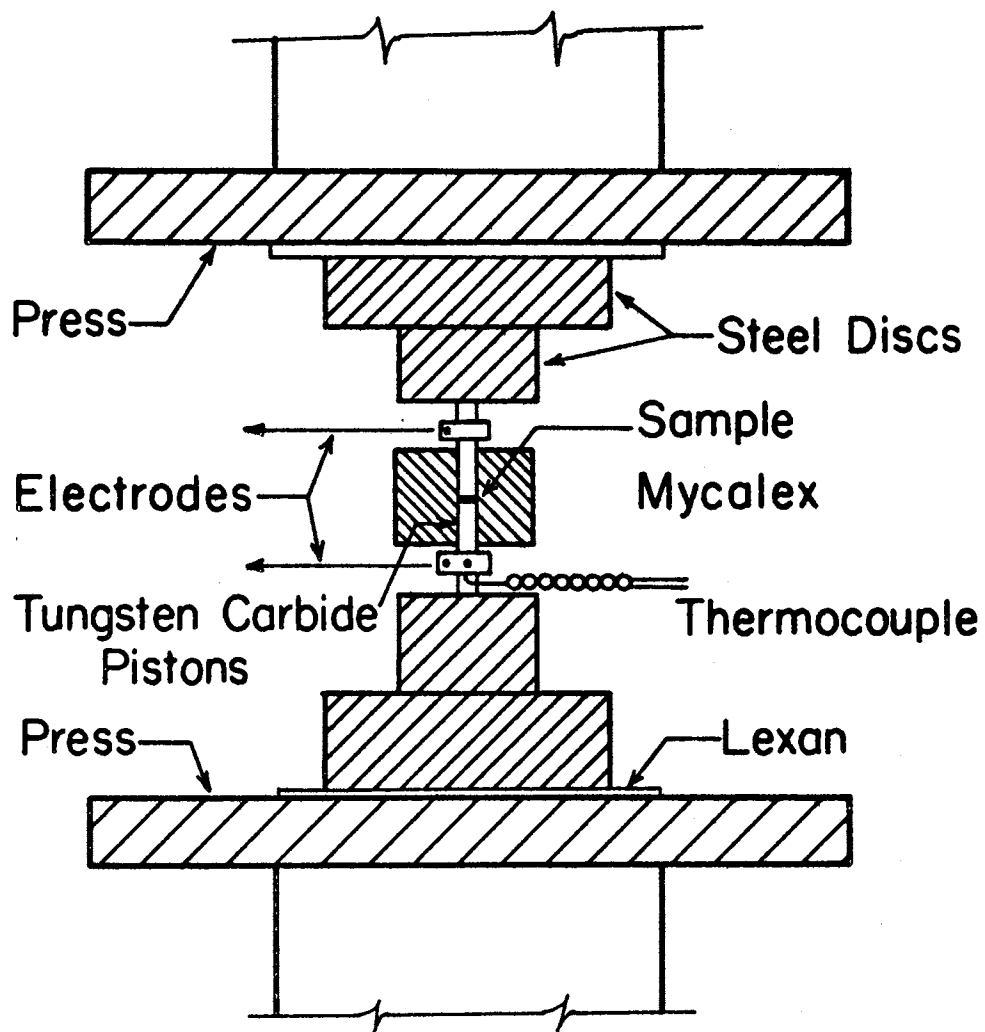
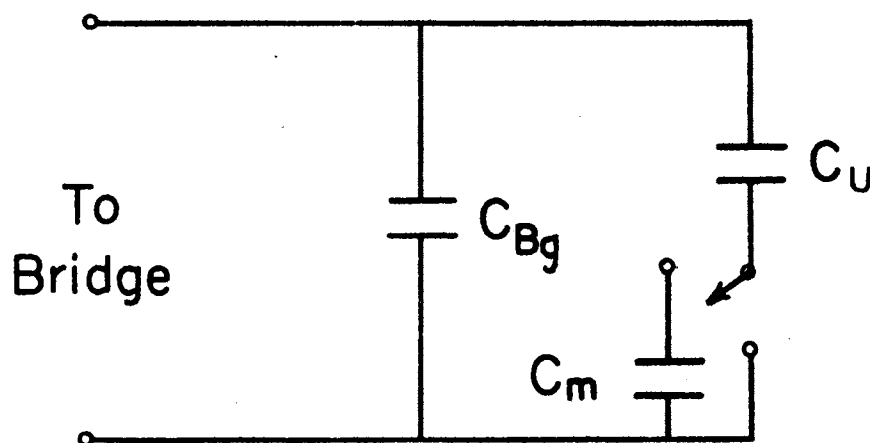


Figure 32. High Pressure Dielectric Cell

capacitance, a bridge balance was determined first with the unknown sample and then with a standard mica capacitor in series with the unknown sample. This produced two balances, from which the actual capacitance contribution of the sample could be computed free from background.

Equivalent capacitance circuits of the systems are shown below.



The initial bridge balance C_1 is given by:

$$C_1 = C_{Bg} + C_u, \quad (31)$$

where C_{Bg} is the background capacitance due to the leads and stray capacitance; and C_u is the parallel capacitance of the sample in the cell.

The second bridge balance with the mica in series yields a new value, C_2 , given by:

$$C_2 = C_{Bg} + (C_u C_m) / (C_u + C_m), \quad (32)$$

where C_m is the capacitance of the mica standard.

By subtracting Eq (32) from Eq (31) and solving for C_u , one obtains:

$$C_u = 1/2 \left\{ \Delta C \pm [(\Delta C)^2 + 4\Delta C C_m]^{1/2} \right\}, \quad (33)$$

where $\Delta C = C_1 - C_2$. The negative sign is to be avoided as it is not physically permissible. This can be seen by choosing $\Delta C \gg C_m$. In the limit as $C_m \rightarrow 0$, from Eq (32) $C_2 = C_B$ and then $\Delta C = C_u$. For Eq (33) to give the correct value, one must take the plus sign only.

Since in some cases the "in place" resistance of the sample may be quite low (<100 ohm), one must exert extreme care that the effective capacitance is being measured correctly. To make certain that such was the case, standard resistors (1%) mounted in parallel with standard mica capacitors whose nominal R_p and C_p values corresponded to the respective values as measured for the sample, were frequently substituted into the unknown arm of the bridge. The balance obtained agreed with the standard values to within 5% at 1 KHz. Below 1 KHz, the reliability drops, while it is improved at frequencies above 1 KHz.

Prior to making electrical measurements, each thoroughly dried sample, initially polycrystalline in form is premolded under high pressures (up to 20 kbar) at moderate temperatures to form a compact pellet of the specimen. The resulting dense pellet is then inserted in the respective high pressure cell, and R_p and C_p are measured with the aid of the Koop's bridge as a function of pressure, temperature, frequency, and \vec{E} -field strength. The dielectric constant and resistivity of the specimen are then determined by the relations:

$$C_p = \epsilon_r \epsilon_0 A/x, \quad (34)$$

where C_p is the parallel equivalent capacitance of the unknown as

obtained from Eq (33), A is the area, x is the thickness, and ϵ_r and ϵ_0 have been previously defined; and

$$\rho = R_p A/x. \quad (35)$$

The thickness of the sample is determined after completion of the experiment.

Results and Discussion

The observed variations in resistivity (or conductivity) and permittivity of the samples studied appear to be consistent in all respects with the proposed model of hyperelectronic polarization (38, 39). These observed effects include the electrical response of the polymers to temperature, pressure, electric field strength, and frequency of applied field. In what follows, these observed effects, which show the consistency of the data with the proposed model, shall be enlarged upon. The theory and behavior of conventional non-polar and dipolar polymers with dielectric constants ranging from 2 to 10 has been presented elsewhere (53, 145, 146, 148-151).

The model of the phenomenon of hyperelectronic polarization presented earlier in this chapter is reviewed in the following paragraphs (Cf. Figure 28). In this type of electrical polarization, one observes the response to an external electric field of an assembly of highly mobile charges lying individually in extended regions of near zero resistance (i. e., in extraordinarily long sequences of associated π -orbitals) but limited in path ultimately by the molecular boundary. The initial

charge separation is that due to normal and easily thermally excited intermolecular exciton and ion formation of long conjugated molecules. This dissociation of charge pairs creates what is in effect an assembly of highly field-sensitive monopoles.

In the absence of an external field, the monopoles will mutually interact to form domains of spiralled and cyclized links of polarization. The collection of domains will exhibit a near-zero overall moment which is easily perturbed by external fields. The field response will be non-linear for it is to be expected from the model of nearly free charges each situated on a very long domain, that small fields will already produce a large displacement of the charge and a large net dipole per charge pair. Because of the kinetic and transitory nature of the individual monopoles, a finite rate of domain reorganization is expected leading to noticeable field dependence, with low frequencies being the most effective. Furthermore, the formation, recombination, and intermolecular transfer rate of the excitons and ions, and hence the monopoles are obviously temperature and pressure dependent, as is known from conduction studies of the ekaconjugated (16, 45, 52, 152) polymers. Accordingly, one expects the degree of hyperelectronic polarization to be both temperature and pressure dependent.

The postulated hyperelectronic polarization fits the observed behavior in five respects as was shown earlier (39). The model correctly fits (1) the unusually high dielectric constants now observed for hydrocarbon derivatives ($\epsilon_r = 50$ to 50,000 compared to $\epsilon_r = 2$ to 7 normally

observed for hydrocarbon derivatives); (2) the observed field dependence both as to sign and magnitude; (3) the observed temperature dependence; (4) the observed pressure dependence; and (5) the observed frequency dependence of the dielectric constant. The present discussion will emphasize the above five aspects of fit based on further observations; and then develop a strong further argument for the concept of hyper-electronic polarization, based upon the relaxation times of polarization and conduction, and upon sample morphology.

To begin with, it is postulated that the A.C. conductivity and polarizability are functionally dependent upon the pressure, temperature, and the frequency and magnitude of the externally applied \vec{E} -field, i. e.,

$$\sigma_{AC} = \sigma(P, T, \vec{E}, \omega); \quad (36)$$

and
$$\epsilon_r = \epsilon(P, T, \vec{E}, \omega). \quad (37)$$

We discussed the dependence of σ_{DC} on P , T , and \vec{E} in Chapter III, and presented there the theoretical model developed by Pohland coworkers (16, 17, 39) [Cf. Eq (20), Chapter III]. There is no reason to suspect this model is not applicable to the case of A.C. measurements. Furthermore, if the sample is properly behaved, one may employ the dispersion relationship linking the real part of $\tilde{\epsilon}_r(\omega)$, i. e., $\epsilon_r(\omega)$, to the imaginary part, $\epsilon_r''(\omega)$, and hence to the conductivity ($\sigma = \omega \epsilon_r''$) or resistivity. By observing the effects of one variable at a time on σ and ϵ_r , while holding the others constant, one may determine analytical expressions for Eqs (36) and (37).

$\sigma(P, \omega)$ and $\epsilon(P, \omega)$

Initial studies were performed on several polymers to investigate the effect of premolding pressure and the effect of pressure variation on σ and ϵ_r as a function of ω . These measurements were made at room temperature ($T = 300^\circ\text{K}$) and under \vec{E} -field strengths of ~ 10 to 50 V/cm. From previous σ versus D.C. \vec{E} -field determinations (Chapter III), it is seen that no appreciable change in conductivity occurs for such small field variations even if the molecular length were $> 10,000 \text{ \AA}$. Hence, the \vec{E} -field is assumed constant.

Sample JM96A, a very resistive polymer ($\rho \sim 10^8$ ohm cm), was examined under two extreme conditions of premolding. The polymer was first examined without any premolding treatment, i. e., the powdered specimen was simply loaded in the mycalex cell (hereafter called Cell I), as shown in Figure 32, and the pressure was increased to 1.38 kbar. Dielectric measurements were then made at that pressure. Following this, the pressure was increased to 4.15 kbar, and the procedure was repeated. Again, at 6.92 kbar, dielectric data was taken. This data is shown in Figure 33.

A second specimen of polymer JM96A was premolded at 10.4 kbar, and was then measured at ~ 0 , 0.7, and 1.38 kbar (Cf. Figure 34). It can be seen by comparing Figures 33 and 34 that premolding at high pressures tends to eliminate the particle to particle voids of the polycrystalline sample, and thus increases the conductivity and dielectric constant.

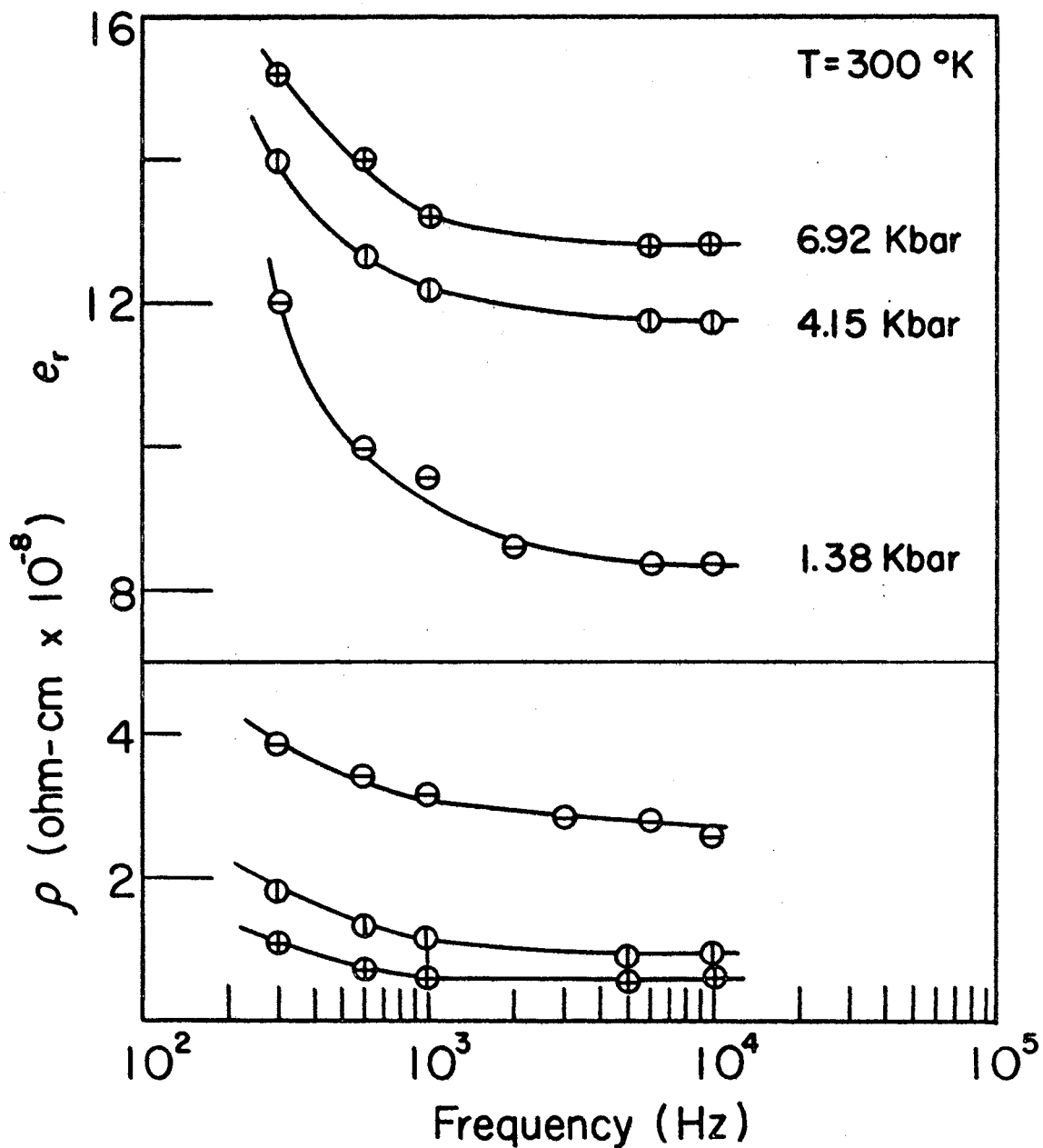


Figure 33. Pressure and Frequency Dependence of the Dielectric Constant and Resistivity for Polymer JM96A (No Premold Pressure Treatment)

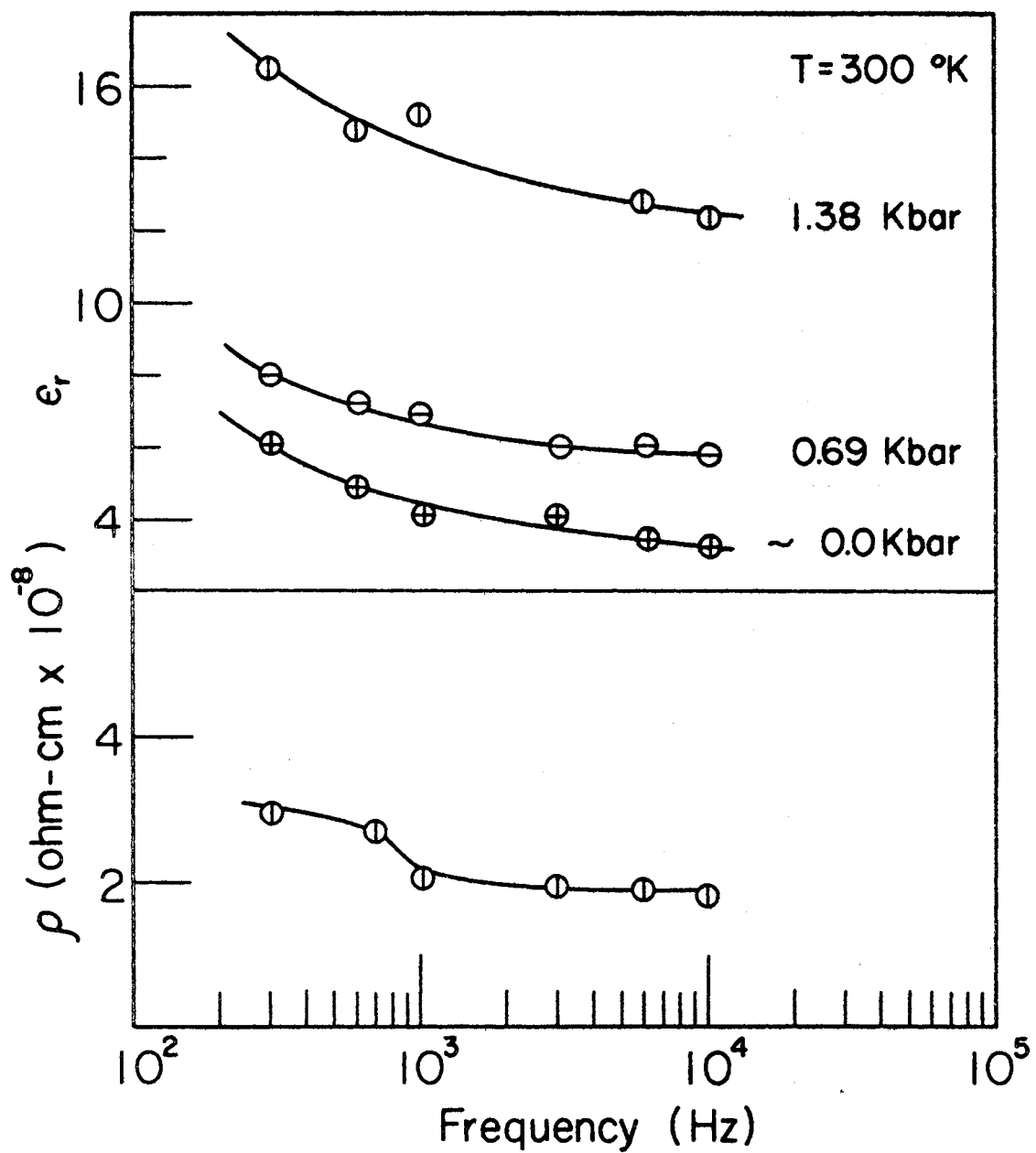


Figure 34. Pressure and Frequency Dependence of the Dielectric Constant and Resistivity for Polymer JM96A (Premolded at 10.4 Kbar)

Further studies of premolding effects on ϵ_r and ρ are shown for polymer JM77B ($\rho \sim 10^6$ ohmcm) in Figure 35. The sample was first premolded at room temperature and 9.5 kbar, after which data was taken in Cell I at room temperature and 1.4 kbar. A second specimen was then premolded at 8.12 kbar, and the above procedure was repeated at 1.4 kbar. This was again repeated on a third specimen which had been premolded at 3.4 kbar. Thus, a marked change is observed in both ρ and ϵ_r , ρ decreasing \approx by a factor of 2, with ϵ_r increasing by a like factor as the premolding pressure is increased \approx by a factor of 2.5. The density was also observed to increase with premolding pressure.

Pohl and Engelhardt (15) observed similar effects on PAQR polymers; however, the density approached a constant value at a pressure of ~ 3 kbar. In view of the behavior exhibited by these polymers, the samples were normally premolded under a pressure of 8 to 10 kbar before data was taken.

The dependence of the dielectric constant and A.C. resistivity on pressure and frequency, as measured at room temperature after exposing the sample to high pressure premolding treatment, was determined for several polymers. Figures 36 through 40 display such results. In all cases, ϵ_r is seen to increase with externally applied pressure, while ρ is seen to decrease accordingly.

This observed pressure dependence on ϵ_r may be understood by recalling that the polarization vector, \vec{P} , as defined by Eq (8) of

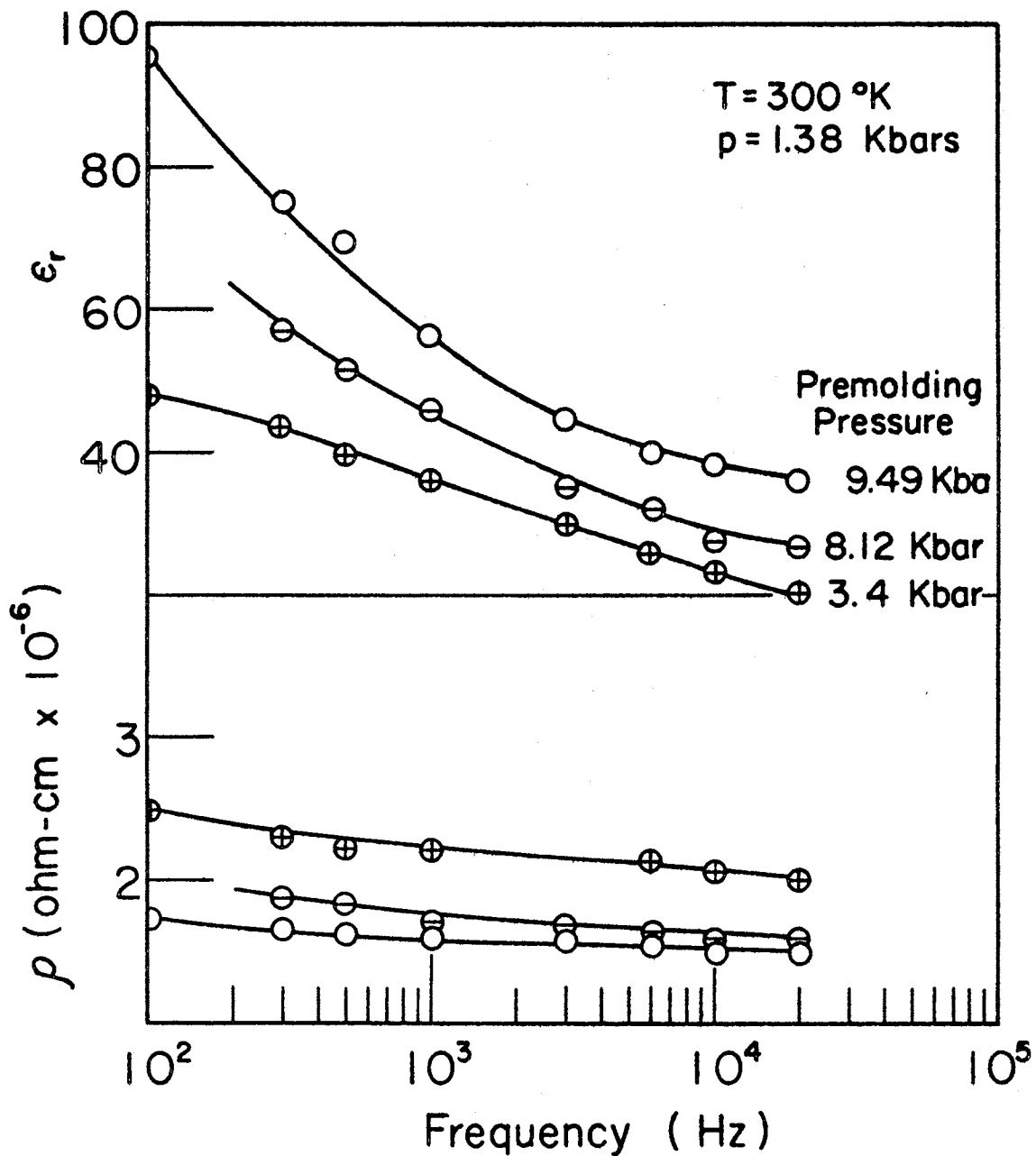


Figure 35. Premolding Pressure and Frequency Dependence of the Dielectric Constant and Resistivity for Polymer JM77B

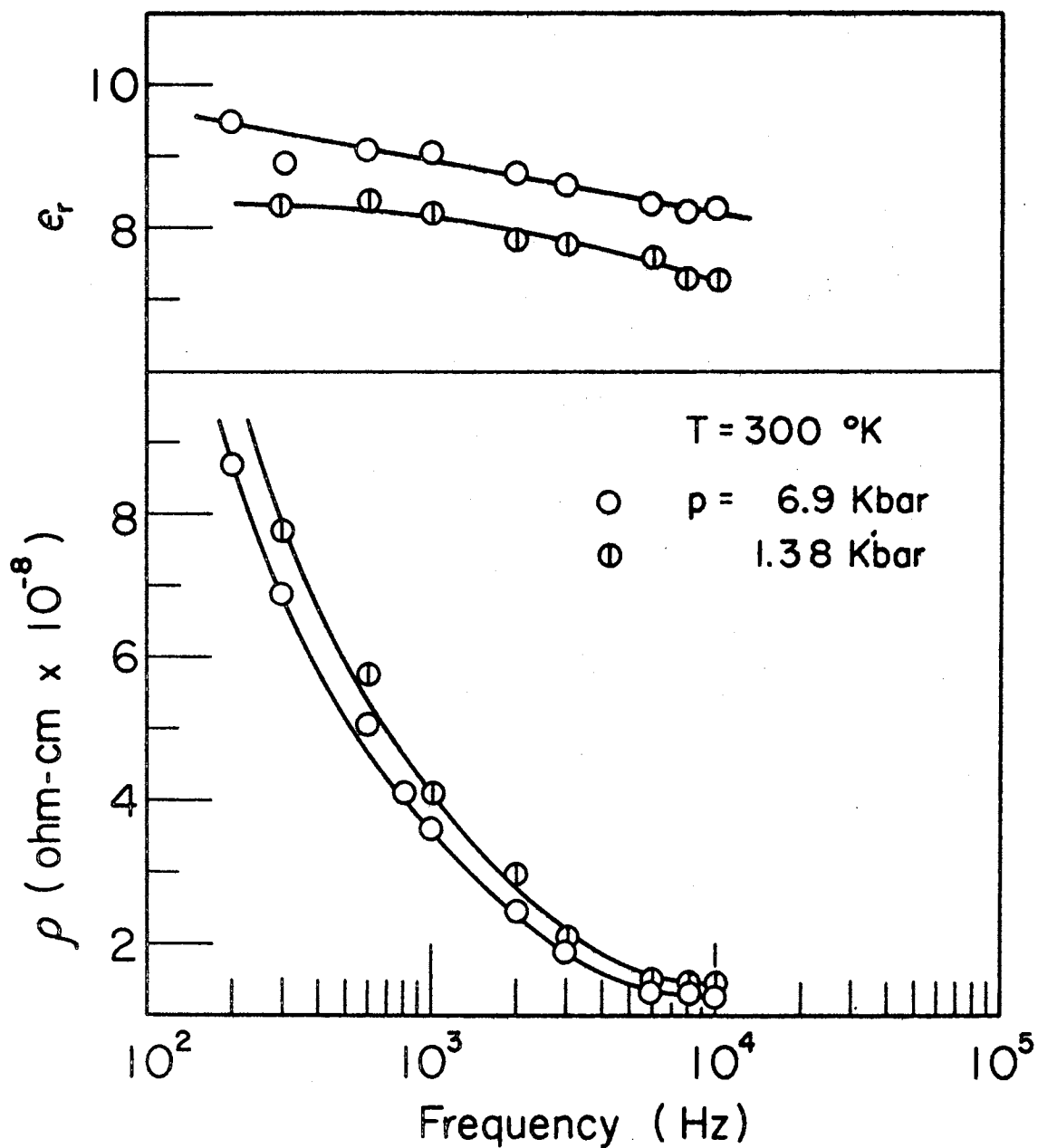


Figure 36. Pressure and Frequency Dependence of the Dielectric Constant and Resistivity for Polymer JM97A (Premolded at 9.6 Kbar)

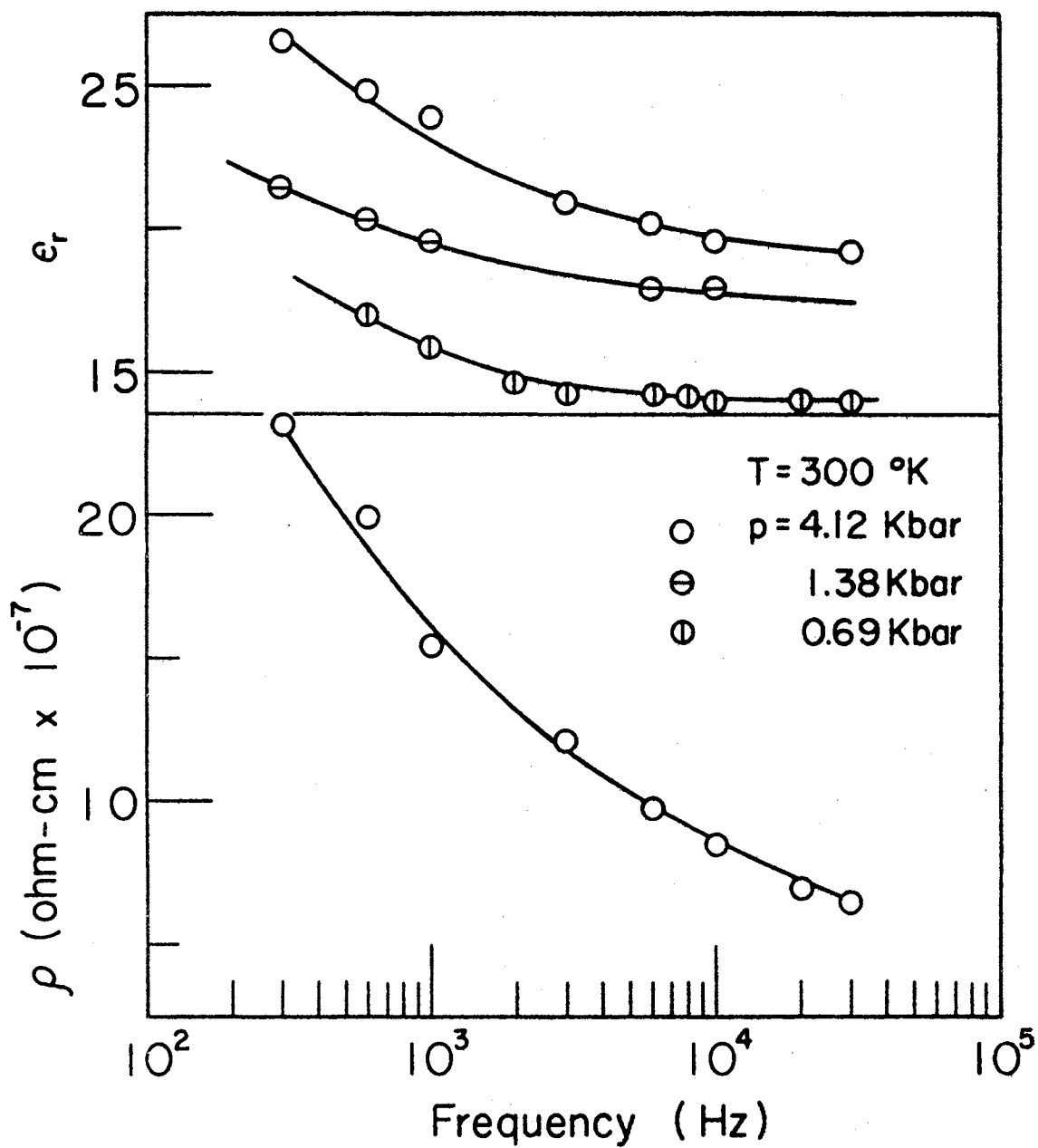


Figure 37. Pressure and Frequency Dependence of the Dielectric Constant and Resistivity for Polymer JM89B (Premolded at 8.3 Kbar)

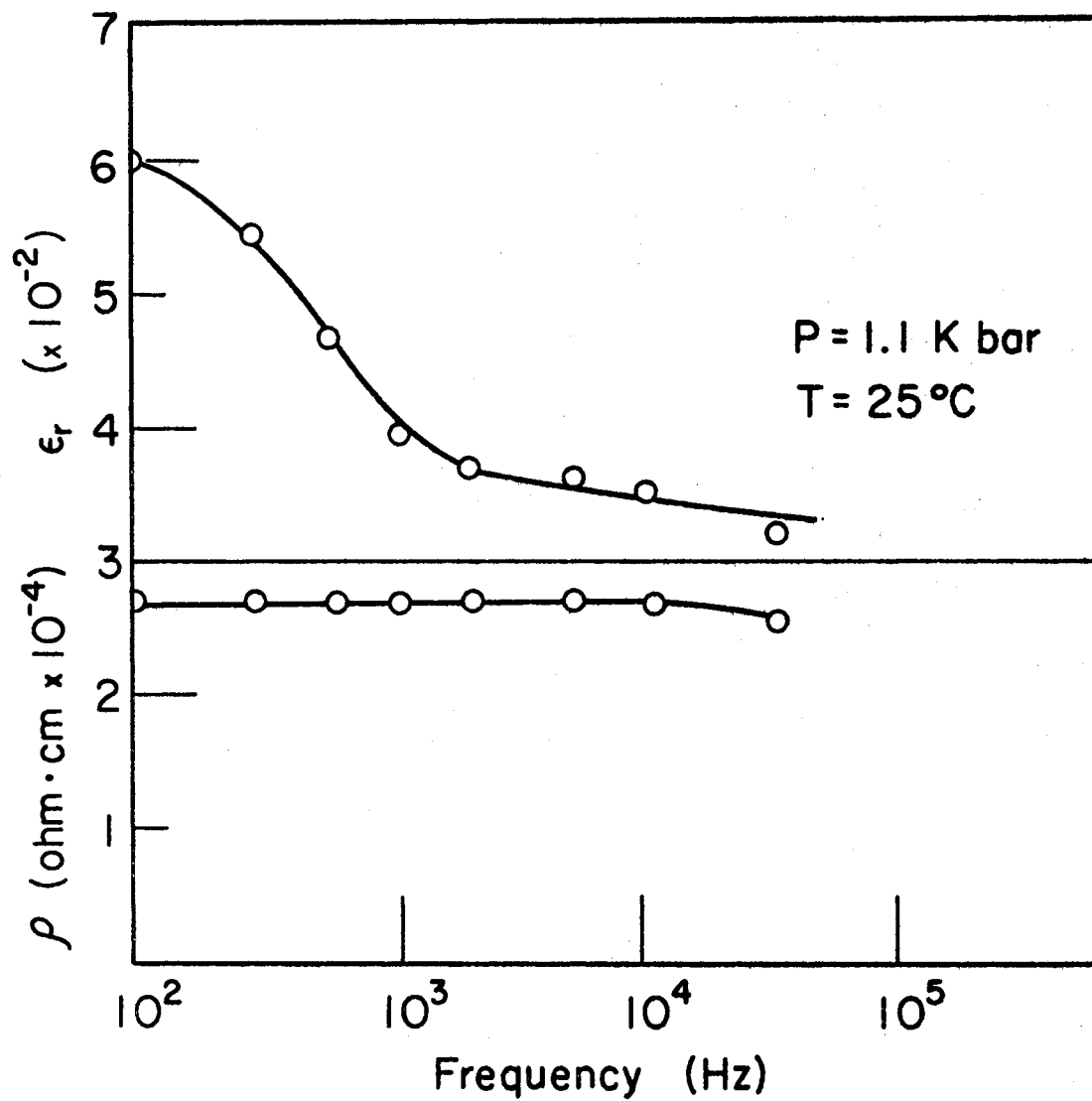


Figure 38. Pressure and Frequency Dependence of the Dielectric Constant and Resistivity for Polymer DPIA. (Premolded at 3.4 Kbar)

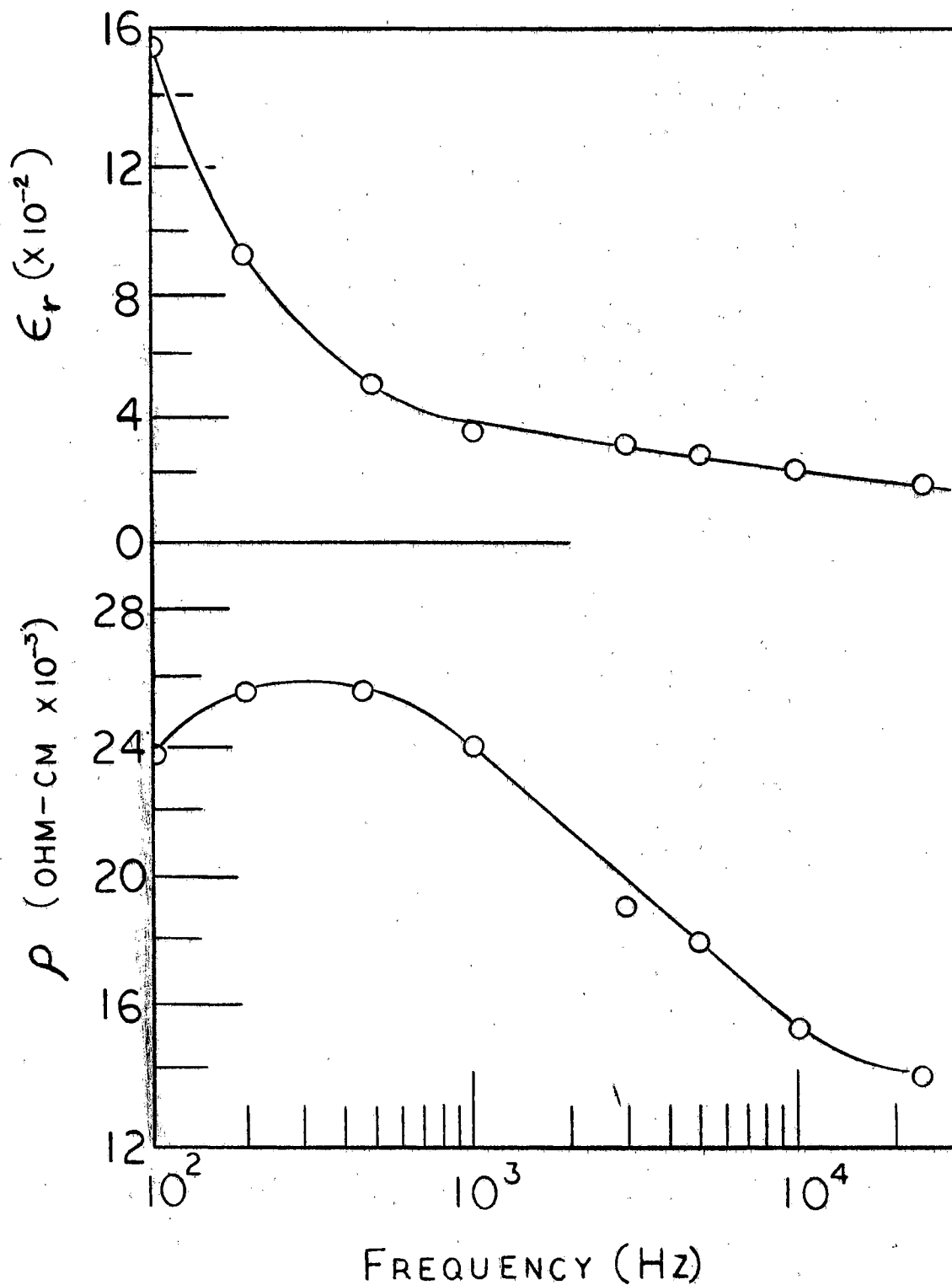


Figure 39. Pressure and Frequency Dependence of the Dielectric Constant and Resistivity for Polymer SK3A (Premolded at 10.6 Kbar)

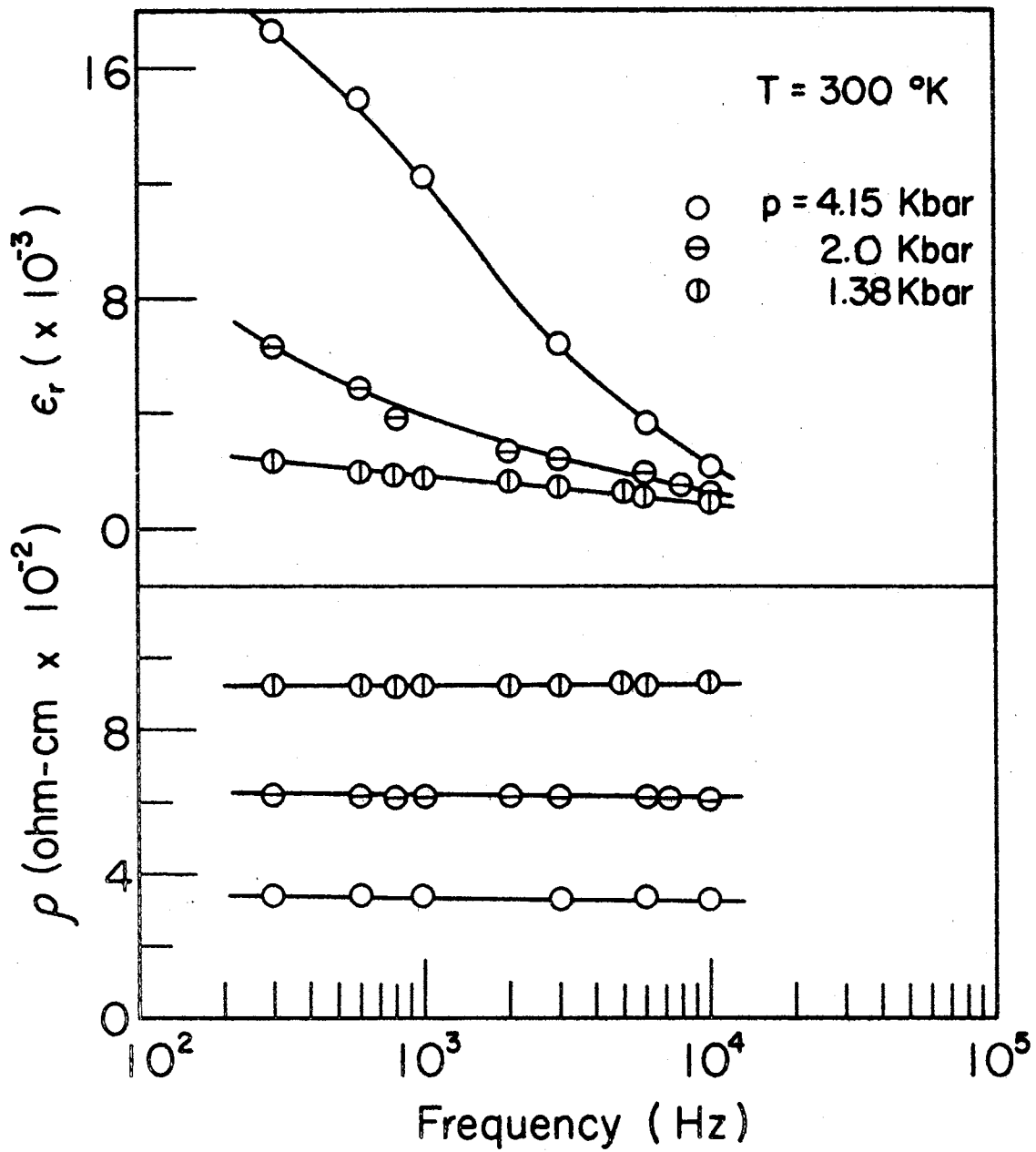


Figure 40. Pressure and Frequency Dependence of the Dielectric Constant and Resistivity for Polymer JM85B (Premolded at 10.9 Kbar)

this chapter, is dependent upon the number of elementary dipoles available to interact with the applied \vec{E} -field.

We have seen in Chapter III, that the D.C. conductivity (or resistivity) for polymeric semiconductors behave according to [Cf. Eq(12), Chapter III]:

$$\sigma \propto \exp (b' P^{1/2}) ; \quad (38)$$

or
$$\rho \propto \exp (-b' P^{1/2}) ; \quad (39)$$

as suggested by Pohl, et.al. (16, 17). Now since $\sigma = n e \mu$, [Eq(4), Chapter III], then:

$$n \mu \propto \exp (b' P^{1/2}) . \quad (40)$$

The mobility, μ , has been seen to be somewhat pressure sensitive in many organic molecular solids (15, 16, 153-158); however it is not strongly dependent on pressure. For example, for anthracene, Kepler (153-154) reports that μ for electrons and holes increases at most by forty percent, while the pressure is increased from 1 bar to 3 kbar (i.e., 3×10^5 percent). Inokuchi, et.al. (28, 156), found the mobility at $P > 100$ kbar to be only 10 to 100 times the value at atmospheric pressure, while the conductivity had increased some 10^5 to 10^7 fold. Bradley, Grace, and Munro (155) concluded the mobility in pathalocyanines was only weakly pressure dependent up to 5 kbar.

Assuming, then, the mobility to be only slightly pressure sensitive, we can approximate Eq (40) by:

$$n \approx A \exp (b' P^{1/2}) , \quad (41)$$

where A is an appropriate constant. Thus, we see the number of carriers is pressure dependent.

Invoking the hyperelectronic polarization model at this point suggests that the degree of polarizability of a macromolecular solid is directly dependent upon the number of exciton or ion monopoles produced; and hence, to the number of charge carriers present on the molecular domains. Thus, if hyperelectronic polarization is to be observed, the polarizability, and hence the dielectric constant, should be observed to be dependent on pressure according to:

$$\epsilon_r \approx A' \exp (b' P^{1/2}) , \quad (42)$$

or
$$\log \epsilon_r \propto P^{1/2} . \quad (43)$$

Typical plots of $\log \epsilon_r$ as determined at 1 KHz versus $P^{1/2}$ are shown in Figure 41. It can be seen that the agreement with Eq (43) is quite good.

For normal inorganic and organic dielectric materials, which exhibit electronic, atomic, and dipolar polarization, Whalley (159) reports that the bulk dielectric constant is expected to vary with pressure according to:

$$\log \epsilon_r \propto P , \quad (44)$$

rather than $P^{1/2}$ as is observed for the macromolecular solids reported in this study.

With regards to the dependence of σ_{AC} or ρ_{AC} on pressures, the 1 KHz values of σ are plotted for several polymers in Figure 41. It is seen that for constant ω ($= 1$ KHz), the A.C. conductivity reacts

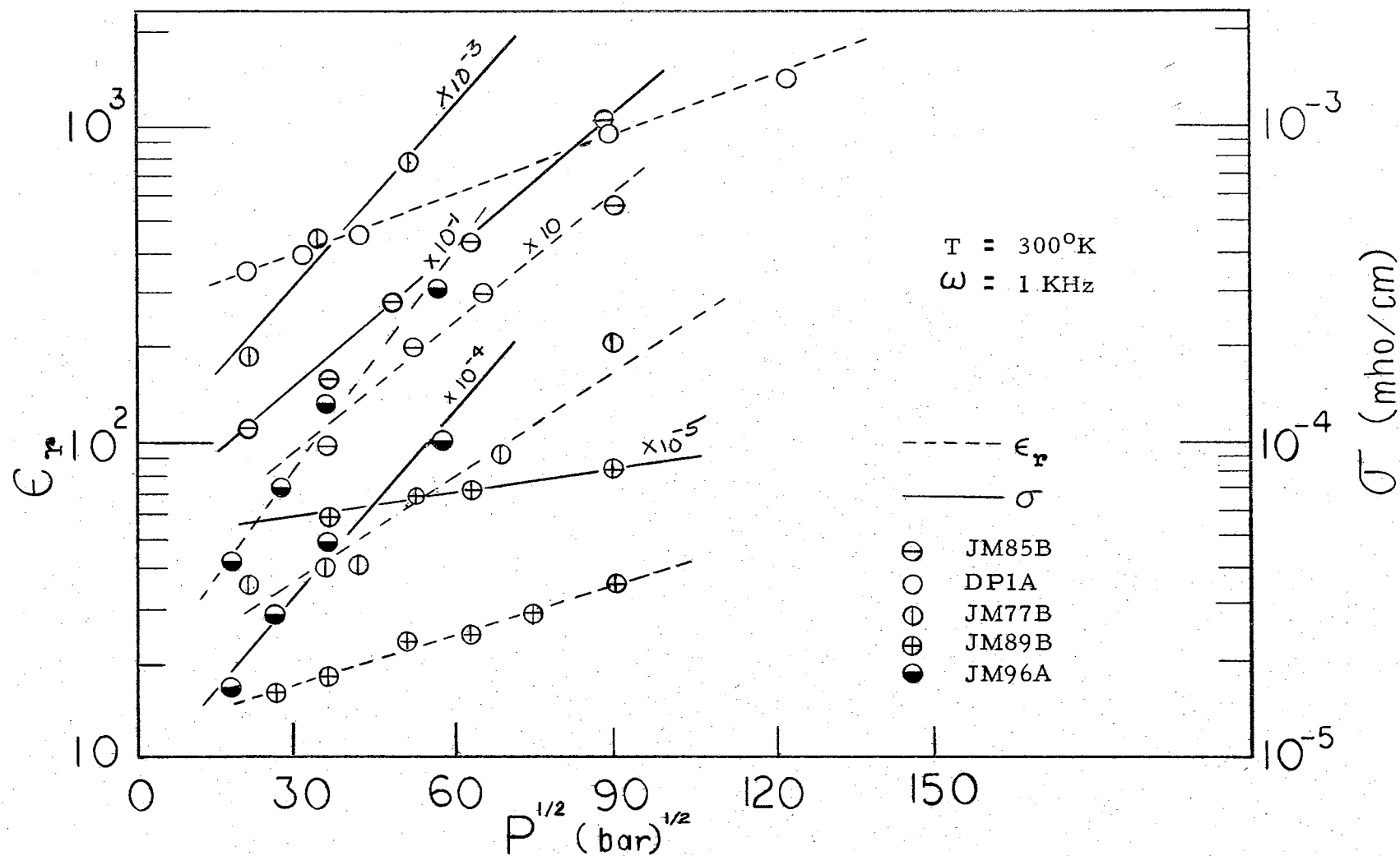


Figure 41. Pressure Dependence of the Dielectric Constant and A.C. Conductivity Measured at 1 KHz for Several Polymers

as does the D.C. conductivity, i. e.,

$$\sigma_{AC} \propto \exp(b'P^{1/2}). \quad (45)$$

The frequency dependence on the dielectric constant and A.C. resistivity is quite pronounced in most cases, with the parameters exhibiting a sharp relaxation in the frequency range of 10^3 to 10^4 Hz. This corresponds to a relaxation time $\tau \sim 10^{-3}$ to 10^{-4} sec. This relaxation phenomenon will be discussed in detail in a later section.

Regarding the conduction mechanism involved in macromolecular organic semiconductors, it was pointed out in Chapter III that the band model is not applicable, but rather the tunneling or hopping model could best be invoked in the case of these polycrystalline solids.

It seems most probable in highly purified polymers that the charge carriers are not molecularly diffusing ions, but are, rather, mobile electrons (or holes) which drift, hop, or tunnel along the molecular sites (45). This is so for at least two reasons: first, there is no sign of electrolytic deposition or polarization upon the passage of large amounts of current (either A.C. or D.C.). Second, the conductivity increases rather than decreases with the application of external pressure. If the carriers were ions, requiring cooperative action of molecules to form large passageways to allow the diffusion of the massive carrier, the application of pressure would tend to diminish this forming of large "holes," and hence, the conductivity would decrease. Rather, the conductivity is seen to increase, as is expected from increased tunneling and hopping made available to mobile electrons as

pressure decreases the average intermolecular distance.

Further support for this electronic hopping model is seen by examining the behavior of σ or ρ with respect to the frequency of the applied \vec{E} -field. Pollak (160) has pointed out that it is difficult to distinguish between band-type conduction and hopping-type conduction by the use of D.C. fields; however, he showed the frequency response of the A.C. conduction to vary according to:

$$\sigma(\omega) \propto \frac{1}{1 + \omega^2 \tau^2} \quad \text{for band;} \quad (46)$$

and

$$\sigma(\omega) \propto \frac{\omega^2}{1 + \omega^2 \tau^2} \quad \text{for hopping;} \quad (47)$$

where τ is the average lifetime of an excited state. It can be seen that Eq (46) decreases with ω while Eq (47) increases with ω . Hence $\sigma(\omega)$ for band-type conduction decreases while $\sigma(\omega)$ for hopping-type conduction increases with ω .

For the macromolecular solids reported in this study, it is seen that ρ decreases with ω , and hence σ increases. This corresponds to the expected behavior for a hopping-type mechanism.

It can be argued on the one hand, that any multiphase solid (polycrystalline, amorphous, ceramic, etc.) can be characterized by a two phase model such as shown in Figure 29 e, resulting in dispersion curves as shown in Figure 30. Thus, for most any multiphase solid, ρ should decrease with ω .

On the other hand, if the material is homogeneous, and ρ is

observed to decrease with ω , it can be safely assumed that the hopping mechanism gives the proper description of the observed dispersion. There are reasons to believe that although the materials examined in this study are polycrystalline, they tend toward homogeneous materials at high pressures. This will be discussed further in a later section.

A further word about the hopping conduction mechanism may be said regarding the pressure effect on ρ at high and low frequencies. If, indeed, the material is homogeneous throughout, then ρ would tend to decrease with ω according to Pollak (160), and ρ would further tend to decrease with the application of high pressure according to Pohl, et. al. (16, 17). However, if the sample is a multiphase material, application of pressure should produce no added significant decrease in ρ at different frequencies.

Stated another way, in terms of Pohl's model [Eqs (13) and (11), Chapter III] :

$$\log \frac{\sigma}{\sigma_0} = \frac{P^{1/2}}{k} (b'' + b_0/T) = \frac{P^{1/2}}{k} b^*,$$

and
$$E'_a = E_a - b_0 P^{1/2};$$

we see that b_0 represents the rate of change of the D.C. activation energy with applied pressure, and $b^* = b'' + b_0 K$ represents the rate of change of D.C. conductivity with applied pressure. If the sample is inhomogeneous, and the resulting dispersion is due to such inhomogeneities rather than to hyperelectronic polarization, then the ap-

plication of pressure should decrease ρ_{AC} in like manner to that of ρ_{DC} , i.e., b^* should not show a frequency dependence.

This is not the case, however. Figure 42 displays typical data for Polymer JM96A at D.C., 1KHz and 10 KHz. It is seen that the slope of the curves and hence b^* is increasing with frequency. Now $b^* = b'' + b_0 / T$ where b'' represents the entropy term and b_0 the energy term. If b^* is to increase with ω , (at constant temperature) then either one or both b_0 and/or b'' must likewise increase. Since b'' is already large with respect to b_0 for most polymers examined (16) it would seem reasonable to assume a change in b_0 with frequency to account for the change in b^* .

Thus, according to the foregoing discussion, the activation energy should exhibit a frequency dependence. This is actually the case as observed. It will be discussed in the next section.

It appears that substantial evidence for the hopping conduction mechanism has been observed, since for an inhomogeneous solid the activation energy should not depend on frequency. It is plausible, however, that it could depend on ω in the case of electron hopping.

In concluding this section, it should be mentioned that in general, the dielectric constant is low (5-25) for polymers with high resistivities ($\sim 10^8$ ohm-cm); is intermediate (40-100) for polymers with intermediate resistivities ($10^5 - 10^6$ ohm-cm); and is quite large (300 - 50,000) for polymers with low resistivities ($10^2 - 10^4$ ohm-cm). We now turn to a discussion of temperature effects on σ and ϵ_r .

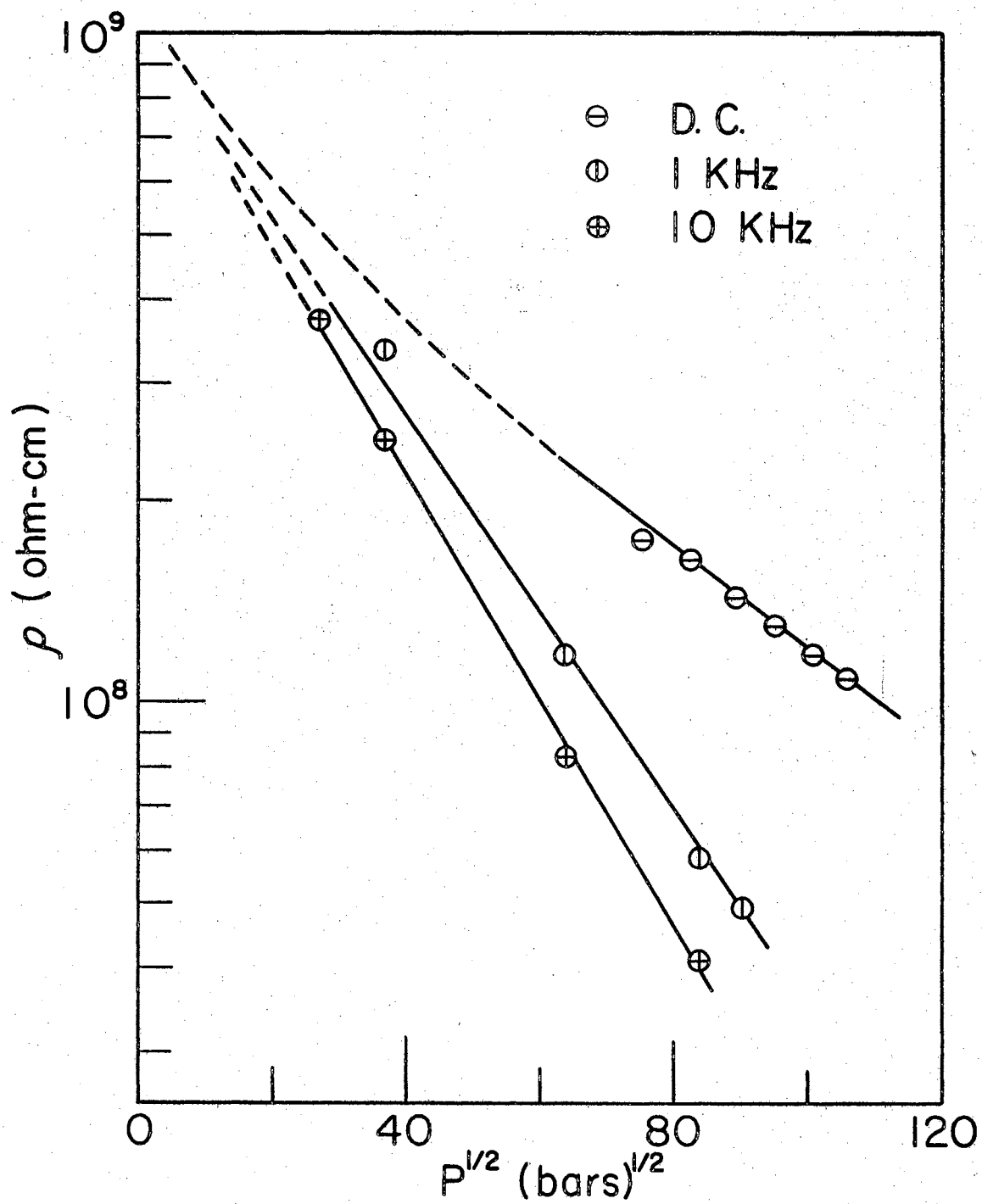


Figure 42. Pressure Dependence of the Resistivity for Polymer JM96A at Various Frequencies

$\sigma(T, \omega)$ and $\epsilon(T, \omega)$

The effect of temperature on the conductivity and dielectric constant of the organic semiconductors was studied in two ranges. The first temperature range was above room temperature, while the second temperature range was down to liquid N_2 and in some cases to liquid He temperature.

Before inserting the samples into the high pressure dielectric cell, they are premolded at 10.4 kbar in a one-eighth inch die with tungsten carbide anvils. The dense pellet is then inserted into a pyrophyllite retaining ring, and the assembly is placed in the proper high pressure cell.

In order to study pressure effects above 5 kbar as well as temperature effects on ϵ_r and ρ , the high pressure resistivity cell (Figure 1) was employed in the high temperature range. For the low temperature range, the Chester-Jones clamp (Cf. Figure 54, Chapter 6) was employed. A steady pressure of ~ 8 kbar was maintained on the specimen by the clamp, while it was examined at very low temperatures.

Typical high temperature behavior of the polymers studied is displayed in Figure 43. There it is seen that for Polymer DP1A, as the temperature is increased, ϵ_r likewise increases while the A.C. resistivity decreases accordingly. These results are in agreement with earlier measurements on PAQR polymers reported by Rosen and Pohl (38, 39).

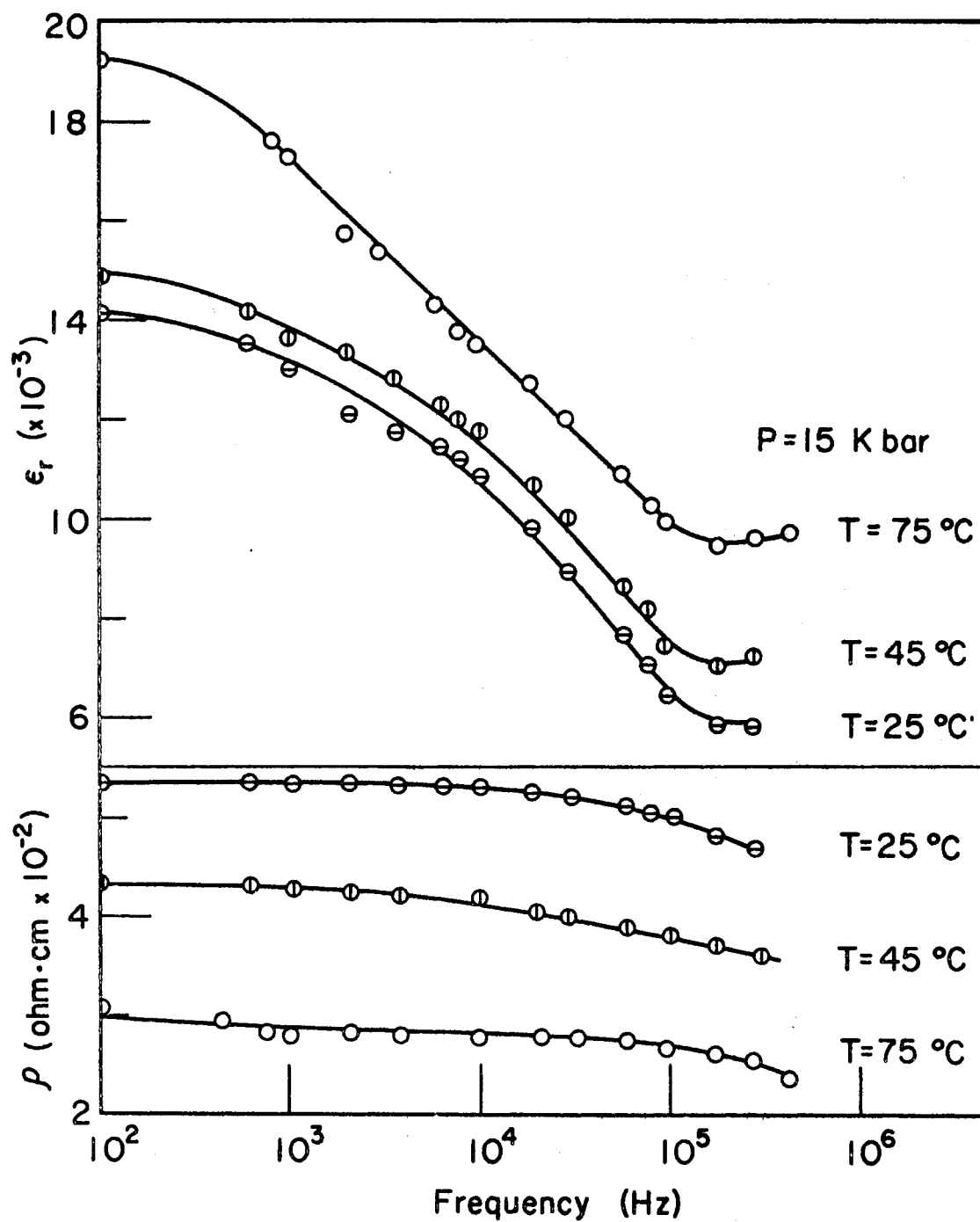


Figure 43. Temperature and Frequency Dependence of the Dielectric Constant and Resistivity for Polymer DPIA (High Temperature)

The pressure effect is very pronounced when one compares the 25°C curve for ϵ_r and ρ of Figure 43 to that of Figure 38. Here, both materials are DP1A, but the former specimen was measured at 15 kbar, while the latter was measured at 1.1 kbar.

Low temperature frequency dependencies of ϵ_r and σ (or ρ) are shown in Figures 44 through 48, as obtained with the aid of Cell III (Chester-Jones Clamp). In many cases, the "in place" resistance of the sample was greater than 11 meg ohms which was the limit of the parallel mode for the bridge used. For such cases, the resistivity was not determined; however, the bridge was used in the "series" mode to determine the capacitance alone.

It is interesting to note the behavior of the dispersion in the polymers studied at low temperatures. Figure 48, in particular, shows the effect. At high temperatures, ϵ_r indicates a very large dispersion, while ρ is practically constant. But as the temperature is lowered such that ρ gets large, then it exhibits a very large dispersion while ϵ_r is practically constant.

Concerning the temperature effect on the dielectric constant, it can be seen from the data displayed in Figures 43 through 48 that the dielectric constant systematically increases with temperature, with the exception of polymers JM85B and JM77B, when there is an intermixing of the 77°K curve with those of higher temperatures. Rosen and Pohl (39) also observed a similar crossing of curves at about 330°K for two polymers.

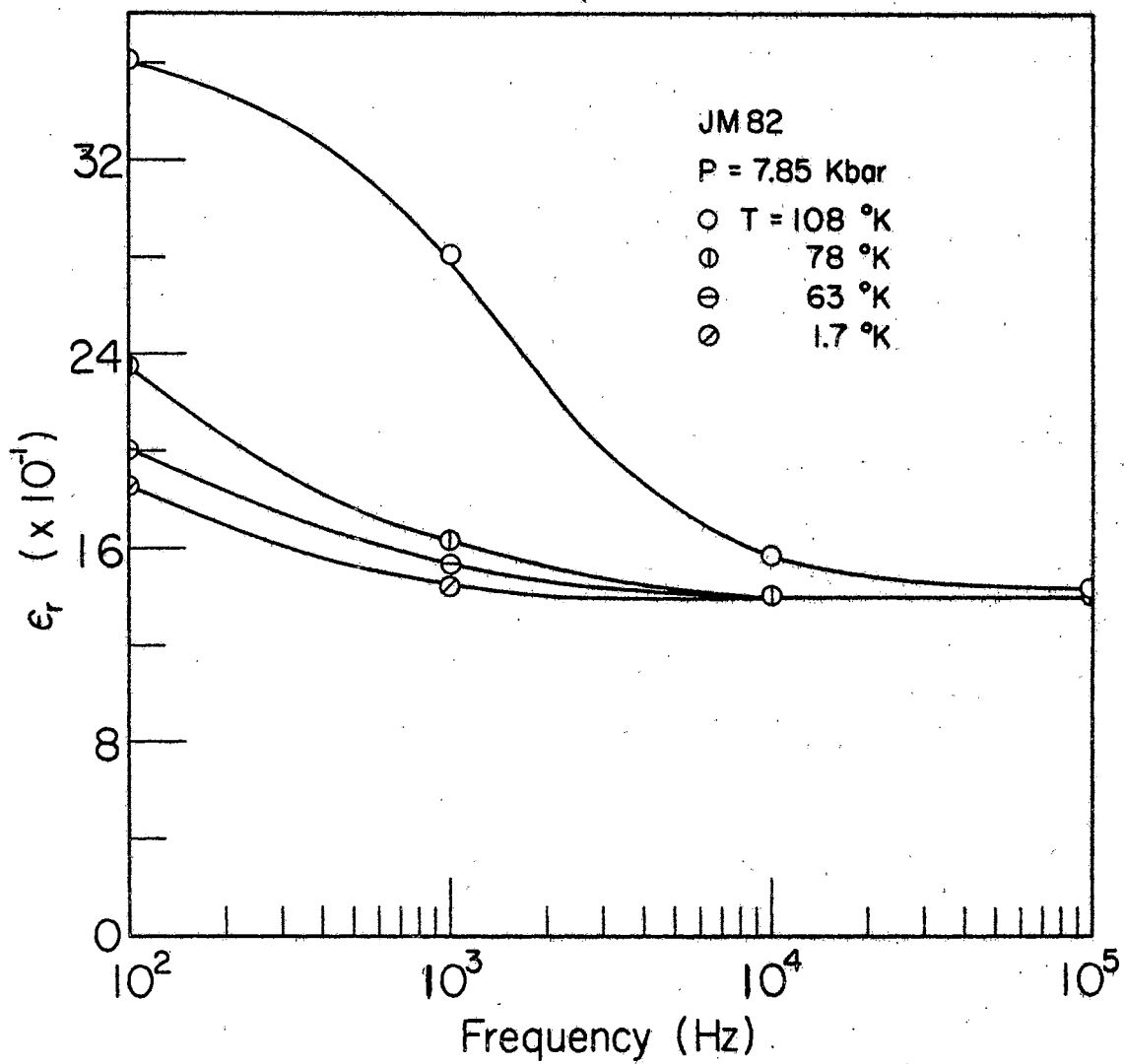


Figure 44. Temperature and Frequency Dependence of the Dielectric Constant and Resistivity for Polymer JM82

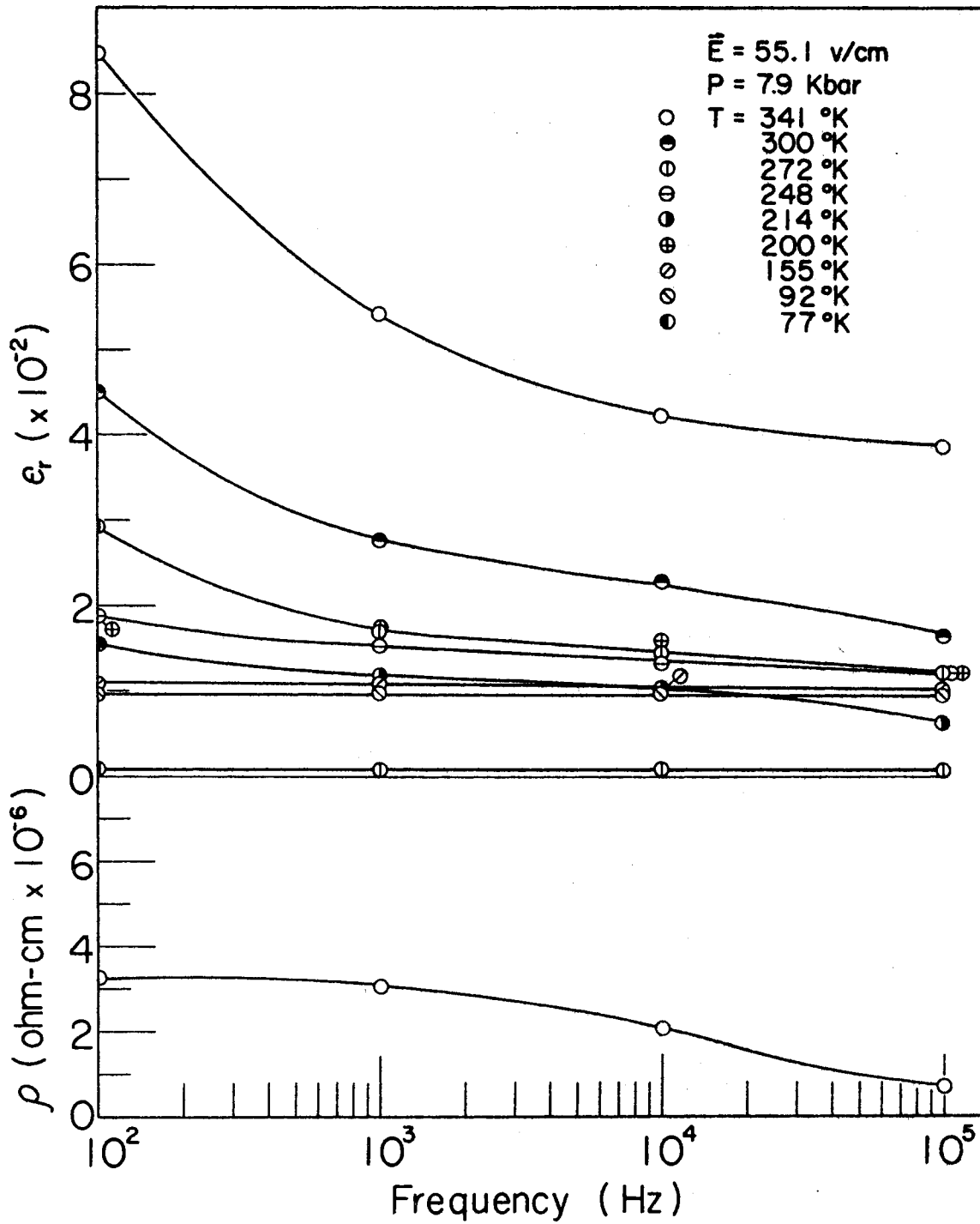


Figure 45. Temperature and Frequency Dependence of the Dielectric Constant and Resistivity for Polymer JM77B

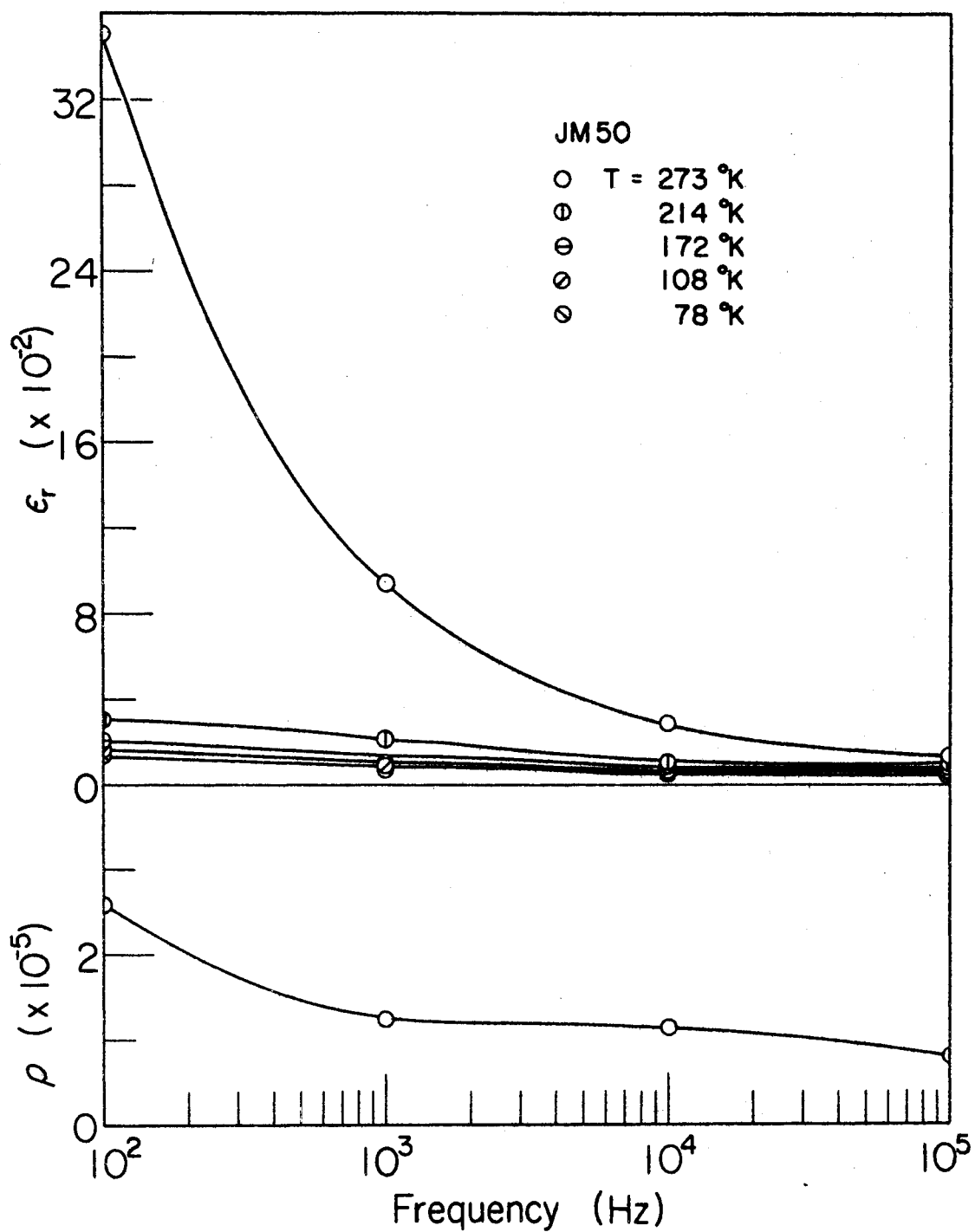


Figure 46. Temperature and Frequency Dependence of the Dielectric Constant and Resistivity for Polymer JM50

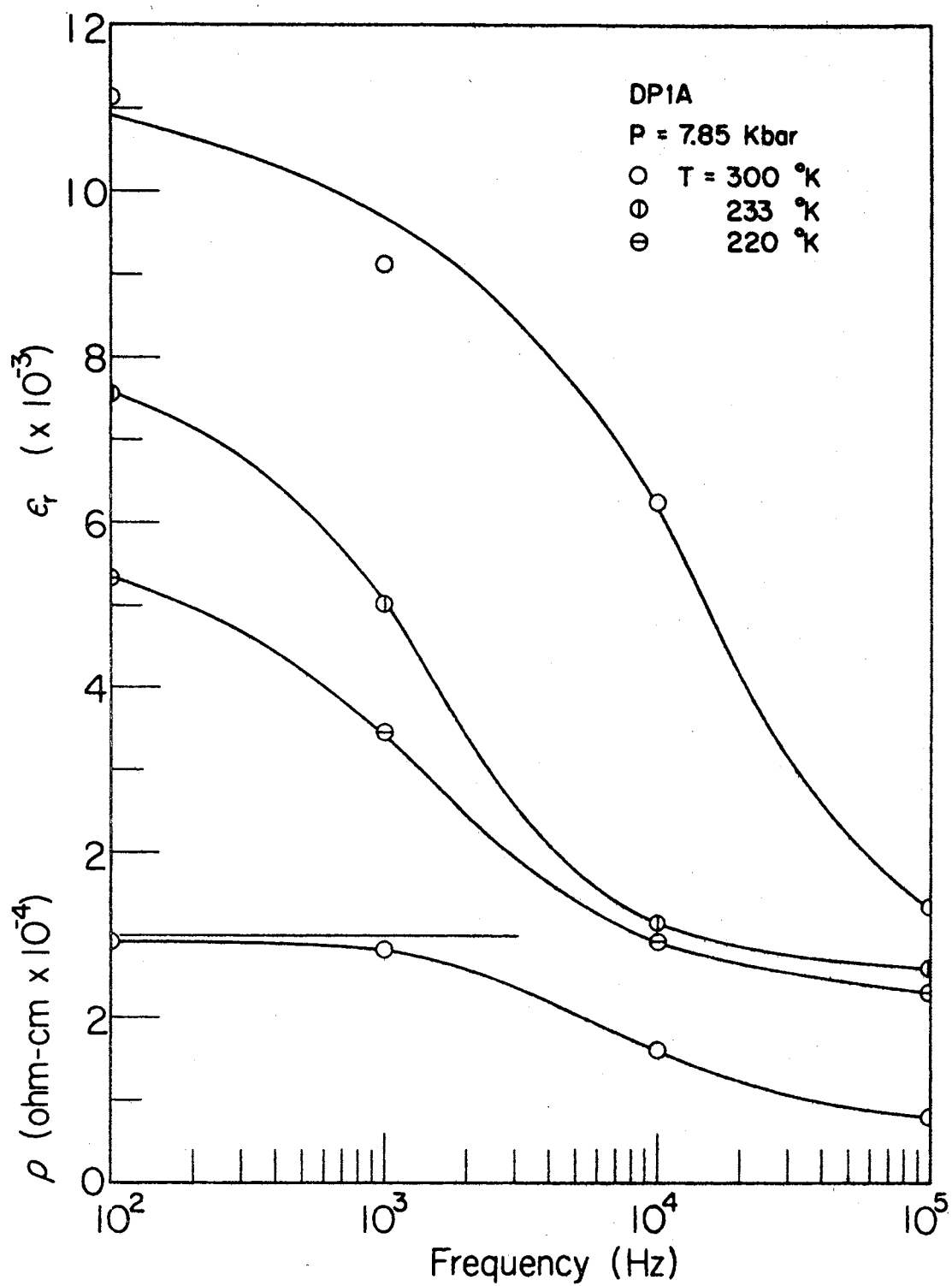


Figure 47. Temperature and Frequency Dependence of the Dielectric Constant and Resistivity for Polymer DP1A

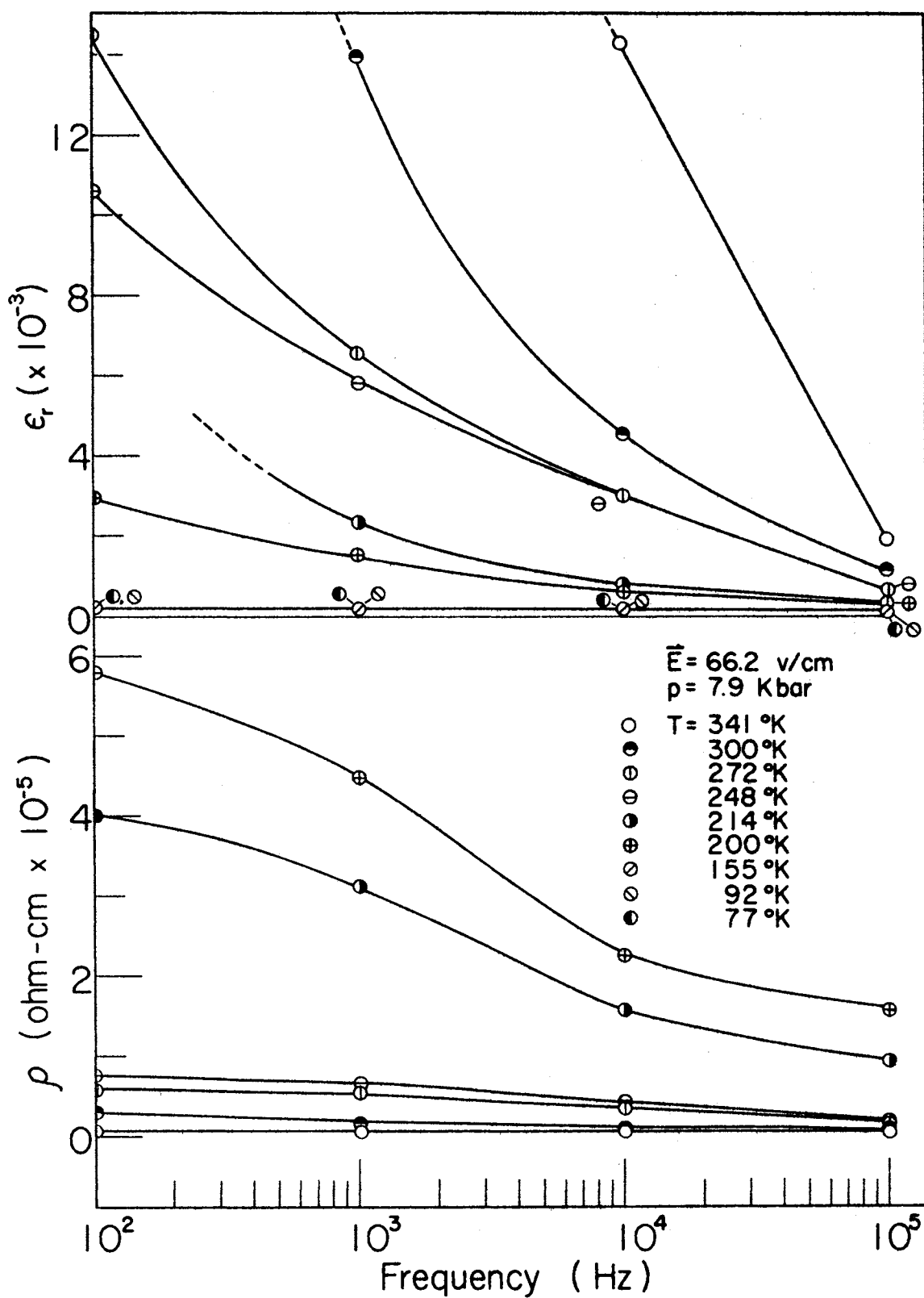


Figure 48. Temperature and Frequency Dependence of the Dielectric Constant and Resistivity for Polymer JM85B

The question then is how should one expect ϵ_r to vary with temperature? Recalling the discussion in the last section on the pressure dependency, we saw that the hyperelectronic polarization would be dependent upon the number of charge carriers present on the molecular domains. This should still hold true in this case, although the pressure is now being held constant. Since the materials being studied are semiconductors, and thus rely on thermal activations to excite carriers into the conduction state, it would seem plausible to expect the polarization, and thus the dielectric constant, to be dependent exponentially on the temperature, i. e.:

$$n \propto \exp(-E_a/kT); \quad (48)$$

and
$$\epsilon_r \propto n = A \exp(-E_a/kT); \quad (49)$$

or
$$\log \epsilon_r \propto -\frac{E_a}{kT}. \quad (50)$$

The dielectric constants for polymers DP1A, JM85B, and JM77B are shown plotted against $1/T$ in Figures 49, 50, and 51 respectively. It is seen that Eq (50) describes their behavior quite well.

According to Whalley, a normal dielectric solid should exhibit the following temperature dependence (159):

$$\log \epsilon_r \propto T, \quad (51)$$

rather than the inverse T dependence as given by Eq (50) which fits the observed behavior of the macromolecular organic semiconductors.

Upon examining the curves for JM85B and JM77B, it appears that there is an anomaly in ϵ_r at $\sim 250^\circ\text{K}$ for JM85B (Cf. Figure 50)

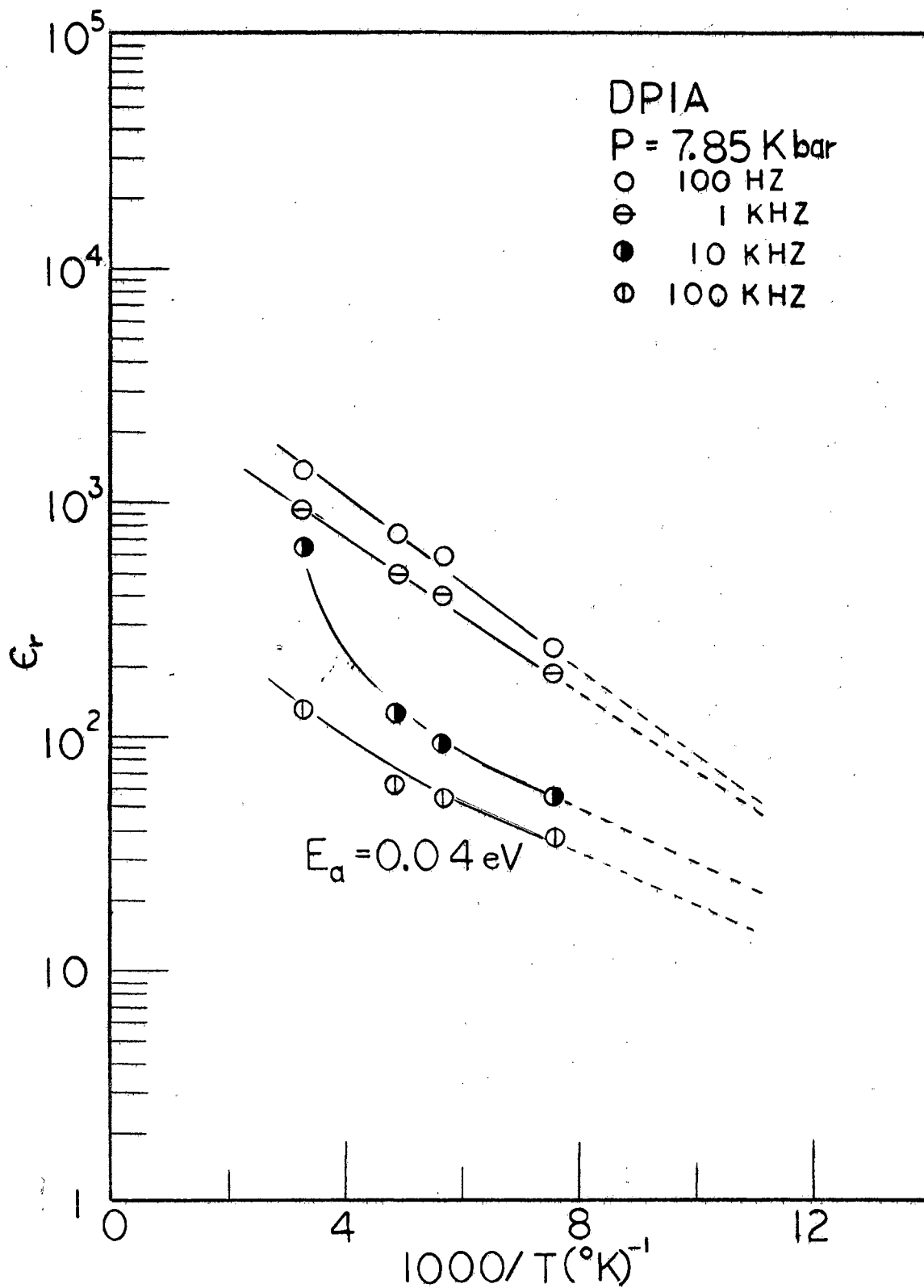


Figure 49. Temperature Dependence of the Dielectric Constant for Polymer DPIA at Various Frequencies

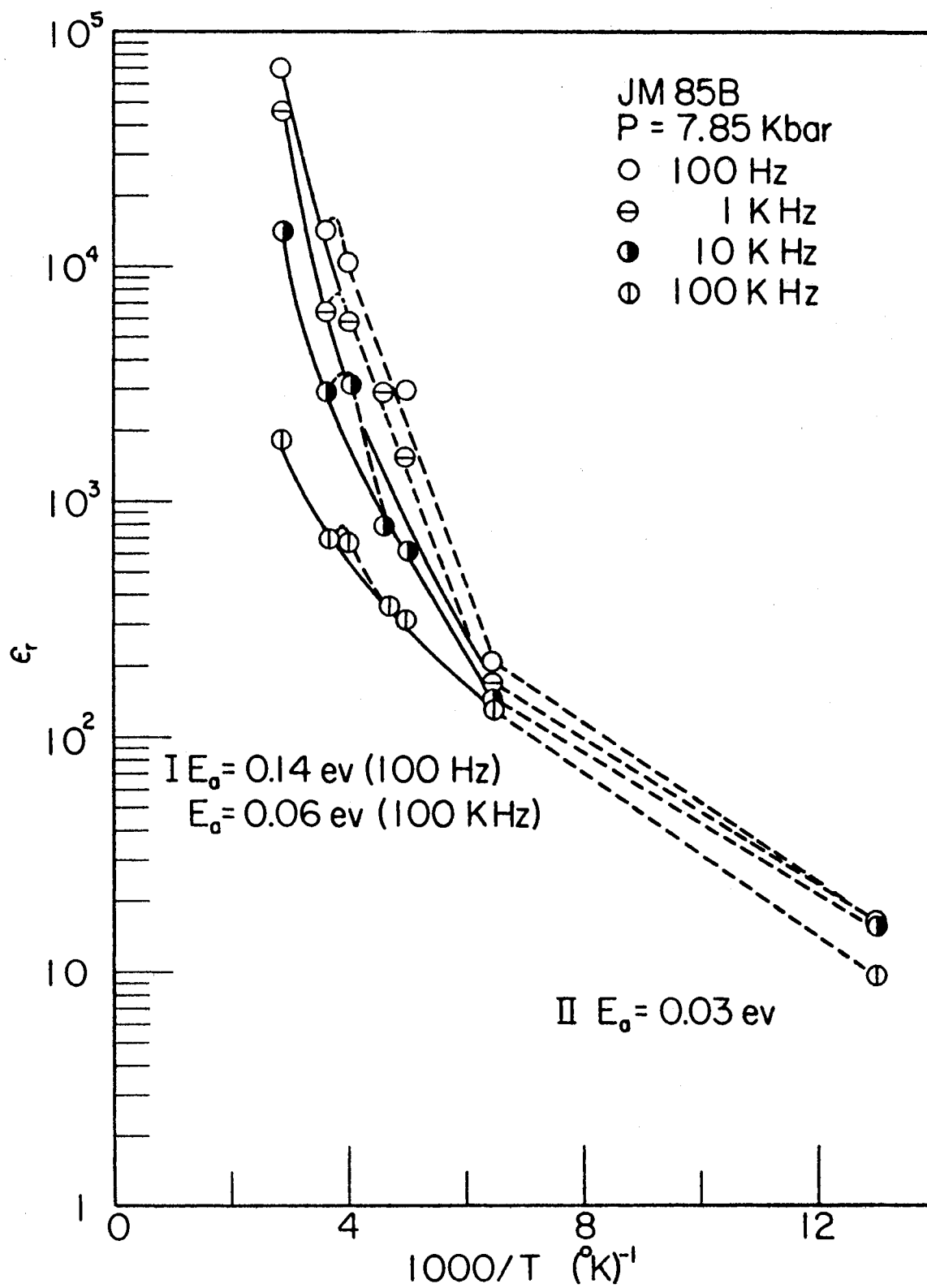


Figure 50. Temperature Dependence of the Dielectric Constant for Polymer JM85B at Various Frequencies

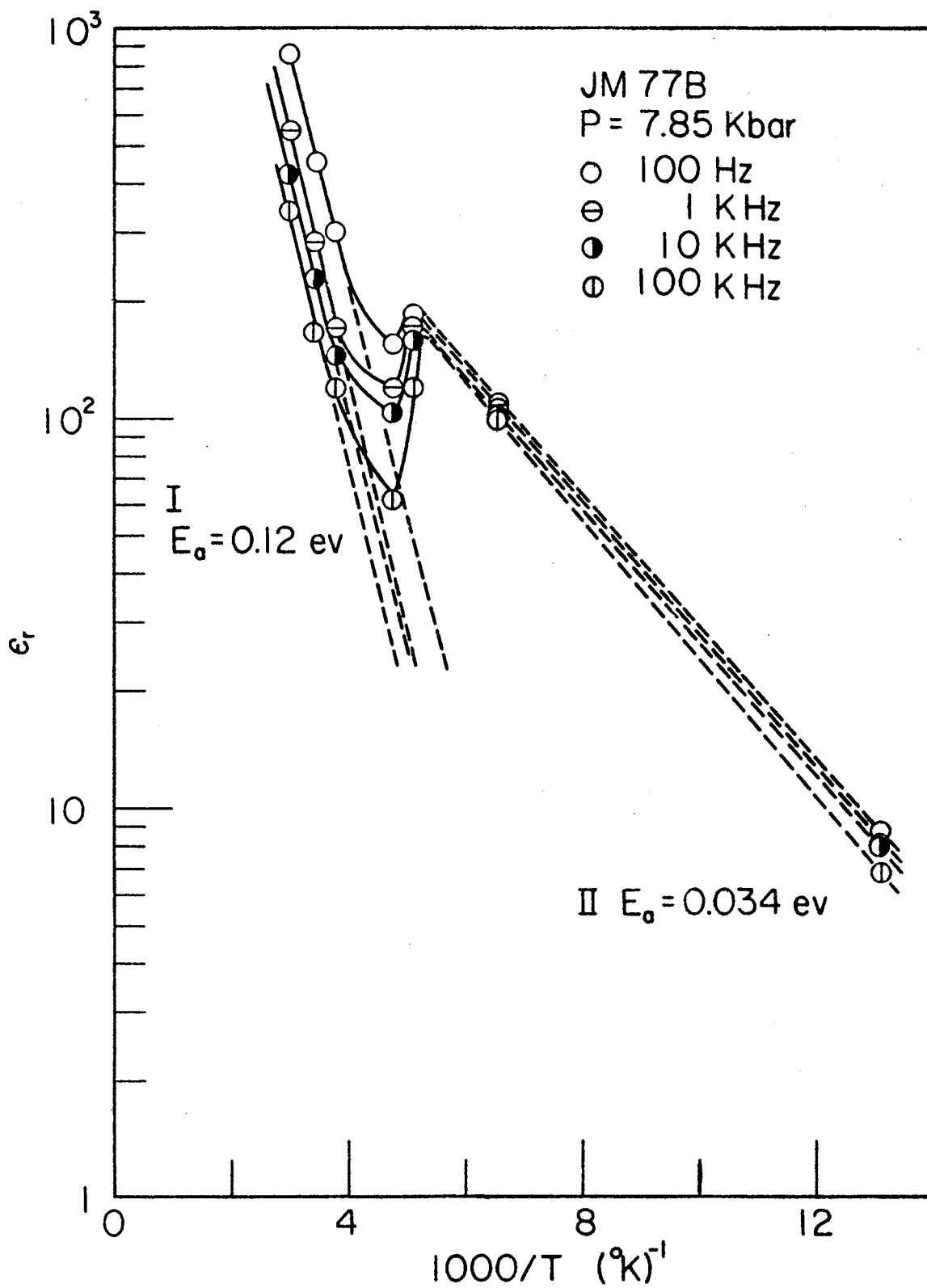


Figure 51. Temperature Dependence of the Dielectric Constant for Polymer JM77B at Various Frequencies

and at $\sim 200^{\circ}\text{K}$ for JM77B (Cf. Figure 51). Since only limited data points were taken in the region from 200°K to 77°K , it is difficult to be entirely conclusive, but it appears that there are two regions for each of these polymers. In the region above the anomalous point, the activation energies for ϵ_r are quite similar to that for the A.C. conductivity, while below the anomalous point, the activation energies for ϵ_r are very similar to that for producing unpaired spins as determined in Chapter IV.

It would appear that at temperatures in excess of 200°K to 250°K , both unpaired spins and carriers localized on molecular domains are contributing to the polarization. But below this temperature, only spins are contributing. This seems reasonable since the unpaired spins may be lying in a shallow trap ~ 0.02 to 0.04 eV below the conduction band. As the sample is cooled, the charge carriers are depleted, but the spins become activated into the conduction band, since the spin activation energy is ~ 5 to 10 times smaller than the charge carrier activation energy.

A comparison of the various activation energies is given in Table X. It is seen that the A.C. conduction activation energy is frequency dependent as was suggested in the last section on pressure effects. This further supports the hopping model of conduction.

In order to further examine the anomalous temperature dependence of ϵ_r , more data points were obtained for sample JM77B and JM85B. The result of the additional data together with the data shown

TABLE X

A COMPARISON OF ACTIVATION ENERGIES

Sample No.	Pressure (kbars)	Temperature Range (K ^o)	E _a (eV)					E _s (eV)
			D. C. σ	A. C.				
				100 Hz		100 KHz		
			σ	ε _r	σ	ε _r		
JM85B	1.8	300-450	0.15					
	31.4	300-450	0.12					
	7.9	250-300	0.15	0.14	0.14	0.08	0.06	
	7.9	77-250	0.12		0.03		0.03	0.021
JM77B	1.8	300-450	0.26					
	31.4	300-450	0.26					
	7.9	200-300	0.15	0.15	0.14	0.14	0.12	
	7.9	77-200	0.08		0.03		0.03	0.024
DP1A	1.8	300-450	0.11					
	31.4	300-450	0.06					
	7.9	150-300	0.10	0.05	0.04	0.04	0.03	
	7.9	77-150	0.04		0.03		0.02	0.033

in Figures 50 and 51 is plotted directly against T in Figure 52. From this result, it appears there is a good possibility that these polymers are ferroelectric. If this were so, one would have a very strong case in favor of the hyperelectronic polarization model. Unfortunately, the experimental arrangement would not permit one to obtain adequate data in the mid temperature range, which is the range of interest. It is possible, then, that the anomalies are due to experimental error.

It is an interesting point, however, to consider that these organic materials may be ferroelectric. If they are, this could explain the anomalous behavior observed by Rosen and Pohl (39) as to the mixing

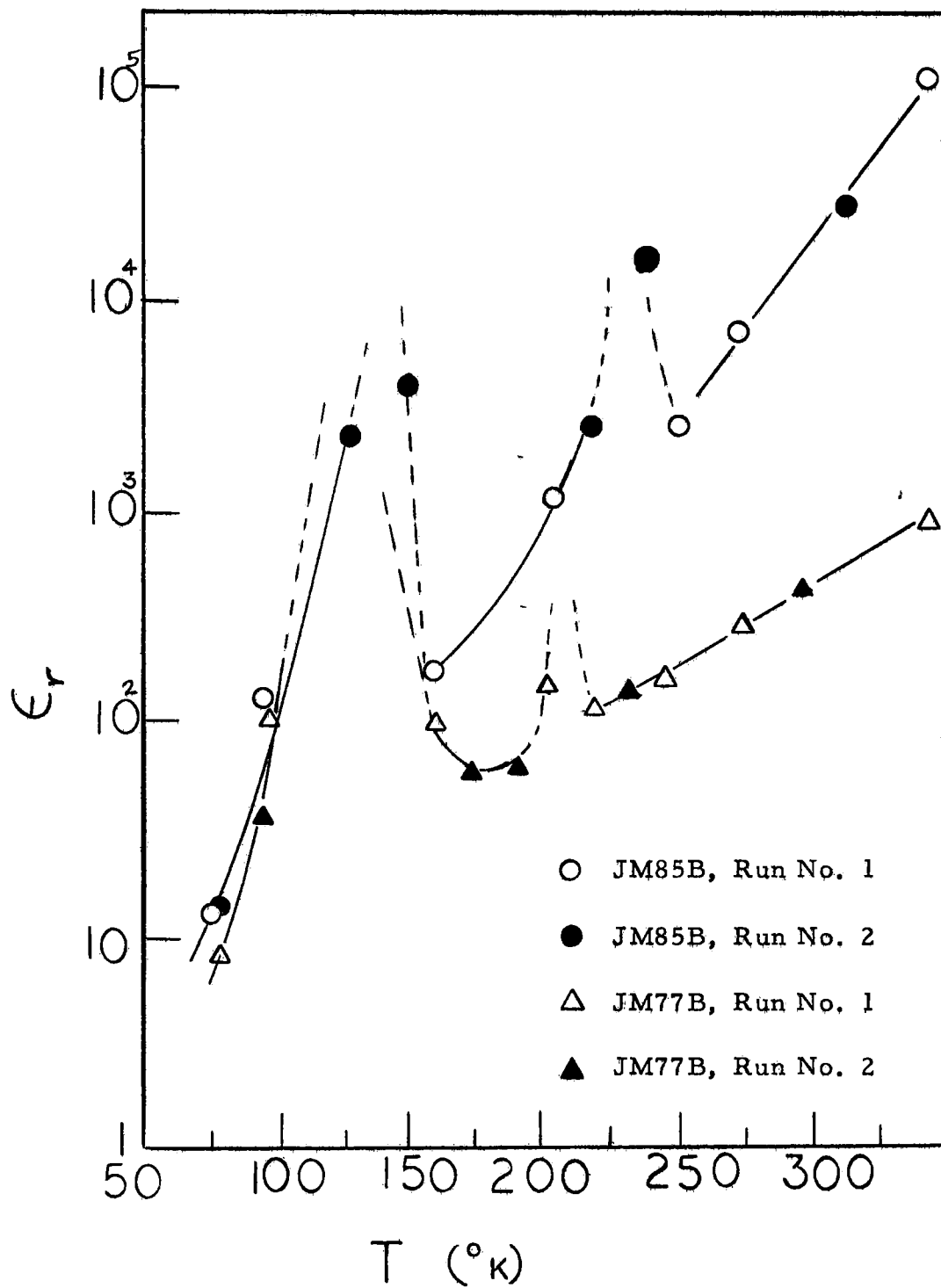


Figure 52. Temperature Dependence of the Dielectric Constant for Polymers JM85B and JM77B at 1 KHz (Possible Ferroelectric Effect)

and crossing of the ϵ_r dispersion curves at various temperatures. It is not totally infeasible to expect organic macromolecular solids to exhibit ferroelectricity, since a number of organics are known to form macroscopic electric dipoles, i. e., electrets. Gutman and Lyons (52) list some 25 organic electrets. Also, many organic solids exhibit extreme piezoresistive effects, and piezoelectric effects, and a few organic complexes have been identified as ferroelectrics. Thus, it appears plausible that macromolecular solids which exhibit hyper-electronic polarization could be ferroelectrics.

Thus far, we have seen that conventional dielectric theory will not account for the observed pressure and temperature dependence of the dielectric constant. However, the hyper-electronic polarization model agrees with both effects. We now turn to a discussion of the \vec{E} -field dependence of σ and ϵ_r .

$\sigma(\vec{E}, \omega)$ and $\epsilon(\vec{E}, \omega)$

The effect of both D.C. and A.C. \vec{E} -field variations on the dielectric constant and conductivity has been examined at room temperature and a variety of pressures. For those polymers examined, it is observed that ϵ_r decreases with increasing \vec{E} -field strength (either A.C. or D.C.), while σ increases accordingly. Since the dependence of σ on \vec{E} -field strength has been discussed in Chapter III, this discussion will be limited to the effects on ϵ_r .

Typical values for ϵ_r at various \vec{E} -fields are shown in Table XI

TABLE XI

DEPENDENCE OF ϵ_r (1 KHz) UPON A.C. \vec{E} -FIELD STRENGTH^(a)

Sample No.	P (kbar)	ϵ_r					
		570 V/cm	340 V/cm	65 V/cm	10 V/cm	6 V/cm	1 V/cm
DP1A	0.7	206	345	708	1188	1675	2520
DP1A	31.4	3700	4216	4820	4850	4900	4920
SK3A	31.4	1148	1345	2180	2310	2440	2560
JM85B	1.89	60400	61050	61450	61900	63300	71200
JM77B	12.6	772	1020	1306	1507	1647	1690

(a) Measured at 300°K under an \vec{E} -field of ~ 50 V/cm.

TABLE XII

DEPENDENCE OF ϵ_r (1 KHz) UPON D.C. \vec{E} -FIELD STRENGTH^(a)

Sample No.	P (kbar)	ϵ_r							
		800 V/cm	600 V/cm	200 V/cm	160 V/cm	120 V/cm	80 V/cm	40 V/cm	0 V/cm
DP1A	1.89	198	208	322	354	396	492	634	898
DP1A	12.6	824	1206	1790	2020	2270	2670	3280	4000
JM85B	1.89	50700	56800		59000			59400	60400
SK3A	12.6	1179	1230	1350	1350	1367	1398	1430	1470
JM77B	12.6	597	790	1006	1068	1159	1312	1608	1970

(a) Measured at 300°K under an \vec{E} -field of ~ 50 V/cm.

and XII for several polymers. Regarding this nearly $1/|\vec{E}|$ dependence of ϵ_r , it is to be expected if one employs hyperelectronic polarization model.

It was postulated earlier that the thermally excited charge carriers are highly delocalized on extremely long molecular domains, in such a manner as to exhibit a near zero polarization in the absence of an \vec{E} -field. Upon the application of an \vec{E} -field, the monopoles are shifted through very long paths, thus creating an unusually large polarization.

Since the monopoles are delocalized in a region of near-zero resistance, it should take only a small amount of energy (and hence a small \vec{E} -field) to completely displace the highly mobile charge to the far end of the molecular domain. As the field strength is increased further, hopping of the carrier from one molecule to another, rather than the oscillation of the carrier within its respective domain, will predominate. This is readily seen since the carrier will be given enough energy from the field change over the long length of the molecular domain ($\sim 4000 \text{ \AA}$) to hop the energy barrier at the end of the domain. After hopping, the motion of the carriers will no longer be in phase with the oscillations of carriers still localized on distant molecular domains, and thus the hyperelectronic polarization effect eventually disappears as the field is increased without limit.

A simple mathematical model which accounts for this $1/|\vec{E}|$ dependence of ϵ_r has been suggested by Pohl and Pollak (161). Consider

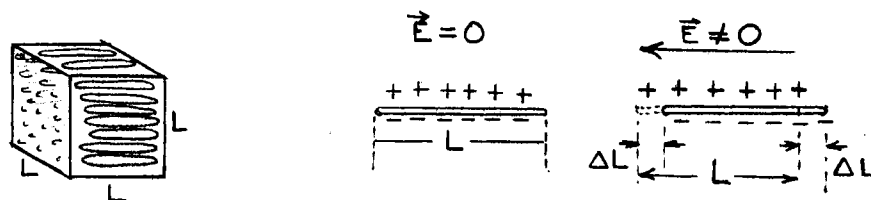
the solid to be composed of highly elongated needle like molecules, of average length $\sim 4000 \text{ \AA}$, and average diameter corresponding to the diameter of a benzene ring ($\sim 4 \text{ \AA}$). Further, assume that the solid possesses localized regions of high order, where the molecules are stacked parallel. Consider at random a unit cube of dimension equal to the average molecular length L to be such a localized region.

The number of charge carriers within the cube is given by the Boltzmann distribution as:

$$n = n_0 \exp(-\Delta E/2kT). \quad (52)$$

The entire cube may be treated as a plasma, since it is in electrical equilibrium; and further, since we are interested in the distortion of the cube when an \vec{E} -field is applied along one of its axes, we shall treat the system as a one dimensional solid only.

Thus, along the line of action of the \vec{E} -field, we treat the system as having a linear charge density λ_h for holes and λ_e for electrons with $\lambda_h = \lambda_e$. (Cf. below.) When an \vec{E} -field is applied, a shift or polarization of the line will occur as indicated below.



Now the linear charge density is given by:

$$\lambda_e = n \times L^2 |e| = \lambda_h, \quad (53)$$

where n = number of carriers/volume, L is the molecular length, and

$|e|$ is the electronic charge.

The work done by the external \vec{E} -field in redistributing the charge is:

$$W = \vec{\mu} \cdot \vec{E} = Q\vec{E} \cdot \Delta\vec{L}, \quad (54)$$

while the increase in internal energy is given by:

$$V = \frac{q_1 q_2}{\epsilon X} = \frac{(\lambda_h \Delta L)(\lambda_e \Delta L)}{\epsilon L}. \quad (55)$$

Now the dipole moment is:

$$\mu = QL = (\lambda_e \Delta L)L = (\lambda_h \Delta L)L, \quad (56)$$

and thus:

$$V = \frac{\mu^2}{\epsilon L^2} \times \frac{1}{L} \quad (57)$$

Equating the work done on the system to the increase in internal energy yields:

$$|\vec{\mu}| |\vec{E}| = \frac{\mu^2}{\epsilon L^3}; \quad (58)$$

or:

$$\epsilon = \frac{\mu}{|\vec{E}| L^3}. \quad (59)$$

Using Eq (53), Eq (59) becomes:

$$\epsilon = \frac{(\lambda \Delta L)L}{|\vec{E}| L^3} = \frac{nL^2 |e| \Delta L L}{|\vec{E}| L^3}; \quad (60)$$

or

$$\epsilon = \frac{n_0 \exp(-\Delta E/2kT) \Delta L |e|}{|\vec{E}|}. \quad (61)$$

Thus

$$\epsilon_r = \frac{\epsilon}{\epsilon_0} = \frac{n_0 \exp(-\Delta E/2kT) \Delta L |e|}{\epsilon_0 |\vec{E}|}. \quad (62)$$

Hence, it is seen from this very simplified model that ϵ_r is inversely

dependent on the \vec{E} -field. It is further seen that it has the proper temperature dependence as discussed in the last section.

Eq (62) may be modified according to Eq (43) to include the pressure dependence, giving:

$$\epsilon_r = \frac{n_o \Delta L |e|}{\epsilon_o |\vec{E}|} \exp(-\Delta E/2kT) \exp(b'P^{1/2}). \quad (63)$$

It should be noted that Eq (63) does not have a time or frequency dependence, i. e., it yields a steady state solution only. To include transient behavior, Eq (63) can be amended to:

$$\epsilon_r = \frac{n_o \Delta L |e|}{\epsilon_o |\vec{E}|} \exp(-\Delta E/2kT) \exp(b'P^{1/2}) [1 - \exp(-t/\tau)], \quad (64)$$

where τ is the relaxation time, or the time for a carrier to diffuse a set distance along the edge of the unit cube.

Eq (64) is seen to satisfactorily agree with the effects observed on the macromolecular solids investigated in this study as can be shown by an example calculation. Choosing typical values for the parameters of a sample to be:

$$\Delta L = L/2 \sim 4000 \text{ \AA}/2 = 2 \times 10^{-7} \text{ M}$$

$$n_o \simeq 10^{21}/\text{cc} = 10^{26}/\text{M}^3$$

$$e = 1.6 \times 10^{19} \text{ coul}$$

$$|\vec{E}| = 25 \text{ V/cm} = 2.5 \times 10^3 \text{ V/M}$$

$$E = 2E_a = 0.5 \text{ eV}$$

$$P = 0$$

$$T = 300^\circ\text{K}$$

$$t = \infty .$$

Then one finds: $\epsilon_r = 1450$.

As the \vec{E} -field increases to 250 V/cm, the calculated ϵ_r drops to 145. On examining the data in Tables XI and XII, it is seen that none of the polymers exhibits a drop in ϵ_r by a factor of 10 when the \vec{E} -field is correspondingly increased by a factor of 10. However, it is seen that in all cases ϵ_r drops with \vec{E} -field. Consider, e.g., polymer JM77B at 40 V/cm (Table XII). When the \vec{E} -field is increased by a factor of ~ 10 , it is seen that ϵ_r drops to $\sim 1/2$ of its original value. Again, this same effect is observed for sample DPlA at pressures of 1.89 and 12.6 kbar in Table XII when the \vec{E} -field is increased from ~ 40 V/cm to ~ 400 V/cm.

Possibly a better choice would be a model that is dependent upon the inverse square root of \vec{E} , or at least \vec{E} to some power smaller than -1. At any rate, the simplified model qualitatively fits the observations.

Tables XI and XII bear out something further. At high pressures, the D.C. \vec{E} -field effect is much more pronounced on ϵ_r than the A.C. \vec{E} -field dependence (e.g., polymer DPlA), while at lower pressures they each have about the same effect on ϵ_r .

With regard to the dispersion and the relaxation times observed in these macromolecular solids, considering $\tau \simeq 10^{-3}$ sec and $t \simeq 1/\omega$, one finds for the example calculation of ϵ_r the expected frequency dependence as shown on the following page.

τ	t	ω	$e^{-t/\tau}$	$1 - e^{-t/\tau}$	ϵ_r
10^{-3}	∞	0	0	1	1450
10^{-3}	10^{-2}	10^2	e^{-10}	1	1440
10^{-3}	10^{-3}	10^3	e^{-1}	0.63	925
10^{-3}	10^{-4}	10^4	$e^{-0.1}$	0.095	138

Thus, it is seen that in all respects regarding the dependence of ϵ_r upon \vec{E} , P , T , and ω , Eq (64) qualitatively accounts for the behavior observed. Hence, the hyperelectronic polarization model seems to fit the observed effects, whereas the normal dielectric theories of polarization do not predict the proper dependencies of ϵ_r upon \vec{E} , P , T , and ω .

Relaxation Times and Dispersion

Convincing evidence for the observance of hyperelectronic polarization in macromolecules can be seen from an examination of the frequency response of the dielectric constant and resistivity. It has already been mentioned that for the samples studied, we saw a strong dispersion in the dielectric constant near a frequency of 1-10 KHz.

The question is raised as to whether this dispersion frequency, indicating a relaxation time on the order of 10^{-3} to 10^{-4} sec, is consistent with what one would expect from a simple treatment of a polycrystalline sample, in which one observes Maxwell-Wagner type polarization (53-60, 145, 146).

In dealing with ceramic or other polyphase materials, one may choose a method of characterizing the sample's electrical behavior from a number of equivalent circuit configurations as was discussed earlier. Considering the simplest circuit (Figure 29 f) as the equivalent configuration for the macromolecular solids, the order of magnitude of the relaxation times will now be estimated.

To arrive at an order of magnitude estimate of the relaxation time, temporarily consider the sample as composed of a one dimensional array of cubic bulk grains of dimension d , separated by air gaps of dimension t . For such a case, the Maxwell-Wagner relaxation time is given by:

$$\tau_{MW} = R_b C_g = (\rho_b d/A) (\epsilon_g \epsilon_o dA/t) = \rho_b \epsilon_g \epsilon_o d/t, \quad (65)$$

where A is the cross section of the grain and gap; ϵ_g and ρ_b are the relative dielectric constant of the gap and resistivity of the bulk grain, respectively; and ϵ_o is the permittivity of free space. The order of magnitude of τ_{MW} for such a system are now estimated by assigning reasonable values to the above parameters.

Consider, for example, Sample DP1A. A bulk resistivity and dielectric constant of $\rho_b = 10^2$ ohm cm and $\epsilon_b = 10$; a gap resistivity and dielectric constant of $\rho_g = 10^{20}$ ohm cm and $\epsilon_g = 1$; a grain size of $d = 10$ micron; and a gap of $t = 1000 \text{ \AA}$ are estimated to be reasonable parameters for the sample. From these values, one calculates the relaxation time from Eq (65) to be:

$$\tau_{MW} = (1 \text{ ohm-M}) (1) (8.85 \times 10^{-12} \text{ Fd/M}) \frac{(10 \times 10^{-6} \text{ M})}{100 \times 10^{-10} \text{ M}}$$

$$\tau_{MW} \simeq 10^{-9} \text{ sec.}$$

This value of τ is far removed from the value observed ($\tau_{\text{obs}} \simeq 10^{-3}$ sec).

One may choose to use a more elegant Maxwell-Wagner model for computing the relaxation times in hopes of obtaining better agreement with the observed τ_{obs} . For example, Takashima (162) has developed an expression for τ for dielectric particles dispersed in a continuous medium given by:

$$\tau_T = (2\epsilon_1 + \epsilon_2) / 4\pi(2\sigma_1 + \sigma_2), \quad (66)$$

where ϵ_1 and σ_1 are the dielectric constant and conductivity of the particles; and ϵ_2 and σ_2 are the dielectric constant and conductivity of the medium. (Note: Here ϵ is not the relative dielectric constant as before used. We therefore, must multiply Eq (66) by ϵ_0 .)

Taking the same values for sample DPIA as used in the above calculation of τ_{MW} , we find:

$$\tau_T = \frac{[2(10) + 1] (8.85 \times 10^{-12} \text{ Fd/M})}{4\pi[2(1) + 10^{-20}] (\text{ohm M})^{-1}}$$

$$\tau_T = 10^{-11} \text{ sec.}$$

This τ does not agree as well with τ_{obs} as does the simple model which was first chosen. Further examples of relaxation times may be tried, such as that developed by Koops (56),

$$\tau_K = \frac{\epsilon_0 \rho_1 \rho_2 (\epsilon_1 + x \epsilon_2)}{x \rho_1 + \rho_2}, \quad (67)$$

where ρ_1 and ϵ_1 are the oxide layer parameters; ρ_2 and ϵ_2 are the bulk grain parameters; and x = ratio of the thickness of the oxide layers to the grains.

Again using the data for Polymer DP1A (and taking Koop's value of $x = 0.45 \times 10^{-2}$), we find:

$$\tau_K = \frac{8.85 \times 10^{-12} \text{Fd/M} (10^{18}) (1) \text{ ohm}^2 \text{M}^2 \quad 1 \quad 0.5 \times 10^{-2} (10)}{(0.45 \times 10^{-12}) (10^{18}) \quad 1 \quad \text{ohm M}},$$

$$\tau_K \approx 10^{-9} \text{ sec.}$$

One could continue using various models such as those developed by Verwey (54), Hilborn (57), and Sillars (59); however, it is apparent that the application of such models will not fit the observed behavior of the dispersion. The anomaly can be removed, however, if one uses the hyperelectronic polarization model in which the molecule is considered to be quite elongated, and is treated as the bulk grain.

Pollak (61) has pointed out in an analysis of Takashima's (162) approach to calculating relaxation times for DNA that Eq (66) is not applicable to the cases of highly elongated molecules. He developed an expression for τ which is appropriate to the case of Maxwell-Wagner mechanism for highly elongated molecules. For such a case of elongated molecules, of length L and diameter b , with $b \ll L$, Pollak's relaxation time, τ_P , is given by two forms; one representing polari-

zation along the long dimension, the other along the short dimension;

$$\tau_L = 2L^2\epsilon / (Cb^2\sigma_L) \quad (68a)$$

$$\tau_b = 2\epsilon / \sigma_b, \quad (68b)$$

where $C = 2 \ln(4L^2/b^2)$; ϵ is an average dielectric constant of the medium and the molecules; and σ_L and σ_b are the conductivities in the respective directions within the molecule.

Since the large domain is dominant for observing hyperelectronic polarization, we are concerned with only Eq (68a) above. Further, since we are interested in an order of magnitude calculation only, Polak (62) has suggested replacing Eq (68a) with:

$$\tau_P \approx \epsilon_o \epsilon_b \rho_b \left[\frac{L}{b} \right]^2. \quad (69)$$

Again, using the parameters chosen for sample DP1A, and in addition using for L the values of $\sim 1500 \text{ \AA}$ as determined by the spin activation measurement and the \vec{E} -field measurement as discussed in Chapter III and IV, and for b , the average chain diameter distance of 4 \AA , one computes τ_P to be:

$$\tau_P = 10(8.85 \times 10^{-12}) Fd/M (1 \text{ ohm M}) \frac{1500 \text{ \AA}}{4 \text{ \AA}}$$

$$\tau_P \approx 10^{-5} \text{ sec.}$$

This calculated τ_P agrees well with the observed τ_{obs} , and lends strong support to the interpretation of the high dielectric constants observed as due to hyperelectronic polarization so postulated earlier.

Table XIII lists estimated parameters for 11 polymers examined

TABLE XIII

ESTIMATED PARAMETERS FOR POLYMERS

Polymer	Bulk Properties					Gap Properties		
	ϵ_b	ρ_b (ohm cm)	d (microns)	L (Å) ^(a)	b (Å)	ϵ_g	ρ_g (ohm cm)	t (Å)
EHE102	10	10^6	1000	100	4	1	10^{20}	10^4
EHE59	10	10^3	100	2500	4	1	10^{20}	10^3
JM77B	10	10^3	10	1900	4	1	10^{20}	10^3
DPIA	10	10^2	10	1500	4	1	10^{20}	10^3
SK3A	10	10^3	10	2500	4	1	10^{20}	10^3
JM85B	10	10^2	10	2000	4	1	10^{20}	10^3
JM82	10	10^2	10	5200	4	1	10^{20}	10^3
JM50	10	10^3	10	15500	4	1	10^{20}	10^3
JM96A	10	10^4	10	2500	4	1	10^{20}	10^3
JM97A	10	10^4	10	2500	4	1	10^{20}	10^3
JM89B	10	10^4	10	2500	4	1	10^{20}	10^3

(a) Obtained from ESR measurements and \vec{E} -field measurements.

in this study, while Table XIV lists the relaxation times as computed by the formulae used for sample DPlA. It is seen that in all cases, the Pollak relaxation time closely agrees with the observed relaxation time.

Hence, from an analysis of the relaxation times, we see that the results indicate normal macroscopic Maxwell-Wagner polarization cannot account for the observed results; however, hyperelectronic polarization or Maxwell-Wagner polarization on the molecular scale can reconcile the anomaly in relaxation times.

Electrode Studies and Sample Morphology

It is well known that macroscopic scale Maxwell-Wagner (interfacial) polarization depends sensitively upon the morphology of the materials present. Typical assemblies of materials exhibiting such Maxwell-Wagner polarization are alternant sheets of metal and insulator or dispersions of metallic spheres in an insulator matrix (145) or compactions of conducting oxide grains surrounded by a thin layer or pellicle of less conductive materials or by voids (54-60). The observed frequency response of the effective dielectric constant and "in-place" resistance of these macroscopically inhomogeneous materials can be simulated "theoretically" by curve fitting, using lumped circuit equivalents with a complex of virtual resistors and capacitors in various series and parallel arrays as has been discussed earlier (54-60, 145, 163). The method of lumped circuit equivalents is a powerful means for giving an "engineering" description of practically any dielectric, even, as von

TABLE XIV

RELAXATION TIMES OF MACROMOLECULAR SOLIDS

Polymer	Relaxation Time (sec)				
	(a) τ_{obs}	(b) τ_{MW}	(c) τ_{T}	(d) τ_{K}	(e) τ_{P}
EHE102	$\sim 10^{-2}$	10^{-4}	10^{-7}	10^{-5}	10^{-2}
EHE59	$\sim 10^{-4}$	10^{-7}	10^{-10}	10^{-8}	10^{-4}
JM77B	$10^{-3} - 10^{-4}$	10^{-8}	10^{-10}	10^{-8}	10^{-4}
DP1A	$10^{-3} - 10^{-5}$	10^{-9}	10^{-11}	10^{-9}	10^{-5}
SK3A	$10^{-3} - 10^{-4}$	10^{-8}	10^{-10}	10^{-8}	10^{-4}
JM85B	$10^{-3} - 10^{-4}$	10^{-9}	10^{-11}	10^{-9}	10^{-4}
JM82	10^{-3}	10^{-9}	10^{-11}	10^{-9}	10^{-4}
JM50	$10^{-2} - 10^{-3}$	10^{-8}	10^{-10}	10^{-8}	10^{-3}
JM96A	10^{-3}	10^{-7}	10^{-9}	10^{-7}	10^{-3}
JM97A	$10^{-2} - 10^{-3}$	10^{-7}	10^{-9}	10^{-7}	10^{-3}
JM89B	$10^{-2} - 10^{-3}$	10^{-7}	10^{-9}	10^{-7}	10^{-3}

(a) τ_{obs} = observed relaxation time.

(b) τ_{MW} = relaxation time as calculated from Maxwell-Wagner methods [Eq (65)].

(c) τ_{T} = relaxation time as calculated by Takashima's method [Eq (66)].

(d) τ_{K} = relaxation time as calculated by Koop's method [Eq (67)].

(e) τ_{P} = relaxation time as calculated by Pollak's method [Eq (69)].

Hippel (145) showed, for water or chlorinated hydrocarbons which are certainly single phase systems. The fact that a given dielectric's behavior can practically always be expressed in terms of lumped circuit equivalents has led some to the erroneous belief that a successful description of the dielectric characteristics by lumped circuit equivalents then implies that the material is displaying macroscopic scale Maxwell-Wagner or interfacial polarization. Such a conclusion is unwarranted, as von Hippel showed in the cases of water and the chlorinated hydrocarbons. In the present case of the study of macromolecular solids which exhibit very high dielectric constants, one could construct a lumped circuit equivalent made of virtual capacitors and resistors in some array which would give an excellent engineering description of a given polymer; but that type of analysis would present no evidence, pro or con, as to the fundamental nature of the polarization processes actually present. An analysis by lumped circuit equivalents cannot in itself distinguish between macroscopic scale Maxwell-Wagner (interfacial) polarization and molecular scale Maxwell-Wagner (hyperelectronic) polarization.

How then can one distinguish between interfacial polarization on the one hand which always involves at least two phases of materials; and on the other, those polarizations which are molecular in their scale of origin? In particular what evidence can be adduced to say that in the polymers under discussion here, the polarization is hyperelectronic plus other molecular scale polarizations rather than macroscopic and

interfacial polarization?

To begin with, it is pointed out that these polymers are single, highly purified materials. Under the conditions of measurement [temperatures up to 150°C, pressures up to 20 kbar (300,000 psi)] , the samples must be void-free, for these pressures are a factor of about ten higher than the compressive or tensile strengths for known organic polymers (164). These polymers cannot therefore be giving rise to an interfacial polarization of a particle-void-particle type, for the dielectric properties vary smoothly with pressure and temperature over all ranges. The dielectric constant, for example, increases steadily with pressure even at the extreme pressures and shows no sign of collapse at the extreme pressures as might be expected for voids in soft materials.

It might be argued that the polymers, here found to have high dielectric constants, have some special gross morphology capable of showing interfacial polarization, such as consisting of conductive particles surrounded by thin pellicles of poorly conductive polymer. Such an argument is very hard to refute for its proponent can always retreat to supposing "insulating monolayers" and the like for which no techniques known to the author would suffice to show as being positively absent. However, the following evidences are considered as constituting considerable grounds for the basence of two such polymeric phases causing the observed high polarization.

First, the pure polymer SK3A, which is Cu(II)-NN¹- dimethyl

rubeanate polymer, is very soft and flows like butter under these pressures. Under high magnification, molded samples show no evidence of physical inhomogeneity. It is furthermore very difficult to conceive that this single substance of high dielectric constant (~ 1600) can maintain a two phase nature, like, for example, in the ceramic or oxide compacts (54-60, 163) with a thin poorly conducting layer always surrounding a conducting region throughout the pressure range and temperature range of the experiment. If conducting regions gain contact across the sample, they "shunt out" the interfacial polarization. Thus, it is concluded that the $\text{Cu(II)-NN}^{\text{I}}$ dimethyl rubeanate polymer is a macroscopically homogeneous polymer displaying hyperelectronic polarization.

Second, if a polymer sample is indeed an assembly of conductive grains each wrapped in a layer of poorly conductive substance, one would expect that harsh physical treatment as by intense and long continued shearing would bring about notable changes in the grain-to-layer distribution and therefore in the interfacial polarization. But exposure of the polymer even to drastic shear produces no particularly significant change, as one can see by inspection of the data of Table XV. The sheared sample, premolded at 20 kbar was subjected to 3° of shear ten times while under 2.5 kbar of uniaxial pressure and in a layer 0.25 mm thick. The dielectric constants for the sheared and unsheared samples agree to within $\pm 10\%$, the precision of measurement.

To further investigate the possibility of the samples being made

TABLE XV

ELECTRODE, THICKNESS, AND SHEAR EFFECTS ON
DIELECTRIC CONSTANT OF POLYMER DPIA^(a)

Pres- sure (Kbar)	Mechanical Treatment	Electrode Material	Sample Thickness t (mm)	ϵ_r			
				100Hz	1KHz	10KHz	100KHz
2.8	Unsheared	WC	0.33	590	451	336	-
1.2	Unsheared	WC	0.25	600	470	342	-
2.5	Unsheared	WC	0.24	750	490	260	172
2.5	Unsheared	WC	0.16	732	485	303	171
2.5	Unsheared	WC	0.13	565	425	336	155
1.5	Unsheared	Pt	0.33	680	480	305	178
2.5	Unsheared	Au	0.24	666	520	280	176
2.5	Sheared (60° at 2.5 kbar)	WC	0.14	680	445	300	162

(a) All entries obtained at 300°K with $\vec{E} \sim 10$ V/cm.

of conducting grains surrounded by a high resistive layer, a study of polarization on grain particle size was performed. Polymer EHE102, is somewhat more dense and physically harder sample, which forms much larger polycrystalline particles than the other polymers, was chosen for this investigation, since it did not exhibit a significant degree of hyperelectronic polarization. At 100 Hz, the dielectric constant of EHE102 varied from ~ 15 to 50 at room temperature under pressures from 1.4 kbar to 20 kbar, respectively. It exhibited only a very slight \vec{E} -field dependency of ϵ_r and σ . (Note, however, that the field measurements indicate a very short molecular length for polymer EHE102, which, when used in the Pollak relaxation equation yields $\tau_P = 10^{-2}$ which is in agreement with the observed τ_{obs} .) Thus, if the polarization as observed in these macromolecular solids is actually due to the grain size, perhaps EHE102 could be made to exhibit a higher polarizability by diminishing the particle size.

Polymer EHE102 was ground in a stainless steel micro-mill, and the resulting powder was sorted through several sieves, resulting in particle sizes ranging from $\gg 125 \mu$ to $\ll 1500 \mu$. Microscopic investigation of the smallest particle size of polymer EHE102 indicated that they were on the order of the size of the particles of those polymers which exhibit high polarizability.

Measurements of the electrical properties of the smallest particles of EHE102 indicated no significant change in ϵ_r nor ρ as compared to those for the largest particles, when each was measured under

similar conditions. This lack of change in ϵ_r with particle size, together with the agreement of relaxation times, would indicate that the absence of high polarizability in polymer EHE102 is due to the small molecular domains. Thus, the polarizability as observed is somewhat smaller but is consistent with the hyperelectronic polarization picture.

It is concluded, then, from the knowledge that these polymers are single substances and from the evidence of microscopic examination, from the observance of high (1600) dielectric constant on a polymer which is physically weak and waxy, and from the unchanging dielectric behavior despite drastic shear and change in particle size, that the observed high polarizability here is not due to the presence of two phases (i. e., interfacial polarization). There remains the possibility that the observed effective high dielectric constants on these polymers is due perhaps to a surface layer effect between the sample and the contacting electrodes of the measuring cell. If this were the case, it should show up on changing sample thickness or on changing electrode materials. As can be seen from the data of Table XV, the experimentally measured dielectric constant is not a function of sample thickness. From the data of Table XV and further from Figure 53, it is seen that the electrode material has no visible effect. It is concluded, therefore, that surface polarization effects are absent or so small as to be within experimental error. They certainly cannot account for the observed high dielectric constants of these polymers.

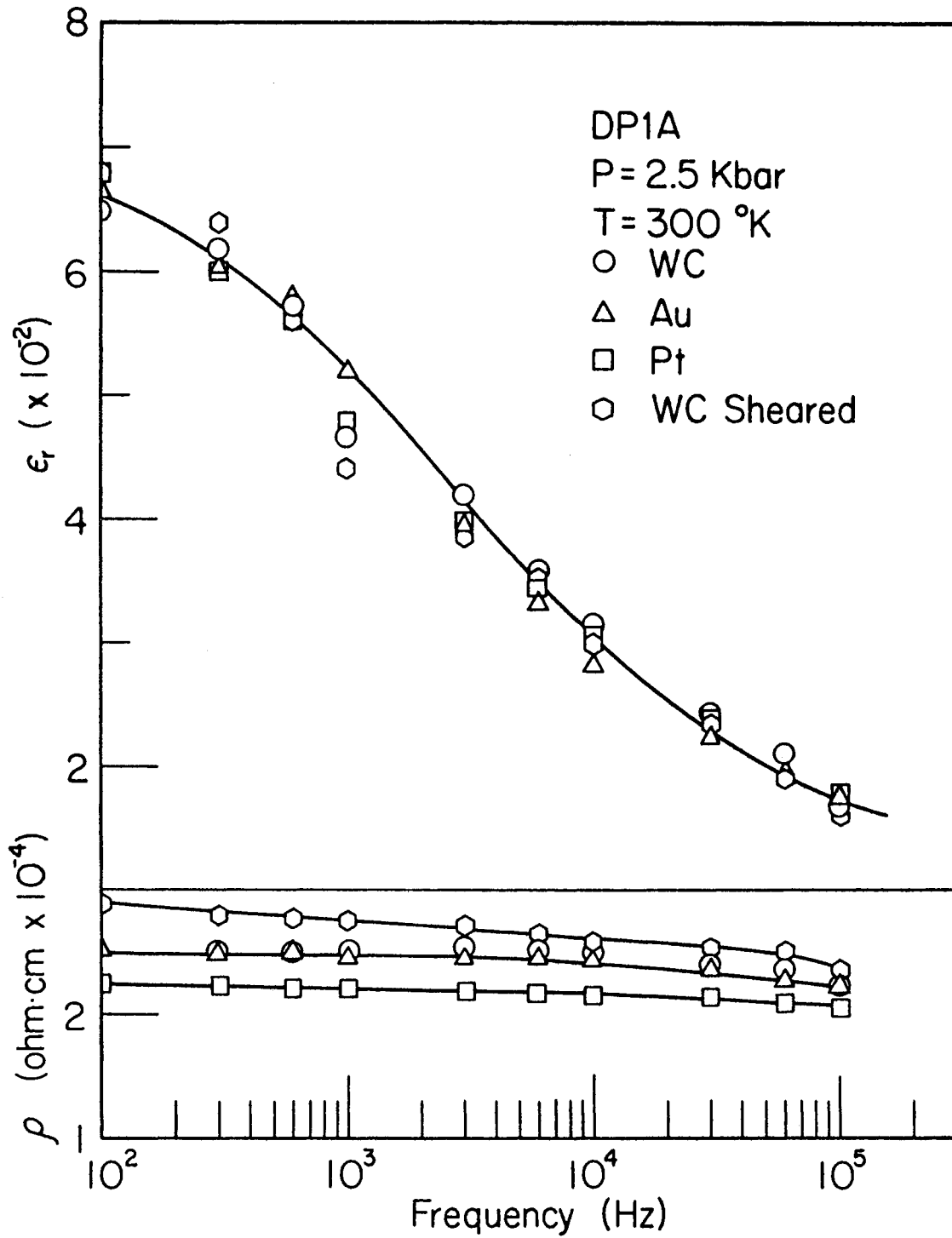


Figure 53. Frequency Dependence of the Dielectric Constant for Polymer DP1A Using Various Electrodes and Mechanical Shearing Stress

Unpaired Spins and O₂ Effects

As mentioned in an earlier section of this chapter, there is an indication that ϵ_r is related to the unpaired spin concentration in the sample by way of a similarity in low temperature activation energies for ϵ_r and S . Since we have seen in Chapter IV that σ is a direct function of the spin density, we would likewise expect ϵ_r to be such, since ϵ_r is found to be larger in materials with high σ 's.

A study of the dependence of ϵ_r on changing the spin concentration was performed on polymer DP1A. After first determining ϵ_r and ρ in air, the specimen was outgassed and quenched with O₂. The electrical properties were once again measured in air. It was found that ρ had slightly decreased, while ϵ_r had decreased considerably. Outgassing of the specimen again, with ϵ_r being determined in an N₂ atmosphere (sample is free from O₂) resulted in an increase in ϵ_r to a value slightly larger than the initial value. In each case, ρ is only slightly effected.

Another DP1A specimen was measured in air, after which it was heated in vacuum to 700°C. ϵ_r and ρ were again determined, with the resistivity being lowered by more than an order of magnitude, while ϵ_r being decreased by \sim a factor of 2-1/2. Outgassing and remeasurement of ϵ_r and ρ in an N₂ atmosphere did not result in a significant change from the heat-treated values.

In each case above, the spin density was determined. The result

indicates that O_2 quenching depletes the spins by a factor of ~ 10 , while heating the sample completely quenched the signal. The O_2 effect is reversible (Cf. Chapter IV) while the heat treatment was irreversible. Apparently pyrolysis of the specimen had occurred at the high temperature, thus accounting for the drop in resistivity. (Pyropolymers are much more conductive than PAQR polymers.)

Hence, it is seen that a direct relation between spins and ϵ_r exists. Although a model has not been worked out to give the qualitative dependence, it is seen that ϵ_r is directly proportional to S in some fashion. This observation is in agreement with the low temperature measurements of ϵ_r , where it was seen that the activation energy for ϵ_r was approximately equal to the spin activation energy below $\sim 200^\circ K$.

A further oxygen effect was observed on ϵ_r . After initial measurements of ϵ_r and ρ with various electrode materials, the specimen was left in air for some time. Further measurements of ϵ_r and ρ indicated that ϵ_r was somewhat larger, and indicated an increased dispersion in ϵ_r when checked with the various electrodes. This effect was shown to be due to the build up of an oxide layer on the surface since outgassing of the specimen and remeasuring ϵ_r in an N_2 atmosphere gave the initial results.

The effect of an O_2 layer was simulated also by using Al electrodes (which were highly oxidized). These measurements indicated a very large dispersion in ϵ_r . In all cases, the oxide layer effect on

ρ was not too pronounced, excepting for the case of the Al electrodes. At all times, when measurements were made on a dry freshly premolded specimen with clean electrodes, there was no difference in the results for ϵ_r as measured with Au, Pt, and WC electrodes as previously stated.

Summary

A.C. polarization and conduction measurements have been made on eleven macromolecular solids which have been previously classified as organic semiconductors. An unusually large polarization was observed in these solids, with dielectric constants ranging as high as 70,000. This unusual and normally unexpected result has been attributed to hyperelectronic polarization.

Hyperelectronic polarization, first suggested by Rosen and Pohl (38, 39), is due to the interaction of an externally applied \vec{E} -field with thermally produced ion or exciton charge pairs which are temporarily localized on extremely long molecular domains of near-zero resistance as are present in highly conjugated macromolecular organic solids.

The observed variations in the dielectric constant, ϵ_r , and conductivity, σ , (or resistivity, ρ) for the materials studied were found to be consistent in all respects with the proposed model of hyperelectronic polarization. In particular, the dielectric constant was observed to be exponentially dependent on $P^{1/2}$, inversely dependent on the applied \vec{E} -field, and exponentially dependent on $-1/T$; while the resis-

tivity was seen to vary exponentially with $-P^{1/2}$, directly with the \vec{E} -field, and exponentially with $1/T$. Both ϵ_r and ρ exhibited dispersion, relaxing at a frequency $\omega \sim 10^3$ to 10^4 Hz, or a relaxation time $\tau \sim 10^{-3}$ to 10^{-4} , with ρ in general showing only mild dispersion, while ϵ_r exhibited pronounced dispersion. A mathematical model was developed which accounts for the observed dependences of ϵ_r and ρ , and which is consistent with the model of hyperelectronic polarization.

By applying Pollak's (160) criteria for detecting band type conduction as opposed to the hopping type conduction, the dispersion of ρ and ϵ_r gives evidence of the hopping model, and hence lends additional support to the model of hyperelectronic polarization. Further support of hyperelectronic polarization was obtained by the resolution of the anomalies in the expected and observed relaxation times of these dispersions which was accomplished by applying Pollak's relaxation model (61, 62).

Low temperature studies of several polymers indicated a connection between ϵ_r and the unpaired spin concentration, S , in the material by way of a similarity in the activation energies for ϵ_r and for S below $\sim 200^\circ\text{K}$. Further direct studies supported this as ϵ_r was seen to vary directly with S , as the spin concentration for a given polymer was changed by various heating and outgassing treatments.

Also, in a couple of polymers, anomalous behavior of ϵ_r in the regions of $T \sim 250^\circ\text{K}$ to 200°K , and again at $T \sim 90^\circ\text{K}$ to 77°K indicated the possibility that these macromolecular organic solids may be ferroelectric in nature. Poor experimental arrangements would not

allow adequate data to be obtained in the mid-temperature range. It is possible that the effects were due to experimental error. However, if these materials were found to be ferroelectric, it would lend more support to the hyperelectronic polarization model, and would further clarify other anomalies in $\epsilon_r - T$ studies reported by Rosen and Pohl(38, 39) earlier.

Since hyperelectronic polarization is observed to exhibit dispersion in the region normally attributed to Maxwell-Wagner surface polarization, it was necessary to establish that the observations were indeed due to hyperelectronic polarization and not to Maxwell-Wagner polarization. This was accomplished by showing:

1. The observed dependence of ϵ_r upon pressure is not what is expected from conventional polarization theories.
2. The observed dependence of ϵ_r upon temperature is not what is expected from conventional polarization theories.
3. The observed dependence of ϵ_r upon \vec{E} -field strength is non-linear and not what is to be expected from conventional polarization theories. For cases reported in the literature for ϵ_r being \vec{E} -field dependent, it is normally attributed to surface polarization and blocking layer capacitance effects.

These effects would be dependent upon the type of electrode used, and upon the sample thickness. Studies performed in this investigation showed that ϵ_r is independent of the electrode used, and also of the sample thickness.

4. The dependence of ϵ_r upon particle size in a polycrystalline sample and hence upon grain-boundary effects was negligible. For Maxwell-Wagner polarization, grain boundaries and surface-bulk effects, etc. play the leading role.
5. The dependence of ϵ_r upon exposure of the sample to severe pressure and temperature treatment and shearing stress was found to be negligible. If the sample were composed of two or more phases, or of voids in the bulk, severe pressure treatment should result in a sharp discontinuity of ϵ_r ; or shearing should rupture the insulating layer and give rise to a drastic change in ϵ_r . These effects were not observed. Further, microscopic examination of the specimen indicated it was a single material and showed no evidence of physical inhomogeneity.
6. The observed dispersion relaxation times ($\tau \sim 10^{-3}$ to 10^{-4} sec) did not agree with the calculated Maxwell-Wagner model relaxation times ($\tau \sim 10^{-9}$ to 10^{-11} sec), but the anomaly between these relaxation times was resolved by applying Polak's (61, 62) model which assumes extremely long molecules, a basic postulate of the hyperelectronic model.

Hence, it is concluded on the grounds of the lack of expected observable Maxwell-Wagner effects, together with the lack of conventional polarization theories to explain the phenomenon of unusually large dielectric constants in materials normally classed as insulators and

plastics; that the observed effects are not due to normal surface-grain boundary polarization of the Maxwell-Wagner type. However, if one assumes the hyperelectronic model to be applicable, whereby: (1) the grain boundary is replaced by the molecule itself; and (2) the relaxation time is modified by the product of the square of the ratio of the molecular length to molecular diameter as suggested by Pollak (61, 62); one then finds the calculated relaxation time is in agreement with the observed relaxation time. Thus, hyperelectronic polarization may be looked upon as Maxwell-Wagner polarization occurring on a molecular scale, and it is concluded that hyperelectronic polarization is the principal contribution to the high polarizabilities of long polymeric ekaconjugated (15, 39, 45) macromolecular solids.

Suggestions for Future Studies

Hyperelectronic polarization has been based upon the concept that highly mobile charges located on highly elongated molecules can exhibit a very large polarization when a weak \vec{E} -field is applied, due to the large dipole moment arm. It has been suggested that these molecules, and hence, the moment arms, are on the order of 4000 \AA in length.

Unfortunately, the polymers in which hyperelectronic polarization has been observed are insoluble, so that the usual osmotic or viscosimetric methods of molecular weight determination are unavailable. Thus, one can not make direct determinations of molecular weights or lengths. As has been discussed in this thesis (Chapter III and IV) there

are two alternate methods, the \vec{E} -field dependence of conductivity, and the spin activation energy, which may be employed to infer the approximate molecular length. Both of these methods are approximate only; but tend to give satisfactory agreement when compared.

In view of the inference that hyperelectronic polarization is molecular in scale, it would be well to study semiconducting polymers which are soluble, such that actual molecular lengths and molecular weights could be obtained, and thus one could investigate the polarization as a function of molecular weight and molecular length. In this fashion, if hyperelectronic polarization is observed, one could accept or reject the hypothesis of its being molecular in origin.

With regard to the possibility of those polymers which exhibit hyperelectronic polarization being ferroelectric, it would be worth while to study those polymers very carefully to determine the ϵ_r dependence on temperature over a very large temperature range.

Further investigation into the morphology of the polymers would also appear in order. It would be well to study the surface of the materials before and after shearing with aid of electron microscopy. In addition, one could utilize a D.C. conductivity noise fluctuation technique to obtain information as to whether the sample is amorphous or polycrystalline. Brophy (165) has shown that plastic deformation of single crystals leads to a considerable increase in the current noise (i. e. fluctuations in σ). Kornfel'd and Sochava (166, 167) further observed that a polycrystalline material is very noisy, with the noise

falling off exponentially with temperature of the sample, while an amorphous material is much less noisy. Further, a liquid polycrystalline melt has almost no noise, i. e., it is below the limit of the detective system. An alternate way of studying sample morphology has been proposed by Stegavik (168) making use of statistical fluctuations in x-ray reflections and x-ray diffractions.

In addition, since it has been established that the dielectric constant is dependent on both the charge carrier and spin densities, one could re-examine the polymers reported in this study to determine qualitatively how ϵ_r varies with spins. In this fashion, one could possibly learn how to modify the polymer chemically (such as was done in the study of the effects of the variation of the acene-anhydride system on conductivity in Chapter III) to produce materials with very high ϵ_r 's but low σ 's. Such a material would be of interest to a host of scientists and engineers.

CHAPTER VI

A SEARCH FOR ORGANIC SUPERCONDUCTORS

Introduction

Superconductivity was discovered in 1911 when Kamerlingh Onnes (169) observed that the electrical resistance of a mercury wire vanished completely as it was cooled below a certain temperature. This temperature is now called the critical temperature (T_c), and as the material is cooled below this temperature, it is said to be transformed from its normal state of high resistance into the superconducting state of zero resistance.

Following his initial discovery of superconductivity, Onnes soon found that lead and tin were also superconducting. He further found that the metal could be transformed from the superconducting state back to its normal state even though it was below the critical temperature, if a current larger than some critical value (I_c) were passed through the wire (170). Later this effect was linked to the magnetic field produced by the current; thus, a magnetic field larger than some critical value (H_c) forces the superconducting metal to return to its normal state of high resistance.

Superconductivity has been discovered in many metallic elements of the periodic system, and also in many alloys, intermetallic compounds, and semiconductors. The range of transition temperatures (T_c) known at the present extends from 18.05°K for the alloy Nb_3Sn to 0.01°K for the semiconductor SrTiO_3 . In 1963, Matthias, Geballe, and Compton (171) listed 26 metallic elements as superconductors.

Prior to the increased activity in the area of organic semiconducting materials in the late fifties (as was mentioned in Chapter I) a suggestion was made by F. London (172) to the effect that some of the more complicated organic macromolecules which play an important role in biochemical processes, might possibly exist in a superfluid state, and hence, might exhibit superconductivity.

In 1964, Little (44) discussed the possibility of synthesizing an organic macromolecule which would exhibit superconductivity. This was followed by another suggestion (63), in which he proposed certain types of organic materials might exhibit superconductivity at room temperature (300°K) and, in fact, at temperatures as high as $2,000^\circ\text{K}$.

This is, indeed, a startling prediction, since the highest transition temperature known for any material to become superconducting is 18°K , well below the predicted 300°K .

As was pointed out in Chapter I, it can be expected from theoretical arguments that solids having a high charge carrier concentration, a high dielectric constant, carriers of large effective mass, and a many valleyed potential surface can be expected to exhibit superconductivity.

From the survey of polymers presented in Chapter III, together with the data presented in Chapter V, it is evident that many of these conductive polymers possess these qualifications, and are, therefore, likely candidates for exhibiting superconductive transitions.

Because of the important need for superconducting materials which could operate in the superconducting state at temperatures above the present limit of 18°K , a study was conducted to survey several of the more conducting polymers characterized in Chapter III, in the hopes of finding one or more which would exhibit superconductivity.

Experimental Background

Following the discovery of superconductivity by Onnes in 1911, many materials were examined for the possible existence of superconducting state. Also, the influences of external agents on superconductivity were studied.

With regard to a material which undergoes a superconducting transition, it has now been established that there is no change in the X-ray diffraction pattern nor in the intensity above and below the transition temperature. Neither is there an appreciable change in the reflectivity in the visible or infra-red range. The photoelectric properties are unchanged, as well as the electron absorption properties. Likewise, the elastic properties and the thermal expansion are not observed to change in the transition. In the absence of magnetic fields, there is no change in volume, and no associated latent heat (170).

Regarding those properties which do change during the transition, the magnetic properties undergo a remarkable change in that the superconducting state excludes magnetic flux; thus, the material behaves as though it were diamagnetic (Meissner Effect). (173) The specific heat is found to change discontinuously at the transition temperature, and in the presence of a magnetic field, there is an associated latent heat of transition. This brings on a small change in volume. The thermoelectric effects, as present in the normal state, disappear in the superconducting state. Also, one finds a discontinuous change in thermal conductivity when a magnetic field is present (170).

If a magnetic field of a certain critical value is applied along the axis of a long superconducting body, a transition occurs, restoring the normal state resistance. This critical field, H_c , is given for many materials by:

$$H_c = H_0 \left[1 - (T/T_c)^2 \right]. \quad (1)$$

It was also observed that if an excess current is passed through the superconductor, the material transforms to its normal state. Silsbee (174) suggested that this effect was probably due to the fact that the current had produced the necessary critical field to restore the normal resistance state. This was later verified by Tuyn and Onnes in 1926 (175), and by Scott in 1948 (176).

The critical temperature may be changed by applying stress to the specimen. In general, a compressional stress lowers T_c while a tensile force raises it. Chemical impurities tend to modify T_c also.

It has been found that at microwave frequencies, the superconducting state has a finite resistance.

Another interesting effect observed in superconduction is the "isotope effect," that is, the critical temperature is found to vary with the isotopic mass. Onnes and Tuyn (175) first studied this effect; however it was observed in the form of an empirical law independently by Maxwell (177) and by Reynolds and coworkers (178) in 1951. Within each series of isotopes, it is observed:

$$M^{\alpha} T_c = \text{Constant}, \quad (2)$$

where $\alpha \approx 0.5$. Since the Debye temperature, Θ , is proportional to $M^{-1/2}$, we have:

$$T_c / \Theta = \text{Constant}, \quad (3)$$

thus linking superconductivity to the interaction of electrons with the lattice vibrations.

Regarding pressure effects on the superconductivity transition temperature, Chester and Jones (68,179) developed a high pressure Bridgman opposed anvil cell which they refer to as a "clamp," capable of exerting up to 44 kbar on the sample while it is immersed in liquid He. With this system, they were able to observe a superconducting transition in bismuth for the first time. They used mutual inductance techniques, made possible by the Meissner effect to observe the transition, (the fact that a superconductor becomes diamagnetic) rather than measuring resistance directly. The transition occurred in Bi at $P \geq 20$ kbar, with $T_c \approx 7^{\circ}\text{K}$. The onset of supercon-

ductivity was associated with changes to a more close-packed crystalline form. They also investigated tin, lead, and thallium at high pressures. T_c for Sn was lowered from 3.7°K to 3.0°K at a pressure of 16 kbar; T_c for Pb was lowered somewhat; while T_c for Tl was lowered from 2.39°K to below 2.35°K at a pressure of 13.4 kbar. Hence, in all cases, dT_c/dP was observed to be negative.

A modification of the Chester-Jones clamp was designed and used by Bowen and Jones (180) to study lead, thallium, and tin. This clamp was designed to produce a very accurate uniform pressure on the specimen, and measurements were made only up to 10 kbar. Transition temperatures were obtained much more accurately as a result of the uniform pressure. As pointed out by Bowen and Jones, and independently by Jennings and Swenson (181), the sharp discontinuity in resistance as the critical temperature is approached offers almost the only possibility of judging directly the uniformity in the pressure distribution on the sample.

Of particular interest is the effect of pressure on T_c for thallium. Early work by Kan and coworkers, (182) and by Fiske (183) reported dT_c/dP as positive for Tl. For all other known superconductors, dT_c/dP was found to be negative, and was predicted to be so by theory. Contrary to this finding, Chester and Jones (68) found dT_c/dP to be negative when measured at high pressure. Further work by Hatton (184), Jennings and Swenson (181), and Bowen and Jones (180) revealed an anomalous behavior, in that T_c first starts to increase with

pressure up to ≈ 2 kbar, maximizes, and then decreases monotonically. Bowen and Jones explained this effect using the BCS model (185) and the Frohlich (186) matrix element for electron-phonon interaction. They attributed the change in slope of transition temperature with pressure to a permanent shift in T_c brought about by the compression.

Other workers who have investigated the anomalous behavior of thallium include a group of Soviet Scientists (187-190). Their approach was to alloy Tl with dilute Bi, Sb, or Hg. Their conclusion was that the $T_c(P)$ behavior could be expressed as a sum of a linearly decreasing term due to the decrease in volume, and a nonlinear term for which changes in the topology of the Fermi surface are responsible.

Gey and coworkers (191-193) have investigated high pressure effects (up to 32 kbar) on the superconducting transition temperature of niobium and thallium under hydrostatic pressure conditions. In the case of Nb, they observed that the application of pressure tends to decrease T_c , up to about 5 kbar, after which T_c minimizes and begins to increase with increasing pressure. The rate of increase of T_c with pressure is quite large and is positive above 10 kbar.

Thallium exhibited inverse behavior to that of Nb, in that T_c rose to a maximum at about 2.5 kbar and then began to drop as pressure continued to increase. Gey studied lattice defects in Tl, and was able to change the behavior of T_c with lattice defects systematically. He concluded that the anomalous behavior in Tl was due to an

anisotropy in the energy gap of the material [a la Markowitz and Kadanoff (194)]. As pressure is applied, the anisotropy changes, due to the smoothing out of the energy gap and the electronic mean free path is reduced, thus causing T_c to increase as pressure is applied. As the anisotropy disappears, at higher pressures, the material tends to behave as most superconductors, exhibiting a negative dT_c/dP .

Luders (195) has studied Nb wires under uniaxial stress (up to 28 kbar), and has found the same behavior as Gey (191).

The Soviet Union Scientists have been keenly interested in the behavior of T_c in materials at extreme pressures, as is evidenced by the published works in the late fifties and the sixties. Brandt and Ginzburg (196) developed a pressure system capable of exerting very homogeneous pressures up to 40 kbar on samples while in a liquid He cryostat. Using this system, they studied the high pressure phases of bismuth. The pressure cell was calibrated using a Sn-II manometer. By observing the superconducting transition for Sn-II, the exact pressure was determined, since ΔT_c for Sn-II is linear with ΔP in the range from 1.5 to 45 kbar. For Bi-II, $T_c = 3.916^\circ\text{K}$ at 25 kbar, with $dT_c/dP \simeq -3.2 \times 10^{-2} \text{ }^\circ\text{K/kbar}$, and Bi-III, $T_c = 7.25^\circ\text{K}$ at 27 kbar, with a very small $dT_c/dP (\leq 0)$. Hysteresis between the phase transitions of bismuth was observed to occur.

Further work regarding high pressure effects has been carried out by Brandt and Ginzburg (197-203). They succeeded in modifying

T_c for cadmium by 80% at 26.4 kbars, from $T_c = 0.5^\circ\text{K}$ at $P = 0$ to $T_c = 0.08^\circ\text{K}$ at 26.4 kbar. They further found that the critical field H_c necessary to destroy superconductivity was lowered almost linearly, with the application of pressure. They also investigated the effects of hydrostatic pressure (up to 26 kbar) and plastic deformation on single crystalline and polycrystalline titanium iodide. It was found that plastic deformation and surface states strongly affect T_c and H_c , while hydrostatic pressures up to 14 kbar had no, or at best little, effect on T_c and H_c for either the single crystalline or polycrystalline forms. Above 14 kbar, it was observed that T_c increases slightly with pressure, i. e., $dT_c/dP \approx + 0.7 \times 10^{-2} \text{ }^\circ\text{K/kbar}$.

Brandt and Ginzburg have also studied the effect of pressure on T_c of zinc, aluminum, thallium, and molybdenum. They report that T_c for Zn is decreased by a factor of 2.7 at 26 kbar from T_c for an unstressed sample. In addition, they report $T_c = 0.91^\circ\text{K}$ for Mo with a slightly positive dT_c/dP .

At the First International Conference on the Physics of Solids at High Pressures, held at Tucson, Arizona in 1965, B. T. Matthias (204) suggested since high pressure had induced a superconducting state in such "non superconductors" as Bi, Sb, and Te, it seemed likely that Ge, Si, As, Be, and possibly Ce could also be transformed to superconductors at elevated pressures.

Shortly thereafter, Wittig (205-206) reported Si and Ge to be superconductors. He investigated the behavior of the electrical

resistance of the Group IV elements, silicon, germanium, tin, and lead, at low temperatures and extreme pressures (up to 160 kbar) in an opposed Bridgman anvil system, i. e., a modified Chester-Jones clamp. Using pyrophyllite to contain the sample, he was able to make four point probe measurements under hydrostatic pressure conditions. For normal Sn ($T_c = 3.72^\circ\text{K}$) and normal Pb ($T_c = 7.19^\circ\text{K}$), he found that higher pressures caused a monotonic decrease in T_c at zero magnetic field, i. e., dT_c/dP is a negative value, until a particular pressure was reached. At this pressure, corresponding to a phase change in the structure of the material, a sharp discontinuity in T_c was observed, after which it was found that $T_c = 5.30 \pm 0.10^\circ\text{K}$ at 113 kbar and zero field for Sn-III, and $T_c = 3.55 \pm 0.10^\circ\text{K}$ at 160 kbar and zero field for Ph-II. As the pressure was increased beyond the respective phase transition points, again it was observed that dT_c/dP was negative.

For the normal state semi-metals, Ge and Si, he found that they became superconducting as high pressure was applied. This was interpreted as the transition of the semi-metal into a true metallic structure. It was observed that $T_c = 5.35 \pm 0.10^\circ\text{K}$ at 115 kbar and zero field for Ge, and $T_c = 6.70 \pm 0.10^\circ\text{K}$ at 120 kbar and zero field for Si. He further found that as the pressure was increased above the phase transition point, that negative values for dT_c/dP resulted.

An interesting observation concerning the Debye temperature of the lattice, Θ , and the critical temperature T_c was made. It

was found for the materials examined that $\Theta/T_c \approx 52$.

Gardner and Smith (207-212) have studied pressure effects on T_c for vanadium, niobium, uranium, lanthanum, and in all cases found that T_c tends to increase with pressure contrary to most superconductors. Specifically, they reported an increase from: $T_c = 5.5^\circ\text{K}$ ($P = 0$) to 6.9°K ($P = 10$ kbar) for La; $T_c = 1.0^\circ\text{K}$ ($P = 0$) to $T_c = 2.3^\circ\text{K}$ ($P = 10$ kbar) for U; $T_c = 9.42^\circ\text{K}$ ($P = 0$) to $T_c = 9.44^\circ\text{K}$ ($P = 10$ kbar) for Nb; and $T_c = 5.05^\circ\text{K}$ ($P = 0$) to $T_c = 5.1^\circ\text{K}$ ($P = 10$ kbar) for V. They conclude the effect is primarily associated with the "isotope effect" mentioned earlier.

It is apparent by now that of the host of materials known to be superconductors, virtually all are elemental types, or alloys. Molecular solids have been studied, but only Te (204), Se (213), and potassium graphite (214) have been reported as undergoing a transition to the superconducting state. Hannay, Geballe, and Matthias (214) succeeded in measuring T_c 's from 0.02°K to 0.55°K for golden colored compounds approximating C_8A , where $A = \text{K, Rb, Cs}$. The blue compounds ($C_{16}A$) did not exhibit superconductivity; neither did the individual components, pyrolytic graphite, nor the alkali metals, at temperatures down to 0.011°K .

Selenium, tellurium, and iodine form crystals which are molecular solids, in that long atom-to-atom distances distinctive of van der Waals forces as well as short interatomic distances characteristic of covalent bonds are present. Se and Te form macromolecular

solids with long chains of atoms linked together. In this simpler type of macromolecular solid, superconduction has been observed. Wittig (213) has reported that under high pressure, Se became superconducting.

Although no organic polymer has been reported to be a superconductor, the enhancement of superconductivity in thin metal films was recently demonstrated by McConnell and coworkers (215), by their depositing organic materials on the film.

In summary, it must be concluded that there are several materials which possess a positive dT_c/dP contrary to the behavior expected for superconductors. To date, it has been observed that Zr (200), La (207), U (210), V (208), Ti (199), and Mo (200) have positive coefficients. In addition, at least two more elements, Nb (91 - 193, 195) and Tl (68, 180, 181, 184, 193) have been observed to exhibit positive coefficients in a certain range of pressure. That pressure has been influential in achieving superconductivity in normal state materials is evidenced by the fact that at least Bi (68), Sb (204), Te (204), Ge (205), Si (205), Se (213), and Sn (206) have exhibited such behavior.

Thus, in the light of such evidence, it appears that high pressure, as applied to certain organic macromolecular solids may be the most promising way of increasing the probable occurrence of a superconducting state, if such transition can be induced.

Theoretical Background

From the time of the discovery of superconductivity in 1911 until the early fifties, the mechanism of the formation of the superconducting state was virtually a mystery. The Bloch theory of metallic conduction could not account for the fact of superconductivity, mainly because it is essentially a "one-electron" theory. As such, it considers only the periodic lattice effect on a single electron, and neglects interactions between electrons themselves. Since electron-electron interactions are at the heart of the present day model of superconduction, it is now apparent why Bloch's theory proved inadequate.

In 1950, both Bardeen(216) and Fröhlich(186) independently produced theories in which interactions between the conduction electrons and the lattice modes (phonons) are considered to give rise to the superconducting state.

Since that time, Bardeen, Cooper, and Schrieffer (185) have developed a very plausible theory (BCS Theory) which will be discussed shortly. It has been successful not only in explaining practically all the experimental data that has accumulated over the past half century, but also in predicting a number of new superconducting phenomena.

The main facts which a superconduction theory must account for are:

- (1) Second-order phase transition at T_c .
- (2) A reciprocal exponential dependence of the electronic specific heat on temperature near $T = 0^\circ\text{K}$. [$c_v \propto \exp(-T_0/T)$].

- (3) Evidence for an energy gap for thermal excitations.
- (4) The diamagnetic behavior in the superconducting state
(Meissner effect). ($\vec{B} = 0$)
- (5) Infinite conductivity ($\vec{E} = 0$).
- (6) Isotope effect ($T_c \sqrt{M} = \text{Constant}$).

BCS Theory

When one considers the electrical properties of metals in the normal state, one deals with a dense and highly degenerate interacting electron gas, i. e., the valence electrons in a metal. Upon entering the metallic state, atoms give up electrons to the Fermi sea, and the positive ions form a more or less regular periodic lattice structure. The electrons in the sea are free to roam about, and consequently interact with the lattice and with each other by scattering and by screened Coulombic interactions.

At normal temperatures, the behavior of metals appears to be well understood. Solution of the Schrödinger wave equation for the periodic potential of the lattice gives the band structure and the Bloch single particle wave functions. These wave functions are plane waves, and propagate freely through the lattice unless scattered by phonons or impurities. In the Bloch approach, they are treated as noninteracting waves.

At low temperatures, where a transition to the superconducting state occurs, the above picture breaks down. At, and below the critical temperature, T_c , the one particle Bloch functions no longer give

an adequate description, since all observations lead to the fact that the electronic wave functions are now highly correlated through an interaction with the lattice.

In order to account for superconductivity, it appears that two conditions must be satisfied. First, there must be some kind of electron-electron attraction, large enough that in spite of the Coulombic repulsion, two electrons can be drawn together to form a stable pair. Second, these "bound pairs" are not free to move about at random in the superconducting state, but must be correlated in some way, i. e., they must all be in the same eigen state (64).

Consider an electron as it moves through the positively charged lattice of a metal. As it approaches one of the lattice centers, an attractive interaction occurs. Since the electron is under the influence of a rather large force due to the application of an external \vec{E} -field, it will be moving at a rather high velocity. Hence, it will not be diverted significantly from its course, but rather the positively charged ion will be drawn toward the electron. Due to the rate at which the electron is traveling, and to its large ionic mass, the ion will not reach the point of maximum excursion before the electron is some distance away. Some distance behind the first electron is a second electron. As it approaches the same point, it will find the lattice somewhat distorted, with a higher concentration of positive charge than normal. This provides an added attractive force, and hence "couples" the second electron to the first. These electron pairs have come to be

known as "Cooper" pairs after L. N. Cooper (217), and the mechanism which produces the attraction is known as the phonon-induced electron-electron interaction, since the distortion of the lattice is related to the phonon coordinate. Thus, the first criterion for the existence of superconductivity is established.

The next step is to coordinate the motion of the "Cooper" pairs. Since the distance between the first electron and the excess charge region which it created is on the order of hundreds of angstroms (64), many other electrons will be moving through this region before the second electron gets there. If they are uncoordinated with respect to electron Number one, then they will produce a random fluctuation in the charge density throughout the lattice, and hence will tend to destroy the correlation between electron one and electron two. It is necessary, then, to pair up a large number of electrons and organize their motion such that they do not interfere with one another. At low temperatures, this would be the case, since the forming of pairs greatly reduces the overall energy of the carriers (due to the binding energy necessary to form the pairs). Thus, the system could spontaneously enter the high correlation state if the temperature were low enough.

This correlation of "Cooper" pairs may be realized if one can provide a strong two particle interaction between electron pairs. An attractive interaction is considered via the exchange of virtual phonons with the lattice, while the short-range Coulomb interaction provides repulsion. (The long-range Coulomb forces are screened out.)

The nature of this two body correlation will be such that if the electronic state designated by the wave vector, $\vec{k} \uparrow$ is occupied in any configuration, then the state $-\vec{k} \downarrow$ must also be occupied. In a normal metal, the probability of finding an electron with spin down a distance \vec{r} from another electron with spin up is given by (217):

$$P_n \uparrow \downarrow (\vec{r}) = 1/4 n^2 \quad , \quad (4)$$

where n is the electron density. The probability of finding electron 2 \uparrow a distance \vec{r} from electron 1 \downarrow without considering where 3, 4,N are located, is just the density of electrons of spin \uparrow , i.e., there is no correlation at all between electrons of opposite spin in the normal metal. In a superconductor, however, correlation is required between the \uparrow and \downarrow spin states. This correlation function may be written as (217):

$$P_s \uparrow \downarrow = 1/4 n^2 + f(\vec{r}, \vec{k}) \quad , \quad (5)$$

where the additive term is the extra correlation produced by the interaction between electron, \vec{r} is the relative coordinate between the two electrons involved, and \vec{k} is the total momentum of the electron pair.

The BCS theory is based on a rather idealized model in which anisotropic effects are neglected. It assumes that the two-body correlations are primarily responsible for the qualitative features of superconductivity, and of the two-body correlations a strong preference exists for singlet zero momentum pairs. It contains three parameters, one dependent on the density of energy states at the Fermi

surface, $N(E_F)$; a second, which is a measure of the average velocity of the electron at the Fermi surface, \vec{v}_F ; and a third, γ , which is dependent on the electron-phonon interaction. The third parameter is determined from the specific heat data, while the first is found from the critical temperature. The second parameter is needed to predict the penetration depth of the field.

The normal state is described by Bloch's individual particle model. The ground state wave function of the superconducting state is formed by taking linear combinations of many low-lying normal state wave functions in which the Bloch states are virtually occupied in pairs, possessing opposite spins and momentum. The average excitation energy of the virtual pairs above the Fermi level is approximately kT_C .

Excited states of the superconducting state are formed by first specifying that certain of the Bloch states are occupied, and then using all the rest to form a linear combination of virtual pair configurations. There is a one to one correspondence between excited states of the normal and of the superconducting states.

Within the approximations mentioned, the extra energy which must be included in the Hamiltonian of the system, due to the pair correlation function, is given by (217):

$$W_s - W_n = W_c = -2N(0) (\hbar\omega)^2 \exp(-2/N(0)V), \quad (6)$$

where W_s , W_n , and W_c indicate the energy of the superconducting state, the normal state, and the correlation energy, respectively;

$N(0)$ is the number energy density of electrons with a given spin at the Fermi surface; and V is the interaction matrix (taken to be a constant) between the state \vec{k} and \vec{k}' , i. e.,

$$-V = \langle \vec{k}' | H_r | \vec{k} \rangle . \quad (7)$$

The criterion for superconductivity to occur is for $V > 0$. The dependence of W_c on $(\hbar\omega)^2$ gives the isotope effect.

From a consideration of the thermodynamics of the superconducting transition region, one finds:

$$kT_c = 1.14 \hbar\omega \exp [-1/N(0)V] \quad (8)$$

$$\frac{T_c^2}{H_0^2} = 0.170 \gamma \quad (9)$$

where
$$\gamma = 2/3 \pi^2 N(0) k^2 \quad (10)$$

and
$$v_F = \hbar^{-1} \left| \frac{\partial E}{\partial \vec{k}} \right|_{E_F} \quad (11)$$

Hence, the three parameters, as were mentioned earlier, are related to the variables as defined above.

It has been determined that the most important contribution to the interaction energy is due to the short wave length phonons. The wave functions were chosen for the superconducting state so as to take maximum advantage of this, by giving a large coherence for short wave length phonons extending over large distances in real space. The coherence length as calculated from the uncertainty principle agrees quite well with that of Pippard (218).

In summary, it may be stated that the BCS theory not only accounts for the main features discussed earlier, i. e.: (1) occurrence

of a second-order phase transition at T_c ; (2) an electronic specific heat $c_v \propto \exp(-T_0/T)$; (3) an energy gap; (4) isotope effect; (5) Meissner effect ($\vec{B} = 0$); and (6) infinite conductivity; but it also accounts for the penetration depth (λ_L); the coherence length (ξ_0); qualitatively explains ring current persistence; and includes the law of corresponding states. For further reference, the reader is referred to the literature (185,216,217).

Little's Organic Superconductor

Making use of the BCS theory, Little (44, 63, 64) has predicted that certain organic macromolecules could exhibit superconductivity, with T_c 's as high as 2,000°K. He has proposed an organic molecule composed of alternate single and double bonded carbon forming a spine, with easily polarizable appendages periodically spaced along the spine, as being a likely candidate to exhibit superconductivity.

In theory, the conjugated carbon system, "the spine," would provide a very low resistance to the conduction electron, and hence, when an electric field were applied, the electron can make its way down the spine with ease. Analogous to the heavy metallic ions, or the lattice points discussed in the last section, are the side groups. As the electron passes close to one of the side chain molecules, it polarizes the molecule, leaving a positive charge at the base of the spine. Since the polarization involves only the displacement of an electron on the side molecule, as opposed to the displacement of a massive metallic ion in the normal metal type superconductor, one would expect a much

greater correlation of electron pairs traveling down the spine.

Little has made calculations on a particular molecule, the spine, composed of a conjugated chain of carbon atoms, while the side-chains are a part of diethylcyanine iodide dye. It appears from a detailed quantum mechanical treatment, and also from a simple isotope effect calculation that T_c should be around 2000°K .

Following Little's initial work (44), Ferrell (219) raised the question as to the validity of applying the BCS model to a one dimensional material, such as Little's organic molecule. He pointed out that the compressional modes of vibration are much more dominant in one dimensional solids than in three dimensional ones. For that reason, he felt that the compressional modes would prevent the long-range ordering required for superconductive phenomena. DeWames, et.al., (220) pointed out an error in Ferrell's work, and stated that at best, Little's figure of $T_c = 2000^\circ\text{K}$ should be "greatly reduced."

McCubbin (221) has also criticized Little's predictions by showing that for normally expected energy gaps in polyene type materials, it is very difficult to expect the interaction term to outweigh the Coulombic repulsion between electrons. He did speculate, however, that other types of organics might be expected to exhibit superconductivity.

Paulus (222) has raised the question about the attractive screening of the electrons in a substituted polyene chain. His calculations on five such molecules indicated that the repulsion was somewhat greater in each case. He states when the attractive interaction arises from

electronic virtual excitations, as opposed to vibrational excitations, the attractive interaction is not nearly large enough to make the total effective interaction matrix positive.

Kuper (223) again has refuted Little's calculations, by showing that electrons constrained to move along a one dimensional path are ineffective in screening the Coulombic field of the "test" charge; and thus, the attractive force is not sufficient to overcome the Coulomb repulsion.

With regard to the above attacks, Little still holds firm in his prediction. In later articles (64, 224), he states that for a one dimensional system, the effect of density fluctuations and thermodynamic fluctuations are such as to yield continuous decrease in resistance with temperature, rather than a discontinuous change as in the "three-dimensional" superconductor. Hence, the one-dimensional effect should only lower T_c rather than exclude the transition completely.

In the light of the current debate on the existence of superconductivity existing in a one-dimensional model, Ginzburg (225) has made a suggestion that surface superconduction (two-dimensional) should be expected, just as surface ferromagnetism. It is suggested that the interaction energy needed to produce superconduction could be changed by applying dielectrics or monolayers on the surface. Mention has been made earlier in this Chapter of such work (215).

The work of Hannay, et.al. (214) on potassium graphite indicated that two dimensional superconductivity could be achieved; yet, a

recent paper by Salzano and Strongin (226) points out that no conclusion can be made about two-dimensional superconductivity, as related to the potassium graphite work.

Also of interest is the recent findings regarding semiconductors being superconductors. In addition, such molecular solids as SrTiO_3 and other mixed titanates have been found to be superconducting (67). Cohen (65) and Gurevich and coworkers (66) had predicted a very strong intravalley electron-phonon coupling was needed to produce a transition into a superconducting state. Indeed, the results on SrTiO_3 indicate the necessary criteria are: (1) high carrier concentration; (2) large effective mass; (3) many valleys in energy bands; and (4) large dielectric constant.

Further comments on the possibility of superconductivity in organic macromolecules, semiconductors, and ferroelectrics have also been made by Keldysh (227). He suggests the possibility of achieving high critical temperatures in organic systems.

Ladik and coworkers (228), have made simple model calculations on a polyene system, and have found that it is quite possible to expect a superconductive state if interband scattering processes are accounted for. Their calculations were based on the excitation of a localized σ -bond, rather than π -type orbitals. Further calculations by Lakik, et. al. (229) which have been performed on different periodic DNA models, indicate an unexpectedly large value for the conductivity of such molecular solids.

Regarding the pressure effect on T_c , as was discussed in Section 2 of this Chapter, Ganguly and Sinha (230) have developed a theory to explain the anomalous behavior. They use perturbations of the BCS theory, which can then lead to intraband or interband scattering of electrons near the Fermi surface. They derive expressions relating T_c to pressure, which accounts for positive and negative dT_c/dP 's, depending upon the magnitude of the relative parameters involved. The agreement of experimental data with the theoretical prediction is very good.

Statement of the Problem

In view of the foregoing discussions, in particular the calculations and predictions of Little (44, 63, 64, 224), Ladik and coworkers (228, 229), and Keldysh (227); together with the suggestions of DeWames and coworkers (220) and McCubbin (221); along with the experimental results of McConnell and coworkers (215) and Hannay and coworkers (214); it would appear that it is certainly a worthy project to examine organic macromolecular solids at low temperatures. Also since Wittig (213) has shown pressure induces a superconducting transition in Se, and since it is a known fact that pressure increases the conductivity of organic solids, it would appear a logical approach to study the organic solids under high pressure, while at liquid He temperature.

Hence, this portion of this thesis describes a study of the electrical conductivity of thirteen organic macromolecular solids at

temperatures down to 1.5°K , and under pressures of up to 10 kbar. All of the materials studied tend to satisfy the four criteria which semiconductors should possess for being potential superconductors, as discussed previously (65 - 67).

Experimental Apparatus and Procedure

In order to achieve the high pressures desired, a miniature Bridgman opposed anvil cell, i. e., a Chester-Jones clamp (68) was constructed in our machine shop from one inch circular stock Be-Cu. The entire clamp was constructed from the same material to insure a minimum of pressure change on the sample when the clamp was immersed in liquid He.

The lower anvil was electrically insulated from the upper electrode and the rest of the clamp housing. In this way, direct resistance measurements could be made. The clamp was designed for both magnetic and electrical measurements; however, this work was involved only with electrical measurements. The clamp assembly is shown in Figure 54. It is drawn approximately to scale. The anvils were hardened to $\approx 350\text{-}420$ Brinell (231) in order to insure minimum distortion at the desired pressures.

A liquid He cryostat was constructed in our glass shop. It consists of two pyrex strip silvered dewars, the inner dewar being approximately three inches in diameter, and equipped with a pumping port for evacuating the jacket. The outer dewar, which holds liquid

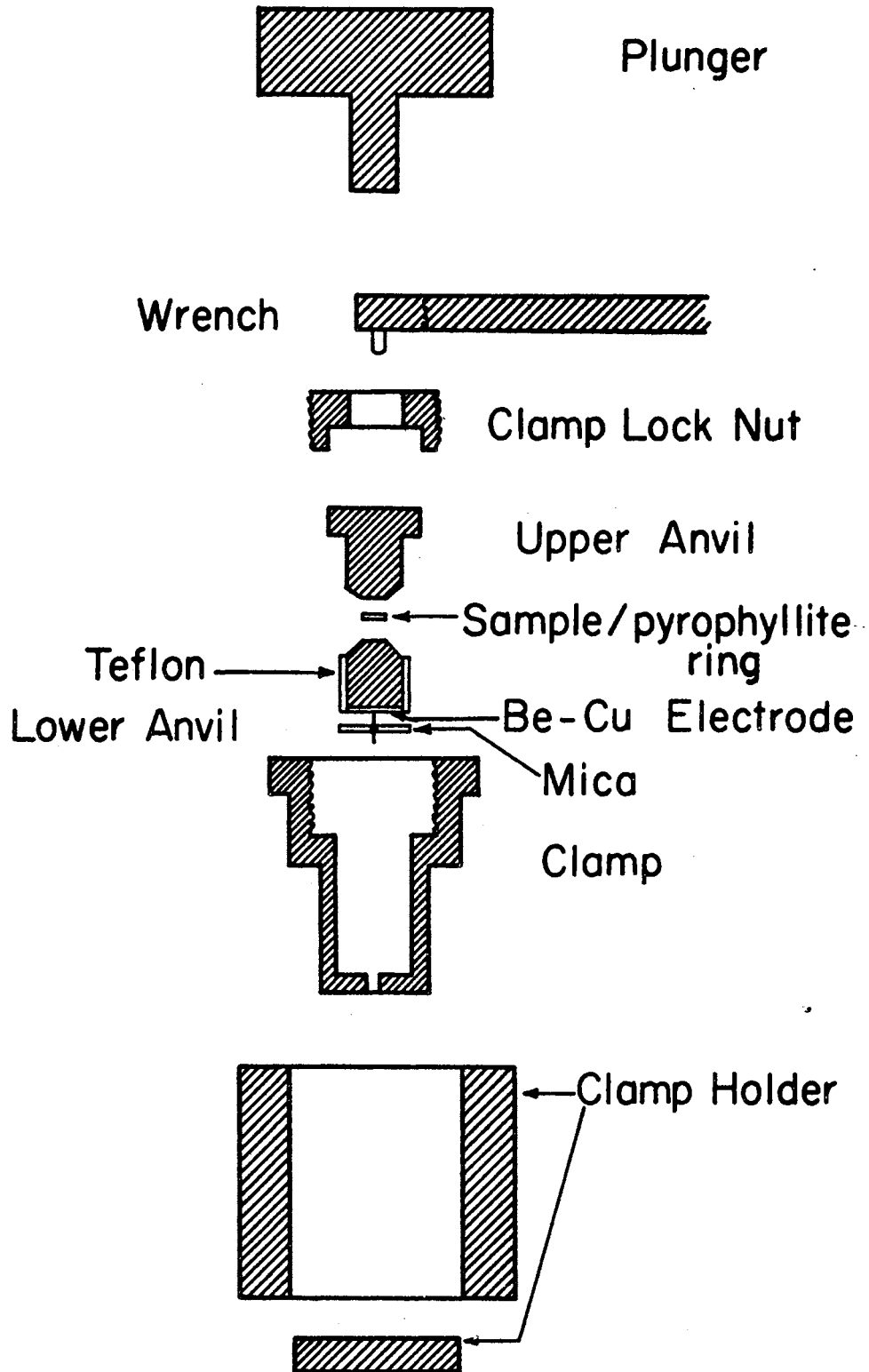


Figure 54. Cross-Sectional View of the Chester-Jones High Pressure Clamp

N_2 , is approximately five inches in diameter. The dewar assembly is shown in Figure 55. It was designed to hold approximately 2 liters of liquid He and 5 liters of liquid N_2 .

To minimize heat losses, the sample holder and the electrical lead shielding tube was made from stainless steel. The stainless tube is silver soldered to the top plate, which is also made from stainless steel. Leveling screws were provided to allow one to line up the inner dewar slit and outer dewar slit in order to determine the level of the He in the inner dewar.

All of the electrical leads are insulated from the system by way of a Stupakoff seal. The leads are waxed in so that a vacuum could be achieved in the inner dewar. An AuCo-Cu thermocouple is placed near the sample in the clamp, and a Keithley 160 A microvolt meter is used to record the temperature of the sample.

Initially, the polymer sample is premolded to 10.4 kbar at room temperature in a one-eighth inch diameter premold die. Carbide (General Electric Carbaloy 80) anvils are used for the premolding treatment. The sample is then weighed, and placed in a pyrophyllite ring. This ring which has a room temperature resistance in excess of 10^{11} ohms acts as a retaining gasket for the pellet. Care should be taken to keep the sample thickness slightly less (≈ 0.001 in.) than the pyrophyllite gasket. The molded pellets have thicknesses which varied from 0.010" to 0.014" and weights from 1.2 mg to 3.8 mg. Their densities ranged from about 1.1 to 1.5 g/cc.

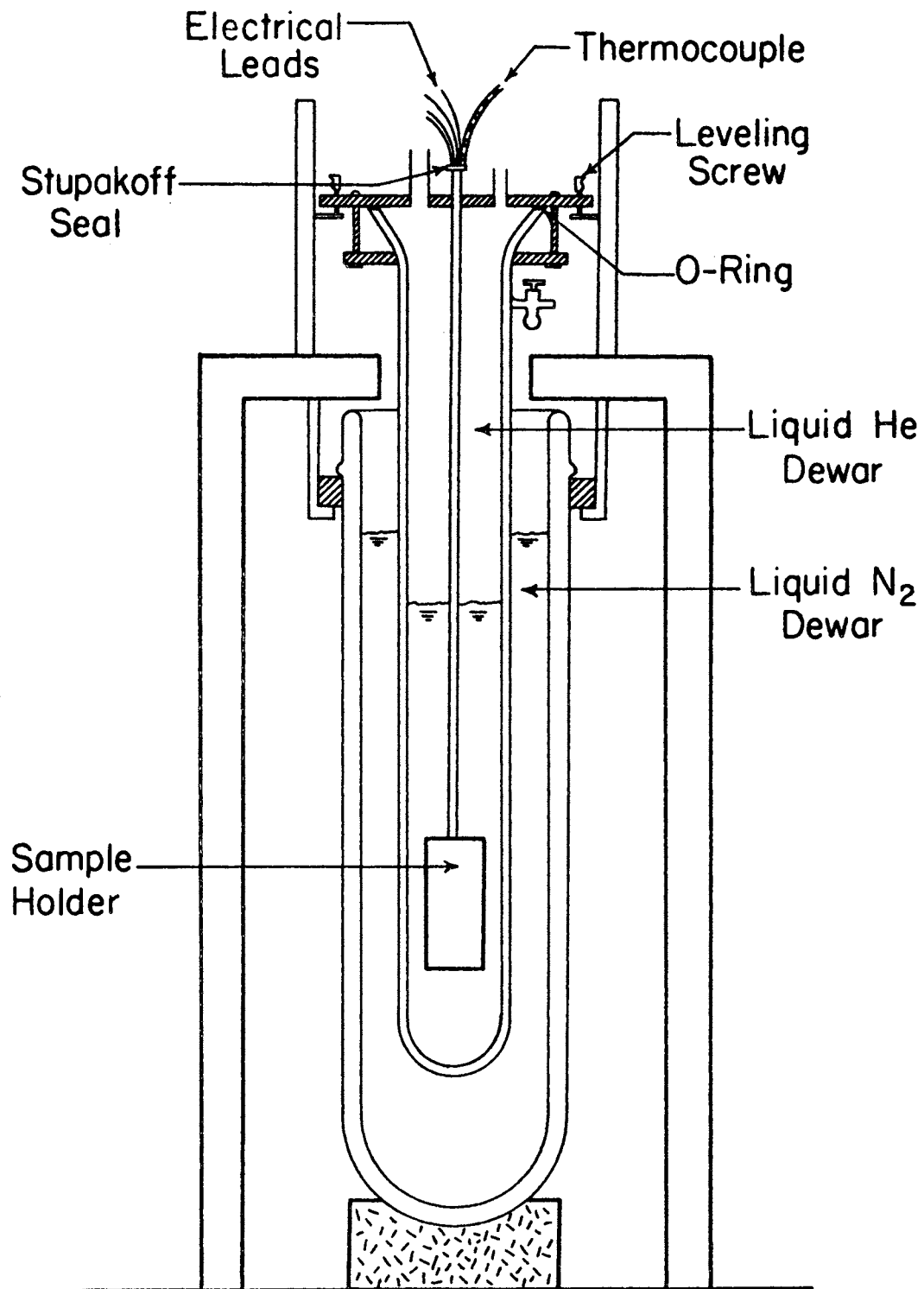


Figure 55. View of the Liquid Helium Cryostat

After the pellet, surrounded by the retaining ring, is placed in the clamp, the clamp assembly is inserted into a press. High pressure is provided by a Pasadena Hydraulic Inc. Model SB230C, 50 ton press. Calibration curves for the press have been presented in Chapter III. Pressure is transmitted to the sample via the plunger. Three complete cycles of pressure are performed (from $\simeq 15$ kbar to $\simeq 2$ kbar) while the resistance of the sample is read on a Simpson 269 ohmmeter.

Following the third cycle of pressure, the clamp lock nut is tightened and the load is released. Some relaxing of pressure is indicated by a slow increase in resistance in time, but the actual pressure on the sample can be determined (since R versus P data has been recorded prior to locking the clamp nut) by extrapolating the R-P curve to the proper value of resistance.

After the sample has been locked in place, the clamp is mounted in the Faraday cage and the necessary electrical connections are made. The thermocouple is also mounted in place. (Note: Normally two samples were mounted in the Faraday cage in two separate clamps. Thus, two samples could be studied simultaneously.)

The clamp assembly is now mounted on the inner dewar, and all hose connections are made as shown in Figure 56. When the pump hoses are properly connected, the helium dewar is sealed to the top plate with an O-ring and is evacuated by opening stopcocks 1, 5, and 7 (cf. Figure 56). The helium dewar jacket is also evacuated by opening stopcock 3 and 4 and closing stopcocks 1, 5, and 8. This process

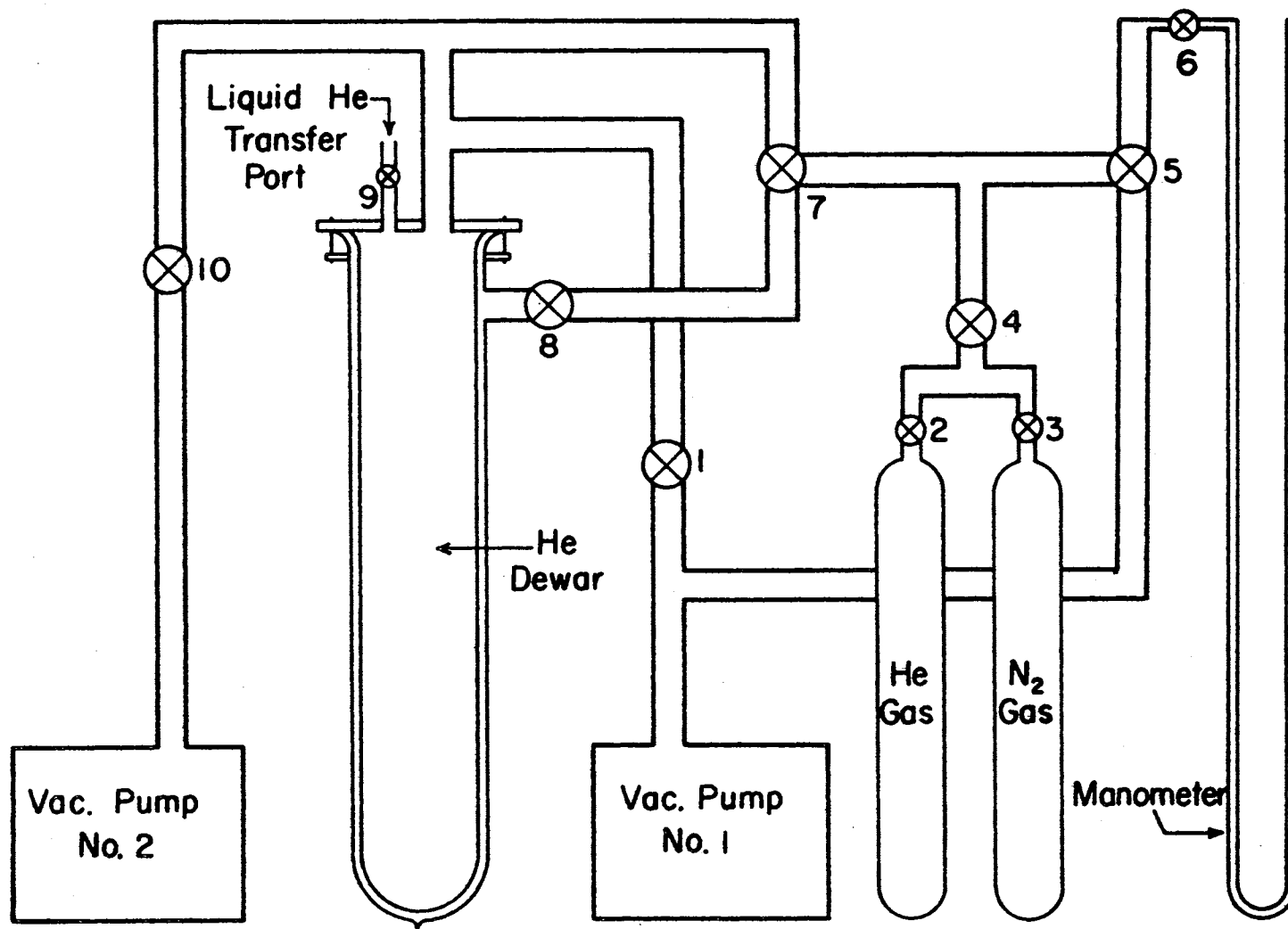


Figure 56. Schematic of the Complete Vacuum System and Exchange Gas System for the Liquid Helium Cryostat

is repeated several times. The helium dewar is then filled to a pressure of one atmosphere with helium gas by opening stopcocks 2, 4, and 7.

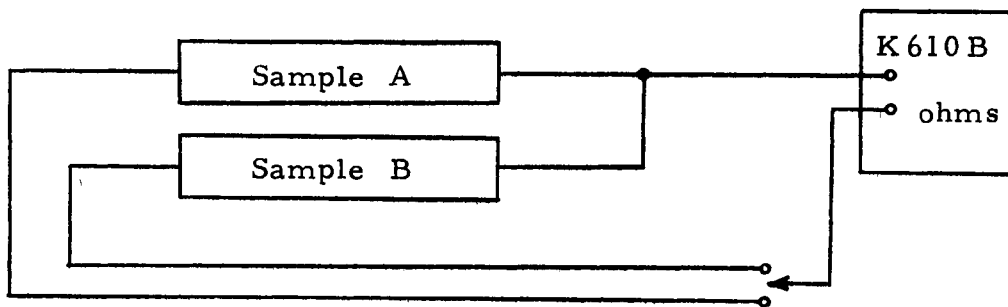
The outer dewar surrounding the helium dewar is now filled with liquid nitrogen. Heat is now slowly withdrawn from the helium dewar until the temperature is lowered to 77°K . During this process, resistance measurements can be taken as a function of temperature. The liquid helium is now transferred through the transfer port 9 (cf. Figure 56). The level of the liquid helium can be observed in the unsilvered portion of the dewars. When the level is above the sample clamp, the transfer tube is removed and the port sealed. Vacuum pump number 2 is then used to reduce the helium vapor pressure. The temperature below the boiling point (4.2°K) is determined by the vapor pressure observed on the manometer and the use of vapor curves. Using this high volume pump, the vapor pressure can be reduced to 4.5 mm Hg (1.7°K).

By following this procedure, it takes from four to eight hours for the inner dewar to reach a temperature of 77°K . An alternate procedure is to put gaseous He in the inner dewar jacket. In this way, due to the high thermal conduction of gaseous He, the inner dewar is cooled to N_2 temperature in about 30 minutes. Care must now be taken, however, to completely pump out the gaseous He from the inner dewar wall before the transfer of liquid He is started.

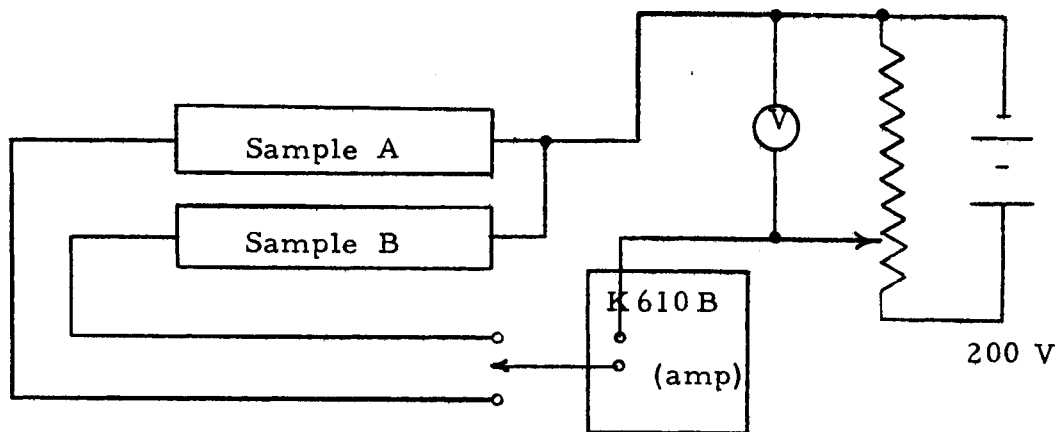
In a few cases, the alternate method was tried; however, due to the difficulty in pumping out the very cold gaseous helium (77°K) from

the tiny volume between the walls of the dewar, it was felt that the first method was superior. In addition, the slower cooling rate insured less thermal lag between the thermocouple recording and the sample temperature, and allowed one to take better data.

Two methods were used to measure the resistivity of the samples using a Keithley 610B Electrometer. The first method consisted of a direct resistance measurement. The circuit for measurement of two samples is shown below.



The second method used, as indicated below, was the measurement of the current through the sample using a known fixed voltage. It is the more accurate of the two, since the samples exhibit \vec{E} -field dependence as was discussed in Chapter III.



In a number of cases, resistance was measured both on the cooling and on the heating cycle. The heating cycle tended to indicate a very large thermal lag between the sample and the thermocouple. Consequently, the data indicated a very large hysteresis. To avoid this effect, data was always recorded on the cooling cycle, and it is this data which is reported in the next section.

Results and Discussion

After reducing the data to resistance values, the resistivity of the sample was calculated from:

$$\rho = \frac{RA}{x} , \quad (12)$$

where R is the resistance in ohms, A is the cross sectional area of the sample in cm^2 , and x is the thickness of the sample in cm.

The resistivity (ρ) is plotted for the 13 samples studied in Figures 57 through 69. Each of the polymers was premolded at 10.4 kbar and taken to ~ 8 kbar in the clamp before the clamp nut was locked in place. Actual pressures on each sample are shown on the corresponding graph.

Virtually all of the samples (11 out of 13) exhibit some form of nonlinearity of $\log \rho$ vs $1/T$. (It should be emphasized that during some of the measurements, the switch used in the resistivity circuit limited the resistance measurements to $\leq 3 \times 10^{10}$ ohms. Such cases are indicated on the graphs, with wide error bars. Also, since the

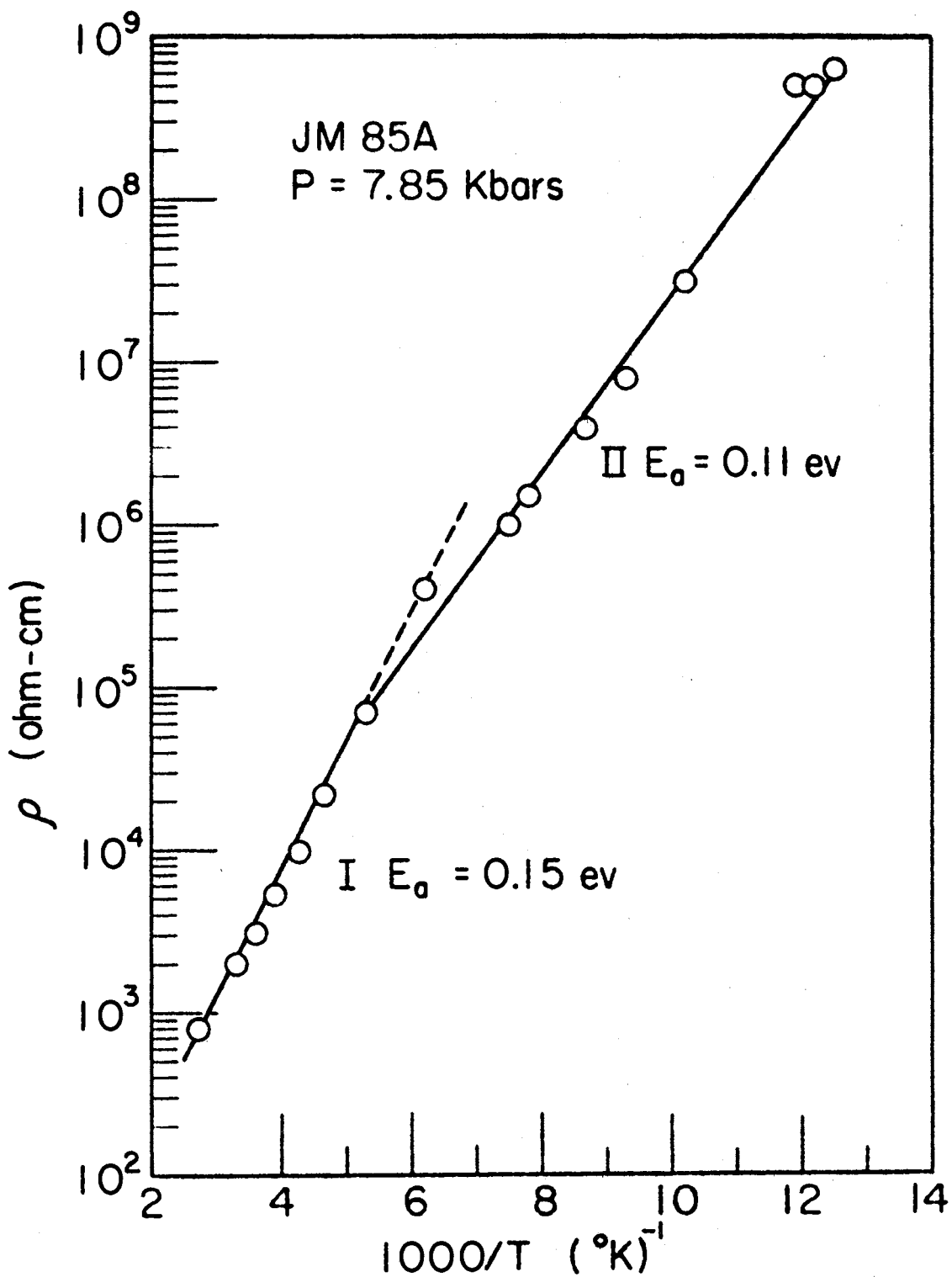


Figure 57. Temperature Dependence of the D.C. Resistivity for Polymer JM85A

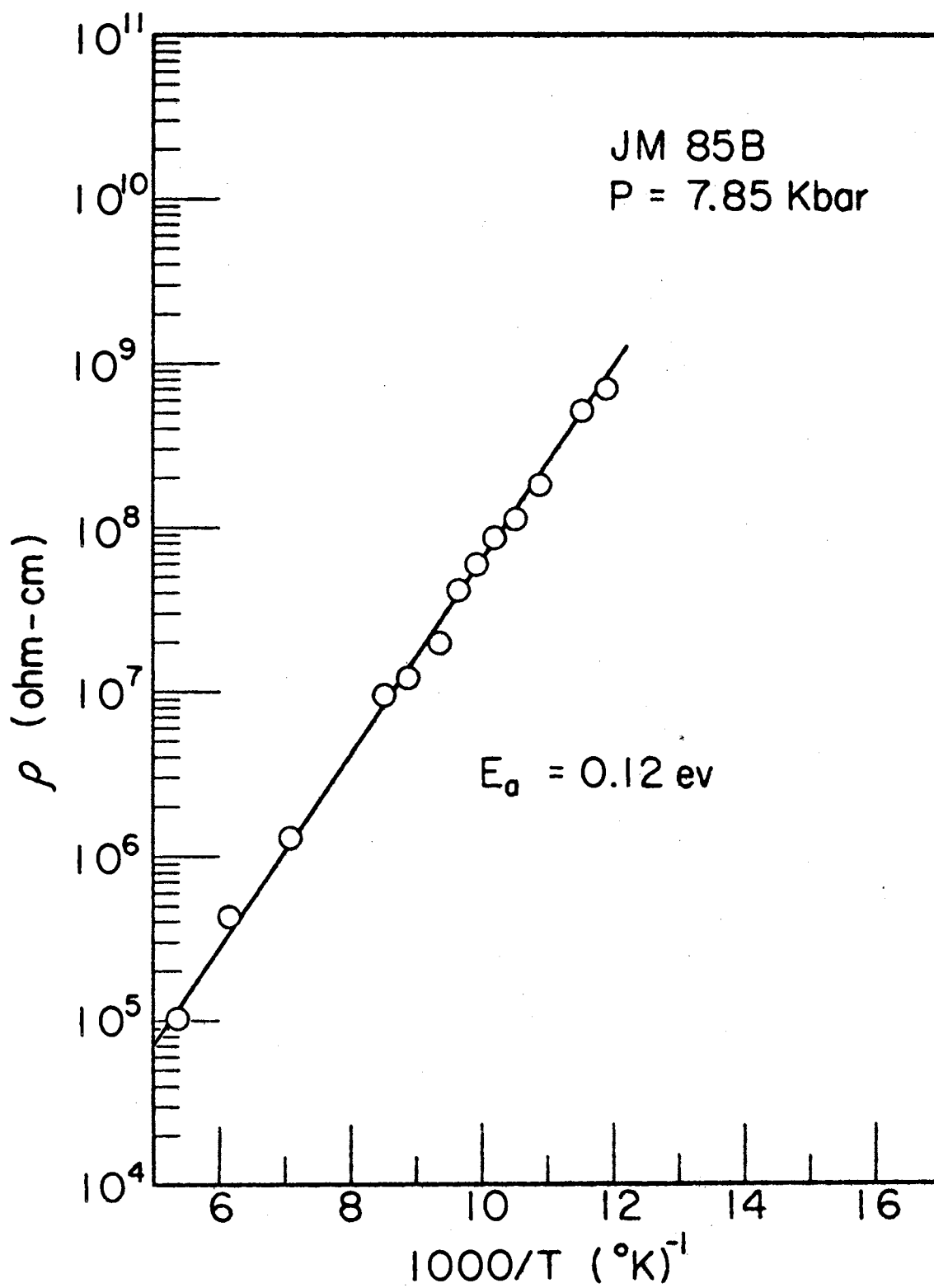


Figure 58. Temperature Dependence of the D.C. Resistivity for Polymer JM85B

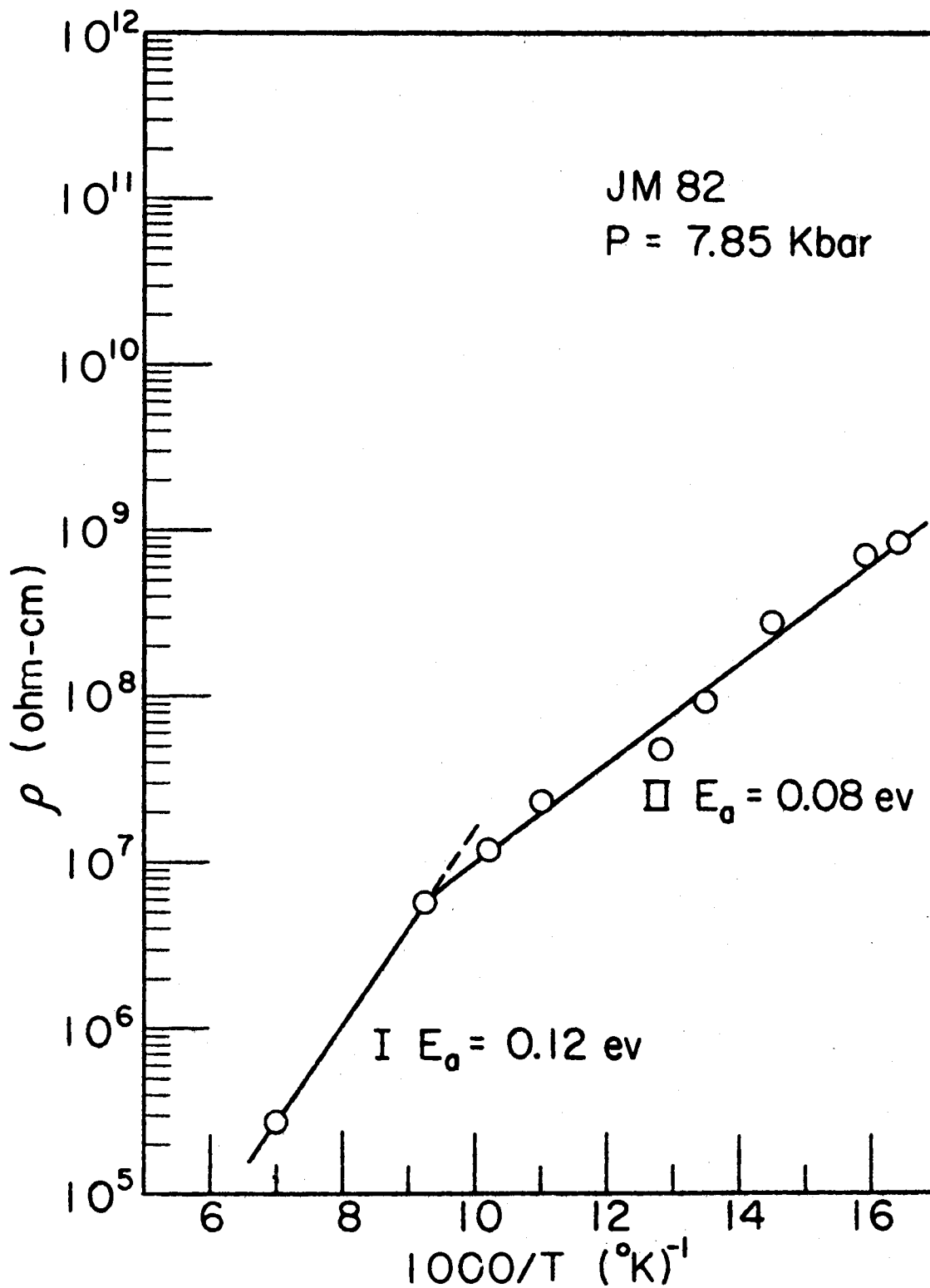


Figure 59. Temperature Dependence of the D.C. Resistivity for Polymer JM82

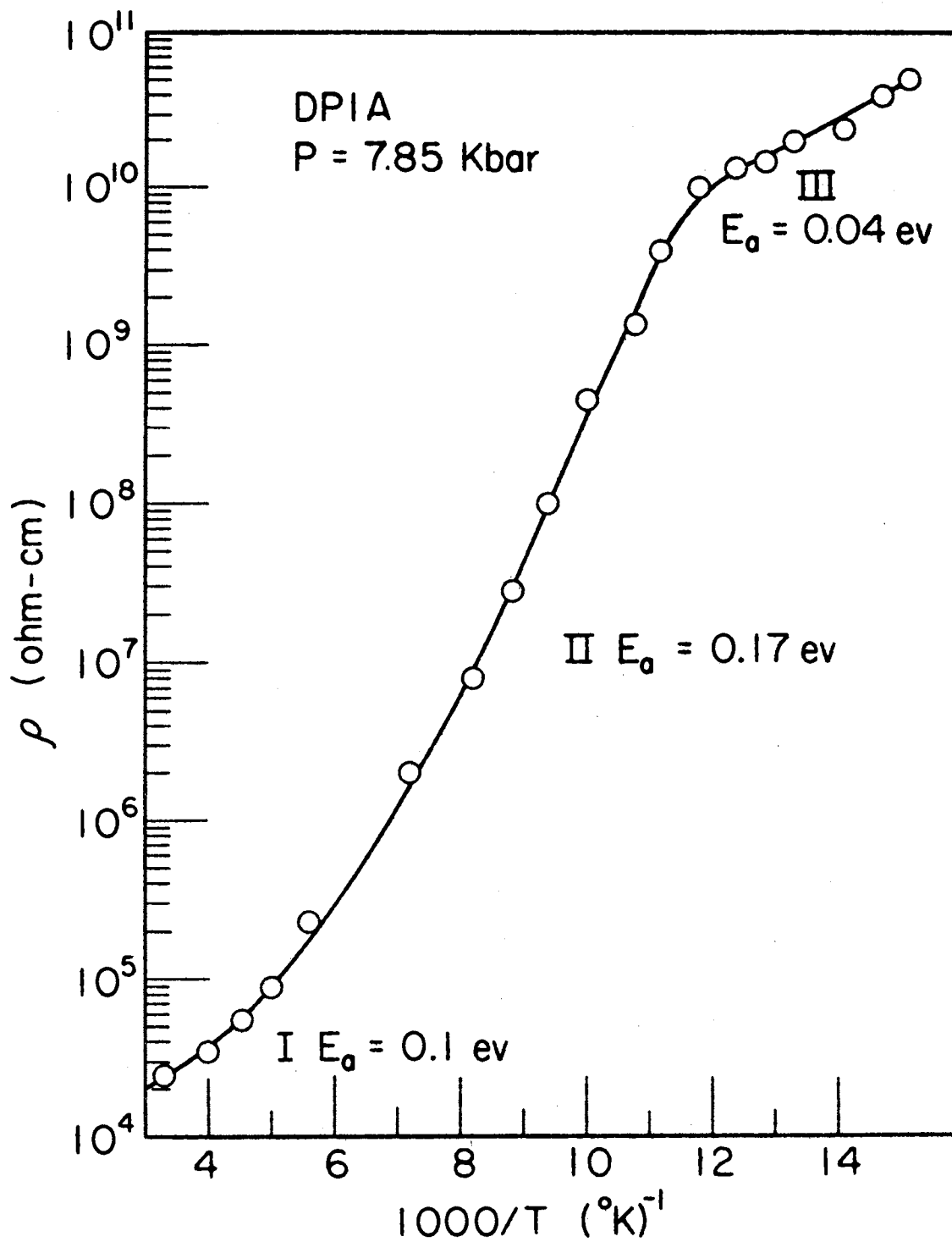


Figure 60. Temperature Dependence of the D.C. Resistivity for Polymer DP1A

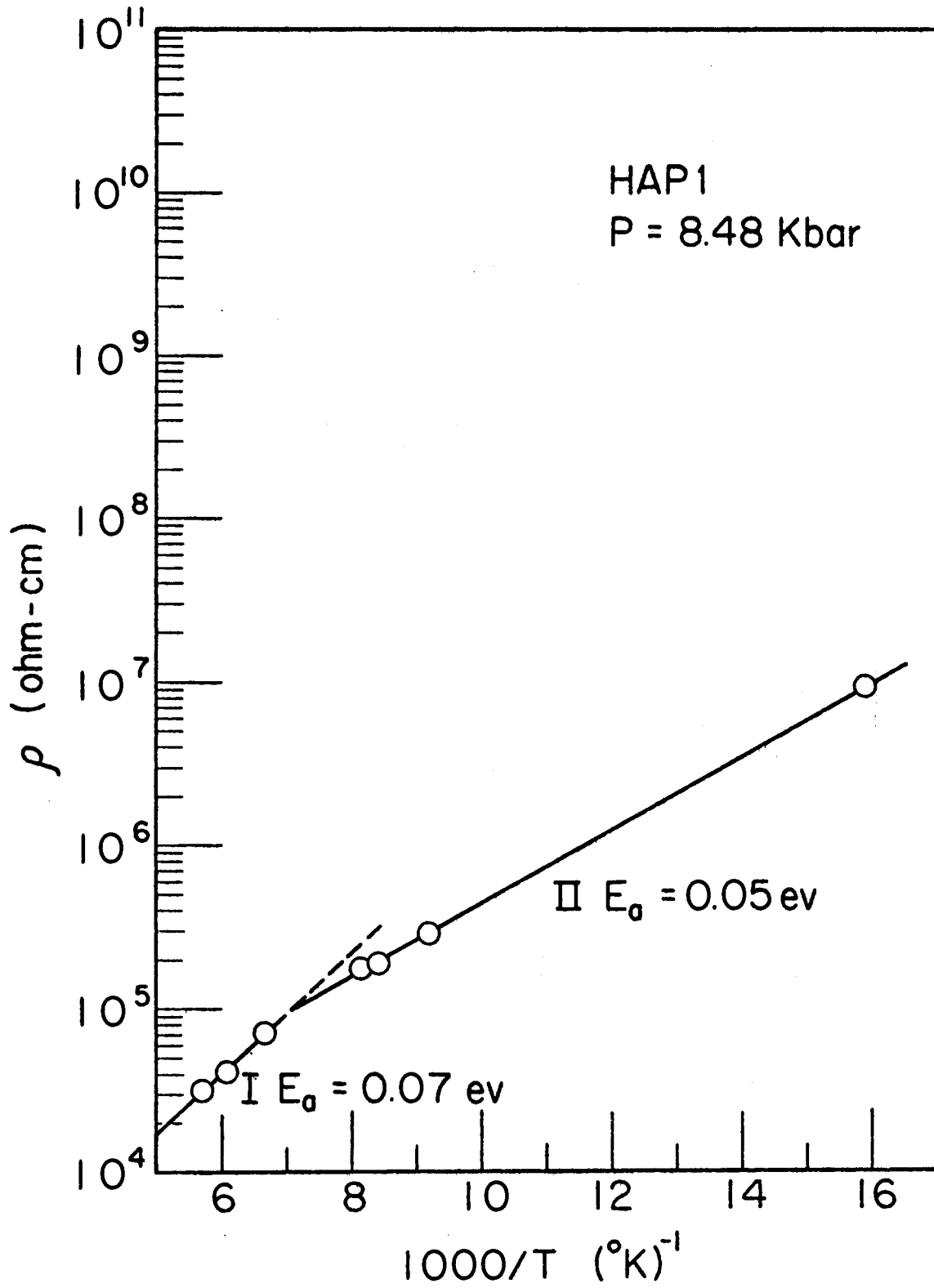


Figure 61. Temperature Dependence of the D.C. Resistivity for Polymer HAP1

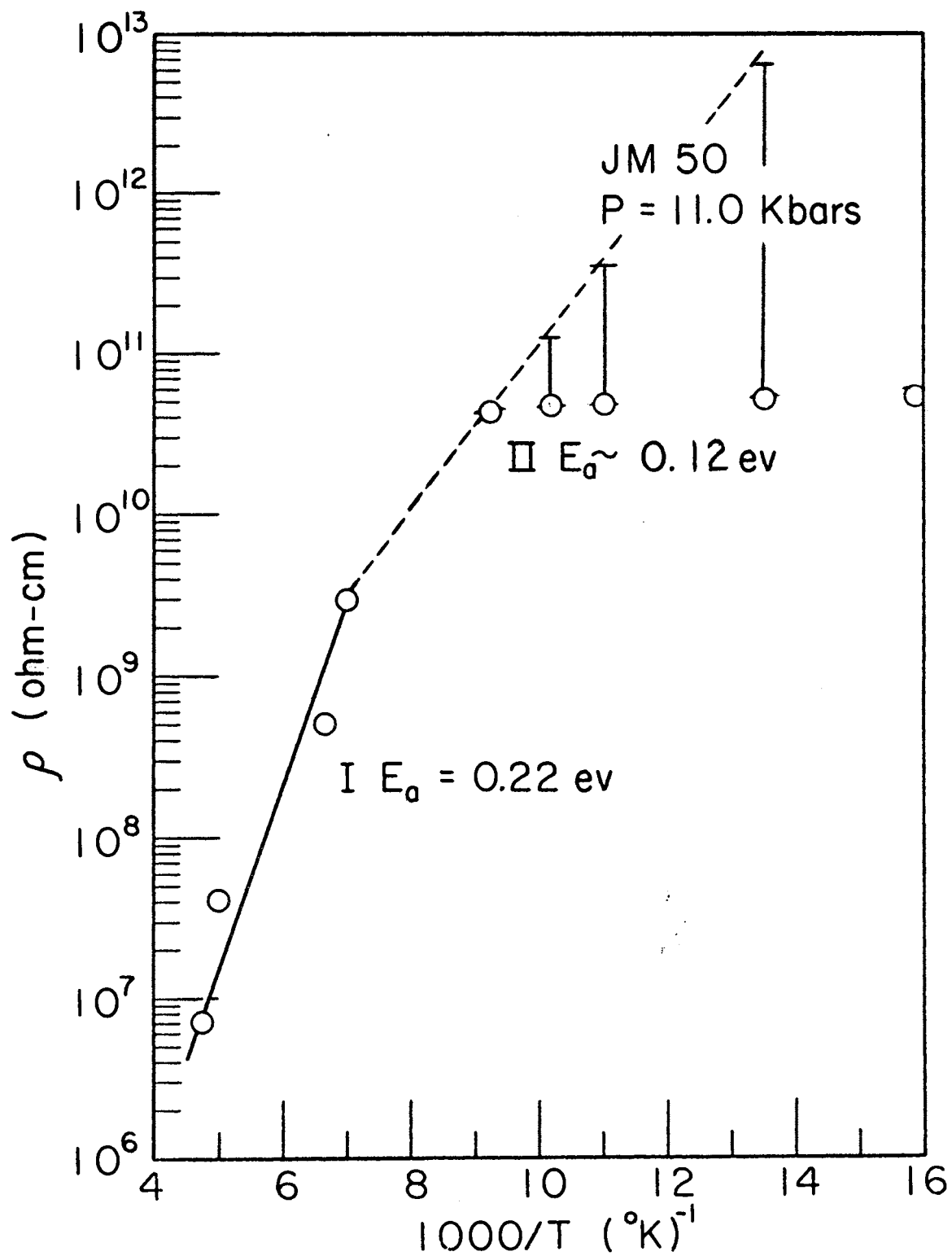


Figure 62. Temperature Dependence of the D.C. Resistivity for Polymer JM50

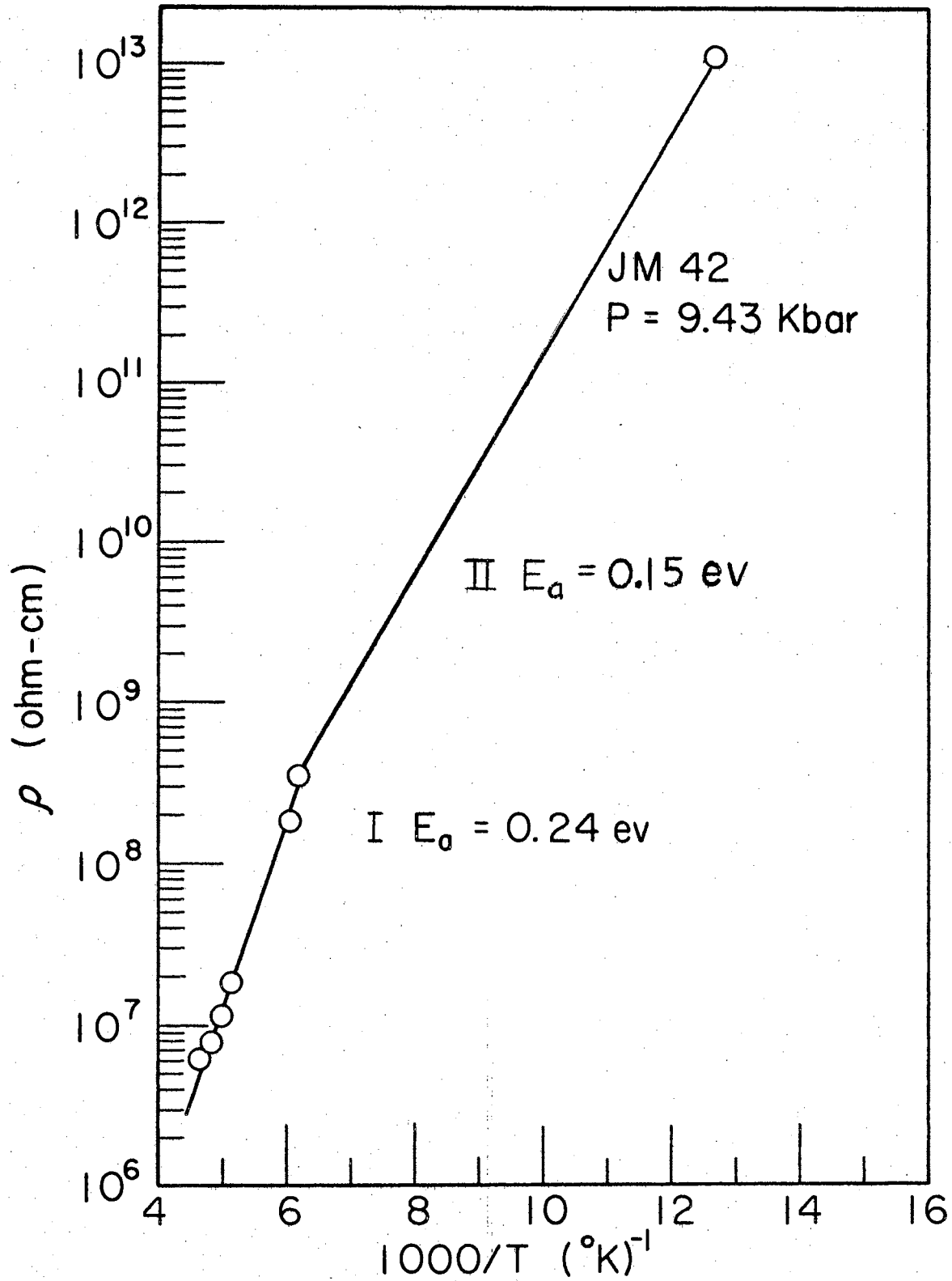


Figure 63. Temperature Dependence of the D.C. Resistivity for Polymer JM42

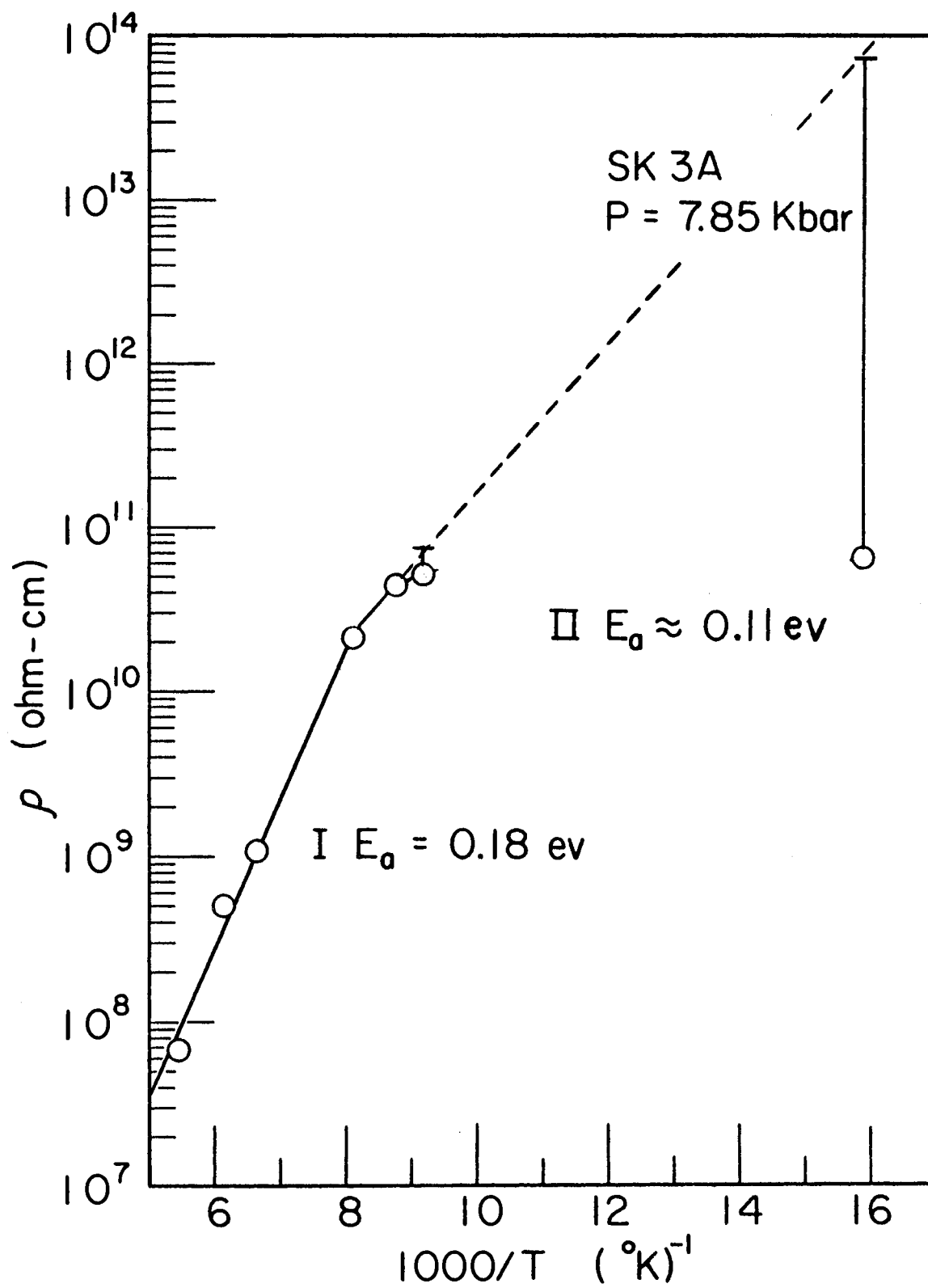


Figure 64. Temperature Dependence of the D.C. Resistivity for Polymer SK3A

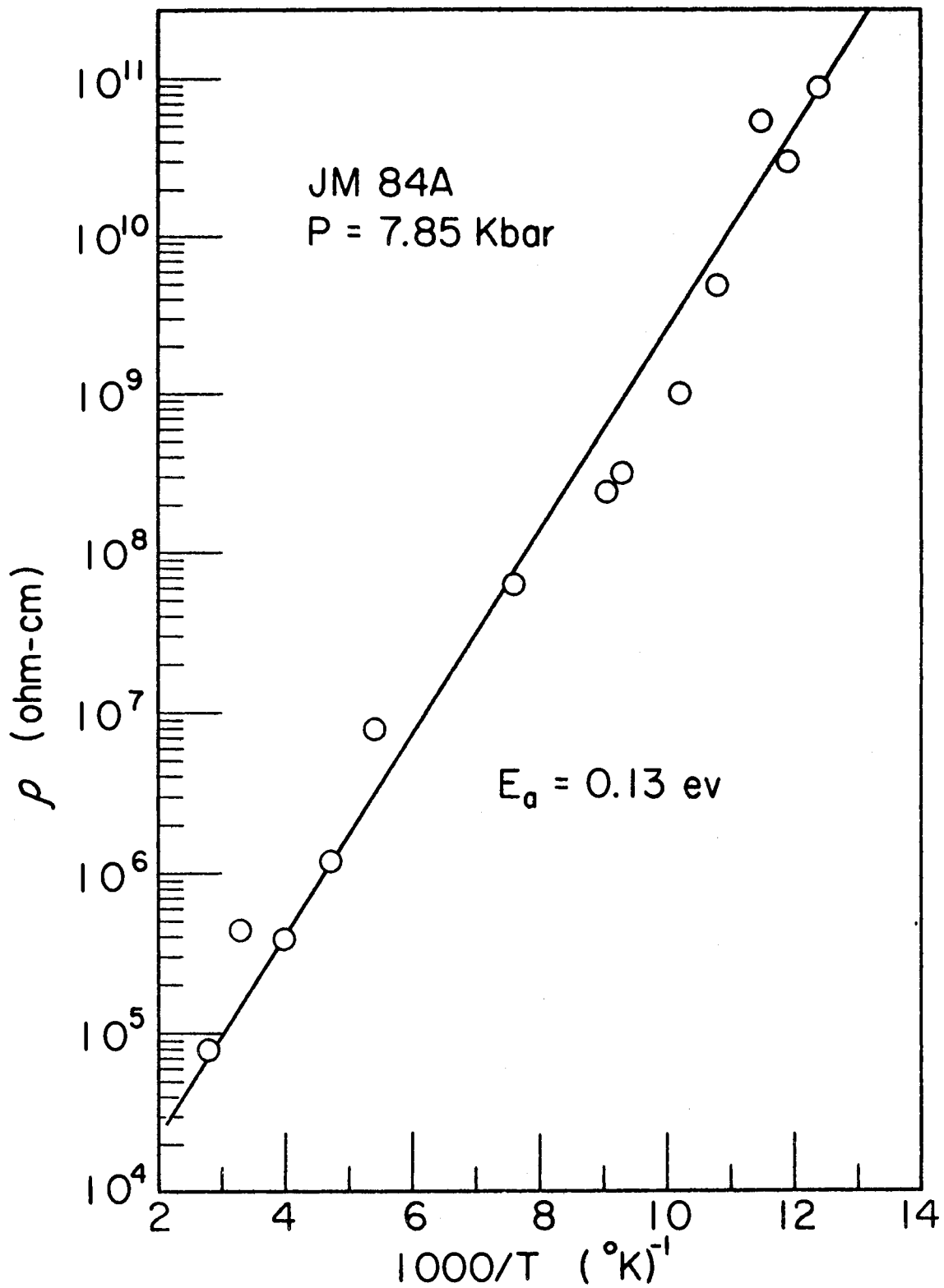


Figure 65. Temperature Dependence of the D.C. Resistivity for Polymer JM84A

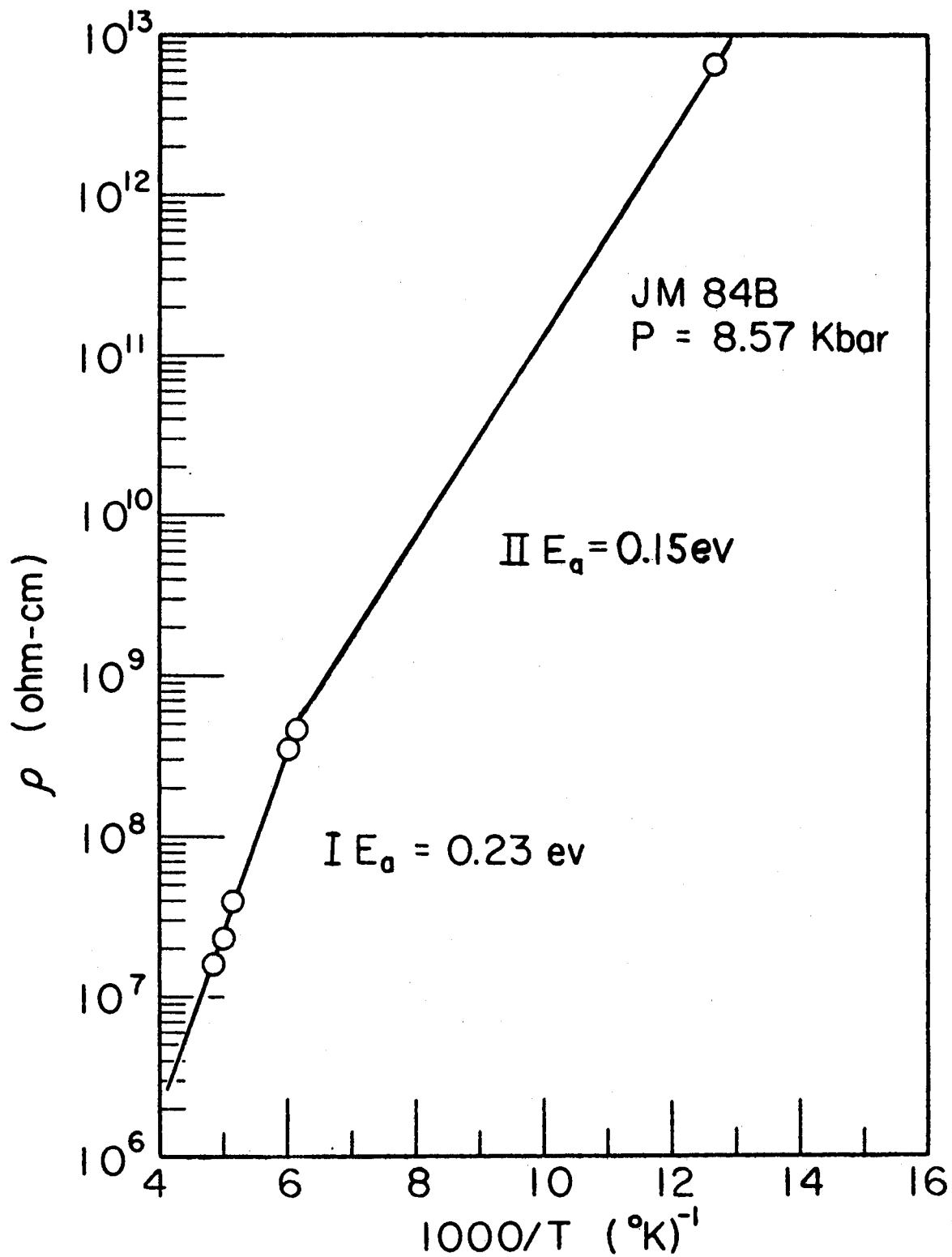


Figure 66. Temperature Dependence of the D.C. Resistivity for Polymer JM84B

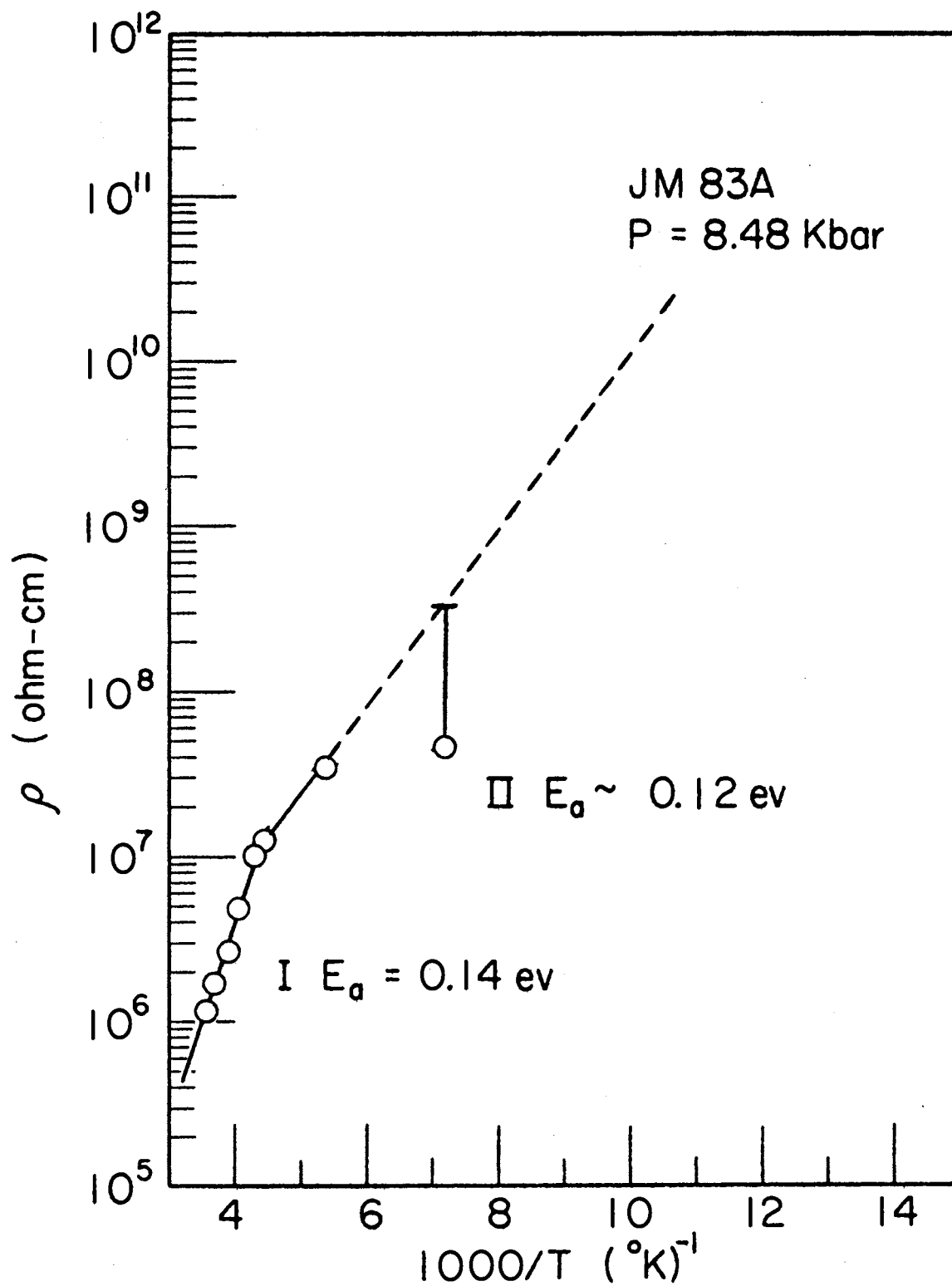


Figure 67. Temperature Dependence of the D.C. Resistivity for Polymer JM83A

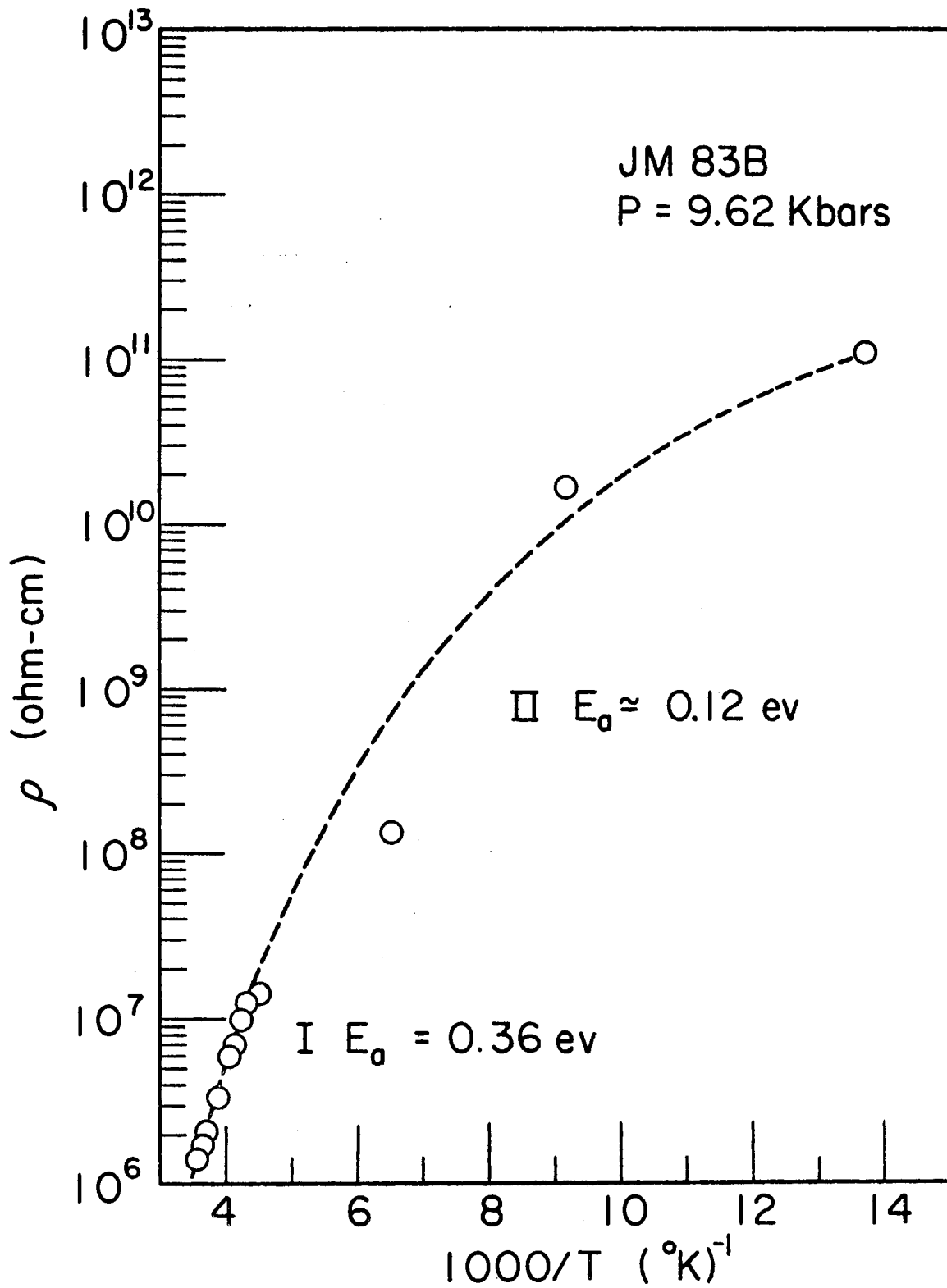


Figure 68. Temperature Dependence of the D.C. Resistivity for Polymer JM83B

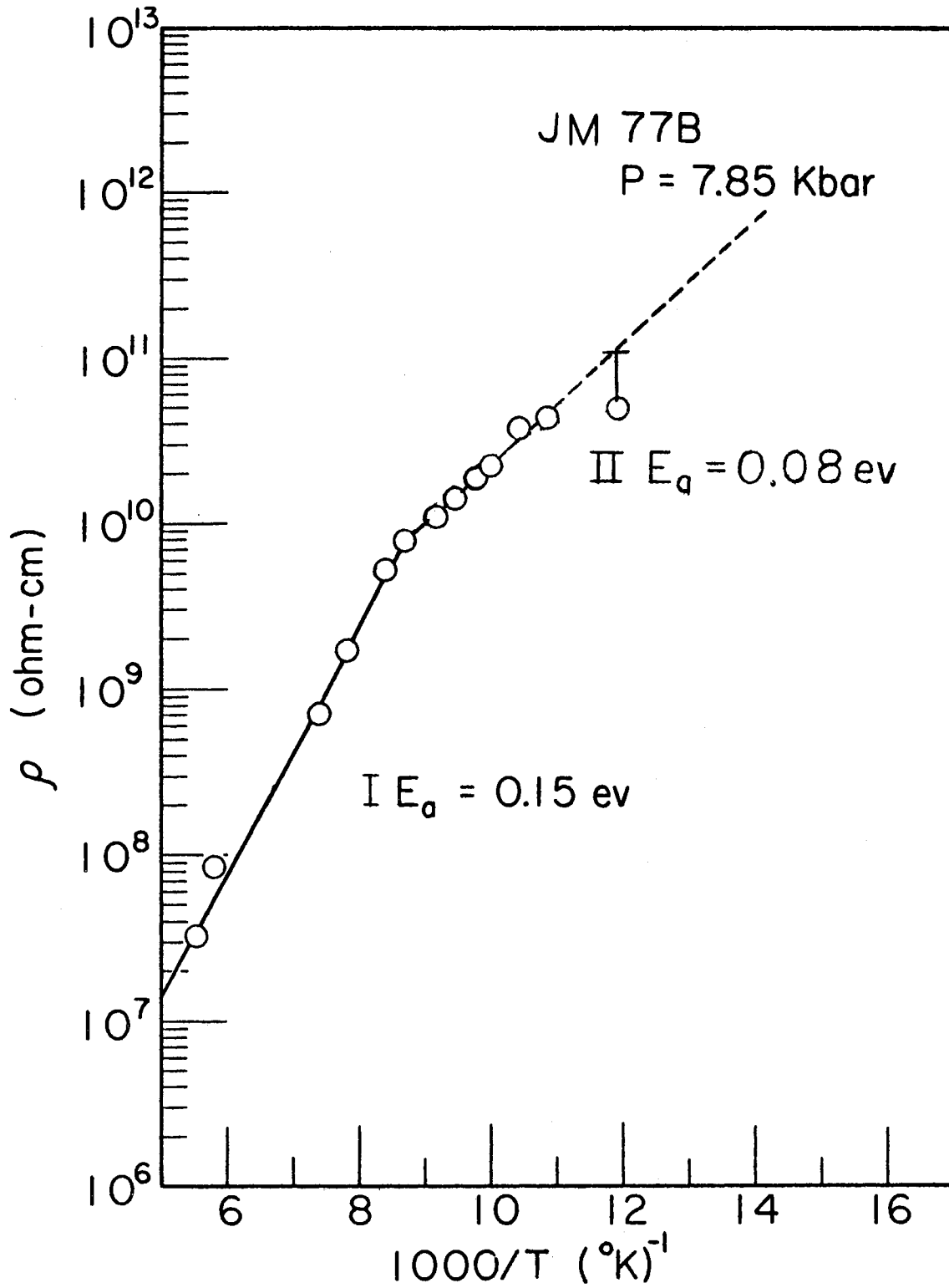


Figure 69. Temperature Dependence of the D.C. Resistivity for Polymer JM77B

limiting resistance of the circuit was $\simeq 3 \times 10^{14}$ ohms, the data at liquid He temperatures for some samples may be only approximate.) Many exhibit two or three linear regions, indicating the presence of several donor or acceptor states in the materials studied. Activation energies for the linear regions are calculated from the equation:

$$\rho = \rho_0 \exp (E_a / kT) \quad (13)$$

where k is Boltzmann's constant; T is the temperature in absolute degrees, and E_a is the activation energy in eV. They are shown on the graphs, and are compared with room temperature activation energies in Table XVI.

Most of the resistivity versus temperature data shown in Figures 57 through 69 covers only the temperature range from room temperature ($1000/T = 3.33^\circ\text{K}^{-1}$) to liquid nitrogen temperature ($1000/T = 13^\circ\text{K}^{-1}$). Resistance measurements were made on all of the samples at liquid He temperature (4.2°K and below), but virtually no detailed data was taken in the range from 4.2°K to 77°K , since the cooling took place too rapidly to allow thermal equilibrium to be achieved within the sample. As was mentioned earlier, data taken on the warm-up cycle tended to indicate the existence of a considerable thermal lag between the thermocouple and the sample. Hence, only limited data was obtained in this temperature range.

In order to extend the data temperature range somewhat, data on sample DP1A, shown in Figure 70, was taken from room temperature to N_2 temperature in the normal way, after which liquid N_2 was

TABLE XVI

ACTIVATION ENERGIES FOR SEVERAL POLYMERS AT
8 KBAR IN VARIOUS TEMPERATURE RANGES

Sample	E_a (eV)		
	(a)	(b)	(c)
	$60^\circ\text{K} \leq T \leq 150^\circ\text{K}$	$150^\circ\text{K} \leq T \leq 300^\circ\text{K}$	$300^\circ\text{K} \leq T \leq 450^\circ\text{K}$
JM85A	0.11	0.15	0.12-0.15
JM85B	0.12	0.12	0.15
JM82	0.08	0.12	
DP1A	0.04-0.17	0.10	0.06-0.10
HAP1	0.05	0.07	
JM50	0.12 ^(d)	0.22	
JM42	0.15 ^(d)	0.24	
SK3A	0.11 ^(d)	0.18	0.35
JM84A	0.13	0.13	0.23
JM84B	0.15 ^(d)	0.23	0.14
JM83A	0.12 ^(d)	0.24	0.23
JM83B	0.12		0.36
JM77B	0.08	0.15	0.25

(a) and (b) E_a determined from data in Chester-Jones Clamp.

(c) E_a determined from data in high pressure cell. (Cf. Chapter III.)

(d) E_a not known accurately, due to inaccurate determination of resistance in this range.

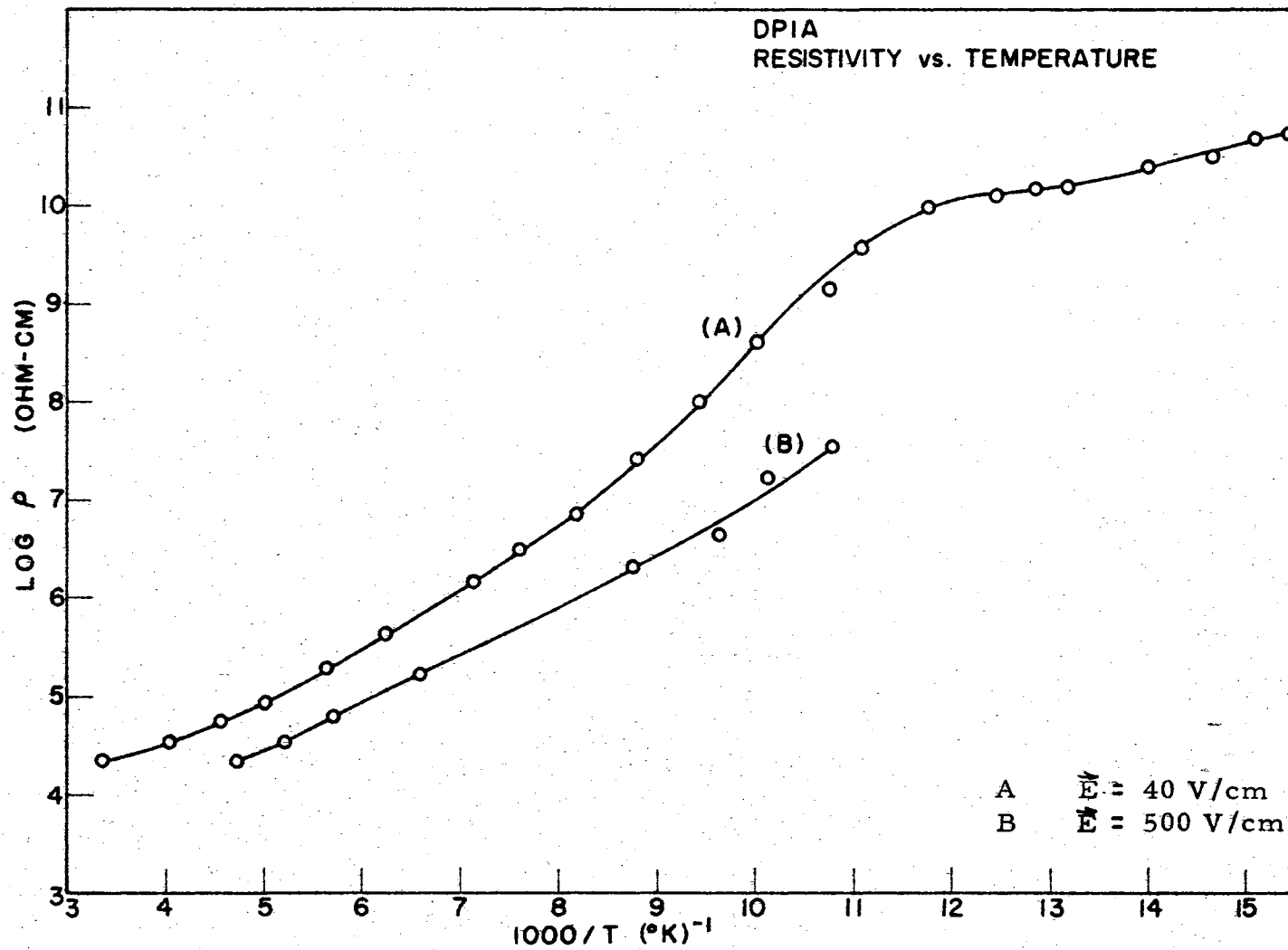


Figure 70. Resistivity-Temperature Curve (pumped Liquid N₂ Temperature) for Polymer DPIA

placed in the inner dewar. By pumping on the liquid N₂, a temperature of 64.5°K was achieved. This extended the data to $1000/T = 15.5^{\circ}\text{K}^{-1}$, and indicated a much lower activation energy in this region than in the region from room temperature down to liquid N₂ temperature.

Multilevel Semiconductors

By examining the activation energies in Table XVI, it can be seen that most of the samples which exhibit two or three activation energies also exhibit proper Boltzmann behavior in that the order of energy levels being populated are from the lowest level at room temperature and above, as indicated by the highest activation energy being found at room temperature; to an intermediate level in the intermediate range temperatures, given by an intermediate value for the activation energy; to the highest level at liquid N₂ temperature, corresponding to the lowest activation energy. Two of the samples (JM84B and DP1A), however, do not follow this trend. There is an inversion in the order of descending activation levels, in that the lowest level tends to occur in the intermediate range. This is not understood in the light of the Boltzmann picture.

One may see this anomaly easier by examining Figure 70, for sample DP1A. Initially, the slope is less than it is in the intermediate temperature range, while in the N₂ range, it again becomes small again. For a well-behaved multilevel type semiconductor, the resistivity slope should be maximum at high temperature, and should

systematically decrease to lower temperatures as each subsequent level becomes dominant.

With regard to the activation energy data, it is further noted that sample JM77B, the most resistive of the lot at room temperature ($\rho = 3.5 \times 10^6$ ohm-cm) tended to exhibit one of the smaller activation energies ($E_a = 0.08$ eV). The attractive interaction between charge carriers must be supplied via the electron-phonon interaction in order to observe a superconducting transition. Since ordinary resistance at room temperature is a measure of this interaction, one might expect a higher resistance material to be a more likely candidate for undergoing a superconducting transition. Indeed, this is the case for metals. The more resistive the metal at room temperature, the more apt it is to become superconducting; and, also the higher the expected T_c (84,217). Of course, the materials being studied are not metals, and due to the large difference in charge carrier densities between the organic state and the metallic state, one probably should not expect this to hold. However, it is an interesting observation.

A further word about the various activation energies for the sample in different temperature regions is in order. One may explain the various linear regions of the resistivity plots by invoking a model which involves the existence of two or more groups of charge carriers in the sample. Using the usual notation, one may write the electrical conductivity σ for the case of three sets of carriers as:

$$\sigma = N_1 |e| \mu_1 + N_2 |e| \mu_2 + N_3 |e| \mu_3 \quad (14)$$

where N_1 , N_2 , and N_3 are the respective carrier densities of the respective carriers; μ_1 , μ_2 , and μ_3 are their respective mobilities; and $|e|$ is the electronic charge. The temperature dependence of each of the carrier concentrations may be written as:

$$\begin{aligned} N_1 &= N_{01} \exp(-E_{a1}/kT); \\ N_2 &= N_{02} \exp(-E_{a2}/kT); \end{aligned} \quad (15)$$

and
$$N_3 = N_{03} \exp(-E_{a3}/kT).$$

Since the total number of carriers, N , is the sum of all contributions:

$$N = N_1 + N_2 + N_3; \quad (16)$$

or:

$$N = N_{01} \exp(-E_{a1}/kT) + N_{02} \exp(-E_{a2}/kT) + N_{03} \exp(-E_{a3}/kT); \quad (17)$$

and the mobility μ is the sum of all mobilities:

$$\mu = \mu_1 + \mu_2 + \mu_3, \quad (18)$$

one then obtains for the conductivity:

$$\sigma = |e| \left[\mu_1 N_{01} \exp(-E_{a1}/kT) + \mu_2 N_{02} \exp(-E_{a2}/kT) + \mu_3 N_{03} \exp(-E_{a3}/kT) \right]. \quad (19)$$

Hence, a conductivity of the form given by Eq (19) could account for the different activations, each becoming dominant in a particular temperature region. The various possible types of carriers which could be available for conduction modes have been discussed by Pohl (45), and were reviewed in Chapter III of this thesis. Pohl considers ionic (intermolecular) excitons, transitory ions (anions in particular); von Hippel polarons; and free holes and electrons as the dominant

sources of conduction enhancement. Since enough data is not available (i. e., the carrier densities and mobilities are not known) to further characterize the sample by this model, it will not be discussed further.

A second model, which also could explain the nonlinear behavior of the resistivity is that of polar scattering Frohlich . (232,233) Here, there is a temperature dependence in the mobility, μ , given by:

$$\mu = A \exp\left[\frac{\Theta}{T} - 1\right], \quad (20)$$

where A is an appropriate constant, and Θ is the Debye temperature. Clearly, this kind of an analysis could also be used to explain the nonlinear and near-independent dependence of the resistance on the temperature.

Filamentary Superconduction

The liquid helium data, as displayed in Table XVII, merits further comment. In several cases, as noted in the footnotes to the Table, the resistivity measured represented an upper limit due to experimental limitations. Excluding these cases, there are four samples that show approximately the same resistance or a slightly higher resistance (which was well below the 10^{14} ohm limit of the open circuit) at 4.2°K than at 77°K . The resistivities of these four samples, JM85A, JM83A, JM83B, and HAP1 are plotted in Figure 71. This behavior is not the expected one for these semiconducting samples: one expects an exponential rise with a drop in temperature from 77 to 4.2°K to a value orders of magnitude above the one observed. For some samples

TABLE XVII

D.C. RESISTIVITIES OF 13 POLYMERS MEASURED AT ~ 8 KBAR
AT LOW TEMPERATURES IN A CHESTER-JONES CLAMP

Sample No.	Resistivity (ohm-cm)		
	T = 300°K	T = 77°K	T = 4.2°K
JM85A	2.47×10^2	1×10^9	1.26×10^{10}
JM85B	3.55×10^2	2×10^9	6.45×10^{13}
JM82	7.35×10^2	4.78×10^7	7.93×10^{10} (a)
DP1A	4.34×10^3	1.6×10^{10}	3.98×10^{14} (b)
HAP1	6.24×10^3	2×10^6	1.95×10^{10}
JM50	5.28×10^4	4.2×10^{10} (a)	5.57×10^{10} (a)
JM42	7.25×10^4	1.1×10^{13}	1.4×10^{13}
SK3A	1.49×10^5	5×10^{10} (a)	6.24×10^{10} (a)
JM84A	1.82×10^5	1.4×10^{11}	3.2×10^{14} (b)
JM84B	1.90×10^5	5.7×10^{12}	6.4×10^{13}
JM83A	4.75×10^5	1×10^8 (a)	6.23×10^{10}
JM83B	7.72×10^5	8.5×10^{10}	9.21×10^{11}
JM77B	3.48×10^6	4×10^{10} (a)	4×10^{10} (a)

(a) Indicates an upper limit on the measured resistivity due to experimental limitations.

(b) Indicates the equivalent open circuit resistance of the apparatus ($\sim 10^{14}$ ohms).

this may be the case as we end up measuring an open circuit resistance [see note (b) in Table XVII]. The reason for the temperature independent resistance in samples JM85A, JM83A, JM83B and HAP1 in

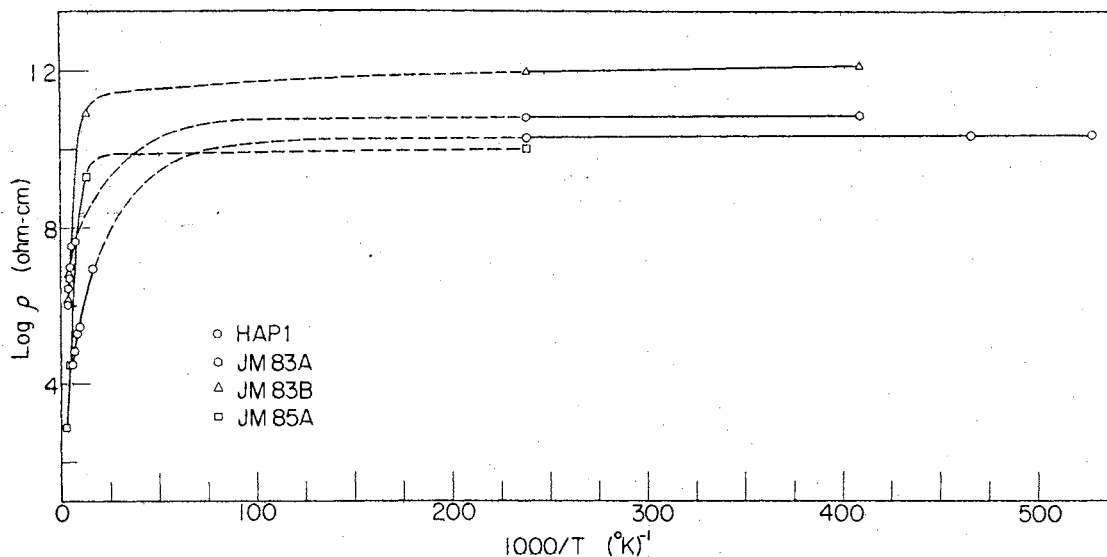


Figure 71. Anomalous Behavior of the Resistivity of Several Polymers at Low Temperatures

the range 4.2 to 77°K is not to be sought using the usual explanation of a degeneracy of the charge carriers, for two reasons: (1) the density of these carriers is probably small, and (2) their effective mass is probably large.

Two possible explanations for this were mentioned earlier (multiple excitation levels with different types of charge carriers; and Fröhlich's polar scattering).

A third possible explanation for the unexpected behavior could be that the semiconductor has both an intrinsic region (above $T \sim 77^\circ\text{K}$) and an extrinsic region. In the intrinsic region, the carrier densities

of conduction band electrons and valence band holes depend only on the nature of the bands and the intrinsic energy gap (E_g) between them. Impurities play a negligible role in the intrinsic semiconductor. However, an intrinsic semiconductor is very sensitive to impurities at low temperatures, since carriers can often be excited from impurity levels for a small expenditure of energy (86). Hence, at some temperature where $kT \sim E'$, E' being the impurity activation energy, the semiconductor could change from an intrinsic type (impurity independent) to an extrinsic type (impurity dependent). This could account for the observed effect also. Inokuchi (233) has observed similar effects in quaterrylene in that the intrinsic behavior of the sample did not persist below $T \sim 370^\circ\text{K}$, when the resistivity was measured in dilute O_2 atmospheres. He attributed the effect to the presence of two acceptor levels due to O_2 impurity; thus quaterrylene, an intrinsic semiconductor in vacuum, is an extrinsic semiconductor in air, or dilute O_2 atmospheres.

Another possible explanation may be the existence of filamentary superconduction. As is well known, the Meissner effect can operate to suppress superconduction. In some known superconductors, the magnetic fields required to convert the superconducting to the normal state need be quite small. Such superconductors are said to be magnetically "soft." To account for the observed limiting of the resistance as low temperatures are approached in these four polymers, we need only assume that the filamentary regions are very "soft" and easily

destroyed singly and to some extent mutually by current pulses in them. The resultant "averaged" conduction as seen by a slow response current device would indicate lowered average resistance of the sample. Alternatively, filaments of superconducting phase could form interior to the surface, again producing a lowered average resistance at low temperatures.

With regard to the above discussion of filamentary superconduction, although most of our data shows that the resistance of our samples at any temperature, there were several instances where a near-zero resistance was observed. Several samples were involved, some exhibiting this effect more than once. A discussion of this effect follows.

On several occasions the electrical resistance of several samples appeared to vanish at low temperatures. The zero resistance of the samples was intermittent, with normal behavior observed most of the time. In these measurements of electrical resistance, two instruments of very different sensitivity were used, a Keithley 610B and a Simpson Model 269 meter. From a description of the following observations, it will be seen that the resistance measured depends on the instrument used as well as on the range selected on each instrument. An interpretation of this is that the current that is passed through the sample in the resistance measurement will be different for each instrument and for each scale setting selected as these are bridge-type instruments. Stated differently, we may conclude that the

sample resistance measured, whether finite or zero, depends on the current passed through the sample. Another feature of these measurements, not easily understood, is that the placement of the thermocouple in electrical, as well as thermal, contact with one of the anvils in the electrical conductivity apparatus influences the observations of vanishing resistance. It is not clear why this placement of the thermocouple should alter the resistance measured, but it is a fact that it does, as will be seen in the description of the measurements which follows:

RUN 1. 22 April '67 DP1A

Observed resistance equal to zero at $\sim 150^{\circ}\text{K}$ using Simpson meter; the resistance later went to 10^3 ohm. When Keithley meter was used on 0.1 volt scale the resistance measured was finite. On this scale the current passed through the sample is 10^{-8} to 10^{-5} ampere. In this run the thermocouple was electrically insulated from the anvils.

RUN 2. 20 May '67 JM85B

Observed $R = 1.7 \times 10^7$ ohm on Keithley at 77°K . A few minutes after changing scales to a higher current setting, the resistance went to zero. A measurement using the Simpson meter indicated $R = 1.5 \times 10^7$ ohm. Checked Keithley, using an external resistor and found it to read properly. Keithley shows $R \simeq 0$ for sample, consistently. Simpson meter showed $R \simeq 3$ ohm once. For this run, the thermocouple was in contact with the anvil.

RUN 3. 25 May '67 JM85A

Observed resistance equal zero at 93°K using Keithley on 10^8 scale. On the Simpson meter $R \sim 8$ ohm, with a slow decrease to 4 ohm. On reversing leads, Simpson read 16 ohm which decreased to 9 ohm. The thermocouple which was in electrical contact with the anvil was observed reading off-scale at this point. On removing one thermocouple lead, the resistances observed on Simpson were: 5 (1 k-ohm scale), 22 (100 ohm scale), 190 (10 ohm scale) and 1000 (on 1 ohm scale). Reversing the leads did not cause a significant change in the resistance measured. On measuring with the Keithley with one arm of the thermocouple removed, we once again observed $R \sim 10^8$ ohm and on going to a lower scale R went to zero again. In this run there was considerably more data to show the resistance going to zero intermittently.

It is not entirely clear whether the observance of a zero resistance was due to experimental difficulties or whether it was a real effect. However, a vanishing resistance has been observed in too many cases for it to be dismissed entirely as an experimental difficulty inherent in our type of electrical resistance measurements. With regard to the observation that different bridge settings on the ohmmeters produced differing resistance values for a given sample, it is a well established fact that \vec{E} -field markedly effects the conductivity. This has been discussed in Chapter III, and a further word on this matter was given in Chapter V. Evidence of this effect on sample DP1A at

temperatures down to 65°K is displayed in Figure 70. Curve (A) corresponds to a lower \vec{E} -field ($\vec{E} \approx 40\text{V/cm}$) while curve (B) is for the higher ($\vec{E} \approx 500\text{V/cm}$). It should be noted that although the effect is noticeable at room temperature, it becomes greatly enhanced as one approaches the liquid N_2 range.

Summary

Electrical resistivities for thirteen macromolecular organic solids have been determined under 8 kbar uniaxial pressure down to pumped liquid He temperatures (1.5°K).

In general, a finite resistance was measured over the entire temperature range; however, during several runs, three samples tended to intermittently exhibit zero resistance in the liquid N_2 temperature range. This effect was reproducible to some degree, and the onset of the effect was observed to be in some manner \vec{E} -field dependent. The zero resistance observation has been attributed to the possibility of the sample entering a superconducting state via filamentary conduction.

Most of the samples exhibited some degree of nonlinearity in the resistivity temperature data. Activation energies were determined over the whole temperature region. In general the samples exhibited two or three linear regions, indicating the possibility of multiple carrier levels and sources, or a region of extrinsic behavior.

Of particular interest was the fact that four samples did not

appreciably change their resistivities in dropping from 77°K to 1.5°K . Although a finite resistance was measured for each sample (10^9 to 10^{12} ohm-cm), it is suspected that filamentary superconduction was occurring. At the onset of the superconduction state, since the sample is soft magnetically, the large magnetic field produced acts via the Meissner effect to revert the sample back to the normal state. The detection system, being somewhat slow in response time, records only the average resistance of the competing processes which continue as long as the sample is below 77°K .

Suggestions for Future Studies

Since all of the work presented in this study involved only electrical resistance measurements, the possibility of filamentary superconduction having been observed suggests the following experiments to study the matter further:

- (1) Use of a magnetic search coil about the sample to search for transitory superconducting current "spikes."
- (2) Direct in-circuit examination by high speed oscilloscope to search for current "spikes."
- (3) Study of the resistance-temperature curve in an external magnetic field varied at least to compensate for any residual magnetism of the earth's field and higher (e. g., 0 - 200 gauss net).
- (4) Study of the resistance-temperature curve as a function of

applied voltage to see if low voltage conditions particularly would allow the "spikes" to persist.

- (5) Measure the specific heat near the anomalous "transition" region in a weak \vec{H} -field. Detection of a discontinuity would indicate superconduction.

In addition, since pressure has both positive and negative effects on the superconducting transition, one could study a given sample extensively to determine the pressure effects at low temperatures. The present clamp is limited to a pressure of about 40 kbar, and this pressure is extremely nonuniform. Recent work by Drickamer (93) has been carried out on 3 organic solids--pentacene, anthracene, and tetracene at liquid N_2 temperatures under uniform pressures up to 400 kbar. It would be interesting to study these samples in such a configuration. On the other hand, Smith and Chu (235) have recently found that high pressures can tend to completely destroy the superconducting transition in a number of metallic superconductors. Thus, it would appear that an extensive study of the effect of varying pressure on the samples is in order.

Regarding other organic systems, one very promising group is the metal-doped pyrolytically derived polymers. Pohl and coworkers (6, 7, 8, 18) have studied these materials earlier, and from their properties, they appear to be very likely candidates for organic superconductors.

CHAPTER VII

SUMMARY AND CONCLUSIONS

This study was conducted to investigate the nature of both the electrical conductivity and the unusually large polarizability (hyper-electronic polarization) as exhibited by certain macromolecular solids, and to examine a number of the specimens at low temperature in an effort to find an organic material which would exhibit superconductivity.

The first phase of the investigation (Chapter III) was concerned with the characterization of twenty-two newly synthesized organic polymers as electronic semiconductors. The conductivity was found to be electronic in nature, and was seen to be considerably increased by the addition of heterocyclic groups which tend to stabilize unpaired electrons.

Part two of the study (Chapter IV) dealt with an investigation of pressure and temperature effects on the energetics of unpaired spin production, and with the electron spin resonance signal of the polymers. A direct correlation between unpaired spins and electronic conduction was observed, indicating a common source for spins and carrier production.

The third portion of the study involved an investigation of the A.C. polarizability and A.C. conductivity, and the effects of pressure

temperature, and \vec{E} -field strength (both magnitude and frequency) on such. An analytical expression relating the dielectric constant, ϵ_r , to variations of pressure, temperature, and \vec{E} -field strength was derived.

Part four, the final phase of the investigation, was concerned with a search for the existence of superconductivity in organic macromolecular solids. On the basis of several anomalous results, it was suggested that filamentary superconduction was observed.

Since each part of this investigation was in itself a complete study, it was written as such, with a summary and conclusion, and with suggestions for further investigations being included in each chapter separately. No further summarization will be given here. The reader is referred to the summary in each respective chapter for further details.

In concluding this paper, suffice it to say that considerable evidence has been presented for the hyperelectronic polarization case as being truly electronic in nature and molecular in scale, rather than being due to surface or grain boundary effects. It is the author's thesis that hyperelectronic polarization is indeed such.

BIBLIOGRAPHY

1. A. Pocchetino, Acad. Kinei Rendiconti 15, 355 (1906).
2. A. Szent-Györgi, Science 93, 609 (1941).
3. D. D. Eley, Nature 162, 819 (1948).
4. A. T. Vartanyan, Acta Physicochim SSSR 22, 201 (1947).
5. R. R. Neiman and R. E. Johnson, Intl. Sci. and Tech., 68 (May, 1964).
6. H. A. Pohl, Proc. Fourth Conf. on Carbon, Ed. S. Mrozowski (Pergamon Press, 1960), p. 241.
7. H. A. Pohl and J. P. Laherrere, Proc. Fourth Conf. on Carbon, Ed. S. Mrozowski (Pergamon Press, 1960), p. 259.
8. H. A. Pohl and J. P. Laherrere, Semiconduction in Molecular Solids, Ed. H. A. Pohl (Ivy -Curtis Press, Philadelphia, 1960), p. 93.
9. H. A. Pohl, Semiconduction in Molecular Solids, Ed. H. A. Pohl (Ivy-Curtis Press, Philadelphia, 1960), p. 9.
10. H. A. Pohl, Chem. Engineering 68, 104 (1961).
11. H. A. Pohl, Electro-Technology 67, 85 (May, 1961).
12. H. A. Pohl, Modern Aspects of the Vitreous State, Vol. II, Ed. J. B. Mackenzie (Butterworths, London, 1962), p. 72.
13. H. A. Pohl, J. A. Bornmann, and W. Itoh, Organic Semiconductors, Ed. J. J. Brophy and J. W. Buttrey (Macmillan, New York, 1962), p. 142.
14. H. A. Pohl, Organic Semiconductors, Ed. J. J. Brophy and J. W. Buttrey (Macmillan, New York, 1962), p. 134.
15. H. A. Pohl and E. H. Engelhardt, J. Phys. Chem. 66, 2085 (1962).

16. H. A. Pohl, A. Rembaum, and A. Henry, *J. Am. Chem. Soc.* 84, 2699 (1962).
17. H. A. Pohl and D. A. Opp, *J. Phys. Chem.* 66, 2121 (1962).
18. H. A. Pohl and S. A. Rosen, *Proc. Fifth Conf. on Carbon*, Ed. S. Mrozowski (Pergamon Press, New York, 1963), p. 113.
19. H. A. Pohl, C. G. Gogos, and C. Cappas, *J. Polymer Sci.* 1A, 2207 (1963).
20. H. A. Pohl, *Progress in Solid State Chemistry*, Vol. I, Ed. H. Reiss (Pergamon Press, New York, 1964), p. 316.
21. H. A. Pohl and R. P. Chartoff, *J. Polymer Sci.* 2A, 2787 (1964).
22. H. A. Pohl, *Electronic Aspects of Biochemistry* (Academic Press, New York, 1964), p. 121.
23. R. G. Kepler, P. E. Bierstedt, and R. E. Merrifield, *Phys. Rev. Letters* 5, 503 (1960).
24. W. J. Siemons, P. E. Bierstedt, and R. G. Kepler, *J. Chem. Phys.* 39, 3523 (1963).
25. R. G. Kepler, *J. Chem. Phys.* 39, 3528 (1963).
26. H. Akamatsu, H. Inokuchi, and Y. Matsunaga, *Bull. Chem. Soc. Japan* 29, 213 (1956).
27. H. Akamatsu, H. Inokuchi, and Y. Matsunaga, *Nature* 175, 168 (1954).
28. I. Shirovani, H. Inokuchi, and S. Minomura, *Bull. Chem. Soc. Japan* 39, 386 (1966).
29. R. Sehr, M. M. Labes, M. Bose, H. Ur, and F. Wilhelm, *Symposium on Electrical Conduction in Organic Solids*, Ed. H. Kallman and M. Silver (Interscience, New York, 1961), p. 309.
30. M. Bose and M. M. Labes, *J. Am. Chem. Soc.* 83, 4505 (1961).
31. J. Kommandeur and L. S. Singer, *Symposium on Electrical Conduction in Organic Solids*, Ed. H. Kallman and M. Silver (Interscience, New York, 1961), p. 325.

32. J. Kommandeur, L. S. Singer, and J. R. Hall, *J. Chem. Phys.* 34, 129 (1961).
33. L. S. Singer and J. Kommandeur, *J. Chem. Phys.* 34, 133 (1961).
34. R. B. Aust, G. A. Samara, and H. G. Drickamer, *J. Chem. Phys.* 41, 2003 (1964).
35. W. H. Bentley and H. G. Drickamer, *J. Chem. Phys.* 42, 1573 (1965).
36. T. N. Anderson, D. W. Wood, R. C. Livingston, and H. Eyring, *J. Chem. Phys.* 44, 1259 (1966).
37. T. N. Anderson, D. W. Wood, R. C. Livingston, and H. Eyring, *J. Phys. Chem.* 70, 360 (1966).
38. H. A. Pohl and R. Rosen, *Bull. Am. Phys. Soc.* 10, 396 (1965).
39. R. Rosen and H. A. Pohl, *J. Polymer Sci.* 4-A1, 1135 (1966).
40. R. D. Hartman and H. A. Pohl, "Carrier Transport and Storage in Organic Semiconductors," A paper read at the Okla. Acad. Sci., Oklahoma State University, Stillwater, Dec. 3-4, 1965.
41. R. D. Hartman and H. A. Pohl, "Hyperelectronic Polarization in Polymeric Semiconductors," A paper read at the Okla. Acad. Sci., University of Okla., Norman, Dec. 2-3, 1966.
42. R. D. Hartman, *Proc. Okla. Acad. Sci.* 47 (1967, In press).
43. R. D. Hartman and H. A. Pohl, *Bull. Am. Phys. Soc.* 12, 409 (1967).
44. W. A. Little, *Phys. Rev.* 134, A1416 (1964).
45. H. A. Pohl, *J. Polymer Sci.* 17C, 13 (1967).
46. A. Rembaum, J. Moacanin, and H. A. Pohl, Progress in Dielectrics, Vol. VI, Ed. J. B. Birks and J. A. Hart (Academic Press, New York, 1965), p. 41.
47. A. V. Airapetyants and B. E. Davydov, *Organ. Poluprov. Akad. Nauk. SSSR Inst. Neftekhim Sinteza, Inst. Poluprov* (1963), pp. 291-315.
48. M. Becher and H. Mark, *Angew. Chem.* 73, 641 (1961).

49. M. Hatano, *Kagaku to Kogyo* 17, 792 (1964).
50. L. D. Rozenshtein, *Organ. Poluprov. Akad. Nauk. SSSR, Inst. Neftekhim Sinteza, Inst. Poluprov* (1963), pp. 143-170.
51. L. D. Rozenshtein, *Organ. Poluprov. Akad. Nauk. SSSR, Inst. Neftekhim Sinteza, Inst. Poluprov* (1963), pp. 171-206.
52. F. Gutmann and L. Lyons, Organic Semiconductors (John Wiley and Sons, New York, 1967).
53. A. von Hippel, Dielectrics and Waves (John Wiley and Sons, New York, 1954).
54. E. J. W. Verwey, Semi-conducting Materials Ed. H.K. Henisch (Butterworths Ltd., London, 1951), p. 151.
55. J. Volger, Semi-conducting Materials Ed. H. K. Henisch (Butterworths Ltd., London, 1951), p. 162.
56. C. G. Koops, *Phys. Rev.* 83, 121 (1951).
57. R. B. Hilborn, Jr., *J. Appl. Phys.* 36, 1553 (1965).
58. C. M. Huggins and A. H. Sharbaugh, *J. Chem. Phys.* 38, 393 (1963).
59. R. W. Sillars, *J. Inst. Elect. Engr. London* 80, 378 (1937).
60. L. G. Van Uitert, *Proc. IRE* 44, 1294 (1956).
61. M. Pollak, *J. Chem. Phys.* 43, 908 (1965).
62. M. Pollak, Private communication (1966).
63. W. A. Little, *Sci. Am.* 212, 21 (1965).
64. W. A. Little, *J. Polymer Sci.* 17C, 3 (1967).
65. M. L. Cohen, *Rev. Mod. Phys.* 36, 240 (1964).
66. V. L. Gurevich, A. I. Larkin, and Y. A. Firsov, *Fiz. Tver. Tela.* 4, 185 (1962). [Engl. Transl.: *Sov. Phys. Uspekhi* 8, 496 (1965).]
67. J. F. Schooley, W. R. Hosler, and M. L. Cohen, *Phys. Rev. Letters*, 12, 474 (1964).

68. P. F. Chester and G. O. Jones, *Phil. Mag.* 44, 1281 (1953).
69. E. H. Engelhardt, Unpublished M.S. Thesis, Princeton University (1961).
70. J. W. Mason, H. A. Pohl, and R. D. Hartman, *J. Polymer Sci.* 17C, 187 (1967).
71. S. Kanda and Y. Saito, *Bull. Chem. Soc. Japan* 30, 192 (1957).
72. S. Kanda and S. Kawaguchi, *J. Chem. Phys.* 34, 1070 (1961).
73. S. Kanda, *J. Chem. Soc. Japan Pure Chem. Sec. (Nippon Kagaku Zasshi.)* 83, 282 (1962).
74. S. Kanda, *J. Chem. Soc. Japan Pure Chem. Sec. (Nippon Kagaku Zasshi.)* 83, 560 (1962).
75. S. Kanda, *J. Chem. Japan Industrial Chemical Sec. (Kogyo Kagaku Zasshi)* 66, 641 (1963).
76. R. D. Hartman, S. Kanda, and H. A. Pohl, *Proc. Okla. Acad. Sci.* 47 (1967, In press).
77. R. D. Hartman, S. Kanda, and H. A. Pohl (To be published).
78. R. A. Van Nordstrand, Private communication, 1966.
79. K. A. Jensen, *Z. Anorg. Chem.* 252, 227 (1944).
80. R. V. G. Evans and C. S. Gibson, *J. Chem. Soc.* 71, 431 (1949).
81. S. Kanda, K. Ito, and T. Nogaito, *J. Polymer Sci.* 17C, 151 (1967).
82. M. Kishita and M. Kubo, Proc. Symp. of Structural Chem. (Tokyo Univ. Press, 1959), p. 69.
83. F. Seitz, The Modern Theory of Solids (McGraw Hill, New York, 1940).
84. C. Kittel, Introduction to Solid State Physics, 3rd. Ed. (John Wiley and Sons, Inc., New York, 1966).
85. A. J. Dekker, Solid State Physics (Prentice Hall, Englewood Cliffs, N. J., 1959).

86. J. Blakemore, Semiconductor Statistics (Pergamon Press, N.Y., 1962).
87. W. Shockley, Electrons and Holes in Semiconductors (Van Nostrand and Co., Inc., Princeton, N.J., 1950).
88. P.W. Bridgman, Collected Experimental Papers (Harvard Press, Cambridge, 1964), Vol. 1-7.
89. R. W. Lynch and H. G. Drickamer, J. Chem. Phys. 45, 1020 (1966).
90. R. W. Lynch and H.G. Drickamer, J.Chem.Phys. 44, 181 (1966).
91. H. G. Drickamer, Sol.St.Phys. 17, 1 (1965).
92. H. G. Drickamer and A. S. Balchan, Modern Very High Pressure Techniques, Ed. R.H. Wentorf (Butterworths, London, 1962).
93. H. G. Drickamer, Science 156, 1183 (1967).
94. H. Akamatsu and H. Inokuchi, J.Chem.Phys. 18, 810 (1950).
95. D. D. Eley, G. D. Parfitt, M. J. Perry, and D. H. Taysum, Trans. Faraday Soc. 49, 79 (1953).
96. D. D. Eley and G. D. Parfitt, Trans. Faraday Soc. 51, 1529 (1955).
97. R. S. Bradley, J. D. Grace, and D. C. Munro, Trans. Faraday Soc. 58, 776 (1962).
98. R. E. Burgess, J. Polymer Sci. 17C, 51 (1967).
99. A. Many, E. Harnik, and D. Gerlich, J.Chem.Phys. 23, 1733 (1955).
100. H. Inokuchi and A. Akamatsu, Sol.St.Phys. 12, 93 (1961).
101. G. E. Pake, Sci. Am. 199, 58 (1958).
102. E. H. Roger, NMR and ESR Spectroscopy, Ed. Varian Associates (Pergamon Press, New York, 1960), p. 1.
103. R. H. Sands, NMR and ESR Spectroscopy, Ed. Varian Associates (Pergamon Press, New York, 1960), p. 44.

104. R. C. Rempel, NMR and ESR Spectroscopy, Ed. Varian Associates (Pergamon Press, New York, 1960), p. 224.
105. D. J. Ingram, Free Radicals as Studied by Electron Spin Resonance (Butterworths, London, 1958).
106. M. L. Randolph, Bull. Am. Phys. Soc. 11, 514 (1966).
107. E. Javoisky, J. Phys. USSR 10, 197 (1946).
108. R. L. Cummerow and D. Halliday, Phys. Rev. 70, 433 (1946).
109. E. M. Purcell, H. C. Torrey, and R. V. Pound, Phys. Rev. 69, 37 (1946).
110. F. Bloch, W. W. Hansen, and M. Packard, Phys. Rev. 69, 127 (1946).
111. R. E. Norberg, Am. J. Phys. 33, 1 (1965).
112. E. M. Purcell, Am. J. Phys. 22, 1 (1954).
113. G. E. Pake, Am. J. Phys. 18, 438 (1950).
114. G. E. Pake, Am. J. Phys. 18, 473 (1950).
115. NMR and ESR Spectroscopy, Ed. Varian Associates (Pergamon Press, New York, 1960).
116. H. S. Jarrett, Sol. St. Phys. 14, Ed. F. Seitz and D. Turnbull (Academic Press, Inc., New York, 1963), p. 213.
117. D. B. Chestnut and W. D. Phillips, J. Chem. Phys. 35, 1002 (1961).
118. D. Bijl, H. Kainer, and A. C. Rose-Innes, J. Chem. Phys. 34, 133 (1961).
119. Z. G. Soos and R. C. Hughes, J. Chem. Phys. 46, 253 (1967).
120. A Rembaum and A. M. Hermann, Bull. Am. Phys. Soc. 10, 1201 (1965).
121. A. M. Hermann and A. Rembaum, J. Polymer Sci. 17C, 107 (1967).

122. R. D. Hartman and S. Kanda, "Semiconduction in Metallo-Organic Polymers," A paper read at the Okla. Acad. Sci., Oklahoma State University, Stillwater, Dec. 3-4, 1965.
123. Y. Okamoto, S. Shah, and Y. Matsunaga, *J. Chem. Phys.* 43, 1904 (1965).
124. G. A. Samara and H. G. Drickamer, *J. Chem. Phys.* 37, 471 (1962).
125. R. B. Aust, W. H. Bentley, and H. G. Drickamer, *J. Chem. Phys.* 41, 1856 (1964).
126. P. W. Bridgman, *Rev. Mod. Phys.* 18, 1 (1946).
127. F. Dacheville and R. Roy, Proc. Fourth International Symposium on Reactivity of Solids, Ed. J. H. Deboer (Elsevier Publ. Co., New York, 1961), p. 502.
128. L. H. Piette, NMR and ESR Spectroscopy, Ed. Varian Associates (Pergamon Press, New York, 1960), p. 207.
129. R. D. Hartman and H. A. Pohl, Submitted to *J. Polymer Sci.* (1967).
130. J. Valasek, *Phys. Rev.* 17, 475 (1921).
131. G. Busch and P. Scherrer, *Naturwiss* 23, 737 (1935).
132. E. Wainer and A. N. Salomon, Titanium Alloy Mfg. Co. Elect. Rep. 8 (1942).
133. A. von Hippel, R. G. Breckenridge, F. G. Chesley and L. Tisza, *Ind. Eng. Chem.* 38, 1097 (1946).
134. B. T. Matthias, *Phys. Rev.* 75, 1771 (1949).
135. B. T. Matthias, *Phys. Rev.* 76, 175 (1949).
136. B. T. Matthias, *Phys. Rev.* 76, 430 (1949).
137. B. T. Matthias, *Phys. Rev.* 76, 1886 (1949).
138. J. K. Hulm, B. T. Matthias, and E. A. Long, *Phys. Rev.* 79, 885 (1950).
139. J. C. Maxwell, Electricity and Magnetism (Clarendon Press, Oxford, 1892).

140. K. W. Wagner, *Archiv. fur. Elektrochem.* 2, 371 (1914).
141. J. W. L. Kohler and C. G. Koops, *Philips Res. Rep.* 1, 419 (1946).
142. E. Blechschmidt, *Physikalische Zeitschrift vereinigt mit dem Jahrbuch der Radioaktivitat und Elektronik* 39, 212 (1938).
143. F. W. Brockman, P. H. Dowling, and W. G. Steneck, *Phys. Rev.* 77, 85 (1950).
144. G. Möltgen, *Zeitsch. fur angew Physik* 4, 216 (1952).
145. A. von Hippel, *Dielectric Materials and Applications* (John Wiley and Sons, New York, 1954).
146. C. P. Smyth, *Dielectric Behavior and Structure* (McGraw Hill Co., New York, 1955).
147. H. V. Malmstadt, C. G. Enke, and E. C. Toren, Jr., *Electronics for Scientists* (W. A. Benjamin, Inc., New York, 1963).
148. H. Fröhlich, *Proc. Roy. Soc. (London)* 185 A, 399 (1946).
149. R. M. Fuoss, *The Chemistry of Large Molecules*, Ed. R. E. Burk and O. Grummitt (Interscience, New York, 1943), Chapter VI.
150. R. M. Fuoss, *J. Am. Chem. Soc.* 63, 2401 (1941).
151. R. M. Fuoss, *J. Am. Chem. Soc.* 63, 2410 (1941).
152. A. Rembaum and J. Moacanin, *Polymeric Semiconductors* (Jet Propulsion Laboratory, Pasadena, California, 1964).
153. R. G. Kepler, *Phys. Rev.* 119, 226 (1960).
154. R. G. Kepler, *Organic Semiconductors*, Ed. J. J. Brophy and J. W. Buttrey (Macmillan Co., New York, 1962), p. 1.
155. R. S. Bradley, J. D. Grace, and D. C. Munro, *Phys. Chem. at High Pressure*, 143 (1964).
156. Y. Harada, Y. Maruyama, I. Shirotani, and H. Inokuchi, *Bull. Chem. Soc. Japan* 37, 1378 (1964).

157. J. L. Katz, S. A. Rice, S. I. Choi, and J. Jortner, *J. Chem. Phys.* 39, 1683 (1963).
158. R. Silbey, J. Jortner, S. A. Rice, and M. T. Vala, Jr., *J. Chem. Phys.* 42, 733 (1965).
159. E. Whalley, Advances in High Pressure Research, Ed. R. S. Bradley (Academic Press, New York, 1966), p. 143.
160. M. Pollak, Physics of Semiconductors Exeter Conference (Institute of Physics and the Physical Society, London, 1962), p. 86.
161. H. A. Pohl, M. Pollak, and R. D. Hartman, Private Communication, 1966.
162. S. Takashima, *J. Mol. Biol.* 7, 455 (1963).
163. H. E. Matthews, Jr., *Proc. Okla. Acad. Sci.* 45, 138 (1965).
164. N. Lange, Handbook of Chemistry (McGraw-Hill Co., New York, 1965), p. 868.
165. J. Brophy, *J. Appl. Phys.* 27, 1383 (1956).
166. M. I. Kornfel'd and L. S. Sochava, *Fiz. Tver. Tela.* 1, 1366 (1959) [Engl. Transl: *Sov. Phys. Sol. St.* 1, 1253 (1959)].
167. M. I. Kornfel'd and L. S. Sochava, *Fiz. Tver. Tela.* 1, 1370 (1959) [Engl. Transl: *Sov. Phys. Sol. St.* 1, 1256 (1959)].
168. K. Stegavik, *J. Appl. Phys.* 37, 2200 (1966).
169. H. K. Onnes, *Commun. Kamerlingh Onnes Lab. Univ. Leiden Suppl.* 34b, 55 (1913).
170. D. Shoenberg, Superconductivity (Cambridge Press, 1952).
171. B. T. Matthias, T. H. Geballe and V. B. Compton, *Rev. Mod. Phys.* 35, 1 (1963).
172. F. London, Superfluids (John Wiley and Sons, Inc., New York, 1950) Vol. I.
173. W. Meissner and R. Ochsenfeld, *Naturwiss* 21, 787 (1933).
174. F. B. Silsbee, *J. Wash. Acad. Sci.* 6, 587 (1916).

175. W. Tuyn and H. K. Onnes, *Commun. Phys. Lab. Univ. Leiden* 174a, 8 (1926).
176. R. B. Scott, *Bur. Stand. J. Res.*, Wash. 41, 581 (1948).
177. E. Maxwell, *Phys. Rev.* 78, 477 (1950).
178. C. Reynolds, B. Serin, W. Wright, and L. Nesbitt, *Phys. Rev.* 78, 487 (1950).
179. P. F. Chester, unpublished Ph.D. Thesis, Queen Mary College, University of London (1953).
180. D. H. Bowen and G. O. Jones, *Proc. Roy. Soc. (London)* A254, 522 (1960).
181. L. D. Jennings and C. A. Swenson, *Phys. Rev.* 112, 31 (1958).
182. L. S. Kan, A. I. Sudovstov, and B. G. Lazarew, *Dokl. Acad. Nauk, SSSR* 69, 173 (1949).
183. M. D. Fiske, *Phys. Rev.* 94, 495 (1954).
184. J. Hatton, *Phys. Rev.* 103, 1167 (1956).
185. J. Bardeen, L. Cooper and J. Schrieffer, *Phys. Rev.* 108, 1175 (1957).
186. H. Fröhlich, *Phys. Rev.* 79, 845 (1950).
187. B. G. Lazarev, L. S. Lazareva, V. I. Makarov, and T. A. Ignat'eva, *Zh. Eksper. Teor. Fiz.* 48 1065 (1965). [Engl. Transl.: *Sov. Phys. JETP* 21, 711 (1965)].
188. V. G. Bar'yakhtar and V. I. Makarov, *Zh. Eksper. Teor. Fiz.* 49, 1934 (1965) [Engl. Transl.: *Sov. Phys.* 22, 1320 (1966)].
189. N. B. Brandt, N. I. Ginzburg, T. A. Ignat'eva, B. G. Lazarev, and V. I. Makarov, *Zh. Eksper. Teor. Fiz.* 49, 85 (1965) [Engl. Transl.: *Sov. Phys. JETP* 22, 61 (1966)].
190. B. G. Lazarev, L. S. Lazareva, T. A. Ignat'eva and V. I. Makarov, *Dokl. Akad. Nauk. SSSR* 165, 74 (1965) [Engl. Transl.: *Sov. Phys. Doklady* 10, 620 (1966)].
191. W. Gey and G. V. Heyden, *Z Physik.* 193, 65 (1966).

192. W. Gey, Sol. St. Commun. 4, 403 (1966).
193. W. Gey, Phys. Rev. 153, 422 (1967).
194. D. Markowitz and L. P. Kadanoff, Phys. Rev. 131, 563 (1963).
195. K. Luders, Z. Phys. 193, 73 (1966).
196. N. B. Brandt and N. I. Ginzburg, Fiz. Tverd, Tela. 3, 3461 (1961) [Engl. Transl.: Sov. Phys. Sol. St. 3, 2510, (1962)] .
197. N. I. Ginzburg, Zh. Eksper. Teor. Fiz. 44, 2104 (1963) [Engl. Transl.: Sov. Phys. JETP, 17, 1415 (1963)].
198. N. B. Brandt and N. I. Ginzburg, Zh. Eksper. Teor. Fiz. 44 1876 (1963). [Engl. Transl.: Sov. Phys. JETP 17, 1262 (1963)] .
199. N. B. Brandt and N. I. Ginzburg, Usp. Fiz. Nauk. 85, 485 (1965). [Engl. Transl.: Sov. Phys. Usp. 8, 202 (1965)].
200. N. B. Brandt and N. I. Ginzburg, Zh. Eksper. Teor. Fiz. 46, 1216 (1964). [Engl. Transl.: Sov. Phys. JETP 19, 823 (1964)] .
201. N. B. Brandt and N. I. Ginzburg, Zh. Eksper. Teor. Fiz. 49, 1706 (1965). [Engl. Transl.: Sov. Phys. JETP 22, 1167 (1966)] .
202. N. B. Brandt and N. I. Ginzburg, Zh. Eksper. Teor. Fiz. 50, 1260 (1966). [Engl. Transl.: Sov. Phys. JETP 23, 838 (1966)] .
203. N. B. Brandt and N. I. Ginzburg, Zh. Eksper. Teor. Fiz. 51, 59 (1966). [Engl. Transl.: Sov. Phys. JETP 24, (1967)].
204. B. T. Matthais, Proceedings of the First International Conference on the Physics of Solids at High Pressures, Tucson 1965 (Academic Press, New York, 1965).
205. J. Wittig, Z. Physik 195, 215 (1966).
206. J. Wittig, Z. Physik 195, 228 (1966).
207. W. E. Gardner and T. F. Smith, Phys. Rev. 138, A484 (1965).

208. W. E. Gardner and T. F. Smith, Phys. Rev. 144, 233 (1966).
209. W. E. Gardner and T. F. Smith, Phys. Rev. 154, 309 (1967).
210. T. F. Smith and W. E. Gardner, Phys. Rev. 140, A1620 (1965).
211. T. F. Smith and W. E. Gardner, Phys. Rev. 146, 291 (1966).
212. T. F. Smith, Phys. Rev. Letters 17, 386 (1966).
213. J. Wittig, Phys. Rev. Letters 15, 159 (1965).
214. N. B. Hannay, T. H. Geballe, B. T. Matthias, K. Andres, P. Schmidt, and D. MacNair, Phys. Rev. Letters 14, 225 (1965).
215. H. M. McConnell, B. M. Hoffman, D. D. Thomas, and F. R. Gamble, Proc. Nat. Acad. Sci. 54, 371 (1965).
216. J. Bardeen, Phys. Rev. 79, 167 (1950).
217. L. N. Cooper, Am. J. Phys. 50, 91 (1960).
218. A. B. Pippard, Proc. Roy. Soc. A216, 547 (1953).
219. R. A. Ferrell, Phys. Rev. Letters 13, 330 (1964).
220. R. E. DeWames, G. W. Lehman and T. Wolfram, Phys. Rev. Letters 13, 749 (1964).
221. W. L. McCubbin, Phys. Letters 19, 461 (1965).
222. K. F. G. Paulus, Molecular Phys. 10, 381 (1966).
223. C. G. Kuper, Phys. Rev. 150, 189 (1966).
224. W. A. Little, Phys. Rev. 156, 396 (1967).
225. V. L. Ginzburg, Phys. Letters 13, 101 (1964).
226. F. J. Salzano and M. Strongin, Phys. Rev. 153, 533 (1967).
227. L. V. Keldysh, Uspekhi. Fiz. Nauk. SSSR 86, 327 (1965).
[Engl. Transl.: Sov. Phys. Uspekhi 8, 496 (1965)] .
228. J. Ladik, G. Biczó¹ and A. Zawadowski, Phys. Letters 18, 257 (1965).

229. J. Lađik, G. Biczó, and E. Elek, *J. Chem. Phys.* 44, 483 (1966).
230. B. N. Ganguly and P. Sinha, *Ind. J. Pure Appl. Phys.* 4, 49 (1960).
231. N. Lange, Handbook of Chemistry (McGraw-Hill Co., New York, 1965), p. 884.
232. C. Kittel, Quantum Theory of Solids (John Wiley and Sons, Inc., 1963), p. 142.
233. H. Fröhlich, H. Pelzer, and S. Zienau, *Phil. Mag.* 41, 221 (1950).
234. Y. Maruyama and H. Inokuchi, *Tech. Rept. ISSP A 194* (The Institute for Solid State Physics, University of Tokyo, Japan, 1966).

VITA

Roger D. Hartman

Candidate for the Degree of

Doctor of Philosophy

Thesis: HYPERELECTRONIC POLARIZATION AND RELATED
ELECTRONIC PROPERTIES OF MACROMOLECULAR
SOLIDS: ORGANIC SEMICONDUCTORS

Major Field: Physics

Biographical:

Personal Data: Born in Kansas City, Missouri, November 4, 1935, the son of Franklin L. and Mona L. Smith Hartman.

Education: Received the Bachelor of Arts degree from William Jewell College, with a major in Physics, in June, 1958; received the Master of Science degree from the University of Arkansas, with a major in Physics, in June, 1960; awarded National Science Foundation Science Faculty Fellowship to work toward the Doctorate in Physics at the Oklahoma State University in June, 1965; attended the University of Uppsala, Uppsala, Sweden, Summer of 1966; completed requirements for the Doctor of Philosophy degree in May, 1968.

Professional Experience: Entered graduate school in June, 1958, and performed research and instructed engineering physics classes as a Graduate Assistant at the University of Arkansas until September, 1960; taught physical science and mathematics as an Instructor of Physical Science at Evangel College, September, 1960 to May, 1961; taught engineering physics as Instructor of Physics at the University of Arkansas from September, 1961 to May, 1962; taught advanced physics and directed the research of three (3) Master of Science candidates at the University of Tulsa, as an Assistant Professor of Physics, September, 1962 to May, 1965; has held Summer appointments as Research Associate at the Los Alamos Scientific Laboratory during 1961, 1962, and 1963; has performed as a

Consultant and Senior Physicist at North American Aviation, Tulsa, during 1964 and 1965; has held the positions of National Science Foundation Science Faculty Fellow and Research Assistant at the Oklahoma State University since June, 1965; has held the position of Assistant Professor of Physics at the University of Tulsa since September, 1967; has performed research in the following areas: solid-gas reactions as related to specific surface areas of adsorbates; plasma physics and thermonuclear reactions; X-ray absorption spectroscopy of solids; has been actively studying electromagnetic properties of molecular solids, since 1963; has conducted studies in electronic properties of macromolecular solids, in particular organic semiconductors, a part of which are described in this thesis, since 1965.

Professional Organizations: American Association of Physics Teachers; American Association of University Professors; American Institute of Physics Student Section; American Physical Society; Oklahoma Academy of Science; Optical Society of America; Red Red Rose Society; Sigma Pi Sigma, National Physics Honor Society; is National Councilor for Sigma Pi Sigma for the Arkansas and Oklahoma region; listed in Who's Who in American Education (1966), and American Men of Science (1966-67).

Publications: "Apparatus for Measuring Relative Roughness Factors of Inert Metals by the Adsorption of Radioactive Iodine." J. Appl. Phys. 34, 1492 (1963) with M. K. Testerman; "Additivity in X-Ray Absorption-Edge Fine Structure of Mixed-Ligand Complexes." Bull. Am. Phys. Soc. 10, 1225 (1965) with R. A. Van Nordstrand and K. W. Schuette; "X-Ray Absorption Spectra and Chemical Bonding." Abstr. Am. Chem. Soc. Tetra-sect. Meet. Okla. 17 (1966) with R. A. Van Nordstrand and K. W. Schuette; "Use of Computers in an Undergraduate Light and Optics Laboratory." Am. J. Phys. 34, 793 (1966); "Application of Matrix Theory to Some Problems in Oscillatory Motion." Proc. Okla. Acad. Sci. 46, 102 (1966) with Y. S. Kim; "Low Resistivity Polyacenequinones." J. Polymer Sci. C17, 187 (1967) with J. W. Mason and H. A. Pohl; "Hyperelectronic Polarization in Polymeric Semiconductors." Proc. Okla. Acad. Sci. 47, (1967, in press); "The Hysteresis of Piezoconduction of Some Metallo-Organic Polymers." Proc. Okla. Acad. Sci. 47 (1967, in press) with S. Kanda and H. A. Pohl; "Relaxation of Hyperelectronic Polarization." Bull. Am. Phys. Soc. 12, 409 (1967) with H. A. Pohl; "Hyperelectronic Polarization in Macromolecular Solids." Submitted to J. Polymer Sci. with H. A. Pohl.